PHYTOCHEMICAL STUDIES AND BIOACTIVITY EVALUATION (DENV-2 NS2B/NS3 PROTEASE) OF *Beilschmiedia glabra* AND *Endiandra kingiana* (LAURACEAE)

SYAZREEN NADIA BINTI SULAIMAN

FACULTY OF SCIENCE
UNIVERSITY OF MALAYA
KUALA LUMPUR

2019

PHYTOCHEMICAL STUDIES AND BIOACTIVITY EVALUATION (DENV-2 NS2B/NS3) OF *Beilschmiedia glabra* AND *Endiandra kingiana* (LAURACEAE)

SYAZREEN NADIA BINTI SULAIMAN

THESIS SUBMITTED IN FULFILMENT OF THE REQUIREMENTS FOR THE DEGREE OF DOCTOR OF PHILOSOPHY

DEPARTMENT OF CHEMISTRY
FACULTY OF SCIENCE
UNIVERSITY OF MALAYA
KUALA LUMPUR

2019

UNIVERSITY OF MALAYA

ORIGINAL LITERARY WORK DECLARATION

Name of Candidate: **Syazreen Nadia Binti Sulaiman**

Matric No: **SHC120035**

Name of Degree: **Doctor of philosophy (PhD.)**

Title of Project Paper/Research Report/Dissertation/Thesis ("this Work"):

PHYTOCHEMICAL STUDIES AND BIOACTIVITY EVALUATION (DENV-2 NS2B/NS3) OF *Beilschmiedia glabra* AND *Endiandra kingiana* (LAURACEAE)

Field of Study: **Organic Chemistry**

I do solemnly and sincerely declare that:

(1) I am the sole author/writer of this Work;
(2) This Work is original;
(3) Any use of any work in which copyright exists was done by way of fair dealing and for permitted purposes and any excerpt or extract from, or reference to or reproduction of any copyright work has been disclosed expressly and sufficiently and the title of the Work and its authorship have been acknowledged in this Work;
(4) I do not have any actual knowledge nor do I ought reasonably to know that the making of this work constitutes an infringement of any copyright work;
(5) I hereby assign all and every rights in the copyright to this Work to the University of Malaya ("UM"), who henceforth shall be owner of the copyright in this Work and that any reproduction or use in any form or by any means whatsoever is prohibited without the written consent of UM having been first had and obtained;
(6) I am fully aware that if in the course of making this Work I have infringed any copyright whether intentionally or otherwise, I may be subject to legal action or any other action as may be determined by UM.

Candidate's Signature Date:

Subscribed and solemnly declared before,

Witness's Signature Date:

Name:

Designation:

PHYTOCHEMICAL STUDIES AND BIOACTIVITY EVALUATION (DENV-2 NS2B/NS3) OF *Beilschmiedia glabra* AND *Endiandra kingiana* (LAURACEAE)

ABSTRACT

Preliminary survey of the dichloromethane crude extracts of two Lauraceae species (*Beilschmiedia glabra* and *Endiandra kingiana*) showed moderate dengue inhibition against dengue type 2 NS2B/NS3 protease with percentage of inhibition by 51.28 ± 13.9% and 65.05 ± 3.7%, respectively. Isolation and purification on the active extracts of the *B. glabra* and *E. kingiana* yielded seventeen compounds. *B. glabra* gave nine compounds; **123**, **124**, **125**, **126**, **127**, **128**, **129**, **130**, and **131**. Among nine compounds, **130**, and **131** were identified as new neolignans which features a rare oxetane moiety in the structure. Meanwhile, *E. kingiana* afforded eight compounds; **132**, **133**, **134**, **135**, **136**, **137**, **138** and **139**, with **136** identified as a new benzofuran. Their structures were elucidated by spectroscopic techniques such as 1D and 2D NMR, UV, IR, LCMS-IT-TOF and comparison with the literature values. All isolated compounds which of had sufficient amount were tested for inhibitory activity against dengue type 2 NS2B/NS3 protease. From *B. glabra*, two compounds, **125** and **130** were tested which showed weak inhibition with percentage inhibition less than 50% towards the dengue type 2 NS2B/NS3 protease. As for *E. kingiana*, five compounds, **134**, **135**, **136**, **137**, and **138** were also subjected to *in vitro* test against NS2B/NS3 protease of DENV-2 where **136** (61.23 ± 7.0%), **137** (69.93 ± 3.3%), and **138** (62.02 ± 6.2%) showed moderate activity with percentage inhibition more than 50%, while the remaining two compounds showed weak inhibition. Therefore, three compounds (**136**, **137** and **138**) with percentage of inhibition more than 50%; were further evaluated in order to determine their respective IC_{50} values. Compound **137** had a higher potency with a lower IC_{50} value compared to the other active compounds towards the protease. Then these three active compounds, **136** (IC_{50} = 403.14 ± 33.03), **137** (IC_{50} = 170.10 ± 5.94), and **138** (IC_{50} = 184.13 ± 2.11) were subjected to molecular

docking studies to provide much clear picture of the site at which the active compounds bind to the protease. Based on molecular docking studies, **136**, **137**, and **138** showed common hydrogen bonding interactions with the oxygen atom in each compound with Asn152 at S2 pocket of DENV-2 NS2B/NS3 protease. However, that was the only similar interactions between these three active compounds. For compound **137** and **138**, both showed similar interaction with Asp129 and Tyr161 of the DENV-2 NS2B/NS3 protease at S1 pocket, however with different type of bonding as **137** having hydrogen bonding while **138** having π-π stacking interaction with the protease. The hydrogen bonding interactions (more stable) resulted for **137** was more active compared to the π-π stacking interaction in **138**. As **136**, being the least potent may cause from having least interaction with the protease that only interacts with Asp129 and Ser135 at S1 pocket.

Keywords: Lauraceae, dengue type 2 NS2B/NS3 protease, *Beilschmiedia glabra*, *Endiandra kingiana*, molecular docking studies

KAJIAN FITOKIMIA DAN PENILAIAN BIOAKTIVITI (DENV-2 NS2B/NS3)

***Beilschmiedia glabra* DAN *Endiandra kingiana* (LAURACEAE)**

ABSTRAK

Kajian awal ekstrak mentah dikhlorometana dari dua spesies Lauraceae (*Beilschmiedia glabra* Kosterm dan *Endiandra kingiana* Gamble) menunjukkan perencatan denggi sederhana terhadap protease NS2B/NS3 denggi jenis 2 dengan peratusan perencatan masing masing sebanyak 51.28 ± 13.9 % dan 65.05 ± 3.7 %. Pengasingan dan penulenan pada ekstrak aktif *B. glabra* dan *E. kingiana* menghasilkan tujuh belas sebatian. *B. glabra* memberikan sembilan sebatian iaitu; **123**, **124**, **125**, **126**, **128**, **129**, **130**, dan **131**. Antara sembilan sebatian yang diasingkan dari *B. glabra*, **130**, dan **131** telah dikenal pasti sebagai sebatian neolignans baru yang mempunyai ciri oksetana yang jarang berlaku dalam struktur. Manakala, *E. kingiana* memberikan lapan sebatian iaitu; **132**, **133**, **134**, **135**, **136**, **137**, **138** dan **139**, dengan **136** dikenalpasti sebagai benzofuran baru. Struktur bagi sebatian yang diasingkan telah dikenalpasti oleh teknik spektroskopi seperti 1D dan 2D NMR, UV, IR, LCMS-IT-TOF dan perbandingan dengan nilai-nilai literatur. Semua sebatian yang mempunyai jumlah yang mencukupi dari *B. glabra* dan *E. kingiana* diuji untuk menghalang aktiviti denggi jenis 2 terhadap protease NS2B/NS3. Dari *B. glabra*, dua sebatian, **125** dan **130** telah diuji yang menunjukkan perencatan yang lemah dengan perencatan peratusan kurang daripada 50% ke atas protease. Walaubagaimanapun, untuk *E. kingiana*, lima sebatian, **134**, **135**, **136**, **137** dan **138** juga tertakluk kepada *in vitro* terhadap protease dengan hanya **136** (61.23% ± 7.0), **137** (69.93% ± 3.3) dan **138** (62.02%) menunjukkan perencatan sederhana dengan perencatan peratusan lebih daripada 50%, manakala sebatian selebihnya menunjukkan perencatan yang lemah. Oleh itu, tiga sebatian (**136**, **137** dan **138**) dengan peratusan lebih daripada 50%; dinilai selanjutnya untuk menentukan nilai IC_{50} mereka. Sebatian **137** mempunyai potensi yang lebih tinggi dengan nilai IC_{50} yang lebih rendah berbanding dengan sebatian aktif yang lain ke arah

protease. Kemudian ketiga-tiga sebatian aktif ini; **136** (IC_{50} = 403.14 ± 33.03), **137** (IC_{50} = 170.10 ± 5.94), dan **138** (IC_{50} = 184.13 ± 2.11) juga tertakluk kepada penyelidikan molekul dok. Kajian molekul dok akan memberi gambaran yang jelas tentang tapak di mana sebatian aktif mengikat kepada protease. Berdasarkan penyelidikan molekul dok; **136**, **137**, dan **138** menunjukkan interaksi yang sama melalui ikatan hidrogen dengan atom oksigen dalam setiap sebatian dengan Asn152 pada poket S2. Walaubagaimanapun, itu adalah satu-satunya interaksi yang sama antara ketiga-tiga sebatian aktif ini. **137** dan **138**, kedua-duanya menunjukkan interaksi yang sama dengan Asp129 dan Tyr161 daripada protease pada poket S1, namun dengan jenis ikatan yang berlainan yang mana **137** mempunyai ikatan hidrogen manakala **138** mempunyai π- π interaksi dengan protease. Disebabkan oleh interaksi ikatan hidrogen (lebih stabil) menghasilkan **137** lebih aktif berbanding dengan interaksi penyusunan π- π pada **138**. Namun bagi sebatian **136**, ianya menunjukkan perencatan yang lemah di sebabkan mempunyai interaksi yang paling sedikit dengan protease yang hanya berinteraksi dengan Asp129 dan Ser135 di poket S1.

Kata kunci: Lauraceae, denggi jenis 2 NS2B/NS3 protease, *Beilschmiedia glabra*, *Endiandra kingiana*, penyelidikan molekul dok

ACKNOWLEDGEMENTS

In the name of Allah, most Gracious, most Merciful, I would like to convey my gratitude to my supervisor, Prof. Dr. Khalijah Awang for her kind supervision, concern, understanding and support throughout the development of this research project.

I would like to express my sincere appreciation to Ms. Nor, Mr. Nordin, Mr. Fateh, Mr. Zakaria, and Mrs. Fiona for their help on the NMR machine. I also thank Mr. Teo Leong Eng, Mr. Din and Mr. Rafly for their collections and identifications of plant materials.

My appreciation extended to my friends in Phytochemistry Laboratory with whom I shared all these wonderful moments over the years; Dr. Azeana, Dr. Joey, Dr. Fadzli, Dr. Norsita, Dr. Nurul, Dr. Chan, Dr. Chong, Dr. Dewi, Mrs. Faizah, Mrs. Julia, Ms. Haslinda, Ms. Aimi, Ms. Shelly, Ms. Tein, Ms. Rosalind, Mr. Remy, Mr. Azrul, Mr. Hafiz, Mr. Faiz, Ms. Mariam, Mr. Aqmal and others for their kindness, support and friendship.

I would like to express my special appreciation to my mother and father, Mrs. Selma and Mr. Sulaiman for your support and encouragement over the past years. To my husband, Mr. Nazrul and my daughter, Ms. Auni Nadia, thank you for being there for me and supporting me in completing my PhD studies. To my father and mother in laws, Mr. Zambri and Mrs. Norrizah, thank you for helping me to take care of Auni when I have conferences and seminars. To my siblings, Mrs. Intan, Mr. Zamri, Mr. Syahrul, Mrs. Nor and Ms Syahira, thank you for being there for me. Without their prayers and relenting support, I could not be here. Finally I would like to thank my incredible late supervisor Professor Madya Dr Mat Ropi Mukhtar for all his guidance throughout my journey in the chemistry field.

TABLE OF CONTENTS

LIST OF SCHEMES

LIST OF FIGURES

LIST OF TABLES

LIST OF SYMBOLS AND ABBREVIATIONS

α	:	Alpha
β	:	Beta
δ	:	Chemical shift
λ	:	Maximum wavelength
µg/mL	:	Microgram per mililitre
µM	:	Micromolar
cm^{-1}	:	Per centimeter
AChE	:	anti-acetylcholinesterase
C_5D_5N	:	Deuterated pyridine
CC	:	Column chromatography
CD_3OD	:	Deuterated methanol
$CDCl_3$	:	Deuterated chloroform
CH_3OH	:	Methanol
$CHCl_3$	:	Chloroform
d	:	Doublet
DCME	:	Dichloromethane extract
dd	:	Doublet of doublet
DENV	:	Dengue virus
DENV-2	:	Dengue virus type 2
DIR	:	Dirigent protein
dt	:	Double of triplet
E	:	Envelope
FA	:	Formic acid
g	:	Gram
HPLC	:	High performance liquid chromatography
Hz	:	Hertz
IC_{50}	:	Concentration required to inhibit 50 % of activity
iNOS	:	Inducible nitric oxide synthase
IR	:	Infrared
J	:	Coupling constant
LRGT	:	Lariciresinol glucosyltranferase
m	:	Multiplicity
m	:	Meter

M	:	Molar
MeOH	:	Methanol
MHz	:	Mega Hertz
NC	:	Nucleocapsid core
nm	:	Nanometer
NS2B	:	Nonstructural protein 2B (essential cofactor)
NS3	:	Nonstructural protein 3
NS3pro	:	Serine protease domain of the NS3 protein
PAL	:	Phenylalanine Ammonia Lyase
PLR	:	Pinoresinol/lariciresinol reductase
PNGT	:	Pinoresinol glucosyltranferase
ppm	:	Part per million
prM	:	Pre-membrane
PSS	:	Piperitol/sesamin synthase
PTLC	:	Preparative thin layer chromatography
q	:	Quartet
s	:	Singlet
SIRD	:	Secoisolariciresinol dehydrogenase
SIRGT	:	Glycosyltransferase
t	:	Triplet
TLC	:	Thin layer chromatography
UV	:	Ultraviolet

LIST OF APPENDICES

CHAPTER 1: INTRODUCTION

1.1 General

There are at least 250,000 species of flowering plants in the world and about 150,000 of them are found in the tropics. In South-East Asia alone, there are 35,000 species of which 8,000 are found in Malaysia. Malaysia is the richest and the oldest rain forest in the world. It may be attributed by the warm and nearly uniform climate which is suitable for the growth of the tropical rain forest (Keng, 1978). Until now, at least 654 species have been reported as endemic to Malaysia. A total of 6,000 floral species have been reported to possess medicinal values in the tropics. From this, a total of 1,230 species have been reported in Malaysia as medicinal plants which are used in traditional medicine (Zakaria & Mohd, 1994). Almost all humans in the world prefer traditional plants as a treatment option and around 80 % of the world population rely on traditional medicines for primary health care (Savithramma et al., 2011).

Recently, there is a trend of people turning towards natural products as remedy. Natural products have become the main source of test materials in the development of drugs based on traditional medicinal practices (Meneses et al., 2009). The demand for plant-based medicines is growing as they are generally considered to be safer, non-toxic and less harmful than synthetic drugs (Abd Kadir et al., 2013).

It has been estimated that approximately over half of the pharmaceuticals in clinical use today are derived from natural products. For centuries, natural substances, particularly plants, have been used to control and treat diseases and this has culminated in the discovery of the majority of modern pharmaceutical agents (Cheuka et al., 2017). As stated by World Health Organization (WHO), each part of the plant is useful and contains active compounds that are important for therapeutic purposes or which are precursors for the synthesis of useful drugs.

Plant derived natural products have long been and will continue to be extremely important as medicinal agents and models for the design, synthesis and semi synthesis of novel substances for treating humankind diseases. Some important plant derived drugs and intermediates that are still obtained commercially by extraction from their whole plant sources are including taxol **1** (*Taxus brevifolia*), vinblastine **2** (*Catharantus roseus*), demecolcine **3** (*Colchicum autumnale*), caffeine **4** (*Camellia sinensis*), cocaine **5** (*Erythroxylum coca*), and morphine **6** (*Papaver somniferum*) (Figure 1.1) (He et al., 1999; Narender, 2012; Javad et al., 2016; Tsuchiya, 2017; Fabiani et al., 2018; Symons et al., 2018).

However, despite these important contributions from the plant kingdom, many plant species have never been described and remain unknown to science and relatively few have been studied systematically to any extent for biologically active chemical constituents. Thus, it is reasonable to expect that new plant sources valuable and pharmaceutically interesting materials remain to be discovered and developed (Newman et al., 2000). In fact, nature is a fantastic reservoir of substance that can be used directly as pharmaceuticals or can serve as lead structures that can be optimized towards the development of new therapeutic agents (Teixeira et al., 2014).

This research work involved the chemical investigation and biological testing from the plant family Lauraceae; *Beilschmiedia glabra (B. glabra*) and *Endiandra kingiana* (*E. kingiana*). This family is well known for producing bioactive compounds with various biological activities (Chen et al., 2006; Rohan A Davis et al., 2009; Mollataghi, A. Hadi, et al., 2012; Salleh, Ahmad, et al., 2015; Azmi et al., 2016).

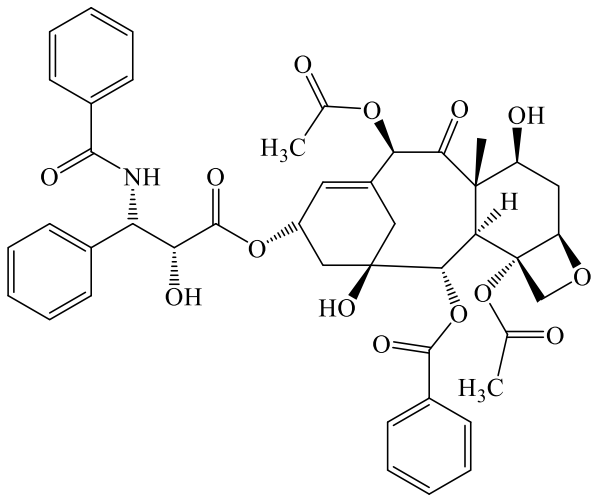

1

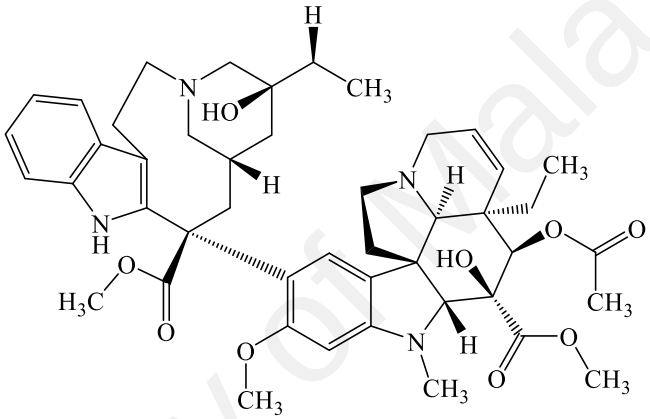

2

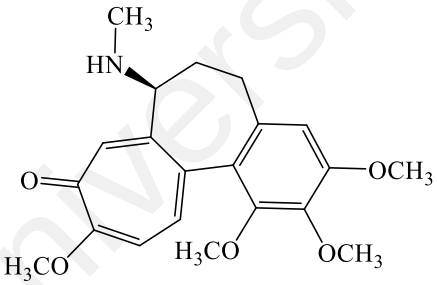

3

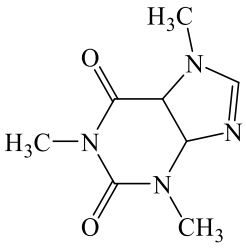

4

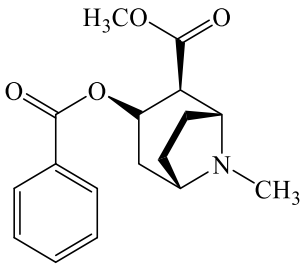

5

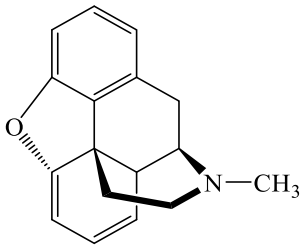

6

Figure 1.1: Chemical constituents of the derived natural products.

1.2 Lauraceae: Botany and distribution

Kochummen (1997) reported that the Lauraceae family consists of 35 genera and 2500 species throughout the warmer parts of the world while in Malaysia it comprises about 16 genera and 213 species (Corner, 1988).

In Malaysia, the members of Lauraceae are known as "***Medang***" or "***Tejur***" and its growth depends on lowland or highland. In the lowland, they are typically small trees of the lower canopy except for a new species which may reach up to 30 meters tall where as in the highland the Lauraceae becomes more abundant reaching the top of the forest canopy. Therefore, the term "oaks laurels forest" is given to this vegetation which lies at 1200-1600m.

Most of Lauraceae species are evergreen, though seasonal in flowering and in the development of new leaves. There are two important features of the Lauraceae family; the presence of aromatic substances in the tissues, and the small flowers with their closely packed sepals and stamens, arranged in circles of trees, open the anters and revealed the pollen.

The leaves of plants in this family are spiral, alternate, opposite, sub-opposite, whorled, entire, and leathery. The color of the new leaves varies from nearly white to pink, purple, red, or brown as in the plants, e.g. Laurel (*Litsea castanea*). The flowers are small, regular, greenish white or yellow, fragrant or with rancid smell, bisexual, or unisexual and united with six sepals in two rows.

Botanically the genera of the Lauraceae are distinguished by details of the stamens which are difficult to make out. In the first six genera: *Cinnamomum. Cryptocarya, Phoebe, Alseodaphne, Dehaasia,* and *Persea* – the flowers and also the fruits are arranged in relatively long stalked panicle produced from the leaf – axils or the end of twigs. While, in the last four genera; *Actinodaphne, Litsea, Neolitsea, and Lindera*- the flowers are grouped in the little heads which are themselves put together to form dense little clusters

in the leaf-axils on the twigs behind the leaves, or on the branches and trunk (Gibbs, 1974; Brossi, 1987; Ng, 1989).

1.3 Lauraceae: Classification of tribes

Classification of Lauraceae can be illustrated in the list below. The classification included 62 genera, mainly found in Southeast Asia and Latin America (*The Plant List*, 2013).

Kingdom: Plantae

Division: Magnoliophyta

Class: Magnoliopsida

Order: Laurales

Family: Lauraceae

Genera:

Table 1.1: Classification genera of Lauraceae family.

Actinodaphne	*Aiouea*	*Alseodaphne*	*Aniba*
Apollonias	*Aspidostemon*	***Beilschmiedia***	*Camphora*
Caryodaphnopsis	*Cassytha*	*Chlorocardium*	*Cinnadenia*
Cinnamomum	*Cryptocarya*	*Dehaasia*	*Dicypelium*
Dodecadenia	***Endiandra***	*Endlicheria*	*Eusideroxylon*
Gamanthera	*Hufelandia*	*Hypodaphnis*	*Iteadaphne*
Kubitzkia	*Laurus*	*Licaria*	*Lindera*
Litsea	*Machilus*	*Malapoenna*	*Mespilodaphne*
Mezilaurus	*Misanteca*	*Mocinnodaphne*	*Mutisiopersea*
Nectandra	*Neocinnamomum*	*Neolitsea*	*Notaphoebe*
Nothaphoebe	*Ocotea*	*Oreodaphne*	*Paraia*
Parasassafras	*Parthenoxylon*	*Persea*	*Phoebe*
Phyllostemonodaphne	*Pleurothyrium*	*Polyadenia*	*Potameia*
Potoxylon	*Povedadaphne*	*Ravensara*	*Rhodostemonodaphne*
Sassafras	*Schauera*	*Sextonia*	*Sinopora*
Sinosassafras	*Syndiclis*	*Systemonodaphne*	*Tetranthera*
Umbellularia	*Urbanodendron*	*Williamodendron*	*Yasunia*

1.4 Challenges in Lauraceae classification

The knowledge of all plants species in the Lauraceae family is still incomplete. As of 1991, approximately 25-30% of neotropical Lauraceae species had not been described. As of 2001, embryological studies had only been completed on individuals from 26 genera yielding a 38.9% level of knowledge, in terms of embryology, for this family (Rohwer et al., 1991).

Additionally, the huge amount of variations within the family for any potential defining characteristic poses a major challenge for developing a reliable classification. It is impossible to describe even one genus or tribe by a single well-defined character. For this reason, all proposed classifications rely on a set of characteristics where the combination presents the most frequently observed traits for the group.

The Lauraceae are nearly all woody trees and shrubs comprising 30 to 50 genera and about 2,000 species. An exception is the vining, leafless, parasitic genus *Cassytha.* The leaves are simple, without stipules, and usually alternate. The flowers are actinomorphic, usually bisexual, and possess a perianth of six, basally connate sepal like segments. The androecium most frequently comprises 4 whorls of 3 stamens each, although the inner whorls are often sterile. The filaments of the inner whorl usually have a pair of enlarged glandular appendages near the base. The anthers dehisce by means of commonly 4, upwardly opening flaps. The single simple pistil has a usually superior ovary with a single pendulous ovule in a solitary locule. The fruit is a berry or a drupe, often surrounded basally by the short, persistent perianth cup. Unlike other Magnoliidae, the endosperm is completely absorbed by the embryo in Lauraceae (Rohwer et al., 1991; Van der Werff & Richter, 1996).

1.5 General appearance and phytomorphology of *Beilschmiedia* and *Endiandra*

The genus *Beilschmiedia* belonging to Lauraceae family, is distributed from Africa and southern Asia to Australia, New Zealand, and in the American tropics (Chaverri & Cicció, 2010). It is one of the largest pantropical genera of the Lauraceae family with about 250 species represented (Nishida, 1999).

Beilschmiedia comprises trees and rarely shrubs and is usually distinguished from other genera of the Lauraceae by the following characteristics: paniculate or racemose inflorescences that are not strictly cymose at the terminal division, bisexual and trimerous flowers with six equals to subequal tepals, six to nine fertile stamens representing the outer two or three whorls, two-celled anthers, and fruits lacking cupules. The leaves are opposite, subopposite, or alternate. Phyllotaxis is usually consistent within a species; however, two species with alternate leaves, *B. crassa* Sach.Nishida and *B. maingayi* Hook.f., have subopposite leaves near the tip of each twig. Leaf shape ranges from ovate to obovate, while leaf size often varies within a given species (Nishida, 2008).

Endiandra is a genus of evergreen trees belongs to the Laurel family, Lauraceae. The genus includes more than 125 species distribute in Southeast Asia, Pacific region and Australia. Meanwhile, 10 species found in Malaysia named; *E. holttumii*, *E. kingiana*, *E. macrophylla*, *E. maingayi, E. praeclara*, *E. rubescens*, *E. wrayi*, *E. sp.1* and *E. sp. 2* (Ridley, 1922; Ng & Phillipson, 1989).

The leaves are alternate, pinnatinerved, with areolate venation (except in *E. introsa*). Inflorescences in axillary and substerminal panicles. Flowers in axillary panicles, usually shorter than the leaves. Flowers bisexual, mostly 3-merous (4-merous in *E. globosa*). Perianth segments 6 or 8, not persistent in fruit. Stamens usually 3 (4–6 in *E. globosa*), anthers 2-locular, dehiscence usually extrorse (introrse in *E. introrsa*); associated glands present or occasionally absent, staminodes usually 3 (sometimes 2–0 in *E. globosa*).

Ovary superior produce fruits in the form of drupe which are free on the receptacles. The seeds are dispersed by animals and birds (Ng & Phillipson, 1989).

The *Beilschmiedia* and *Endiandra* genera are morphologically similar. The leaves of the *Beilschmiedia* species tend to coarser venation pattern than those of *Endiandra*, a genus often misidentified as *Beilschmiedia*. However, there are many exceptions, such as *B. glauca* having a very fine venation pattern and *E. clavigera* Kosterm. having a very coarse venation pattern. As for the number of stamens, the six stamens in *Beilschmiedia* species always represent the first and second whorls, not the second and third whorls as seen in *Endiandra.* Sometimes specimens with relatively long oblong fruits of *Endiandra* are misidentified to *Beilschmiedia*. Long oblong fruits with obtuse base and apex are rather rare for *Beilschmiedia*, but more common for *Endiandra* in Borneo and the Malay Peninsula. However, there are some exceptions in this tendency because both genera have a wide variation in fruit shape. As mentioned by Van der Werff (2001), fruiting specimens can often not be assigned to either genus with certainty because of their similarity in fruit and vegetative characters (Nishida, 2008).

1.6 *Beilschmiedia glabra* Kosterm

B. glabra Kosterm (Figure 1.2), locally known as "*kayau temblouh"* or "*kayuh tefuluh*" is distributed in Peninsular Malaysia, Borneo and Kalimantan. The trees are up to 35 m tall and the twigs are colored greenish brown. The leaves are evenly distributed, blade relatively coriaceous, ovate to elliptic, base cuneate, apex acute, margin usually flat. It also has 6-9 pairs of secondary veins, almost immersed above, slightly raised below with minor tertiary veins. It also has filaments longer than anthers in all the stamens. Fruits of this species are ellipsoid with a pointed apex with 3.0 - 4.5 cm across on 2.5 cm drying brown stalk (Nishida, 2008).

Figure 1.2: *B. glabra* Kosterm (left: leaves and fruit; right: bark).

1.7 *Endiandra kingiana* Gamble

E. kingiana Gamble (Figure 1.3), is a large sub-canopy tree growing up to 33 m tall and 210 cm girth. The leaves are 2 cm long, stout, hairy to glabrous, leathery thick blade and elliptic to oblong. Fruits are oblong shape with 3 cm across on 1.5 cm, shiny green to drying brown. The species can be found in Pahang, Perak, Kelantan, Negeri Sembilan, Johor and Borneo (Burkill, 1966; Whitmore & Ng, 1989).

Figure 1.3: *E. kingiana* Gamble (left: leaves and flower; right: bark).

1.8 Problem statement

Dengue is the most prevalent anthropod-borne viral infection of human. It is estimated that dengue virus infection is 50 – 100 million per year globally in over 100 tropic and sub-tropic countries where over 2.5 billion people are at risk. Out of these 2.5 billion people at risk, 1.8 billion which is more than 70% are in Asia Pacific countries (Abd Kadir et al., 2013).

The development of vaccines and antiviral therapy has seen little success but no licensed antiviral therapy is currently available yet for dengue virus (Sampath & Padmanabhan, 2009). The control of the disease is focused on the control of mosquito vector, which is costly and often met with limited success (Gubler, 1998). Therefore, the search for the lead compounds and derivatives with their information on the structures and activities is needed in discovering novel inhibitor for the development of anti-dengue.

Two genera of Lauraceae family, *Beilschmiedia* and *Endiandra* are widely used in traditional medicine and are sources of various classes of secondary metabolites such as endiandric acid derivatives, amides and alkaloids, flavonoids, lignans and neolignans (Ndjakou Lenta et al., 2015). Among these types of secondary metabolites found, one of the most common are flavonoids. Flavonoids, which are polyphenolic natural products that are found mainly in plants, are well known due to their different biological properties including dengue antiviral activity (Moghaddam et al., 2014). Some previously reported, flavonoids demonstrated significant inhibitory activity against dengue virus such as quercetin, baicalein, baicalin and fisetin (Hassandarvish et al., 2016). Even though a number of plants are known for their dengue antiviral activity, few investigations have been published related to isolation (identification) of compounds from plants and subsequent evaluation of their dengue related antiviral activities (Teixeira et al., 2014).

Evidence has also shown that the secondary metabolites of *Cryptocarya chartacea* Kosterm, which is a plant from the Lauraceae family is active towards dengue antiviral

activity with IC_{50} value of 1.8 to 4.2 µM (Hassandarvish et al., 2016). Since *B. glabra* and *E. kingiana*, the plants which are the subjects of the current study are in same family as *C. chartacea*, therefore there is a strong possibility that the secondary metabolites of *B. glabra* and *E. kingiana* also could showed significant values against dengue antiviral activity.

Preliminary screening of the dichloromethane crude extracts (at 200 µg/ mL) of the bark of *E. kingiana* has proven to be a moderate inhibitor against dengue-2 NS2B/NS3 protease (65.05 ± 3.73 %) but not a good inhibitor towards *B. glabra* (51.28 ± 13.90 %).

1.9 Objectives of the research

The principal objectives of the present PhD work were as follows:

i- to isolate and purify the secondary metabolites from the active extracts of the bark of *B. glabra* Kosterm and *E. kingiana* Gamble,

ii- to characterize the isolated secondary metabolites using spectroscopic techniques such as NMR, FTIR, LCMS-IT-TOF, and UV-Vis spectroscopy,

iii- to screen the inhibitory activities of the isolated secondary metabolites against dengue virus type 2 (DENV-2) using NS2B/NS3 protease in order to identify the compound(s) which are responsible for moderate and low inhibitions towards DENV-2 NS2B/NS3 protease of the extracts,

iv- to carry out molecular docking studies on the compound(s) that possess more than 50 % inhibition at 200 ppm towards the DENV-2 NS2B/NS3 protease, in order to investigate the site at which the active compound(s) bind the enzymes.

CHAPTER 2: GENERAL AND CHEMICAL ASPECTS

2.1 Introduction

Plants have been explored by chemist for their chemical compounds and their related medicinal values. Throughout this exploration many compounds and drugs were identified and studied. The studies have been aimed at compounds that are of the pharmaceutical interest in the scope of medicinal importance.

Phytochemical studies of Lauraceae plants have produced various type of compounds such as carbohydrates, lipids, amino acids, proteins, polyphenol, essential oils, terpenes, aromatic compounds and alkaloid constituents. The production of those phytochemicals from the Lauraceae plants has been the subject of a number of comprehensive articles (Banning et al., 1982; Kochummen, 1997; Fischer et al., 1999).

Beilschmiedia is one of the largest pantropical genera in the Lauraceae, comprising about 250 species (van der Werff, 2003; Nkeng-Efouet & Rao, 2012). Most of its species grow in tropical climates, but few of them are native to temperate regions, and they are widespread in tropical Asia, Africa, Madagascar, Australia, New Zealand, North America, Central America and South America (van der Werff, 2003; Nkeng-Efouet & Rao, 2012). Regarding *Endiandra*, there are about 125 species found throughout the tropical regions, including 10 species in Malaysia (Burkill, 1966; Ng, 1989; Mabberley, 2008).

2.2 Medicinal values from *Beilschmiedia* species

Several *Beilschmiedia* species have been applied as traditional medicines in various parts of the world (Salleh, Ahmad, et al., 2015) . They have been used in local medicine to treat various conditions, including infectious disease, malaria, cancer and gastrointestinal infections (Talontsi et al., 2013; Kuete et al., 2014). Some of the medicinal uses from the bark of *B. pahangensis* are the bark being crushed and mixed

with water and used as a drink after childbirth, it is also used to relieve stomach pains and also to treat diarrhea (Wiart, 2006). In Indonesia, the wood of *B. madang,* is traditionally employed as decoction in the treatment as an antimalarial preparation (Kitagawa et al., 1993). The lists of the various medicinal uses of other *Beilschmiedia* species in distinct parts of the world are shown in Table 2.1.

Table 2.1: Medicinal uses of several *Beilschmiedia* species.

Species	Locality	Plant parts and medicinal uses
B. pahangensis	Malaysia	Bark: as a drink after childbirth, to relieve stomach pains and to treat diarrhea (Wiart, 2006)
B. tonkinensis	Malaysia	Leaves: for easing pain and broken bone (Wiart, 2006)
B. madang	Indonesia	Wood: the decoction as an antimalarial preparation (Kitagawa et al., 1993)
B. cryptocaryoides	Madagascar	Fruits/bark: to treat infectious disease and malaria (Talontsi et al., 2013)
B. acuta	Cameroon	Leaf: cancer and gastrointestinal infection (Kuete et al., 2014)
B. anacardioides	Cameroon	Stem/bark: treat uterine tumours, rubella, rheumatisms, bacterial and fungal infections (Nkeng-Efouet & Rao, 2012) Seeds: used as spices (Nkeng-Efouet & Rao, 2012)
B. lancilimba	Cameroon	Used to cure skin bacterial infections (Nkeng-Efouet & Rao, 2012)
B. manii	Cameroon	Used to treat dysentery and headache. It also used as an appetite stimulant (Nkeng-Efouet & Rao, 2012)

2.3 Phytochemical studies from *Beilschmiedia* species

Among the 250 species, only 15 species of *Beilschmiedia*; *B. glabra, B. madang, B. brevipes, B. elliptica, B. kunstleri, B. alloiophylla, B. tsangii, B. erythrophloia, B. obscura, B. anacardioides, B. pulverulenta, B. volckii, B. ferruginea, B. cryptocaryoides* and *B. zenkeri* have been phytochemically investigated.

These investigations led to the isolation and characterization of various classes of secondary metabolites, of which endiandric acid derivatives, amides and alkaloids, flavonoids, lignans and neolignans, and also miscellaneous compounds (cyanogenic glycosides, benzopyran, benzenoid, terpenes, benzaldehyde, and fatty acid) (Chen et al., 2006; Lenta et al., 2009; Mollataghi, A. Hadi, et al., 2012; Salleh, Ahmad, et al., 2015).

Previous studies of chemical constituents isolated from the *B. glabra* have led to the isolation of alkaloids; beilschglabrines A **7**, beilschglabrines B **8**, butanolides; subamolide D **9**, subamolide E **10**, steroids; β-sitosterol **11,** β-sitostenone **12**, 24-methylenelanosta-7,9(11)-diene-3β,15α-diol **15**, triterpenes; lupeol **13,** taraxerol **14**, and sesquiterpene; germacrene D **16**, β-selinene **17**, δ-cadinene **18**, β-eudesmol **19**, β-caryophyllene **20**, γ-gurjunene **21**, caryophyllene oxide **22** (Salleh, Ahmada, et al., 2015; Salleh, Ahmad, Khong, & Zulkifli, 2016; Salleh, Ahmad, Khong, Zulkifli, et al., 2016). As for their biological studies, compound **7** and **8** exhibited moderate activities towards DPPH radical scavenging (IC_{50} 115.9 μM), acetylcholinesterase (IC_{50} 50.4 μM) and lipoxygenase (IC_{50} 32.8 μM) assays (Salleh, Ahmad, Khong, Zulkifli, et al., 2016), meanwhile other biological studies are tabulated in Table 2.2.

The other chemical constituents isolated from *Beilschmiedia* species, and their references are listed in Table 2.2. Although there are reports on the crude extracts of these species exhibit antifungal, antibacterial, antimicrobial, antioxidant, and anti-inflammatory; however, the number of active compounds isolated from them are still limited.

Table 2.2: Chemical constituents isolated from *Beilschmiedia* species and their biological activities.

Species and site of collection	Compound name	Compound type	Biological activities
B. glabra (bark); Malaysia	Beilschglabrines A **7** Beilschglabrines B **8**	Alkaloids	Both compounds showed moderate activities towards DPPH radical scavenging (IC_{50} 115.9 μM), acetylcholinesterase (IC_{50} 50.4 μM) and lipoxygenase (IC_{50} 32.8 μM) assays (Salleh, Ahmad, Khong, Zulkifli, et al., 2016).
B. glabra (leaves); Malaysia	Subamolide D **9** Subamolide E **10** β-sitosterol **11** β-sitostenone **12** Lupeol **13** Taraxerol **14** 24-methylenelanosta-7,9(11)-diene-3β,15α-diol **15**	Lignans Steroids Triterpenes Steroids	All compounds were tested for DPPH radical scavenging, antimicrobial, acetylcholinesterase and lipoxygenase inhibitory activities. Subamolide D **9** and Subamolide E **10** displayed strong lipoxygenase assay with an IC_{50} value of 5.1 and 5.5 μM, respectively (Salleh, Ahmad, Khong, & Zulkifli, 2016).
B. glabra (leaves and barks); Malaysia	Germacrene D **16** β-selinene **17** δ-cadinene **18** β-eudesmol **19** β-caryophyllene **20** γ-gurjunene **21** Caryophyllene oxide **22**	Terpenes	All compounds showed moderate activity for antioxidant, antimicrobial, and anti-inflammatory activities. (Salleh, Ahmada, et al., 2015).

'Table 2.2, continued'

Species and site of collection	Compound name	Compound type	Biological activities
B. madang (wood); Indonesia	Dehatrine **23**	Alkaloid	Dehatrine **23** was tested for antimalarial acticity. It exhibit a potent inhibitory activity (IC_{50}= 0.17 and IC_{90}= 3.6 µM) against the proliferation of malarial pathogen *Plasmodium falciparum* (Kitagawa et al., 1993).
B. madang (stem bark); Malaysia	Madangones B **24** (+)-kunstlerone **25**	Neolignans	Both compounds were tested for antioxidant, acetylcholinesterase inhibitory and anti-inflammatory activitites. Compound **24** exhibited the highest level of activity on the COX-2 model and acetylcholinesterase inhibition assay, with IC_{50} values of 27.4 and 70.3 µM, respectively. Compound **25** displayed the strongest DPPH radical-scavenging activity with an IC_{50} values of 68.7 µM (Salleh, Ahmad, Yen, Zulkifli, et al., 2016).
B. brevipes (leaves); Malaysia	(6,7-Dimethoxy-4-methylisoquinolinyl)-(4'-methoxyphenyl)-methanone **26**	Alkaloid	Nob biological activities reported (Pudjiastuti et al., 2010).

'Table 2.2, continued'

Species and site of collection	Compound name	Compound type	Biological activities
B. elliptica (stem bark)	Laurelliptine **27**	Alkaloid	Not reported any biological activities (Nkeng-Efouet & Rao, 2012).
B. kunstleri (leaves); Malaysia	(+)-kunstlerone **25** (+)-norboldine **28** (+)-cassythicine **29** (+)-boldine **30**	Neolignan Alkaloids	(+)-kunstlerone **25** was tested for antioxidant activity using DPPH radical scavenging activity. The results shown that it possess potent antioxidant activity with scavenging capacity of SC_{50} = 20.0 µg/mL (Mollataghi et al., 2011).
B. kunstleri (bark); Malaysia	(-)-kunstleramide **31**	Dienamide	(-)-kunstleramide **31** was tested for antioxidant activity using DPPH radical scavenging activity and cytotoxic effect. It exhibit poor dose-dependent inhibition of DPPH activity, with an IC_{50} value of 179.5 µg/ml, but show a moderate cytotoxic effect on MTT assays of A549, HT-29 and WRL-68 with EC_{50} values of 44.74, 55.94 and 70.95 µg/mL, respectively (Mollataghi, A. Hadi, et al., 2012).

'Table 2.2, continued'

Species and site of collection	Compound name	Compound type	Biological activities
B. alloiophylla (barks); Costa Rica	2-hydroxy-9-methoxyaporphine **32** Laurotetanine **33** Liriodenine **34** Oreobeiline **35**	Alkaloids	These compounds were tested for anti-acetylcholinesterase (AChE), and anti-α-glucosidase assays. Compounds **32-34** have significant anti-AChE activity with IC_{50} values of 2.0, 3.2 and 3.5 μM, respectively that is comparable with the AChE inhibitory activity of huperzine A (IC_{50} = 1.8 μM), a standard substrate AChE inhibitor and is used as prescribed drug to treat Alzeimer's disease. While oreobeiline **35** was significantly active in α-glucosidase inhibitory activity with IC_{50} values of 8.0 μg/mL (Mollataghi, Coudiere, et al., 2012).
B. tsangii (roots); Taiwan	Tsangibeilin C **36** Endiandric acid M **37**.. Beilschminol **38** (+)-5-hydroxybarbatenal **39**	Lignans (Endiandric acid) Lignan Sesquiterpene	Among the isolates, endiandric acid M **37** exhibited moderate an inducible nitric oxide synthase (iNOS) inhibitory activity, with an IC_{50} value of 31.70 μM (Y. T. Huang et al., 2012).

'Table 2.2, continued'

Species and site of collection	Compound name	Compound type	Biological activities
B. tsangii (leaves); Taiwan	4α,5α-epoxybeilschmin B **40** Beilschmin D **41** Beilschmin A **42** Beilschmin B **43**	Lignans	Among the isolates, beilschmin A **42** and beilschmin B **43** exhibited potent antitubercular activities (MICs = 2.5 and 7.5 µg/mL, respectively) against Mycobacterium tuberculosis 90 µg/mL (Chen et al., 2007).
B. tsangii (stem); Taiwan	Tsangin A **44** Tsangin B **45**	Lignans	All compounds exhibit potent cytotoxic, with IC_{50} value of 0.81, and 0.42, respectively, against the P-388 cell line (Chen et al., 2006).
B. erythrophlo ia (seeds); Taiwan	Cordycepiamide B **46** Cordycepiamide D **47**	Lignans	Compounds were evaluated for their inhibition on nitric oxide (NO) release by macrophages. Among the tested compounds, Cordycepiamide D **47** showed the most NO inhibitory effects, with the inhibition of 17.4 % NO production in LPS stimulated RAW264.7 cells at 10 µM (Chang et al., 2017).

'Table 2.2, continued'

Species and site of collection	Compound name	Compound type	Biological activities
B. erythrophloia (stem); Taiwan	Beilschamide **48**	Lignan	Beilschamide **48** was tested *in vitro* against CCRF-CEM (human lymphoblastic leukemia) cell line. It exhibit cytotoxic effect with IC_{50} value of 21.2 µg/mL against CCRF-CEM cell line (Chen et al., 2015).
B. erythrophloia (roots); Taiwan	Suberosol B **49** Erythrophloin C **50**	Sesquiterpene Lignan (Endiandric acid)	All the isolated compounds were tested *in vitro* against *M. tuberculosis* H37Rv. Both compounds (**49** and **50**) exhibited antitubercular activity with MIC = 28.9 and 50 µg/mL, respectively. The clinically used antitubercular agent ethambutol (MIC = 6.25 µg/mL) was employed as the positive control (P.-S. Yang et al., 2009).
B. erythrophloia (roots): Taiwan	Dehydrooligandrol methyl ether **51** Farnesylol **52**	Benzopyran Benzenoid	Not reported any biological activities (P.-S. Yang et al., 2008).
B. obscura (roots)	Obscurine **53**	Cyclostachine acid	Not reported any biological activities (Lenta et al., 2011).

'Table 2.2, continued'

Species and site of collection	Compound name	Compound type	Biological activities
B. anacardioides (stem/bark); Cameroon	Beilschmiedic acid A **54** Beilschmiedic acid B **55** Beilschmiedic acid C **56**	Lignan (Endiandric acids)	All compounds were evaluated *in vitro* against five strains of microbes for antibacterial activities. Among all, beilschmiedic acid C **56** showed strong activity against *Bacillus subtilis*, *Micrococcus luteus* and *Streptococcus faecalis* with MIC values of 5.6, 0.7 and 22.7 µg/mL, respectively (Chouna et al., 2009).
B. anacardioides (stem/bark); Cameroon	Beilschmiedic acid D **57**	Lignan (Endiandric acid)	Not reported any biological activities (Chouna et al., 2010).
B. anacardioides (stem/bark); Cameroon	Beilschmiedic acid F **58** Beilschmiedic acid G **59**	Endiandric acids	Not reported any biological activities (Chouna et al., 2011).
B. pulverulenta (stem/bark); Malaysia	(+)-yangambin **60** (+)-sesartemin **61** (+)-excelsin **62** (+)-sesamin **63**	Lignans	All compounds exhibited significant inhibition in AChE/BChE assays with (+)-yangambin **60** being the most potent compare to the other lignans with IC_{50} values of 179.8 and 168.8 µM, respectively (Salleh, Ahmad, Yen, & Zulkifli, 2016).

'Table 2.2, continued'

Species and site of collection	Compound name	Compound type	Biological activities
B. volckii (leaves); Australia	Magnolol **64**	Neolignan	Not reported any biological activity (Banfield et al., 1994).
B. ferruginea (leaves and flowers); Vietnam	Ferrugineic acid B **65** Ferrugineic acid C **66** Ferrugineic acid D **67** Ferrugineic acid J **68**	Lignans (Endiandric acids)	These compounds were assayed for Bcl-xL and Mcl-1 binding affinities. Ferrugineic acids B, C and J (**65**,**66** and **68**) exhibited significant binding affinity for both antiapoptotic proteins Bcl-xL (K_i = 19.2, 12.6 and 19.4 µM, respectively) and Mcl-1 (K_i = 14.0, 13.0 and 5.2 µM, respectively), and ferrugineic acid D **67** showed only significant inhibiting activity for Mcl-1 (K_i = 5.9 µM) (Apel et al., 2014).
B. cryptocaryoides (Bark); Madagascar	Cryptobeilic acid A **69** Cryptobeilic acid B **70** Cryptobeilic acid C **71** Cryptobeilic acid D **72** Tsangibeilin B **73**	Beilschmiedic acids	All compounds displayed moderate antibacterial activity against *Escherichia coli* 6r3, *Acinetobacter calcoaceticus* DSM 586, and *Pseudonamas stutzeri* A1501, with the minimum inhibitory concentrations ranging from 10-50 µM, respectively (Talontsi et al., 2013).

'Table 2.2, continued'

Species and site of collection	Compound name	Compound type	Biological activities
B. zenkeri (Bark); Cameroon	5-hyroxy-7,8-dimethoxyflavanone **74** Beilschmieflavonoid A **75** Beilschmieflavonoid B **76**	Flavonoids	All compounds were tested for their antiplasmodial activitiy against the W2 strain of *Plasmodium falciparum*. Compound **74** exhibited antiplasmodial activity with IC_{50} values of 9.3 µM (Lenta et al., 2009).

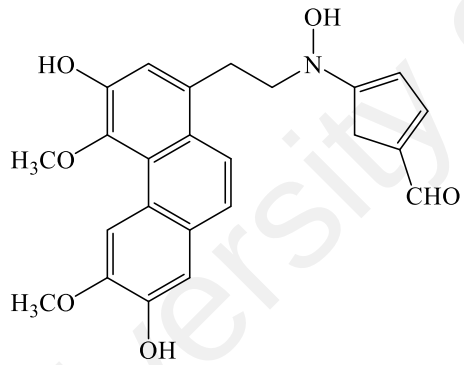

7

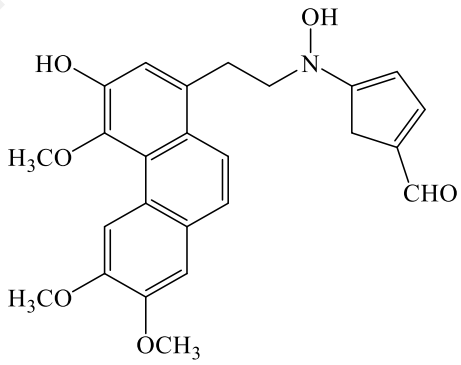

8

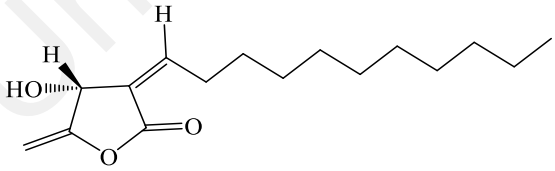

9

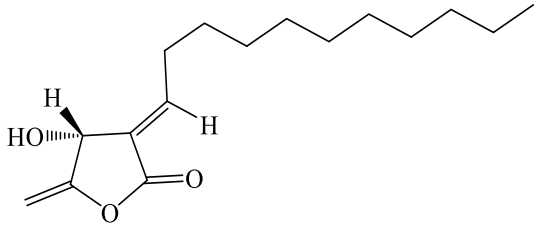

10

Figure 2.1: Chemical constituents isolated from *Beilschmiedia* species.

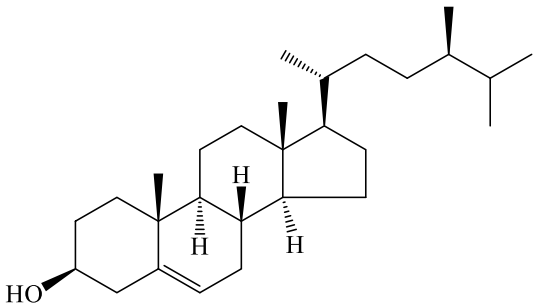

11

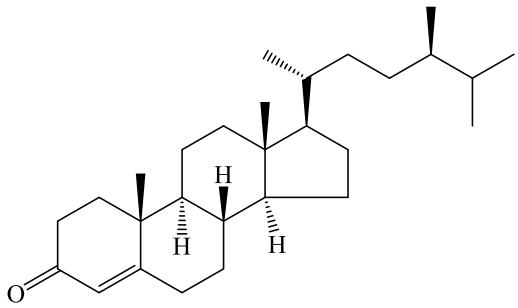

12

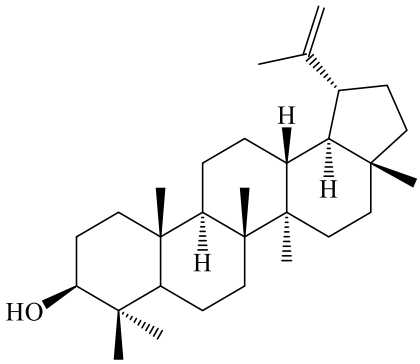

13

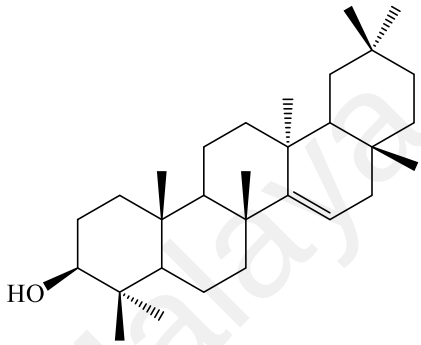

14

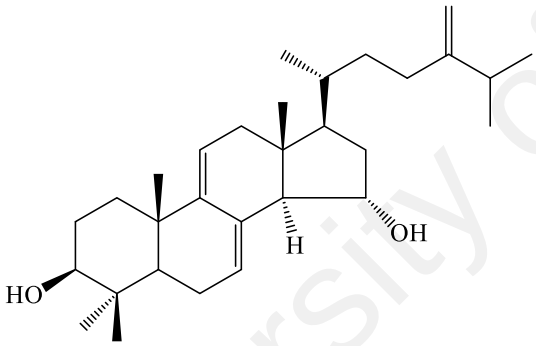

15

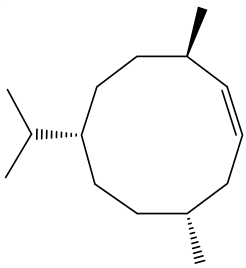

16

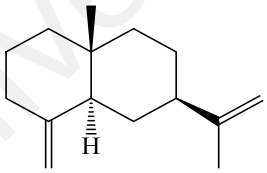

17

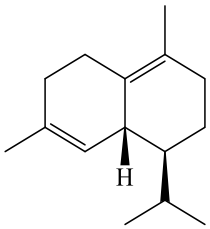

18

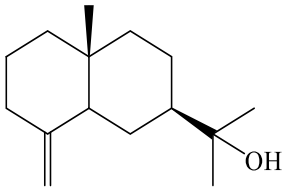

19

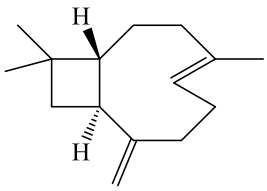

20

'Figure 2.1, continued'

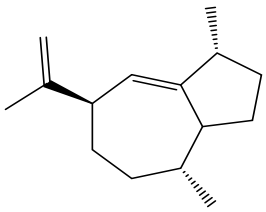

21

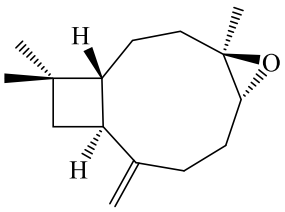

22

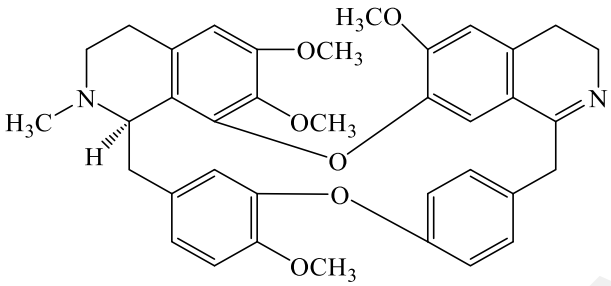

23

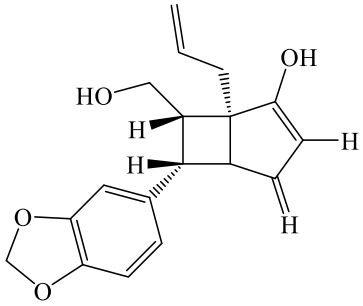

24

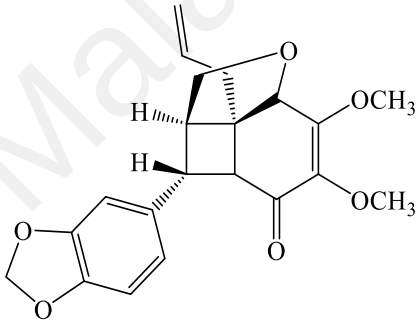

25

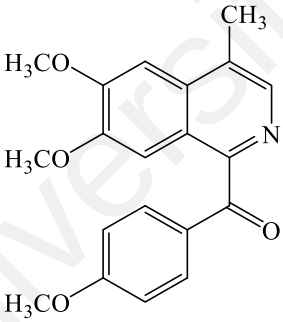

26

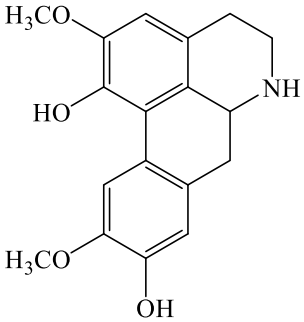

27

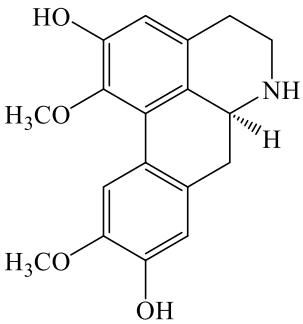

28

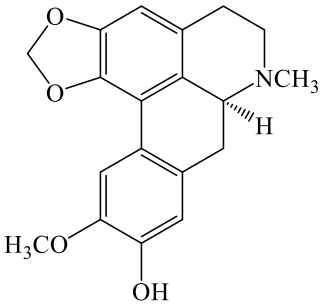

29

'Figure 2.1, continued'

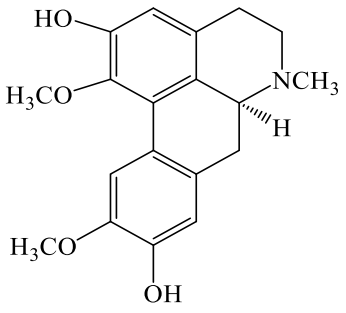

30

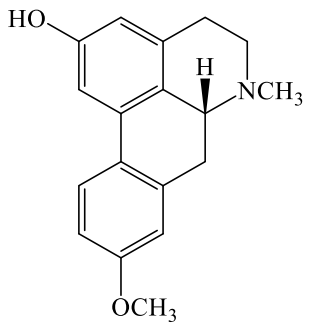

32

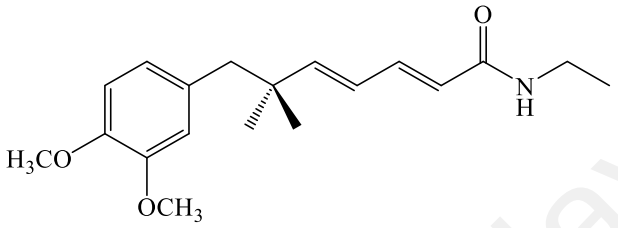

31

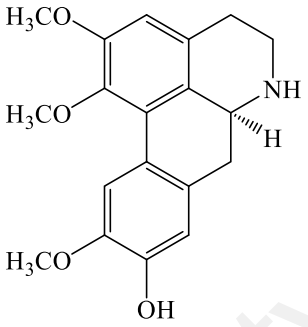

33

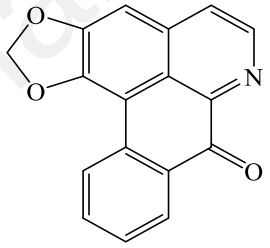

34

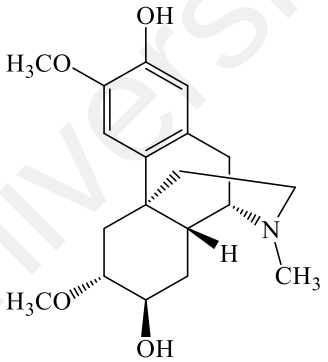

35

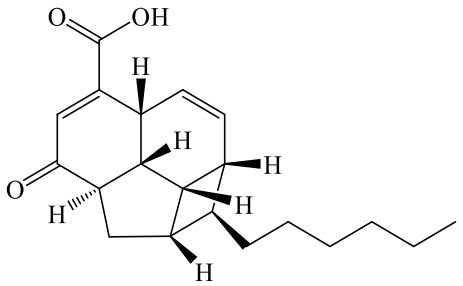

36

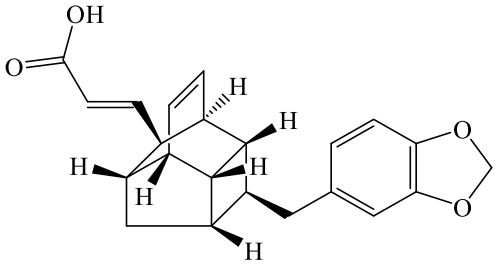

37

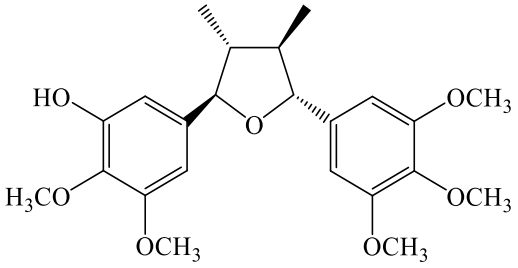

38

'Figure 2.1, continued'

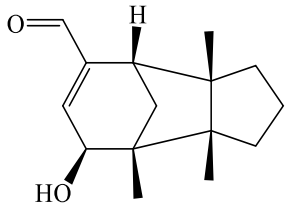

39

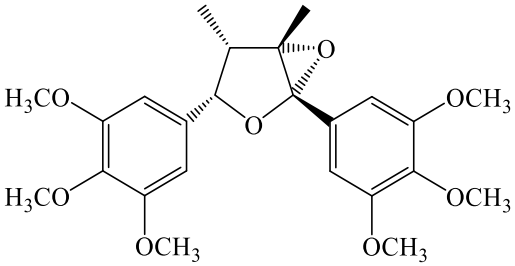

40

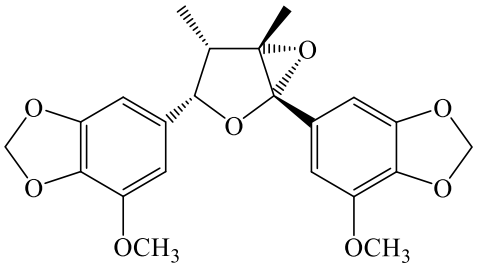

41

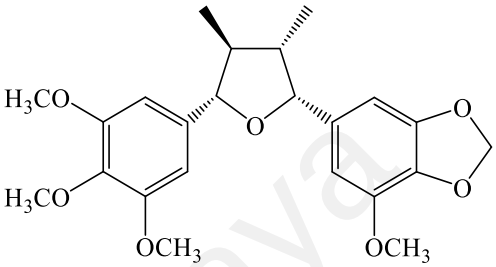

42

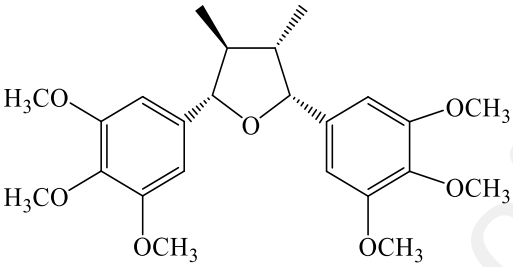

43

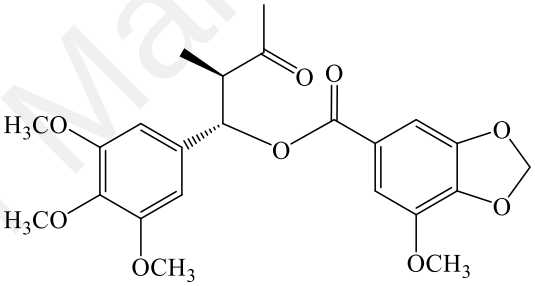

44

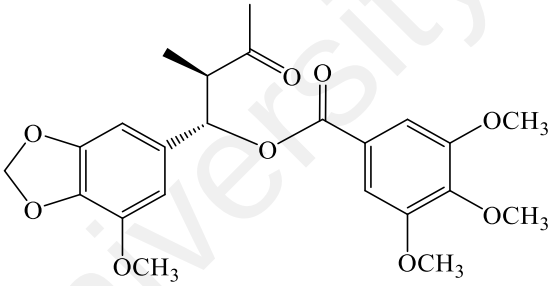

45

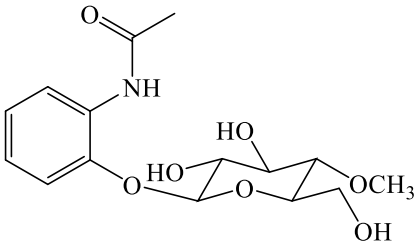

46

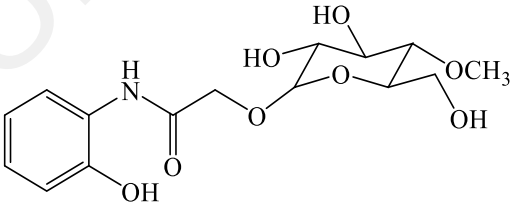

47

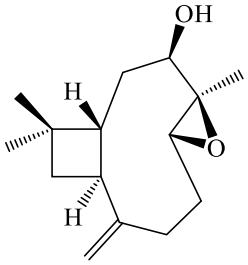

49

'Figure 2.1, continued'

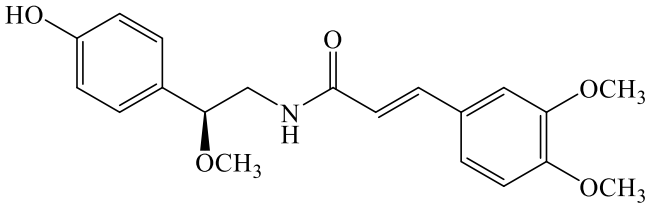

48

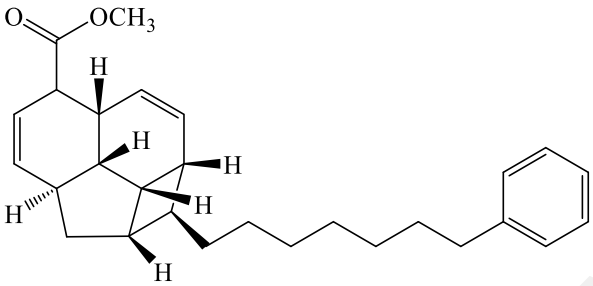

50

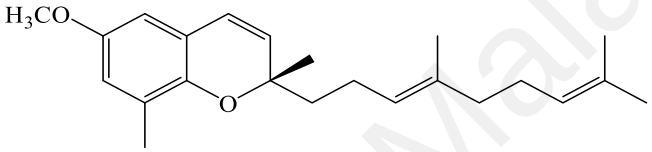

51

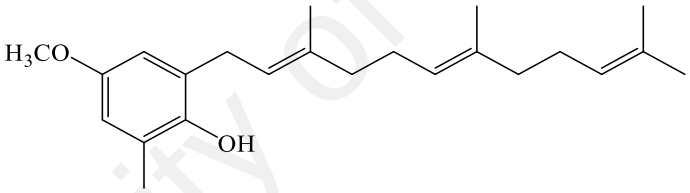

52

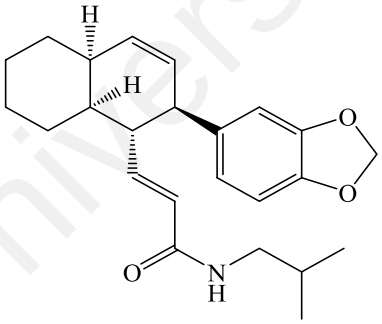

53

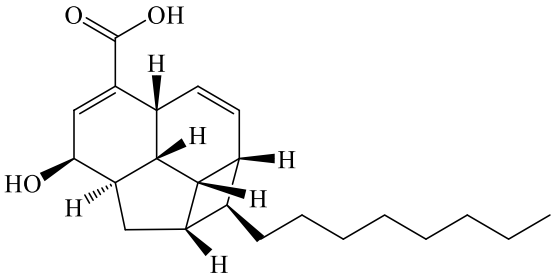

54

'Figure 2.1, continued'

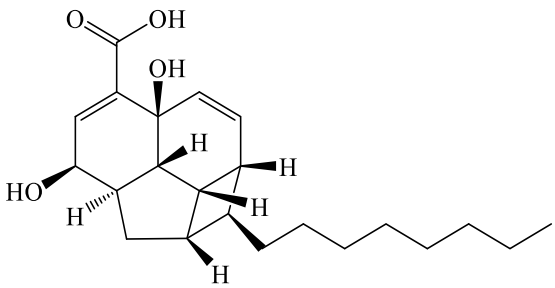

55

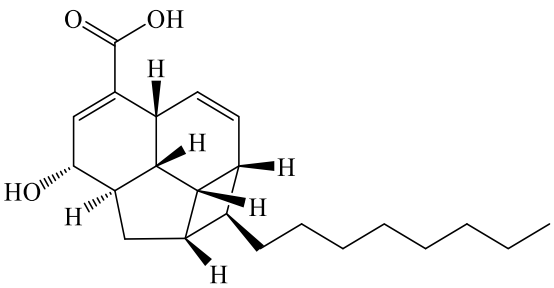

56

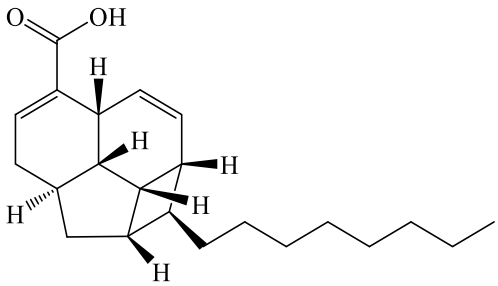

57

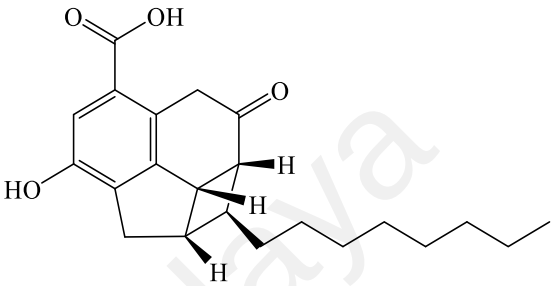

58

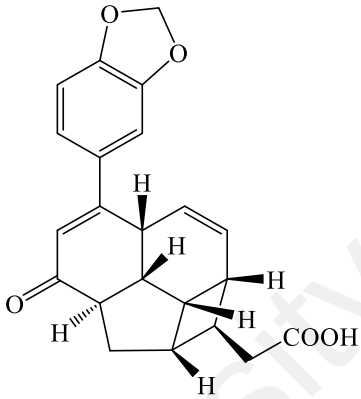

59

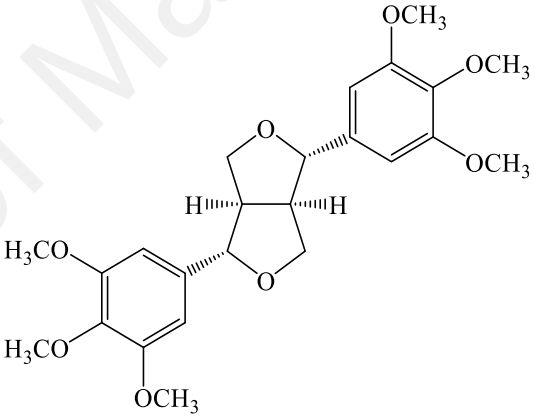

60

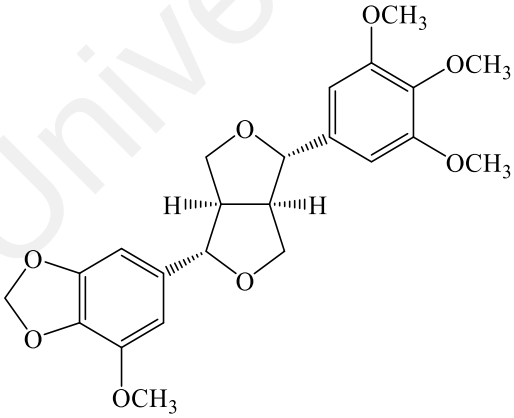

61

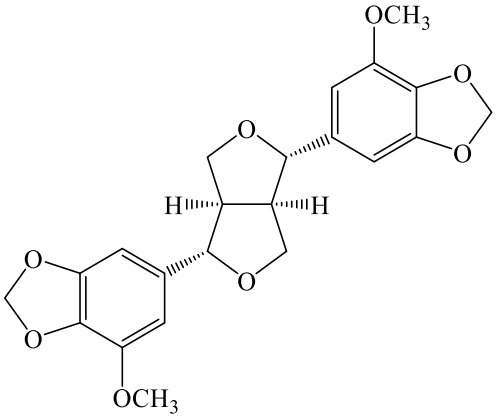

62

'Figure 2.1, continued'

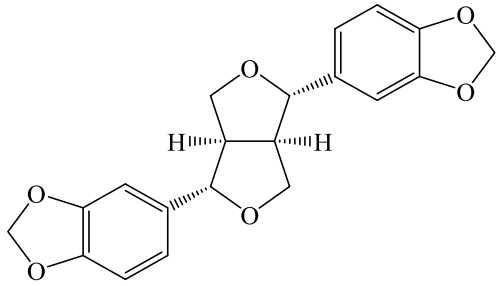

63

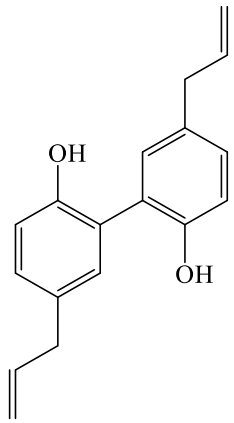

64

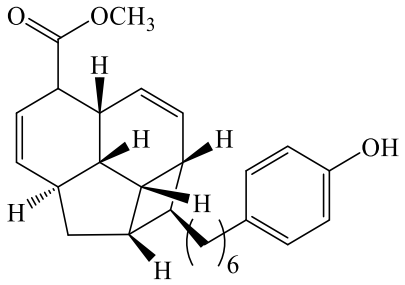

65

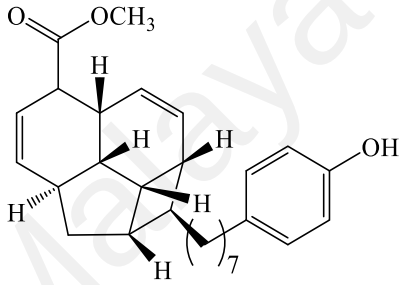

66

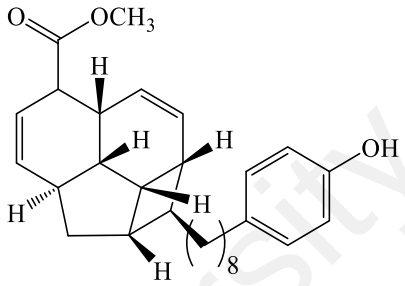

67

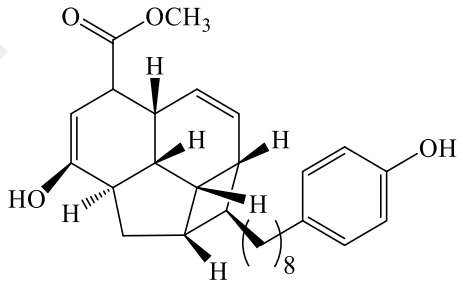

68

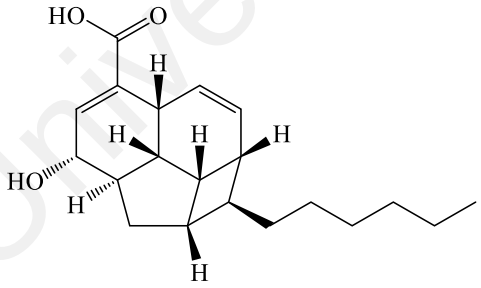

69

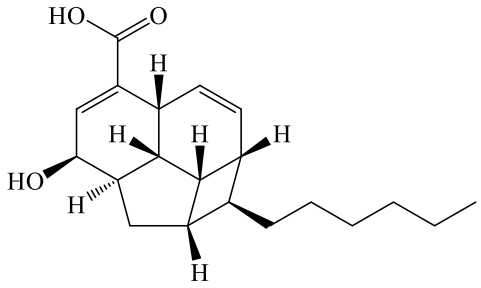

70

'Figure 2.1, continued'

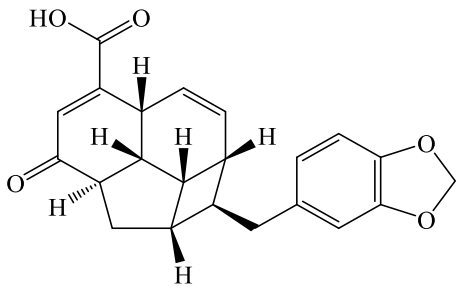

71

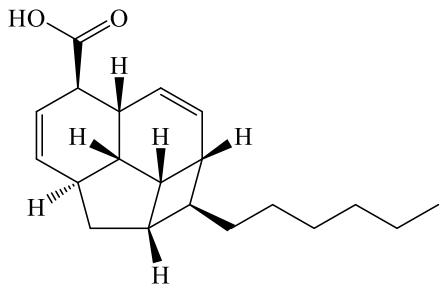

72

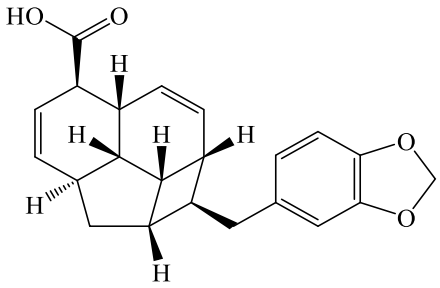

73

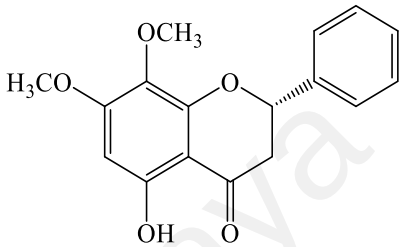

74

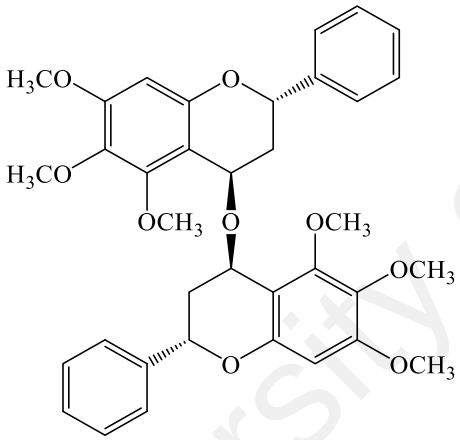

75

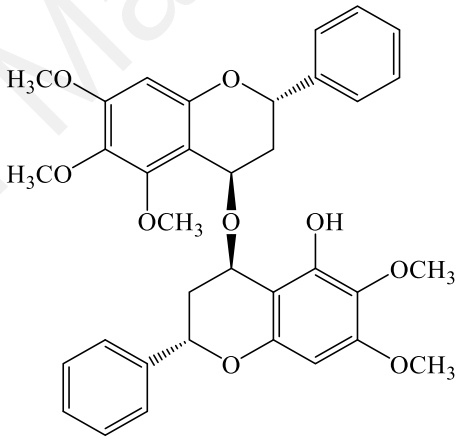

76

'Figure 2.1, continued'

2.4 Phytochemical studies from *Endiandra* species

Among 125 *Endiandra* species found throughout the tropical regions, only eight species of *Endiandra; E. kingiana, E. anthropophagorum, E. oligandra, E. introrsa, E. jonesii, E. monothyra, E. baiilonii, E. xanthocarpa* have been study for their phytochemicals (Bandaranayake et al., 1981; Banfield et al., 1994; Rohan A. Davis et al., 2007; Ndjakou Lenta et al., 2015). Interestingly, these plants have been reported to consist of endiandric acids derivatives which has an unprecedented pentacyclic carbon skeleton described for the first time in higher plants (Leverrier et al., 2011). These plants are also reported to contain lignans, neolignans and sesquiterpenes (Ndjakou Lenta et al., 2015).

Previous studies on *E. kingiana* studied by Azmi's group have led isolation series of endiandric acid analogues named kingianic acid A **77**, kingianic acid B **78**, kingianic acid C **79**, kingianic acid D **80**, kingianic acid E **81**, kingianic acid F **82**, kingianic acid G **83**, kingianic acid H **84** and kingianic acid I **85**. These compounds were screened for Bcl-xL and Mcl-1 binding affinities and cytotoxic activity on various cancer cell lines. Kingianic acid E **81** showed moderate cytotoxic activity against human colorectal adeno-carcinoma (HT-29) and lung adenocarcinoma epithelial (A549) cell lines, with IC_{50} of 15.36 ± 0.19 μM and 17.10 ± 0.11 μM, respectively (Azmi et al., 2014).

The other chemical constituents found in *Endiandra* species and their bioactivities are shown in Table 2.3 below. Only cytotoxic activity and antiapoptotic have been reported throughout centuries. Therefore, it is important to further explore their pharmacological activities due to their very interesting structures. As for medicinal values of the *Endiandra* species, to author knowledge there is no information available to date.

Table 2.3: Chemical constituents isolated from *Endiandra* species and their biological activities.

Species and site of collection	Chemical constituents isolated	Type of compounds	Biological activities
E. kingiana (Bark); Malaysia	Kingianic acid A **77** Kingianic acid B **78** Kingianic acid C **79** Kingianic acid D **80** Kingianic acid E **81** Kingianic acid F **82** Kingianic acid G **83** Kingianic acid H **84** Kingianic acid I **85**	Endiandric acids	These compounds were screened for Bcl-xL and Mcl-1 binding affinities and cytotoxic activity on various cancer cell lines. Kingianic acid E **81** showed moderate cytotoxic activity against human colorectal adeno-carcinoma (HT-29) and lung adenocarcinoma epithelial (A549) cell lines, with IC_{50} of 15.36 ± 0.19 µM and 17.10 ± 0.11 µM, respectively (Azmi et al., 2014).
E. kingiana (bark); Malaysia	Kingianin O **86** Kingianin P **87** Kingianin Q **88**	Endiandric acids	These compounds were screened for Mcl-1 binding affinities. All compounds (**86**, **87**, and **88**) exhibited weak binding affinity for the anti-apoptotic protein Mcl-1 with K*i* values of > 33, 30 and > 33 µM, respectively (Azmi et al., 2016).

'Table 2.3, continued'

Species and site of collection	Chemical constituents isolated	Type of compounds	Biological activities
E. anthropophagorum (bark); Australia	Endiandrin A **89** Endiandrin B **90** (-)-Dihydroguaiaretic acid **91**	Lignan	All compounds were evaluated for their cytotoxicity towards human lung carcinoma cells (A549). (-)-Dihydroguaiaretic acid **91** was found to be the most potent cytotoxin with an IC_{50} value of 7.49 µM (Rohan A Davis et al., 2009).
E. oligandra (bark); Australia	Endiandric acid A **92**	Endiandric acids	No biological activity reported (Nkeng-Efouet & Rao, 2012).
E. introrsa (leaves); Australia	Methylenedioxyendiandric acid A **93** Endiandric acid B **94**		
E. jonesii (bark and leaves): Australia	Endiandric acid C **95**		
E. monothyra (Bark): Australia	Magnolol **64**	Neolignan	No biological activity reported (Banfield et al., 1994).
E. baillonii (Bark): Australia	(-)-ishwarane **96** (-)-α-copaene **97**	Sesquiterpenes	
E. xanthocarpa (Bark); Australia	(+)-sesamin **63**	Lignan	

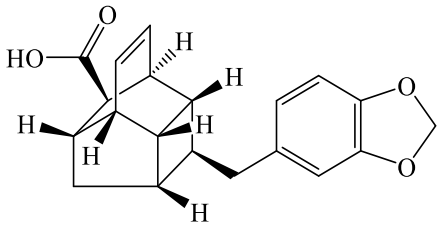

77

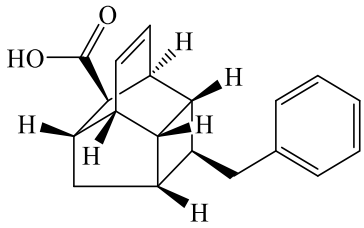

78

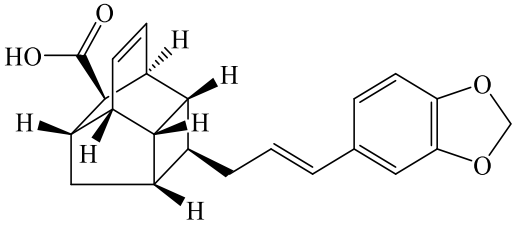

79

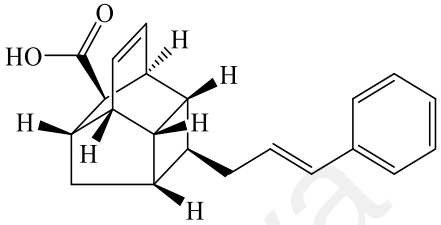

80

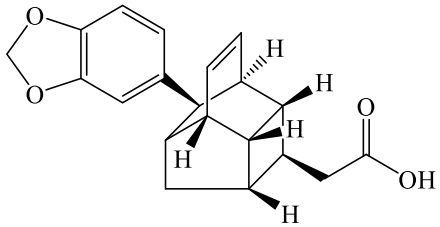

81

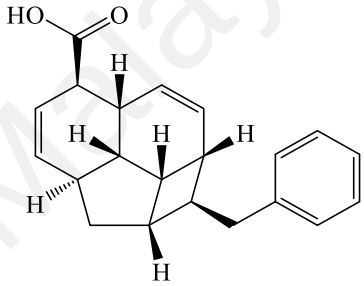

82

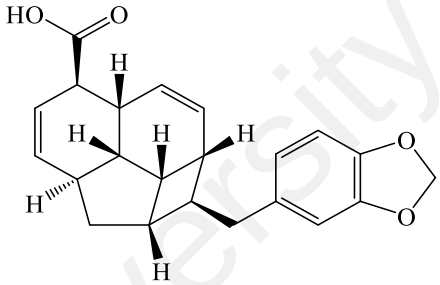

83

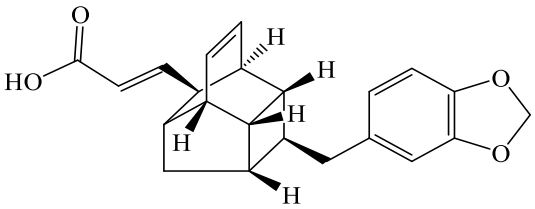

84

Figure 2.2: Chemical constituents isolated from *Endiandra* species.

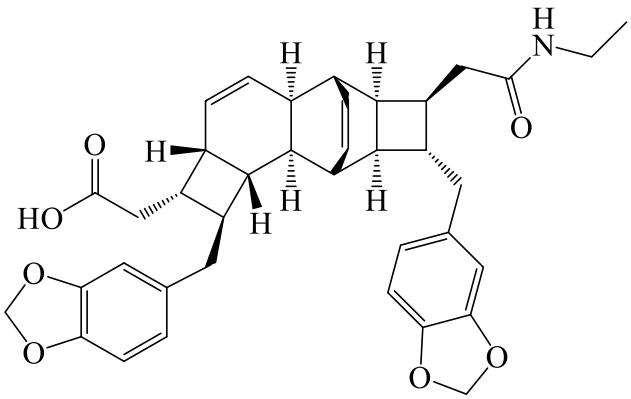

86

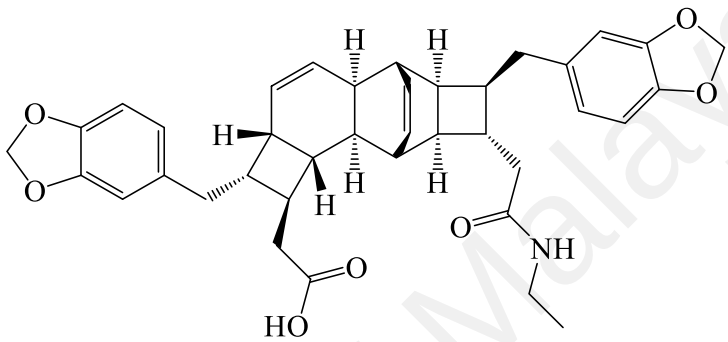

87

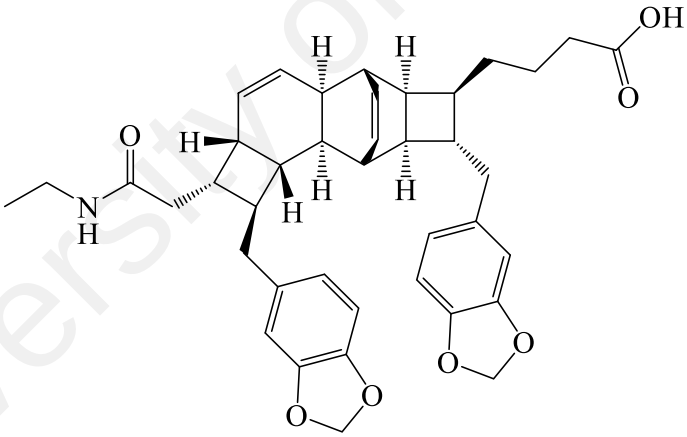

88

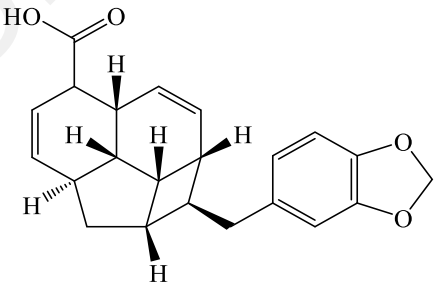

85

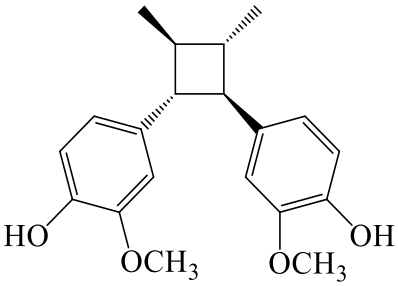

89

'Figure 2.2, continued'

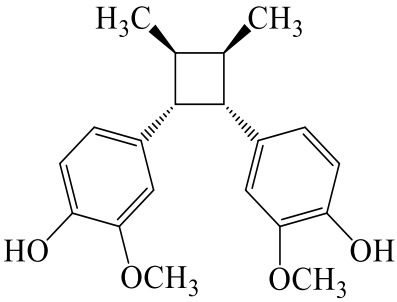

90

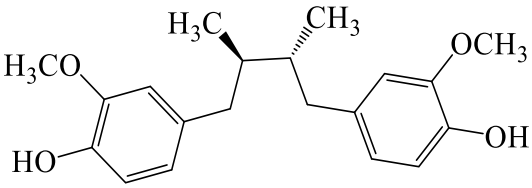

91

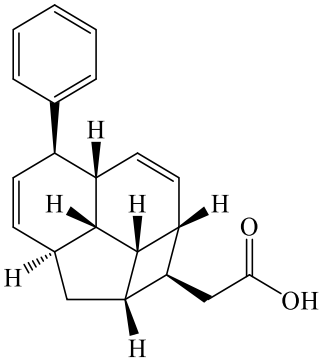

92

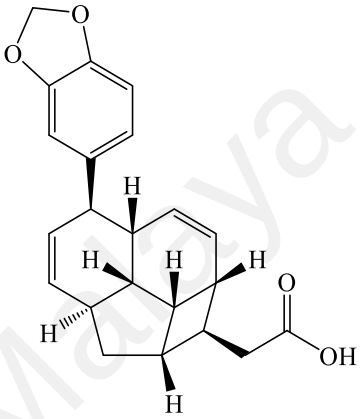

93

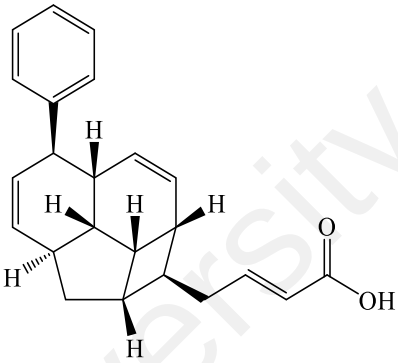

94

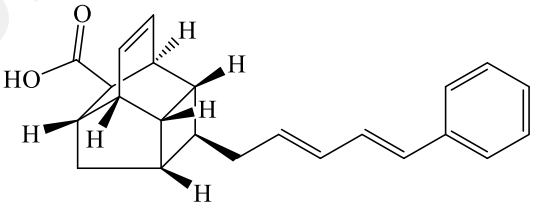

95

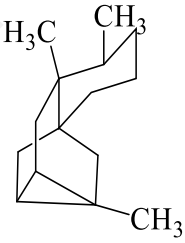

96

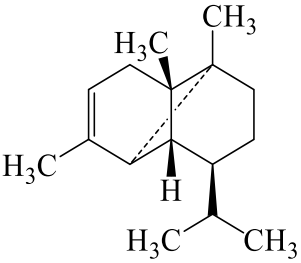

97

'Figure 2.2, continued'

2.5 Comparison between the secondary metabolites isolated from the *B. glabra* and *E. kingiana* in the current and previous investigations

Previous investigations of *B. glabra*, have led to the isolation of the diverse types of chemical constituents such as alkaloids, butanolides, steroids, sesquiterpenes, and triterpenes (Salleh, Ahmada, et al., 2015; Salleh, Ahmad, Khong, & Zulkifli, 2016; Salleh, Ahmad, Khong, Zulkifli, et al., 2016). Meanwhile for *E. kingiana*, these plants are reported to contain endiandric acid derivatives only (Leverrier et al., 2010; Leverrier et al., 2011; Azmi et al., 2014; Azmi et al., 2016).

Even though there are previous investigations of *B. glabra* and *E. kingiana*, the reports on the biological activities are still limited. Preliminary evaluation of *B. glabra* indicated the crude extracts of this species (with the number of active compounds isolated from them are still limited) exhibit antifungal, antibacterial, antimicrobial, antioxidant, and anti-inflammatory; meanwhile, as for *E. kingiana*, only cytotoxic activity and antiapoptotic have been reported to date. Although being limited, there are reports on the biological activities of *B. glabra* and *E. kingiana*, however none are on the dengue antiviral activity. Generally, many plants worldwide show strong inhibitory effect on the dengue antiviral activity.

To date, 32 varied species have been found having the potential to treat dengue; among those species are *Cryptocarya chartacea* (Lauraceae), *Tephrorosia madrensis* (Fabaceae), *Boesenbergia rotunda* (Zingiberaceae) and *Zostera marina* (Zosteraceae). Since the secondary metabolites of *C. chartacea*, which is a plant from the Lauraceae family is active towards dengue antiviral activity with IC_{50} value of 1.8 to 4.2 μM (Hassandarvish et al., 2016), therefore there is a strong possibility that the secondary metabolites of *B. glabra* and *E. kingiana* (the plants in the current study, which are in same family as *C. chartacea*) also show significant values against dengue antiviral activity. Hence, the phytochemical investigation in this research towards *B. glabra* and

E. kingiana was equally important in producing interesting compounds, structurally and biologically.

2.6 Phytochemical composition

Among the metabolites found in *B. glabra* and *E. kingiana*, the most commons are phenylpropanoids, lignans and neolignans, flavonoids and triterpenes. The biosynthesis of these common metabolites is discussed in following subchapter.

2.6.1 Phenylpropanoids

Phenolic compounds are a various group of aromatic chemical compounds which containing at least one benzene ring; commonly with hydroxyl groups. Many herbal phenolic compounds have three carbon side chains and are called phenylpropanoid. Some studies have classified the phenolic compounds in plants into several families as illustrated in Table 2.4 (R. Huang et al., 1999).

2.6.1.1 General biosynthesis of phenylpropanoids

The general phenylpropanoid metabolism generates an enormous array of secondary metabolites based on the few intermediates of the shikimate pathway as the core unit. The resulting hydroxycinnamic acids and esters are amplified in several cascades by a combination of reductases, oxygenases, and transferases to result in an organ and developmentally specific pattern of metabolites, characteristic for each plant species (Vogt, 2010). The various characteristic of the general phenylpropanoid pathway not only produce common lignin or flavonoid biosynthesis, but it also feeds into a variety of other aromatic metabolites such as coumarins, phenyl volatiles and hydrolyzable tannins (Vogt, 2010).

Table 2.4: Classification of some phenolic constituents in plants.

Number of carbons	Skeleton	Phenol Families
C_6	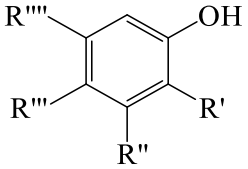	Simple phenol
C_6-C_1	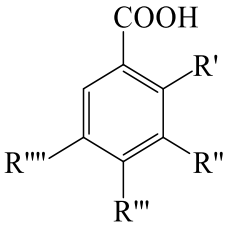	Phenolic acid and derivatives
C_6-C_2	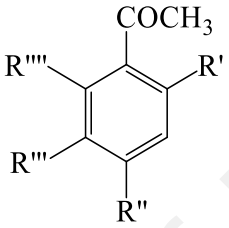	Acetophenones and phenylacetic acids
C_6-C_3	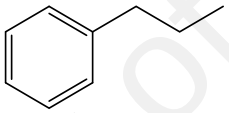	Phenylpropanoids and derivatives
C_{15}	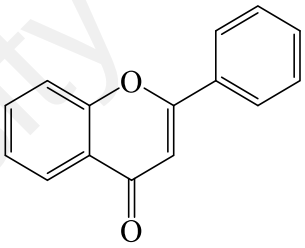	Flavones
C_{15}	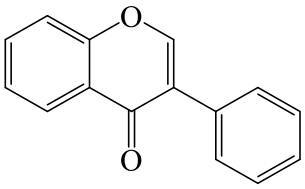	Isoflavones and isoflavonoids
C_{15}	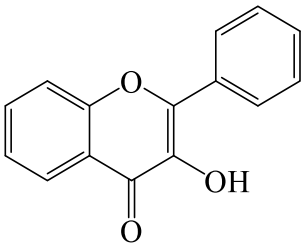	Flavonols and derivatives

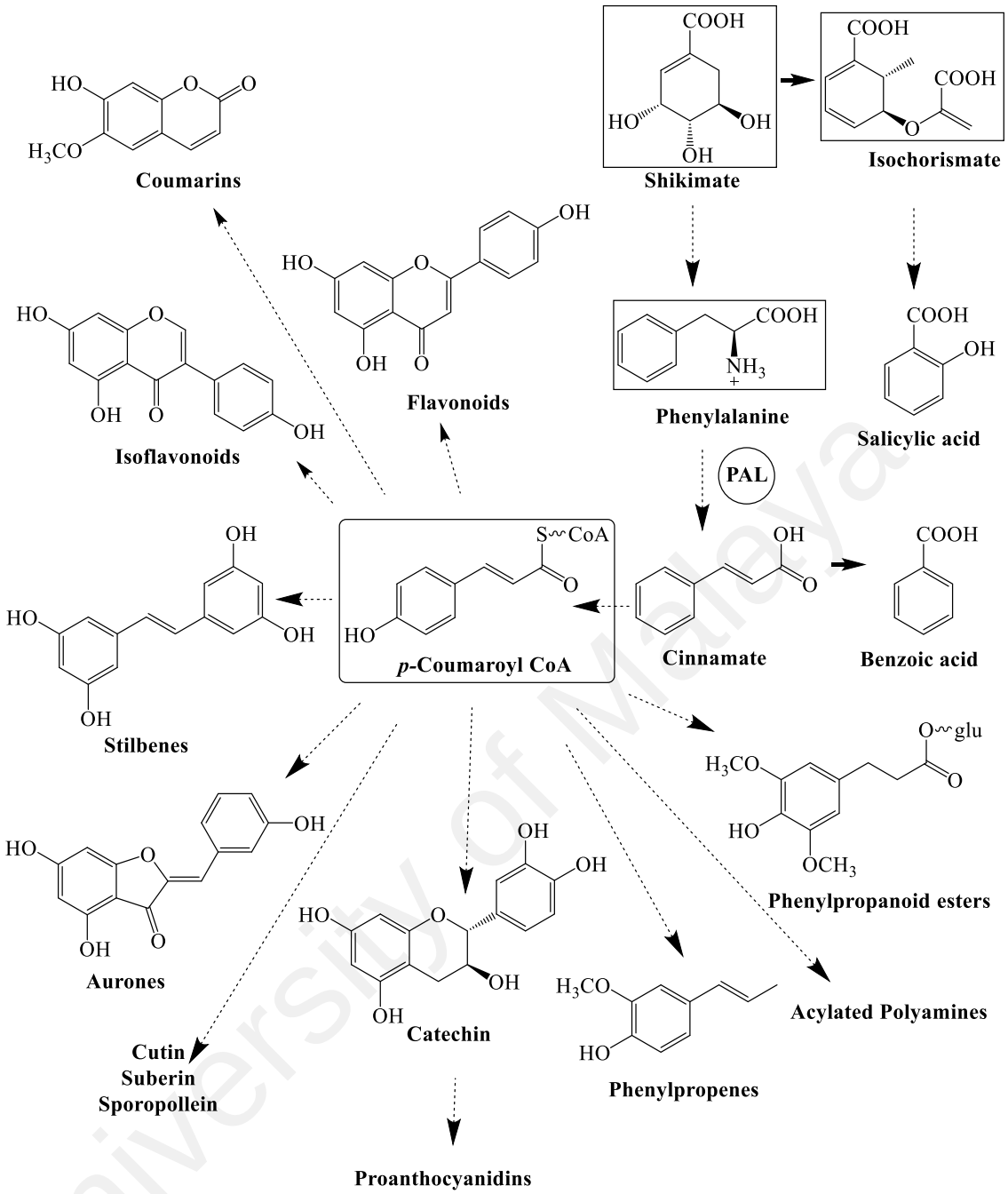

Scheme 2.1: Diversification of phenylpropanoids on the general phenylpropanoids pathway.
*The metabolites of the shikimate pathway and the central metabolite, (*p*-Coumaroyl CoA) are in the box
*PAL- phenylalanine ammonia lyase
Source: Vogt, T. (2010). Phenylpropanoid Biosynthesis. Molecular Plant, 3(1), 2-20

2.6.2 Lignans and neolignans

Lignans and neolignans are formed by enantioselective dimerization of two coniferyl alcohol **107** units which originate from cinnamic acid **102** which are related

biochemically to the metabolism of phenylalanine. The general biosynthesis of coniferyl alcohol **107** are shown in the Scheme 2.7. Lignans and neolignans are a large group of natural products characterized by the coupling of two C_6-C_3 units (**a**). When the two C_6-C_3 units are linked by a bond between positions 8 and 8′ (β, β′-bond) the compound is referred to and named as a lignan (**b**). In the absence of the C-8 to C-8′ bond, and where the two C_6-C_3 units are linked by other bond (e.g., 3-3′ instead of 8-8′) it is referred to and named as a neolignan (c) (Figure 2.3) (Teponno et al., 2016).

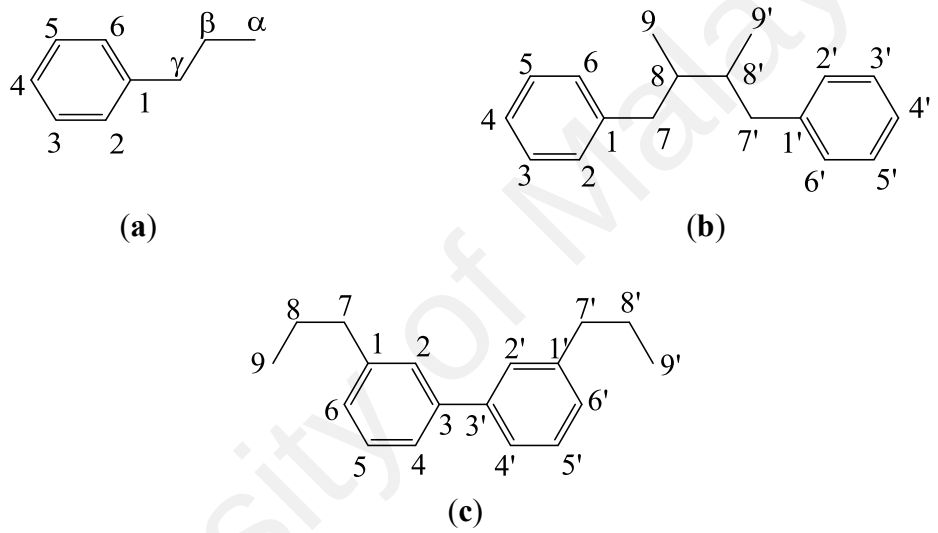

Figure 2.3: Skeletons of lignan and neolignane.

Lignans are classified into eight groups based on their structural patterns, including their carbon skeletons, the way in which oxygen is incorporated into the skeletons, and the cyclization pattern. These are arylnapthalene, aryltetralin, dibenzocyclooctadiene, dibenzylbutane, dibenzylbutyrolactol, dibenzylbutyrolactone, furan, and furofuran (Figure 2.4). Neolignans consist of 15 subtypes designated as NL1 to NL15 and no special names have been assigned to them (Figure 2.5) (Teponno et al., 2016).

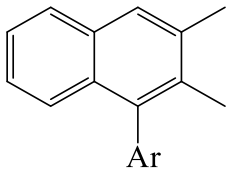

Arylnaphthalene

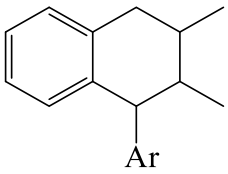

Aryltetralin

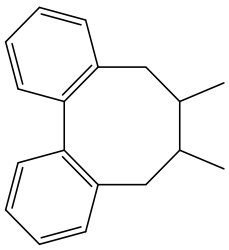

Dibenzocyclooctadiene

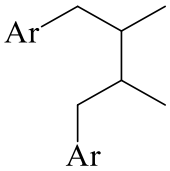

Dibenzylbutane

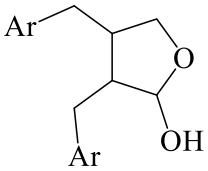

Dibenzylbutyrolactol

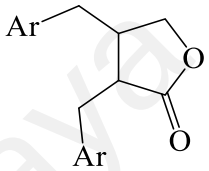

Dibenzylbutyrolactone

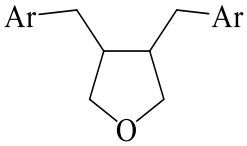

3,4-dibenzyltetrahydrofuran

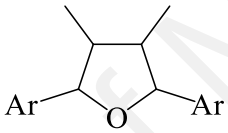

2, 5-diaryltetrahydrofuran

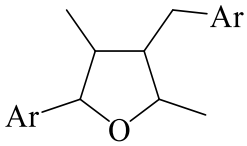

2-aryl-4-benzyltetrahydrofuran

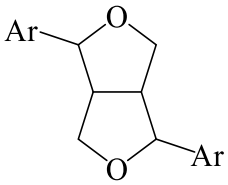

Furofuran

Figure 2.4: Subtypes of classical lignans (Ar = aryl).

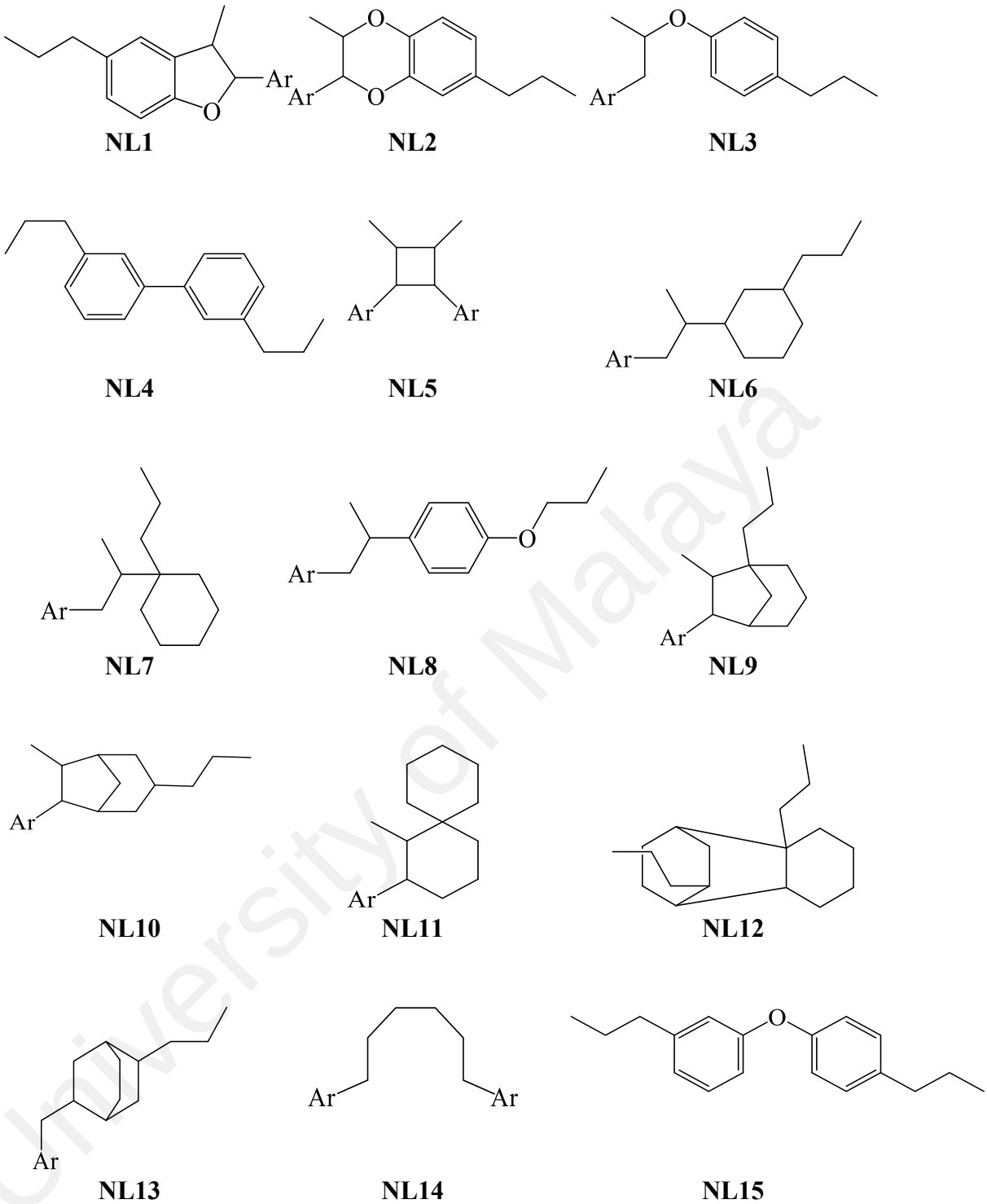

Figure 2.5: Subtypes of neolignans (NL).

2.6.2.1 General biosynthesis of lignans and neolignans

Coniferyl alcohol **107** which originates from cinnamic acid **102** is biochemically related to the metabolism of phenylalanine. Chorismic acid **98** is transformed into prephenic acid **99** *via* a Claisen rearrangement, which transfers the phosphoenolpyruvate derived side-chain so that it becomes directly bonded to the carbocycle, and thus builds up the basic carbon skeleton of phenylalanine **101**. L-phenylalanine was formed by decarboxylation aromatization of prephenic acid **99** yields phenylpyruvic acid, and pyridoxal phosphate-dependent transaminaton. Deamination of phenylalanine **101** initiated the biosynthesis of coniferyl alcohol **107** by phenylalanine ammonialyase to form cinnamic acid **102**, which is then hydroxylated by a P450 enzyme, cinnamate 4-hydroxylase, to form *p*-coumaric acid **103**. Coniferyl alcohol **107** is derived from the reduction of coumaric acid *via* coenzyme A ester to an aldehyde which is further reduced in the presence of a NADPH molecule. Formation of the coenzyme A ester facilitates the first reduction step by introducing a better leaving group ($CoAS^-$) for the NADPH-dependent reaction (Scheme 2.2) (Teponno et al., 2016).

The general biosynthesis of lignans with 9-(9′)-oxygen is very well studied that is clearly revealed by some important results obtained in last couple of years. This type of lignan is formed by enantioselective dimerization of two coniferyl alcohol **107** units with the aid of a dirigent protein (DIR) to give rise to pinoresinol **108** (furofuran). Pinoresinol **108** is then reduced to secoisolariciresinol **112** (dibenzybutane) by pinoresinol/lariciresinol reductase (PLR), *via* lariciresinol **110** (furan), which is in turn oxidized to afford matairesinol **114** (dibenzylbutyrolactone) by secoisolariciresinol dehydrogenase (SIRD) (Scheme 2.3). The conversion from coniferyl alcohol **107** to matairesinol has been demonstrated in various plant species, which strongly suggest that this is the general biosynthetic pathway of lignans (H. Satake et al., 2013; Honoo Satake et al., 2015). Pinoresinol **108** also undergoes glucosylation by a putative pinoresinol

glucosyltranferase (PNGT). Such glycosylation is highly likely not only to suppress the chemical reactivity of a phenolic hydroxyl group of pinoresinol but also to potentiate high water solubility of pinoresinol aglycone, resulting in large and stable amounts of pinoresinol (Teponno et al., 2016). Similar to pinoresinol, lariciresinol **110** and secoisolaiciresinol **112** can be glycosyltransferase (SIRGT), respectively. Piperitol **115** is metabolized from pinoresinol **108**, followed by further conversion into (+)-sesamin **63** by piperitol/sesamin synthase (PSS), a cytochrome P450 family enzyme, CYP81Q1, which is responsible for the formation of two methylenedioxy bridges (Scheme 2.3).

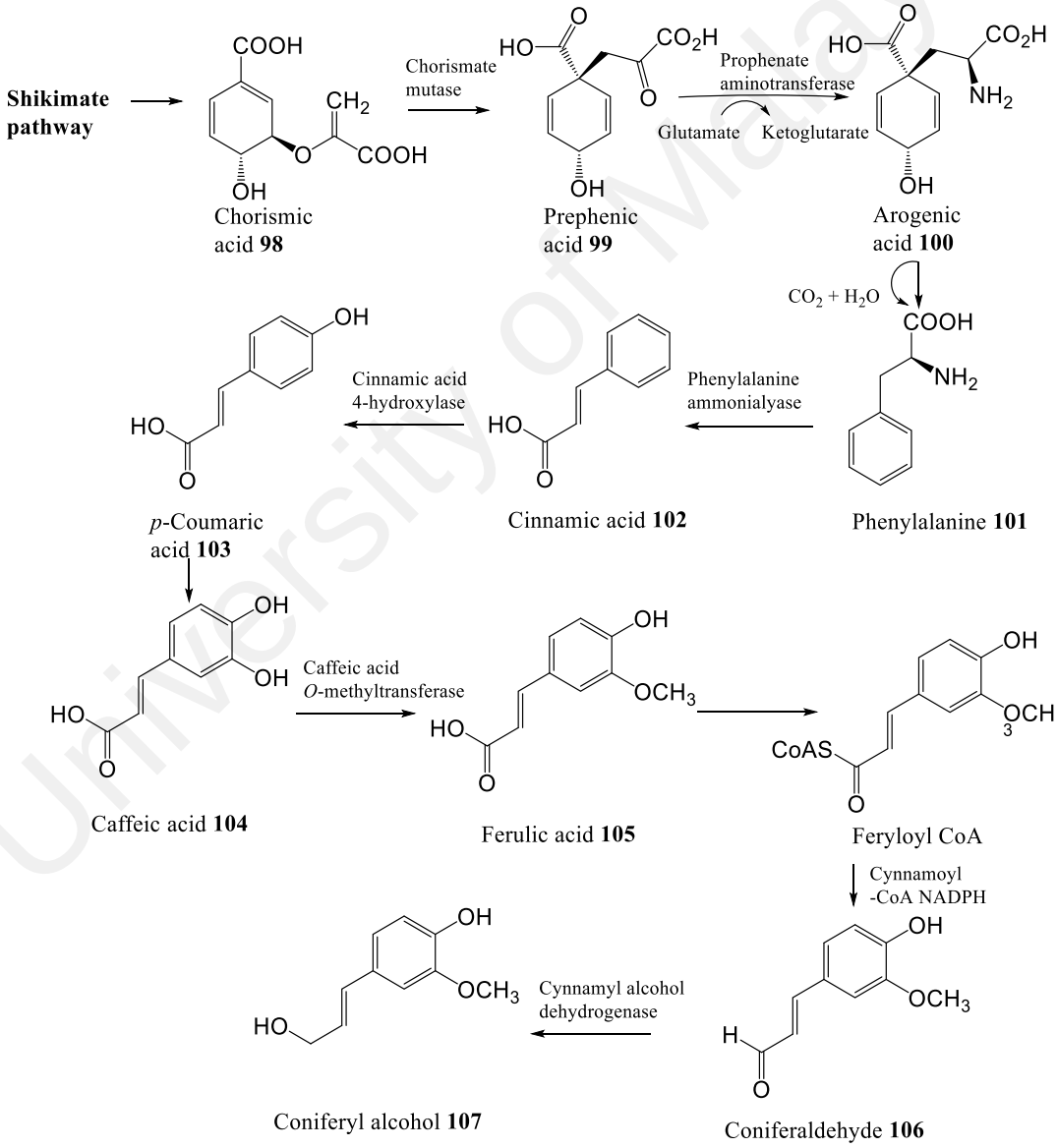

Scheme 2.2: Biogenesis of coniferyl alcohol.

Source: Teponno, R. B., Kusari, S., and Spiteller, M. (2016). Recent advances in research on lignans and neolignans. Natural Product Reports, 33(9), 1044-1092

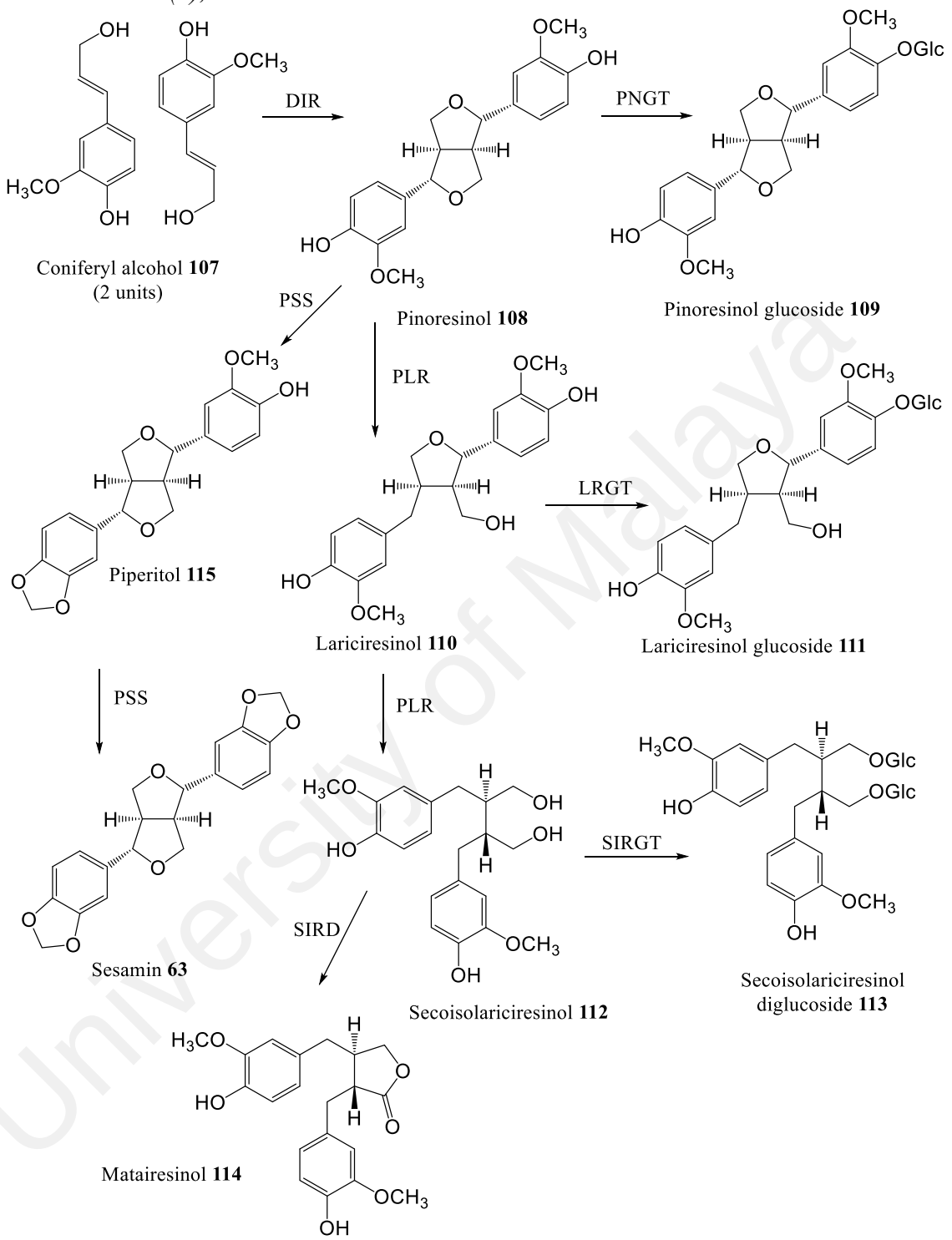

Scheme 2.3: General biosynthetic pathways of major lignans.
*DIR-Dirigent protein *SIRD-Secoisolariciresinol dehydrogenase
*SIRGT-Glycosyltransferase *PLR-Pinoresinol/lariciresinol reductase
*PSS-Piperitol/sesamin synthase *PNGT-Pinoresinol glucosyltranferase
*LRGT-Lariciresinol glucosyltranferase
Source: Teponno, R. B., Kusari, S., and Spiteller, M. (2016). Recent advances in research on lignans and neolignans. Natural Product Reports, 33(9), 1044-1092

2.6.3 Flavonoids

Flavonoids are a group of heterocyclic organic compounds present naturally in plants. The terms "flavonoids" is used to embrace all compounds having their structures based upon fifteen-carbon skeleton arranged in C_6-C_3-C_6 fashion. The two C_6 units from aromatic nuclei and the C_3 unit links them either forming an open chain connection (**a**) or it may be fused with 'A' ring thereby giving rise to another heterocyclic ring often called 'C' ring (**b**) (Figure 2.6) (Harborne, 2007).

Figure 2.6: Subtypes of neolignans (NL).

There are 14 classes of flavonoids based on the difference of the position of substituent such as flavanone (**c**), flavone (**d**), isoflavone (**e**). dihydroflavonol (**f**), flavonol (**g**), and chalcone (**h**) (Figure 2.7) (Havsteen, 2002; Panche et al., 2016).

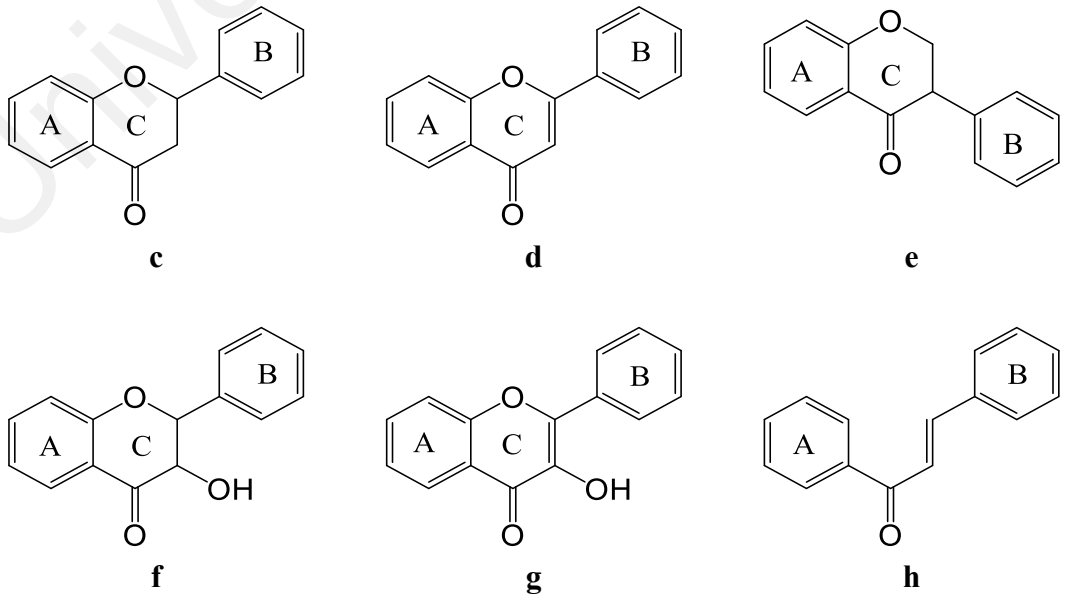

Figure 2.7: Class of flavonoids.

2.6.3.1 General biosynthesis of flavonoids

Structural diversion in the known type of flavonoids emanates principally due to variation in the oxidation level of C_3-portion of the molecule. The range of oxidation level extends from highly reduced catechin type to highly oxidized flavonol. All the flavonoid variants share a common biosynthethic pathway that incorporates the precursors from both "Shikimate" and "Acetate-Malonate" pathways, the first flavonoids being formed immediately following the confluence of the two pathways is the chalcone. All other variants are derived from this by a variety of routes (Scheme 2.4) (Harborne, 2007; Tuan et al., 2016).

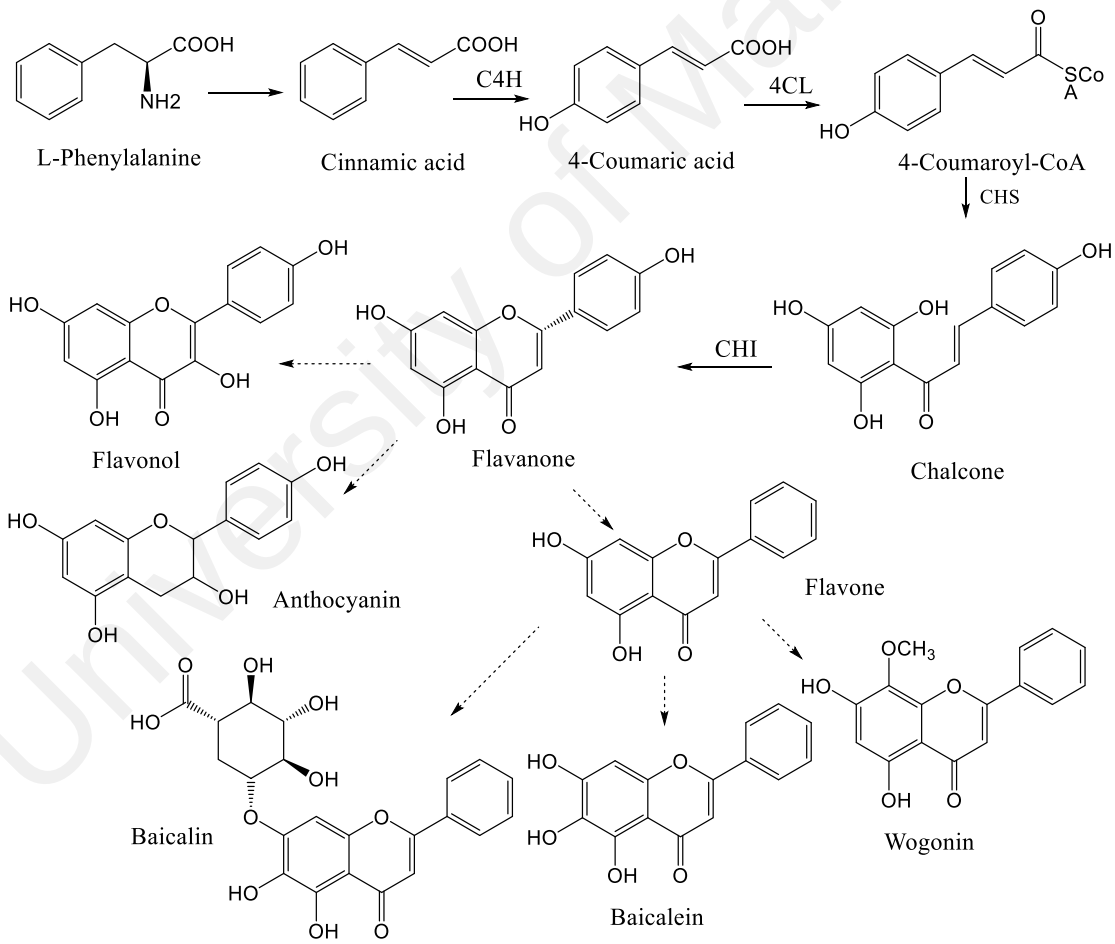

Scheme 2.4: General biosynthetic origin of flavonoids.
* CHI-chalcone-isomerase *C4H-cinnamate 4-hydroxylase
Source: Tuan, P. A., Kim, Y. S., Kim, Y., Thwe, A. A., Li, X., Park, C. H., Lee, S. Y., and Park, S. U. (2016). Molecular characterization of flavonoid biosynthetic genes and accumulation of baicalin, baicalein, and wogonin in plant and hairy root of Scutellaria lateriflora. Saudi Journal of Biological Sciences. 5(7), 70

2.6.4 Triterpenes

Triterpenes are terpenes consisting six isoprene units with the molecular formula of $C_{30}H_{48}$. Many triterpenes occur in their free form, while others occur as saponin or in special combined form. Triterpenoids are modified triterpenes, where methyl groups are moved or removed, or oxygen atoms added. It is generally made up of either tetracyclic (6-6-6-5 tetracycles) or pentacyclic (6-6-6-6-5 or 6-6-6-6-6 pentacycles) ring system with an alicyclic hydrocarbon as the C-17 side chain (R. Xu et al., 2004).

2.6.4.1 General biosynthesis of triterpenoids

Triterpenoids are formed by the cyclization of squalene 2,3-epoxide **116**. In triterpenoids biosynthesis, the squalene 2,3-epoxide will fold to form either mono-, di-, tri-, tetra-, penta-, or acyclic triterpenoid skeletons. In general, all squalene 2,3-epoxides are activated by cationic attack. A cascade of cation-olefin cyclization generate a cyclic carbocation, which then rearranges and cyclizes further (R. Xu et al., 2004).

The squalene 2,3-epoxide **116** was maintained in a *chair-boat-chair-boat* conformation **117**. The subsequence cyclization leads to a protostreyl cation **118**. Through a series of Wagner-Meerwein 1,2-shifts and the subsequent formation of a double bond, lanosterol **119** was created. Lanosterol is a typical animal triterpenoid from which all animal sterols are derived.

As for *chair-chair-chair-boat* conformation **120**, squalene 2,3-epoxide folded to form a dammarenyl cation **121** which then undergoes a series of Wagner Meerwein 1,2-hydride and methyl migrations, commonly known as backbone rearrangements to produce skeletal type such as dammaranes **122**. The triterpenoid skeletons cyclized via the *chair-boat-chair-boat* (CBCB) and *chair-chair-chair-boat* (CCCB) conformation respectively as shown in Scheme 2.5 below.

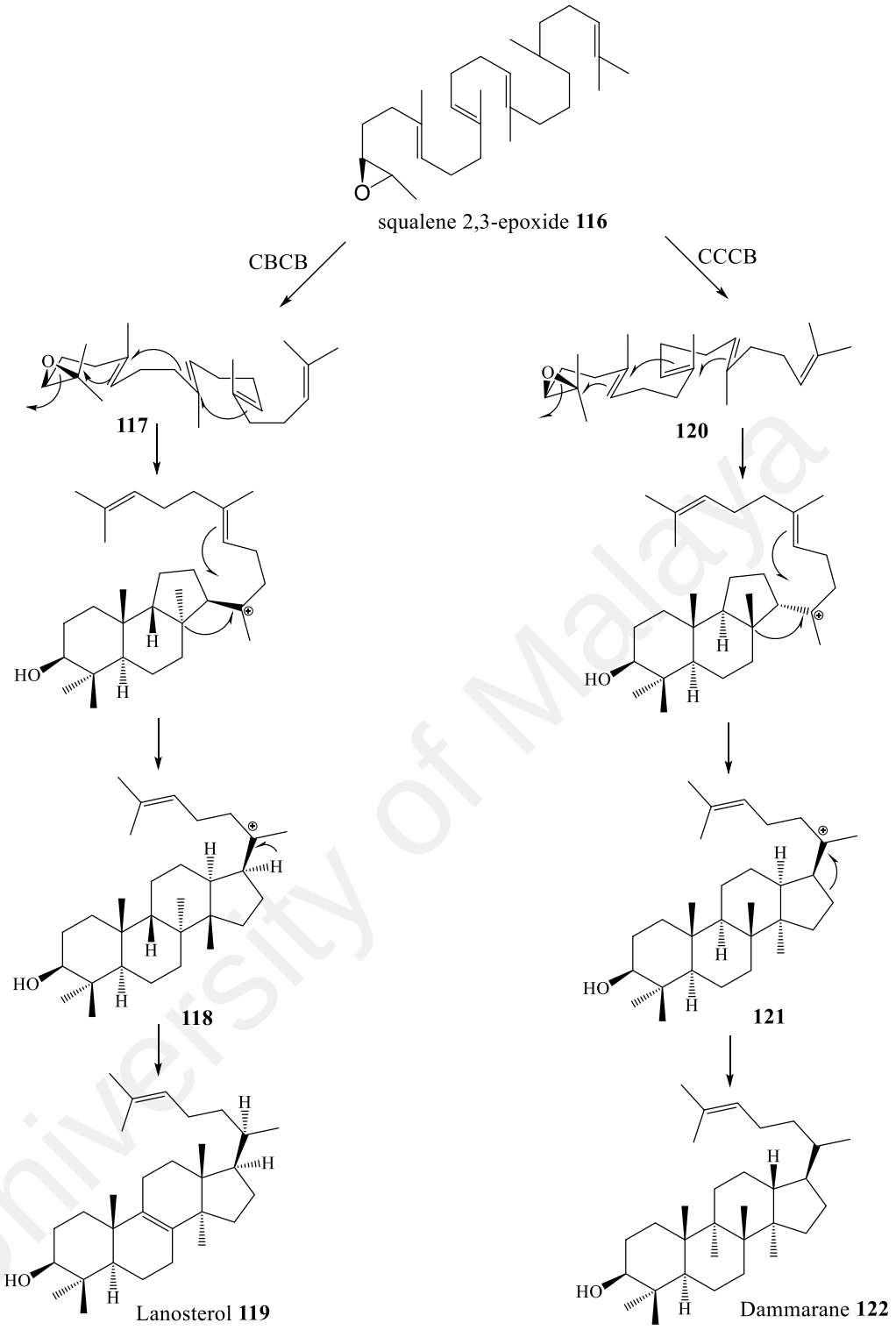

Scheme 2.5: Formation of sterols/triterpenoids through different type of cyclization. *Source: Xu, R., Fazio, G. C., and Matsuda, S. P. T. (2004). On the origins of triterpenoid skeletal diversity. Phytochemistry (Elsevier), 65(3), 261-291*

CHAPTER 3: EXPERIMENTAL

3.1 Plant material

The bark of *B. glabra* was collected at Sungai Tekam Reserve Forest, Jerantut, Pahang with a voucher specimen (KL4846). While the bark of and *E. kingiana* was collected from Kuala Lipis, Pahang with a voucher specimen (KL4828). The plant specimens were identified by Mr. Teo Leong Eng and Mr. Din Mat Nor of the phytochemical group and have been deposited at the Herbarium of the Department of Chemistry, University of Malaya, Kuala Lumpur, Malaysia.

3.2 Chemicals and reagents

1. *Hexane
2. *Dichloromethane
3. *Methanol
4. Methanol AR grade
5. Methanol spectroscopy grade
6. Chloroform, $CDCl_3$ with 99.8 atom % D
7. Pyridine, C_5D_5N with 99.8 atom % D
8. Silica Gel 60 for column chromatography, (0.040-0.063 mm)
9. TLC Aluminium Sheets, Silica Gel 60 F_{254}, 20 cm x 20 cm
10. Silica Gel 60 F_{254}, pre-coated glass plates 20 cm x 20 cm x 0.5 mm
11. Celite
12. Ferric Chloride
13. Vanillin
14. Ammonia vapour
15. Tris-HCl (buffer)

* Solvents were distilled prior to use

3.2.1 Preparation of detecting reagent

The identification for the isolated compounds with different type of skeleton were detected by various reagent. The reagents were vanillin, ammonia vapor and 1 % ferric chloride. The procedure for the preparation of the used reagent were described below:

3.2.1.1 Vanillin

Vanillin (0.5 g) in 2.0 mL concentrated H_2SO_4 was added to 8.0 mL of ethanol to produce spray reagent. Vanillin reagent was sprayed to the dried chromatography TLC plates. The TLC plate was heated at 100-110°C until full development of colour occurred. The occurrence of blue, red, pink, brown, dark green, grey or purple indicated the presence of phenylpropenes and simple terpenes.

3.2.1.2 Ammonia vapour

The plates were placed above a tank containing a solution of ammonia. Fluorescence under UV before and after exposure to the ammonia vapour were marked. Fluorescence under long wave might only indicate the presence of flavonoids while fluorescence under short and long wave might indicate the presence of phenyl propanoids.

3.2.1.3 1 % Ferric Chloride

Ferric chloride (1 g) was dissolved in 100 ml of methanol. TLC plate was dipped into the reagent after been developed using various solvent systems. An immediate change of color on the TLC indicated the presence of phenolic compounds.

3.3 Extraction, isolation and purification of the secondary metabolites from the barks of *B. glabra* and *E. kingiana*

The method of extraction of barks of *B. glabra* and *E. kingiana* were described in section 3.3.1. For the isolation of the crude extract from both plants, it were brief in detailed in section 3.3.2. Lastly, for the purification of the pure compounds will be discussed further in section 3.3.3.

3.3.1 Extraction procedure

The extraction process was carried out using simple maceration method. The dried, ground barks of *B. glabra* and *E. kingiana* were first defatted with hexane for 3-days period. Then the hexane extract was filtered and dried in a rotary evaporator. The plant material was then dried up and followed by extraction with dichloromethane (CH_2Cl_2) for 48 hours and repeated twice. The liquid extracts were dried under reduced pressure using rotary evaporator. After that, the whole procedure was repeated once again with methanol to obtain the methanol extract. The yields of the crudes from the bark extracts of each plant are given in Table 3.1.

Table 3.1: Yield of crude extracts from the barks of *B. glabra* and *E. kingiana*.

Species	Amount (kg)	Yield of crude (g)	Percentage yield (%)
B. glabra	1.5	Hexane: 2.0	0.13
		CH_2Cl_2: 4.3	0.29
		Methanol: 7.2	0.48
E. kingiana	2.0	Hexane: 4.2	0.21
		CH_2Cl_2: 20.5	1.03
		Methanol: 35.2	1.76

3.3.2 Isolation techniques

The crude extracts of CH_2Cl_2 from the barks *B. glabra* and *E. kingiana* were further investigated using various separation techniques such as Thin Layer Chromatography

(TLC), Column Chromatography (CC), Preparative Thin Layer Chromatograhpy (PTLC), and High-Performance Liquid Chromatography (HPLC) to obtain pure compounds.

3.3.2.1 Thin Layer Chromatography (TLC)

Aluminium supported silica gel 60 F_{254} plates were used to visualize the spots of the isolated compounds on the TLC. Ultra-violet light (254 and 365 nm) was used to examine the spots on the TLC before spraying with or dipped into the reagent.

3.3.2.2 Column Chromatography (CC)

CC using silica gel 60 (70-230 mesh ASTM) was used for the isolation and purification of compounds. The ratio of silica gel to the sample for the CC was approximately 30:1. A slurry of silica gel was used as an adsorbent while the elution was carried out using desired solvent systems.

3.3.2.3 Preparative Thin Layer Chromatograhpy (PTLC)

PTLC was employed for the separation of the compounds that could not be achieved through CC. Silica gel plate was loaded with 20 mg of sample. The plate was placed in a covered glass chamber and developed with a suitable solvent system. The separated compounds were visualized under UV lights and the region marked. The marked region was then scraped off and placed into a conical flask to repeatedly extract using desired solvents.

3.3.2.4 High Performance Liquid Chromatography (HPLC)

HPLC was performed for the polar fractions from which the separation of the compounds could not be achieved through CC and PTLC. HPLC were performed on four devices:

i- Semi-preparative HPLC separations using a Waters auto purification system equipped with a sample manager (Waters 2767)

ii- A binary pump (Waters 2525)

iii- A column fluidics organizer (Waters SFO)

iv- Photoiodide Array Detector (190-600 nm, Waters 2998)

The polar fractions were eluted with a mixture of solvents between MeOH/H_2O in the presence of 0.1 % formic acid as a buffer. The purification was done using Agilent® Pursuit XRs (250 x 4.6 mm, 5.0 µm) C18 column. Prior to analysis, all solvents and fractions were filtered with a nylon membrane filter that has a pore size of 0.45 µm. The fractions were eluted at a flow rate of 3.3 mL/min.

3.3.3 Purification of compounds from dichloromethane extracts of *B. glabra* and *E. kingiana*

The dichloromethane (CH_2Cl_2) extract was subjected to column chromatography (CC) separation over silica gel (Merck silica gel, 720-230 mesh) as the stationary phase. All separations were carried out using gradient elution method. The solvent used was CH_2Cl_2 and methanol which acted as mobile phase. The eluents were collected in the test tubes (10 ml). The alternate test tubes were then tested on thin layer chromatography (TLC) for purity. Test tubes which gave spots with same R_f values on the TLCs were combined and treated as a fraction. Each fraction was subjected to repeated CC or preparative TLC until a single spot on the TLC was obtained. Certain fractions were subjected to semi-preparative C_{18} HPLC, using gradient elution with methanol-H_20 + 0.1 % formic acid to give desired compounds.

The CH_2Cl_2 crude extract (2.2 g) of *B. glabra* was purified by an open CC eluting to give 6 major fractions (A-F). Fraction B (42 mg) was separated by CC over silica gel, eluting gradiently with CH_2Cl_2: MeOH to furnish **123** (1.3 mg) and **124** (0.9 mg).

Fraction C (177.0 mg) was purified by preparative TLC eluted with a CH_2Cl_2: CH_3OH (98:2) solvent system to furnish **125** (2.0 mg), **126** (8.4 mg) and **127** (1.0 mg). Fraction D (98.0 mg) was further subjected to preparative TLC eluting with a CH_2Cl_2: CH_3OH (95:5) to give **128** (1.9 mg) and **129** (1.3 mg). Finally, fraction E (125.0 mg) was purified using preparative TLC again eluted with CH_2Cl_2: CH_3OH (93:7) solvent system to give **130** (6.0 mg) and **131** (1.6 mg).

As for *E. kingiana*, the crude CH_2Cl_2 extract (8.0 g) was purified by an open CC eluting with gradient solvent system 90:10 to 30:70 CH_2Cl_2: CH_3OH to give 5 major fractions (A-E). Fraction A (52 mg) was separated by preparative TLC eluted with a CH_2Cl_2: CH_3OH (98:2) solvent system to furnish **132** (1.1 mg) and **133** (1.0 mg). Fraction C (162.0 mg) was also purified by preparative TLC eluted with a CH_2Cl_2: CH_3OH (97:3) solvent system to yield **134** (2.4 mg), **135** (1.0 mg) and **136** (2.6 mg). For fraction C (77.0 mg) and D (60.0 mg), HPLC was used during purification of these fraction. In this stage, reverse phase analytical and semi-preparative HPLC were performed and the compounds were eluted with a mixture of solvents between CH_3OH/H_2O in the presence of 0.1% formic acid as a buffer to give **137** (1.6 mg), **138** (2.7 mg) from fraction C and **139** (1.2 mg) from fraction D. The parameters for the isolation and the chromatogram of the compounds **137**, **138** and **139** are shown in subchapter below.

The schematic flow of the isolation of all the compounds from the barks of *B. glabra* and *E. kingiana* are simplified in Scheme 3.1 and Scheme 3.2 respectively.

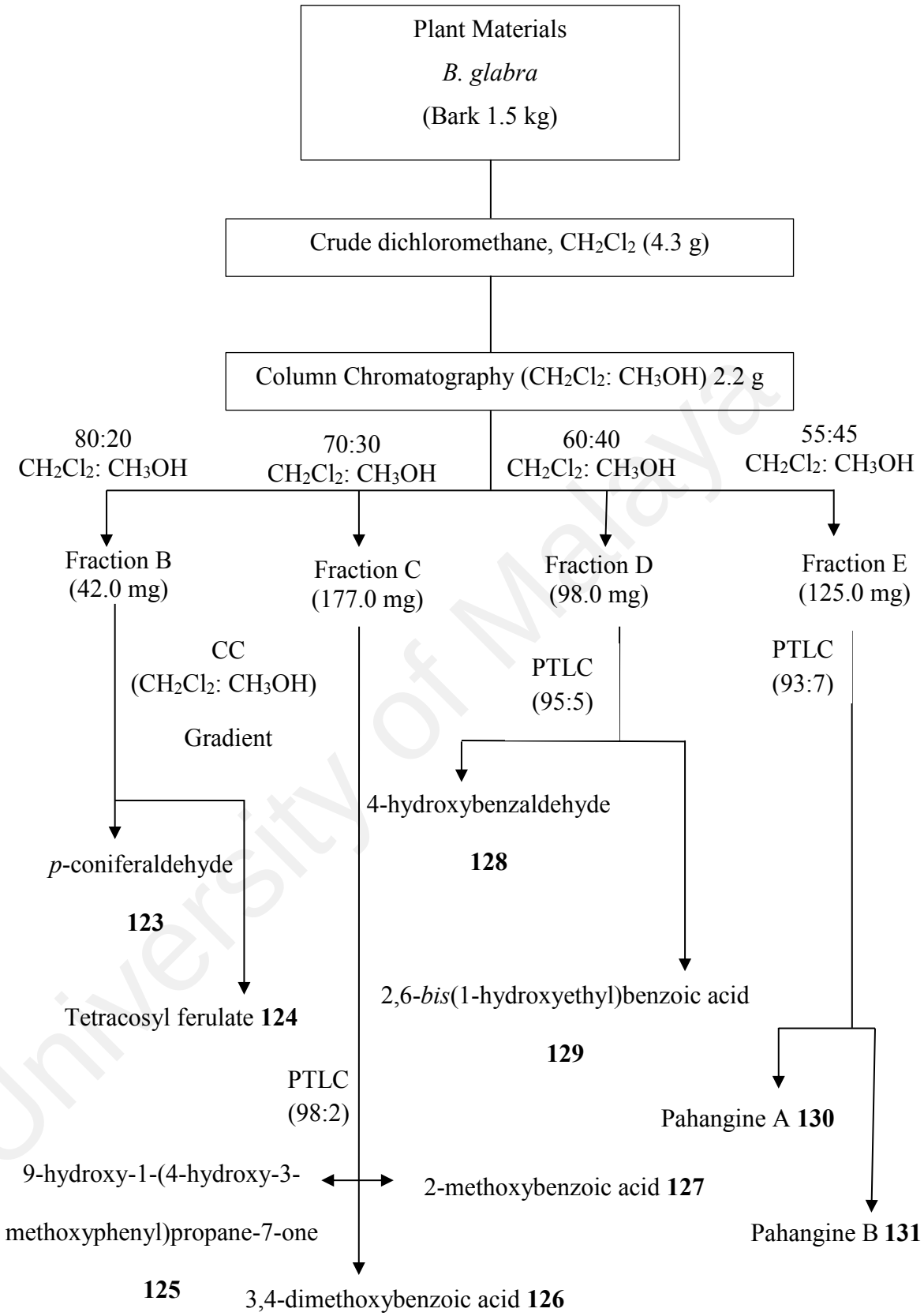

Scheme 3.1: Purification of compounds from the bark of *B. glabra*.

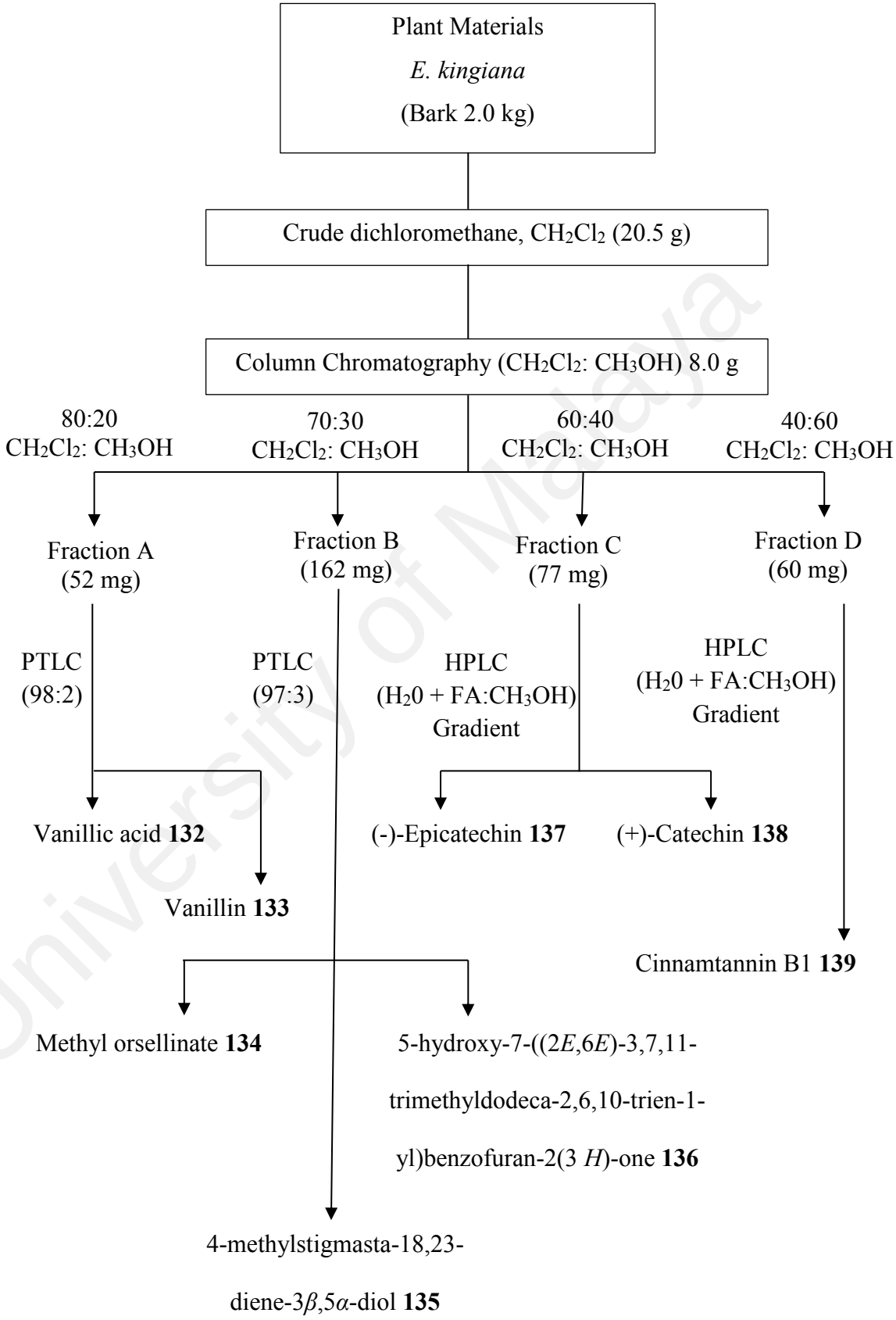

Scheme 3.2: Purification of compounds from the bark of *E. kingiana*.

3.3.3.1 HPLC chromatograms

The isolation and chromatograms for the fraction C and D were shown in Table 3.2, Table 3.3, Figure 3.1 and Figure 3.2 which yielded **137**, **138** and **139** respectively.

Table 3.2: HPLC solvent system for fraction C.

Time (min)	Flow rate (mL/min)	% A2 (H_20 + 0.1 % formic acid)	% B2 (CH_3OH)
0.0	3.3	95.0	5.0
20.0	3.3	70.0	30.0
30.0	3.3	70.0	30.0
31.0	3.3	0.0	100.0
36.0	3.3	0.0	100.0

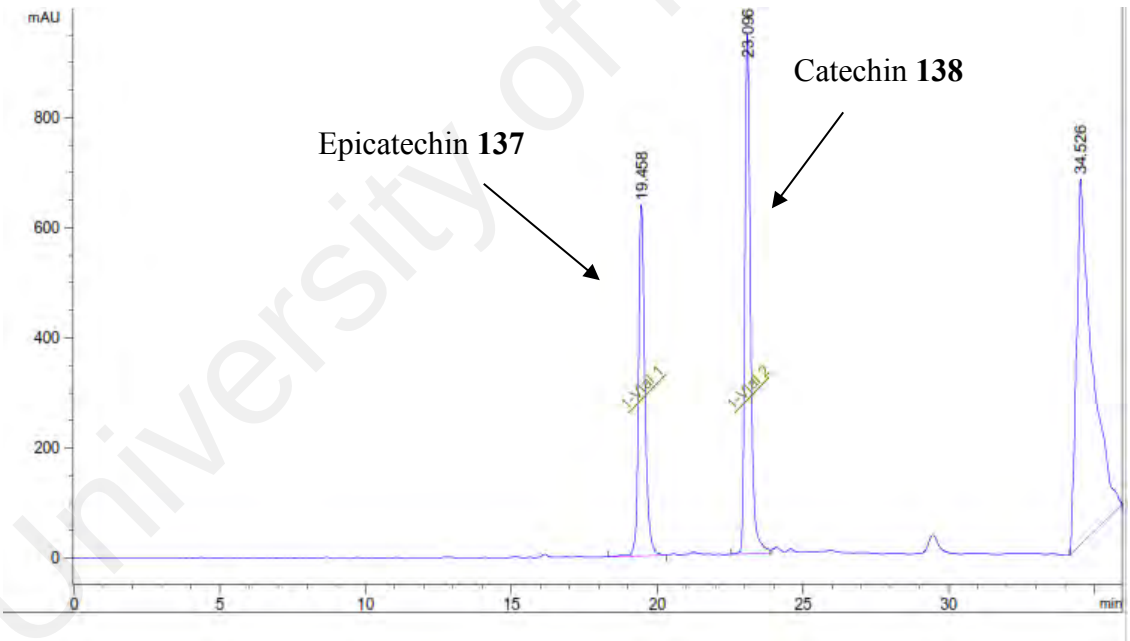

Figure 3.1: HPLC chromatogram of fraction C.
Serial collections: Epicatechin **137** (**t_R** 19.5min, 1.6 mg)
Catechin **138** (t_R 23.1min, 2.7 mg)

Table 3.3: HPLC solvent system of fraction D.

Time (min)	Flow rate (mL/min)	% A2 (H_20 + 0.1 % formic acid)	% B2 (CH_3OH)
0.0	3.3	95.0	5.0
20.0	3.3	70.0	30.0
26.0	3.3	70.0	30.0

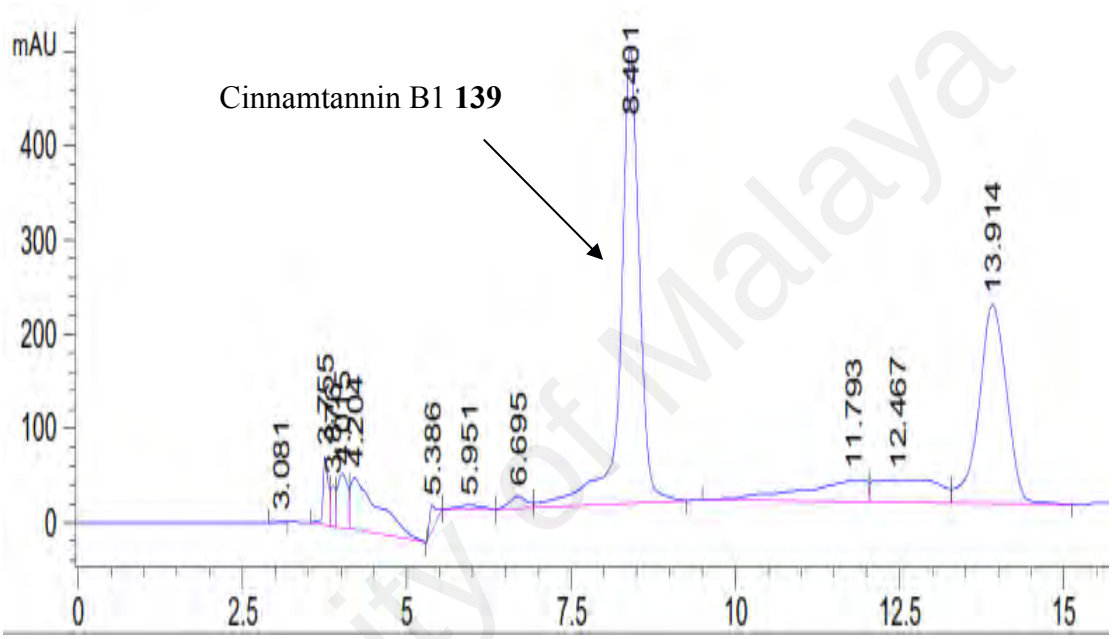

Figure 3.2: HPLC chromatogram of fraction D.
Serial collections: Cinnamtannin B1 **139** (t_R 8.4 min, 1.2 mg)

The list of isolated compounds from both plants (*B. glabra* and *E. kingiana*) have been tabulated in Table 3.4 and Table 3.5.

Table 3.4: List of eluent and fractions of respective compounds from *B. glabra*.

Compounds	Eluent CH_2Cl_2: CH_3OH	Fraction	R_f	Weight (mg)
p-Coniferaldehyde **123**	99:1	36-43	0.71	1.3
Tetracosyl ferulate **124**	99:1	36-43	0.89	0.9

'Table 3.4, continued'

Compounds	Eluent CH_2Cl_2: CH_3OH	Fraction	R_f	Weight (mg)
9-Hydroxy-1-(4-hydroxy-3-methoxyphenyl)propane-7-one **125**	98:2	55-67	0.52	2.0
3,4-Dimethoxybenzoic acid **126**	98:2	55-67	0.70	8.4
2-Methoxybenzoic acid **127**	98:2	55-67	0.81	1.0
4-Hydroxybenzaldehyde **128**	98:2	75-82	0.52	1.9
2,6-*Bis*(1-hydroxyethyl)benzoic acid **129**	98:2	75-82	0.65	1.3
Pahangine A **130**	95:5	119-130	0.62	6.0
Pahangine B **131**	95:5	119-130	0.75	1.6

Table 3.5: List of eluent and fractions of respective compounds from *E. kingiana*.

Compounds	Eluent CH_2Cl_2: CH_3OH	Fraction	R_f	Weight (mg)
Vanillic acid **132**	98:2	15-20	0.58	1.1
Vanillin **133**	98:2	15-20	0.34	1.0
Methyl orsellinate **134**	97:3	26-30	0.82	2.4
3-Methylstigmasta-20,23-diene-3β,5α-diol **135**	97:3	26-30	0.65	1.0
5-Hydroxy-7-((2*E*,6*E*)-3,7,11-trimethyldodeca-2,6,10-trien-1-yl)benzofuran-2(3 H)-one **136**	97:3	26-30	0.43	2.6

Table 3.6: List of eluent and fractions of respective compounds from *E. kingiana* isolated with HPLC.

Compounds	Eluent HPLC H_20 + FA: CH_3OH	Fraction	R_t (min)	Weight (mg)
(-)-Epicatechin **137**	See Table 3.4	60-65	19.5	1.6
(+)-Catechin **138**	See Table 3.4	60-65	23.1	2.7
Cinnamtannin B1 **139**	See Table 3.5	80-85	7.5	1.2

3.4 Characterization of compounds isolated from the barks of *B. glabra* and *E. kingiana*

Structural identification of the isolated compounds was carried out on the basis of IR, NMR, LCMS-IT-TOF and UV spectroscopic techniques.

3.4.1 Infrared spectroscopy (IR)

IR spectra were recorded using a Perkin-Elmer System 400 FT-IR Spectrometer. Spectra were obtained using a sodium chloride (NaCl) window with chloroform as the solvent. The range of measurement was from 4000 to 600 cm^{-1}.

3.4.2 Nuclear magnetic resonance spectroscopy (NMR)

The 1D (^1H, ^{13}C, DEPT Q and DEPT 135) and 2D-NMR (COSY, HSQC and HMBC) spectra were recorded on a BRUKER Advance III NMR spectrometer (400 or 600 MHz). The samples were dissolved in deuterated chloroform ($CDCl_3$) and pyridine-D_5 (C_5D_5N) in 180 mm x 5 mm NMR tubes.

3.4.3 Liquid chromatography mass spectrometry-ion trap-time of flight (LCMS-IT-TOF) and electrospray ionization mass spectrometry (ESIMS)

The LCMS-IT-TOF and ESIMS spectra were obtained using an Agilent 6530 with a SPD-M20A diode array detector coupled to an IT-TOFF mass spectrometer.

3.4.4 Ultra-violet spectroscopy (UV)

The UV spectra were obtained using a Jasco V530 UV-Vis Spectrophotometer. The stock solutions were prepared by adding 10 mL spectral grade methanol which were used for dissolving of 0.1 mg of each compound.

3.5 Physical data of the isolated compounds

Pahangine A 130

Pahangine A	: $C_{20}H_{21}NO_6$
UV nm	: 404, 332
IR v_{max} cm^{-1}	: 3354, 1670
$[\alpha]_D^{25}$	: +37.5
Mass spectrum *m/z*	: 372.1447 $[M+H]^+$
^{1}H-NMR δ ppm	: see Table 4.2
DEPT-Q NMR δ ppm	: see Table 4.2

Pahangine B 131

pahangine B	: $C_{20}H_{22}O_7$
UV nm	: 404, 332
IR v_{max} cm^{-1}	: 3420, 1727
$[\alpha]_D^{25}$	: +12.5
Mass spectrum *m/z*	: 397.1298 $[M+Na]^+$
^{1}H-NMR δ ppm	: see Table 4.3
DEPT-Q NMR δ ppm	: see Table 4.3

***p*-Coniferaldehyde 123**

p-coniferaldehyde	: $C_{10}H_{10}O_3$
UV nm	: 220
IR v_{max} cm^{-1}	: 1720
Mass spectrum *m/z*	: 179.0993 $[M+H]^+$
^{1}H NMR δ ppm	: see Table 4.4
^{13}C-NMR δ ppm	: see Table 4.4

Tetracosyl ferulate 124

Tetracosyl ferulate	: $C_{40}H_{70}O_4$
UV nm	: 321, 278
IR v_{max} cm^{-1}	: 3410
Mass spectrum *m/z*	: 615.5507 $[M+H]^+$
^{1}H-NMR δ ppm	: see Table 4.5
DEPT-Q NMR δ ppm	: see Table 4.5

9-Hydroxy-1-(4-hydroxy-3-methoxyphenyl)propane-7-one 125

9-hydroxy-1-(4-hydroxy-3-methoxyphenyl)propane-7-one	: $C_{10}H_{12}O_4$
UV nm	: 321
IR v_{max} cm^{-1}	: 3271, 1628
Mass spectrum *m/z*	: 197.0853 $[M+H]^+$
^{1}H-NMR δ ppm	: see Table 4.6
^{13}C NMR δ ppm	: see Table 4.6

3,4-Dimethoxybenzoic acid 126

3,4-dimethoxybenzoic acid	: $C_9H_{10}O_4$
UV nm	: 220
IR v_{max} cm^{-1}	: 1725
Mass spectrum *m/z*	: 183.0703 $[M+H]^+$
^{1}H-NMR δ ppm	: see Table 4.7
^{13}C NMR δ ppm	: see Table 4.7

2-(Methoxy)benzoic acid 127

2-(methoxy)benzoic acid	: $C_8H_8O_3$
UV nm	: 220, 230
IR v_{max} cm^{-1}	: 1720
Mass spectrum *m/z*	: 153.0565 $[M+H]^+$
^{1}H-NMR δ ppm	: see Table 4.8
DEPT-Q NMR δ ppm	: see Table 4.8

4-Hydroxybenzaldehyde 128

4-hydroxybenzaldehyde	: $C_7H_6O_2$
UV nm	: 220, 230
IR v_{max} cm^{-1}	: 1731, 3401
Mass spectrum *m/z*	: 123.0565 $[M+H]^+$
^{1}H-NMR δ ppm	: see Table 4.9
^{13}C NMR δ ppm	: see Table 4.9

2,6-*Bis*(1-hydroxyethyl)benzoic acid 129

2,6-*bis*(1-hydroxyethyl)benzoic acid	: $C_{11}H_{14}O_4$
UV nm	: 220, 230
IR v_{max} cm^{-1}	: 3251, 1704
Mass spectrum *m/z*	: 211.0954 $[M+H]^+$
^{1}H-NMR δ ppm	: see Table 4.10
^{13}C NMR δ ppm	: see Table 4.10

Vanillic acid 132

vanillic acid	: $C_8H_8O_4$
UV nm	: 220, 230
IR v_{max} cm^{-1}	: 1725
Mass spectrum *m/z*	: 169.0703 $[M+H]^+$
^{1}H NMR δ ppm	: see Table 4.11
^{13}C NMR δ ppm	: see Table 4.11

Vanillin 133

vanillin	: $C_8H_8O_3$
UV nm	: 220, 230
IR v_{max} cm^{-1}	: 3401, 1695
Mass spectrum *m/z*	: 153.0456 $[M+H]^+$
^{1}H NMR δ ppm	: see Table 4.12
^{13}C NMR δ ppm	: see Table 4.12

Methyl orsellinate 134

methyl orsellinate	: $C_9H_{10}O_4$
UV nm	: 230

IR v_{max} cm^{-1}	: 3401, 1628
Mass spectrum *m/z*	: 183.0286 $[M+H]^+$
^1H NMR δ ppm	: see Table 4.13
^{13}C NMR δ ppm	: see Table 4.13

5α-Cholesta-20,24-diene-3β,6α-diol 135

5α-Cholesta-20,24-diene-3β,6α-diol	: $C_{30}H_{50}O_2$
UV nm	: 195
IR v_{max} cm^{-1}	: 3430, 2941
Mass spectrum *m/z*	: 444.3434 $[M+H]^+$
^1H NMR δ ppm	: see Table 4.14
^{13}C NMR δ ppm	: see Table 4.14

4-hydroxy-6-(9,13,17-trimethyldodeca-8,12,16-trienyl)-2(3H)-benzofuranone 136

4-hydroxy-6-(9,13,17-trimethyldodeca-8,12,16-trienyl)-2(3 H)-benzofuranone	: $C_{23}H_{30}O_3$
UV nm	: 217
IR v_{max} cm^{-1}	: 1470, 1457, 1725, 3402
Mass spectrum *m/z*	: 355.2243 $[M+H]^+$
^1H NMR δ ppm	: see Table 4.15
^{13}C NMR δ ppm	: see Table 4.15

(-)-Epicatechin 137

(-)-epicatechin	: $C_{15}H_{14}O_6$
UV nm	: 280
IR v_{max} cm^{-1}	: 1470, 1457, 3402
Mass spectrum *m/z*	: 291.1432 $[M+H]^+$
^1H NMR δ ppm	: see Table 4.16
^{13}C NMR δ ppm	: see Table 4.16

(+)-Catechin 138

(+)-catechin	: $C_{15}H_{14}O_6$
UV nm	: 276

IR v_{max} cm^{-1}	: 1470, 1457, 3402
Mass spectrum *m/z*	: 291.1432 $[M+H]^+$
^1H NMR δ ppm	: see Table 4.17
^{13}C NMR δ ppm	: see Table 4.17

Cinnamtannin B1 139

cinnamtannin B1	: $C_{45}H_{36}O_{18}$
UV nm	: 280
IR v_{max} cm^{-1}	: 1470, 1457, 3402
Mass spectrum *m/z*	: 863.40 $[M-H]^-$
^1H NMR δ ppm	: see Table 4.18
^{13}C NMR δ ppm	: see Table 4.18

CHAPTER 4: RESULTS AND DISCUSSION

4.1 Secondary metabolites isolated from the barks of *B. glabra* and *E. kingiana*

The barks of *B. glabra* and *E. kingiana*, belonging to the Lauraceae family were studied in detail for their chemical constituents. The dichloromethane extracts of bark from these two species have been subjected to extensive chromatography separation such as column chromatographie, preparative TLC and HPLC, to yield seventeen pure compounds.

Nine compounds were isolated from *B. glabra* which consists of neolignans and cinnamic acid derivatives. Two neolignans were pahangine A **130** (new), and pahangine B **131** (new). Seven cinnamic acid derivatives, *p*-coniferaldehyde **123**, tetracosyl ferulate **124**, 9-hydroxy-1-(4-hydroxy-3-methoxyphenyl)propane-7-one **125**, 3,4-dimethoxybenzoic acid **126**, 2-methoxybenzoic acid **127**, 4-hydroxybenzaldehyde **128**, and 2,6-*bis*(1-hydroxyethyl)benzoic acid **129** were also isolated from this plant.

The chemical study of *E. kingiana* yielded eight compounds consists of cinnamic acid derivatives, stigmasterol, benzofuran and flavonoids types. The cinnamic acid derivatives were vanillic acid **132**, vanillin **133**, and methyl orsellinate **134**. A stigmasterol; 5α-Cholesta-20,24-diene-3β,6α-diol **135** and a benzofuran; 4-hydroxy-6-(9,13,17-trimethyldodeca-8,12,16-trienyl)-2(3 H)-benzofuranone**136** (new) were isolated from this plant. Subsequently, 3 flavonoids such as (-)-epicatechin **137,** (+)-catechin **138** and cinnamtannin B1 **139** were also isolated from this plant.

The structural elucidation of those seventeen compounds shall be discussed in detail through spectroscopic methods, principally NMR experiments. The elucidated compounds have been arranged according to their skeletal types and presented in Table 4.1. Of the compounds elucidated, two were new neolignans possessing an oxetane ring (**130** and **131**). Complete ^{1}H, ^{13}C, DEPT-Q and HMBC spectral data were given for all compounds and also by comparison with the literature data for the known compounds.

Table 4.1: The isolated compounds from *B. glabra* and *E. kingiana*.

Compounds	Plants	Types	Pages
Pahangine A **130**	*B. glabra*	Neolignan	69
Pahangine B **131**	*B. glabra*	Neolignan	78
p-Coniferaldehyde **123**	*B. glabra*	Cinnamic acid derivatives	86
Tetracosyl ferulate **124**	*B. glabra*	Cinnamic acid derivatives	90
9-Hydroxy-1-(4-hydroxy-3-methoxyphenyl)propane-7-one **125**	*B. glabra*	Cinnamic acid derivatives	95
3,4-Dimethoxybenzoic acid **126**	*B. glabra*	Cinnamic acid derivatives	100
2-Methoxybenzoic acid **127**	*B. glabra*	Cinnamic acid derivatives	104
4-Hydroxybenzaldehyde **128**	*B. glabra*	Cinnamic acid derivatives	108
2,6-*Bis*(1-hydroxyethyl)benzoic acid **129**	*B. glabra*	Cinnamic acid derivatives	112
Vanillic acid **132**	*E. kingiana*	Cinnamic acid derivatives	117
Vanillin **133**	*E. kingiana*	Cinnamic acid derivatives	121
Methyl orsellinate **134**	*E. kingiana*	Cinnamic acid derivatives	125
5α-Cholesta-20,24-diene-3β,6α-diol **135**	*E. kingiana*	Stigmasterol	130
4-hydroxy-6-(9,13,17-trimethyldodeca-8,12,16-trienyl)-2(3H)-benzofuranone **136**	*E. kingiana*	Benzofuran	137
(-)-Epicatechin **137**	*E. kingiana*	Flavonoid	144
(+)-Catechin **138**	*E. kingiana*	Flavonoid	148
Cinnamtannin B1 **139**.	*E. kingiana*	Flavonoid	152

4.1.1 Pahangine A 130

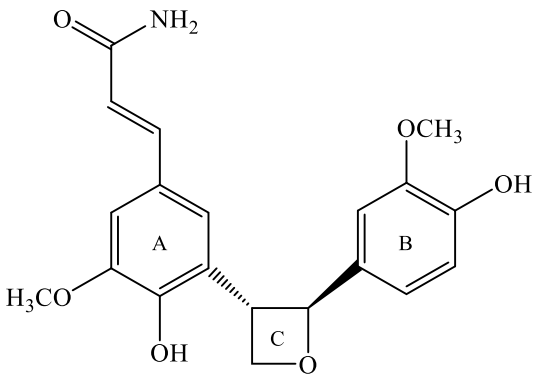

130

Compound **130** was isolated as yellow amorphous solid, $[\alpha]_D^{25}$ = +37.5. It was assigned the molecular formula $C_{20}H_{21}NO_6$ as deduced from its positive LCMS-IT-TOF spectrum (*m/z* 372.1447 $[M+H]^+$; calcd. for $C_{20}H_{22}NO_6$, 372.1442), consistent with eleven degrees of unsaturation (DoU); which can be accounted to ring A (4 DoU), ring B (4 DoU), oxetane ring C (1 DoU) and two double bonds (2 DoU). The IR spectrum of **130** indicated the presence of hydroxyl (3354 cm^{-1}) and conjugated carbonyl (1670 cm^{-1}) functionalities (Sulaiman et al., 2018).

The ^{1}H NMR spectrum (Figure 4.3) of **130** established the existence of two olefinic protons, five aromatic signals, and two methoxy groups (δ_H 3.77, and δ_H 3.66). The two *trans* olefinic protons resonated at δ_H 8.11 and δ_H 6.98, with a pair of doublets having a coupling constant of 15.7 Hz. The aromatic protons in ring A, H-2 and H-6, appeared as broad singlets at δ_H 7.37 and δ_H 7.15 while, three aromatic protons in ring B, H-2′, H-5′ and H-6′ gave signals of an ABX spin system at δ_H 7.31 (d, J = 1.8), δ_H 7.22 (d, J = 8.1 Hz) and 7.21 (dd, J = 8.1 and 1.8 Hz) respectively. In addition, **130** was postulated to form a rare oxetane ring, of which H-7′ was detected as a doublet (J = 6.9 Hz) at δ_H 6.09 together with two methylene protons at δ_H 4.21 (dd, J = 12.2 and 6.1 Hz, H_2-9′) and a methine proton δ_H 3.94 (dd, J = 12.2 and 6.9 Hz, H-8′).

The DEPT-Q NMR spectrum (Figure 4.4) revealed the presence of twenty carbons; seven sp^2 quaternary carbons, seven sp^2 methines, two sp^3 methines, one sp^3 methylene, two methoxys and, one carbonyl carbon of an amide. Two olefinic carbon signals corresponding to C-7 at δ_C 140.9 and C-8 at δ_C 119.8 were readily assigned due to the distinguish feature of α,β-unsaturated carbonyl system. The signals at δ_C 88.9 (C-7′), δ_C 54.1 (C-8′), and δ_C 63.7 (C-9′) were characteristic of sp^3 carbons of an oxetane ring (Fleming & Gao, 1997).

The COSY and HMBC correlations between H-7′, H-8′ and H_2-9′ (Figure 4.5 and Figure 4.6) confirmed the presence of the oxetane system which is connected to ring A and B through C-3 and C-1′.

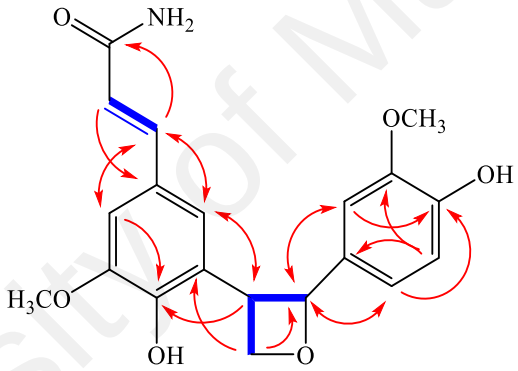

130

Figure 4.1: ^{1}H-^{1}H COSY (blue line) and HMBC (red arrows) correlations of **130**.

The assignment of the relative configuration of **130** was deduced through values of the coupling constants between H-7′ and H-8′. According to the reports on the synthesised isomeric diphenyloxetanes (Fleming & Gao, 1997; Saphier et al., 2005), the *trans* isomers (6.9-7.6 Hz) has a lower coupling constant as compared to the *cis* isomers (8.7-9.3 Hz). Compound **130** showed coupling constant with the values of 6.9 Hz, thus suggesting a *trans* configuration. This hypothesis is strengthened by the NOESY spectrum which showed correlations between H-9′a with H-8′ and H-9′b with H-7’ only, therefore implying that H-8’ and H-7’ are *trans* to each other (Figure 4.2). Based on all

the spectroscopic evidences aforementioned, pahangine A was structurally elucidated as **130**, which is a new neolignanamide isolated from *B. glabra* (Sulaiman et al., 2018).

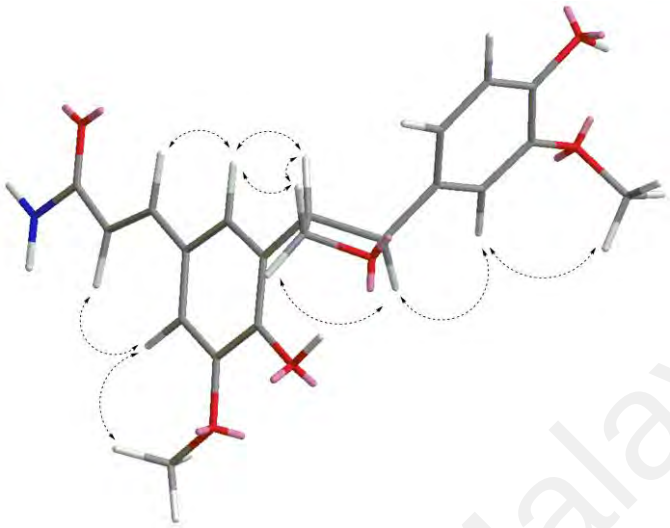

Figure 4.2: NOESY correlations of **130**.

According to Scheme 4.2, pahangine A **130** proposed as originating from radical pairing of ferulic acid and coniferyl alcohol which were possibly derived from *p*-coniferaldehyde **123** and tetracosyl ferulate **124**, where both were isolated from this plant. It is proposed that ferulic acid and coniferyl alcohol undergo one-electron oxidation of the phenol groups which is shown in Scheme 4.1. One-electron oxidation of phenol groups allow delocalization of the unpaired electron, giving resonance forms in which the free electron resides at position *ortho* for ferulic acid and as for coniferyl alcohol conjugation occurs at the side-chain (Cordell, 2002). Radical pairing of resonance structures which was followed by enolization, intramolecular nucleophilic attack from the hydroxyl group and subsequent amidation of aliphatic carboxylic acids moiety to give pahangine A **130**.

Table 4.2: ^{1}H (400 MHz), ^{13}C (100 MHz) and HMBC NMR data of pahangine A **130** (δ in ppm) in C_5D_5N.

Position	δ_H (*m*, *J* in Hz) in C_5D_5N (**130**)	δ_C in C_5D_5N (**130**)	HMBC correlation (H⟶C)
1	-	129.3	
2	7.37 (br s)	117.5	C4, C6, C7, C8′
3	-	130.7	
4	-	150.5	
5	-	144.7	
6	7.15 (br s)	112.3	C2, C4, C7
7	8.11 (d, *J* = 15.6)	140.9	C1, C2, C6, C8, C9
8	6.98 (d, *J* = 15.6)	119.7	C1, C9
9	-	168.5	
1′	-	132.9	
2′	7.31 (d, *J* = 1.8)	110.6	C7′, C6′, C1′, C4′
3′	-	148.6	
4′	-	148.1	
5′	7.22 (d, *J* = 8.1)	116.3	C1′, C3′
6′	7.21 (dd, *J* = 8.1, 1.8)	119.6	C2′, C7′, C4′
7′	6.09 (d, *J* = 6.9)	88.9	C3, C2′, C6′, C8′, C9′
8′	3.94 (dd, *J* = 12.2, 6.9)	54.1	C2, C3, C4, C1′, C7′, C9′,
9′	4.21 (dd, *J* = 12.2, 6.1)	63.7	C3, C7′, C8′
5-OMe	3.77 (s)	55.8	C5
3′-OMe	3.66 (s)	55.6	C3′

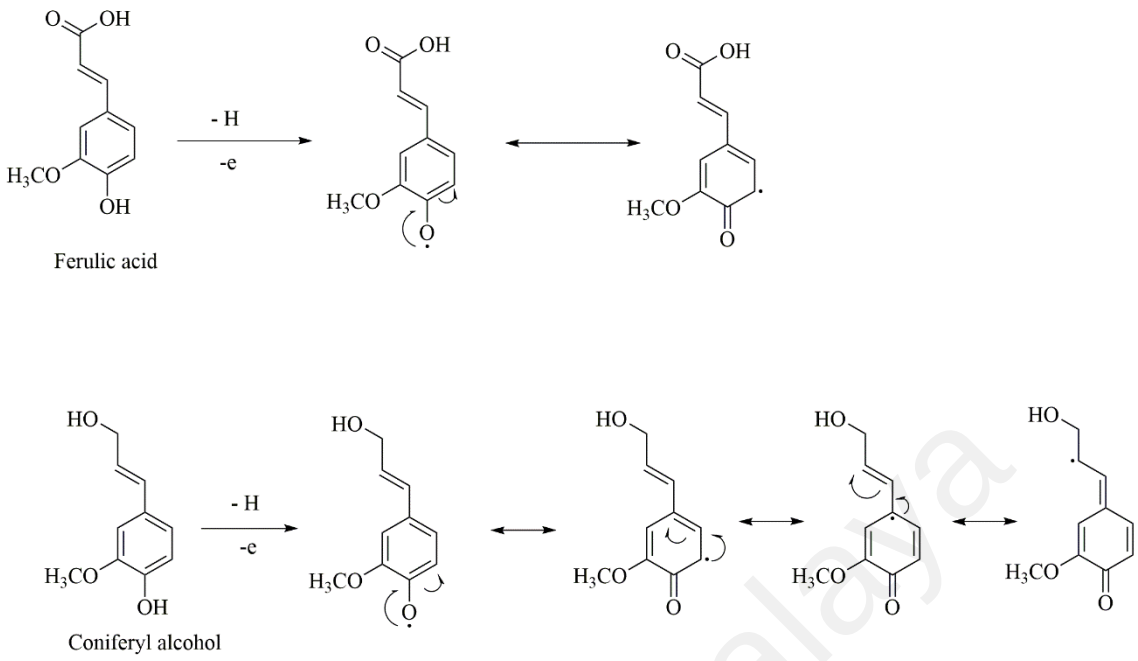

Scheme 4.1: Resonance forms of free radical of ferulic acid and coniferyl alcohol.

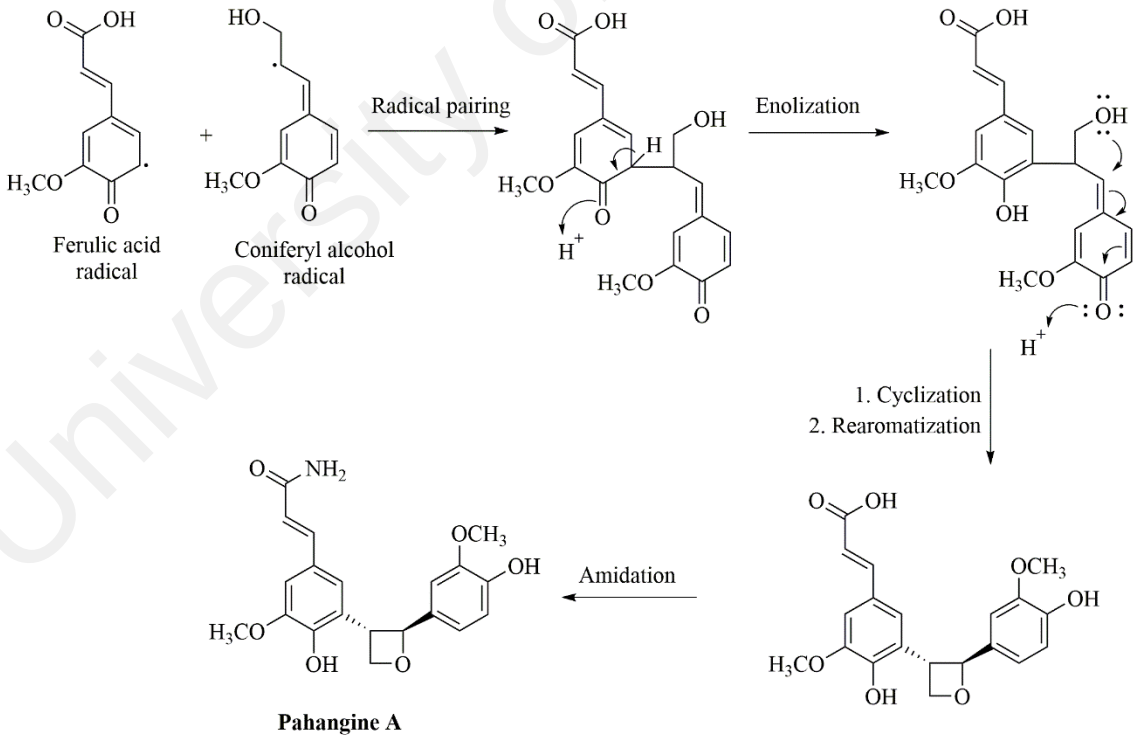

Scheme 4.2: Hypothetical biosynthetic pathway of pahangine A **130**.

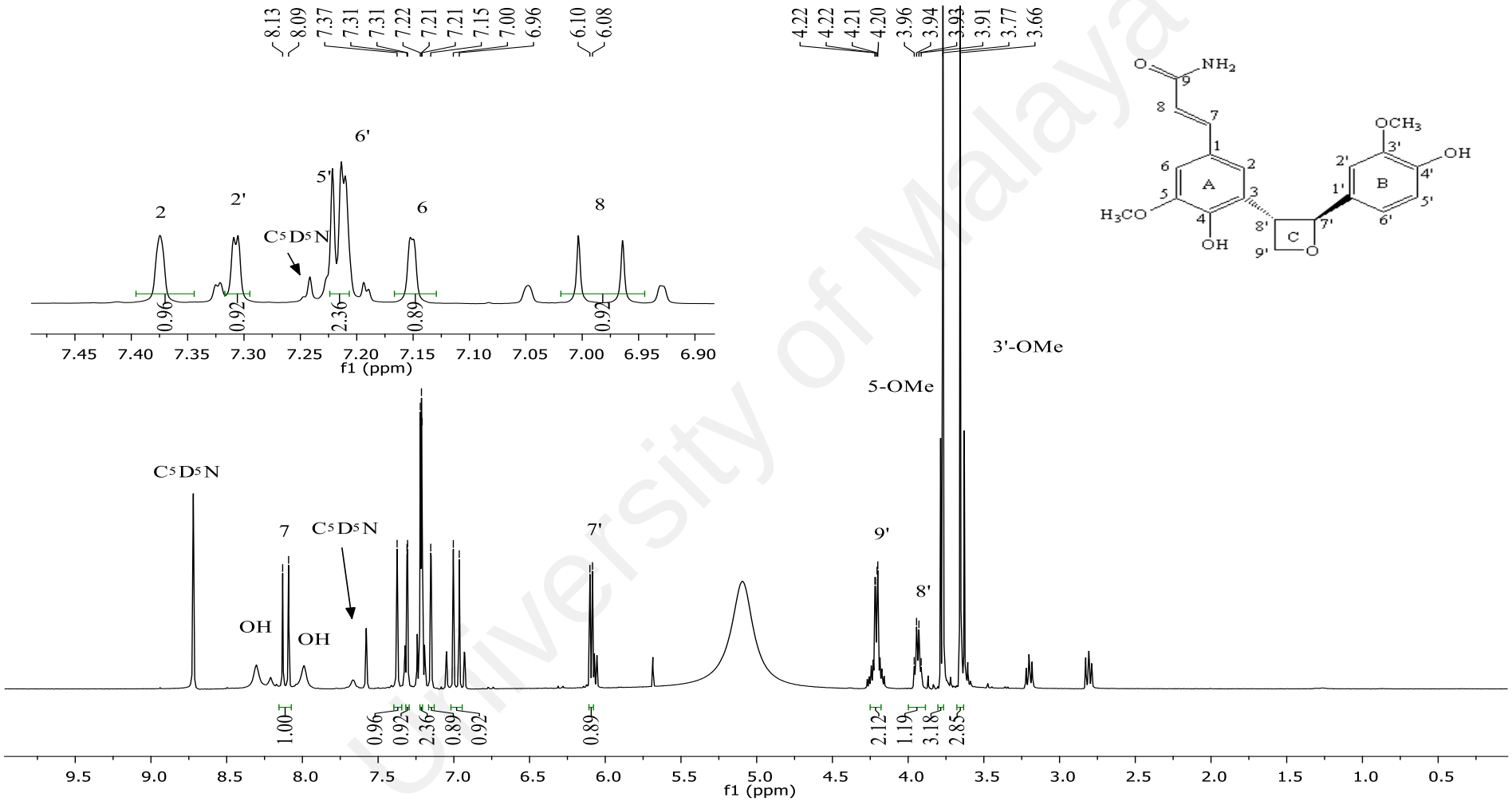

Figure 4.3: ^{1}H NMR spectrum of pahangine A **130**.

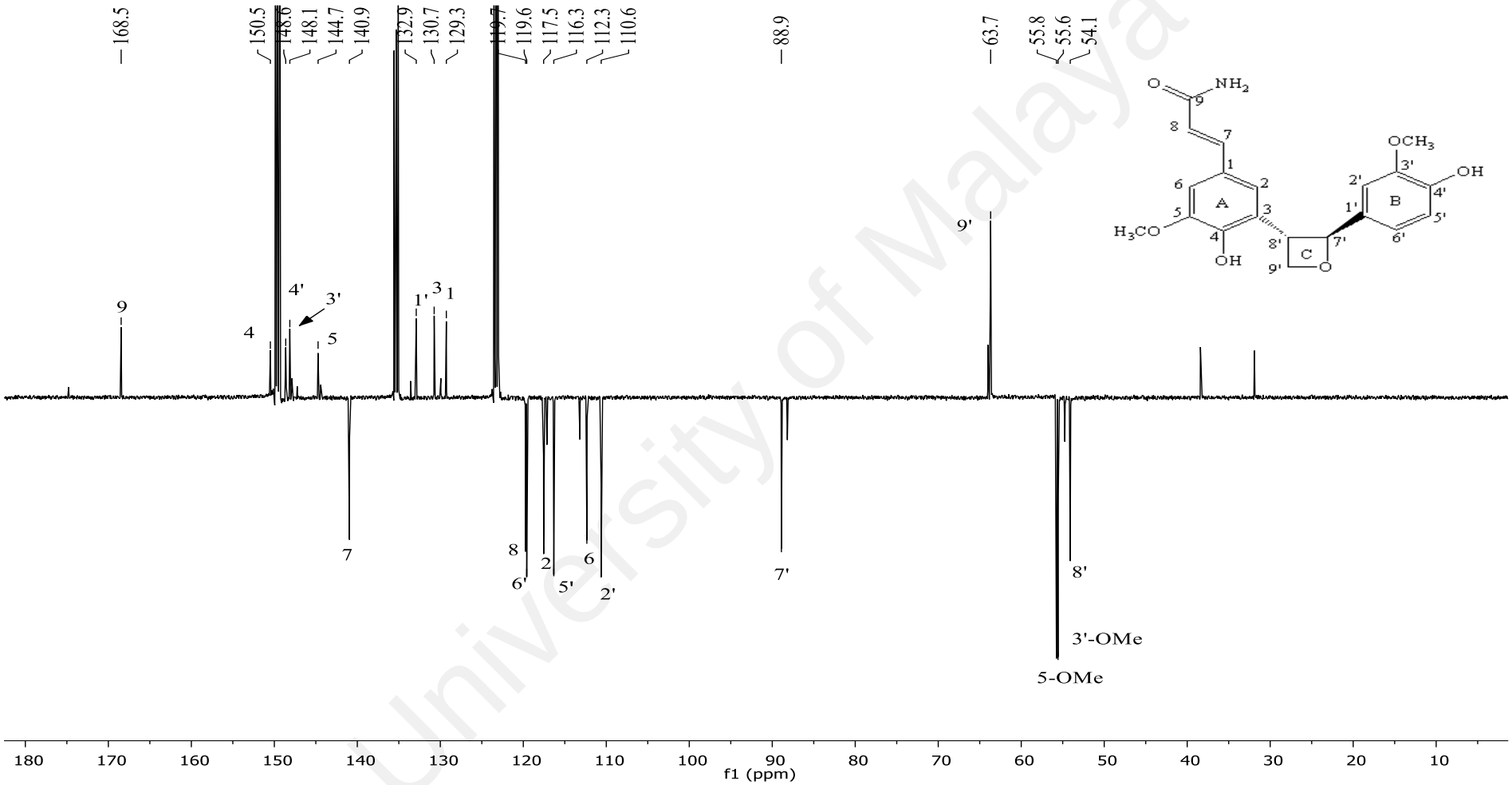

Figure 4.4: DEPT-Q NMR spectrum of pahangine A **130**.

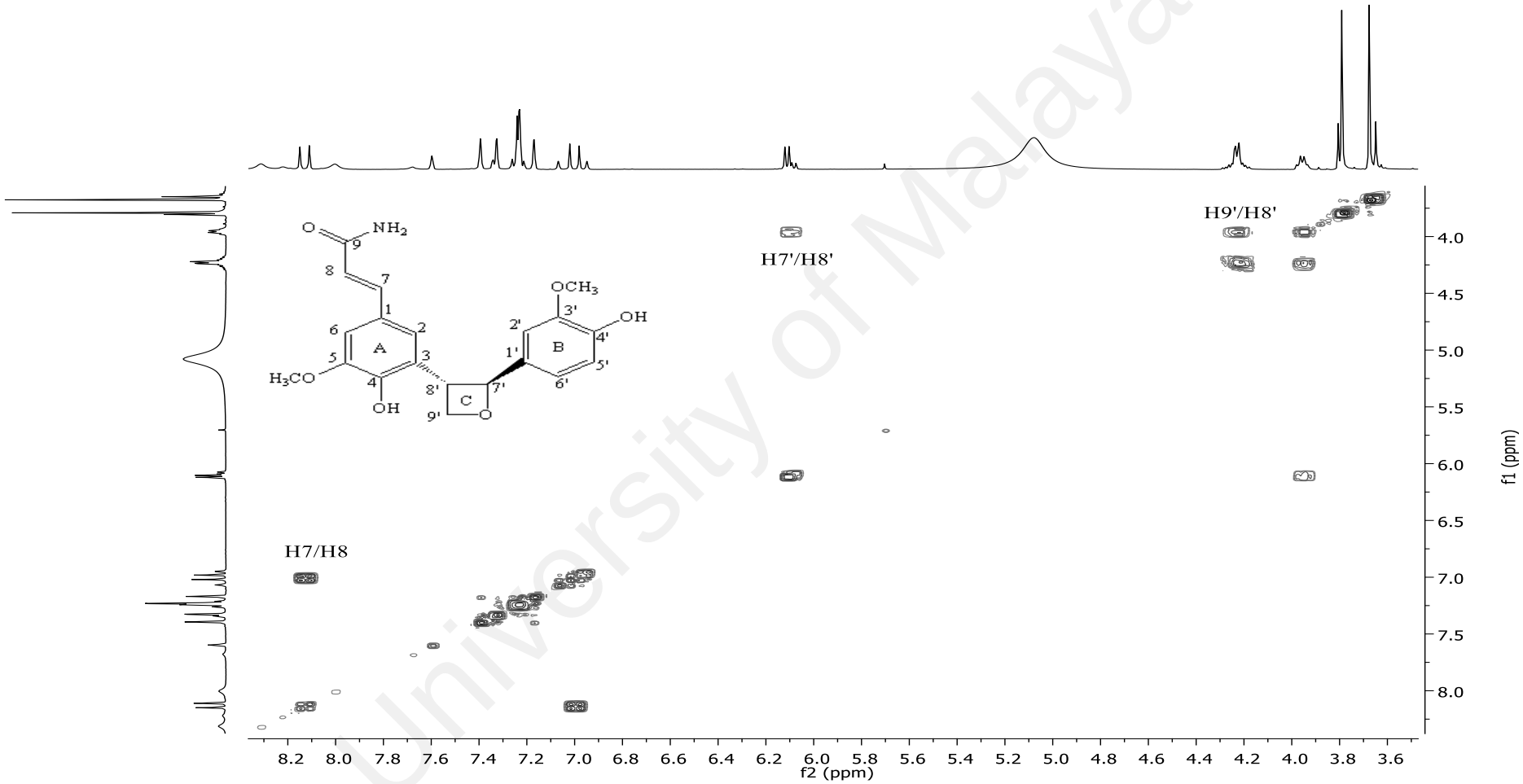

Figure 4.5:COSY NMR spectrum of pahangine A **130**.

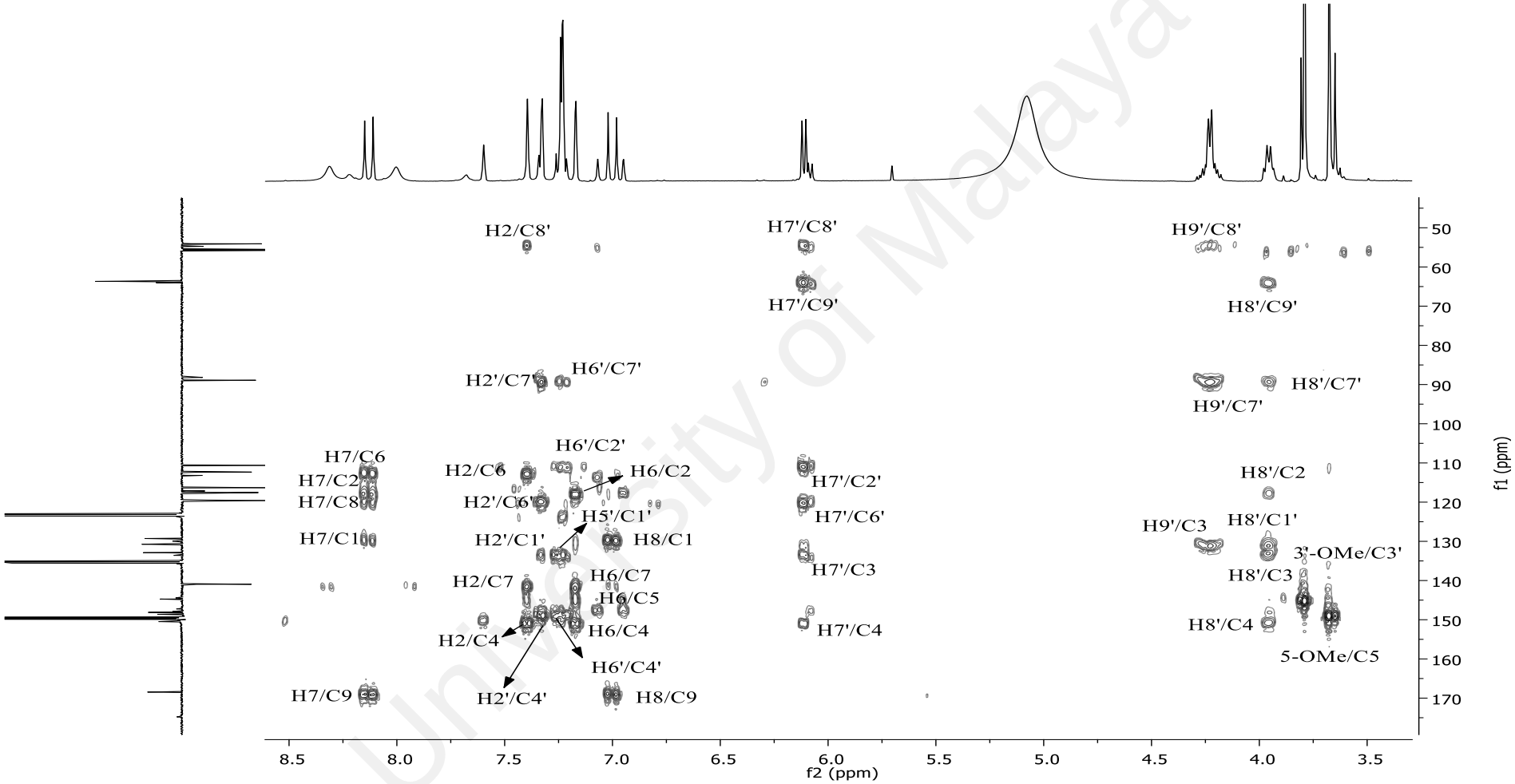

Figure 4.6: HMBC NMR spectrum of pahangine A **130**.

4.1.2 Pahangine B 131

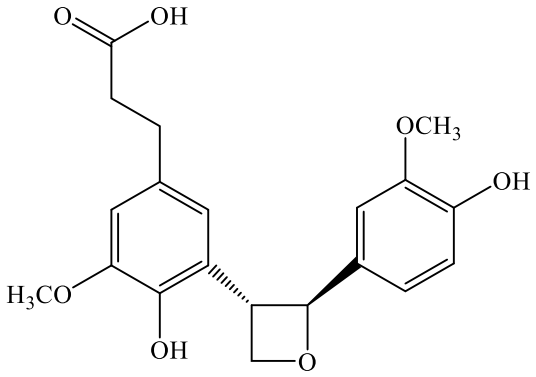

131

Compound **131** was obtained as a yellow amorphous solid with $[\alpha]_D^{25}$ = +12.5 (c=0.50, $CHCl_3$). Its molecular formula as $C_{20}H_{22}O_7$ with ten degree of unsaturation was deduced from its positive LCMS-IT-TOF (397.1298 $[M+Na]^+$; calcd. for $C_{20}H_{22}NaO_7$,397.1258) spectrum. The broad IR absorption band at 3420 cm^{-1} was attributed to the hydroxyl group whereas the band at 1727 cm^{-1} was due to carboxylic acid moiety (Sulaiman et al., 2018).

The ^{1}H NMR spectrum (Figure 4.7) of **131** was similar to pahangine A **130** except for the signals associated with the α,β-unsaturated carbonyl system at position 7, 8 and 9. Unlike **130**, which possessed an olefinic group at position 7 and 8, **131** was suggested to accommodate the methylene protons. This view was supported by a set of triplet appeared at δ_H 2.93 and δ_H 2.53 attributable to the methylene protons; H_2-7 and H_2-8 respectively. However, **131** retained the rare oxetane moiety which was clear from the H-7′ methine signal that appeared as a doublet (J = 7.5 Hz) at δ_H 5.54. However, as for H-8′ methine and H-9′ methylene signals, it appeared as multiplet at δ_H 3.63 and δ_H 3.95, respectively.

From the DEPT-Q NMR spectra (Figure 4.8), the observation of C-7′ and C-8′ methine carbons signal at δ_C 87.9 and δ_C 53.7 along with C-9′ methylene carbon signal at δ_C 63.8 which matched closely with the corresponding carbon signals in **130**; C-7′ (δ_C 88.9), C-8′ (δ_C 54.1) and C-9′ (δ_C 63.7), thus confirmed the existence of an oxetane

moiety. However, comparison between **130** and **131** revealed that they differed by the shift values of the carbon signals associated with C-7 and C-8. The C-7 (δ_C 31.3) and C-8 (δ_C 37.9) were deduced to be hydrogenated, which was in contrast to the olefinic carbons of C-7 (δ_C 140.9) and C-8 (δ_C 119.8) in **130**. This view was also supported by the fact that **131** had one less degree of unsaturation compared to **130**.

The COSY spectrum (Figure 4.9) gave rise to an off-diagonal signal that linked H-7′ with H-8′ and H-9′, thus proving the oxetane moiety. In the HMBC spectrum (Figure 4.10), the correlations from H-7′ methine and H-9′ methylene signals to C-2′ and C-3, respectively were important, as it substantianted the existence of the oxetane group.

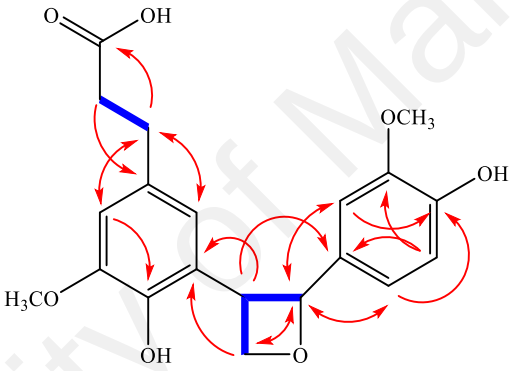

131

Complete analyses of 1D and 2D NMR spectra indicated that **131** is a new neolignan, thus named pahangine B. The NMR data of **131** are provided in Table 4.4. The hypothethical biosynthesis pathway of **131** is presented in Scheme 4.3.

The pahangine B **131** is thought to originate from radical pairing of ferulic acid and coniferyl alcohol which possibly derived from *p*-coniferaldehyde **123** and tetracosyl ferulate **124**, where both were isolated from the same source. The **131** first underwent one-electron oxidation of the phenol groups, which was the same process that has been elaborated in the proposed biogenetic pathway of **130**. The C3-C4 bond underwent stabilization of an enol by electron delocalization in the enolization step, which resulting intramolecular nucleophilic attack from the hydroxyl group at C-9′ in the following step

to form an oxetane moiety. This is followed by the hydrogenation of olefinic carbons at C-7 and C-8 to give pahangine B **131**.

Table 4.3: ^{1}H (400 MHz), DEPT-Q (100 MHz) and HMBC data of pahangine B **131** (δ in ppm) in $CDCl_3$.

Position	δ_H (m, *J* in Hz) in $CDCl_3$ (**131**)	δ_C in $CDCl_3$ (**131**)	HMBC correlation (H⟶C)
1	-	133.0	
2	6.70 (d, *J* = 2.9)*	116.0	C4, C6, C7, C8′
3	-	128.0	
4	-	146.7	
5	-	144.3	
6	6.70 (d, *J* = 2.9)*	112.5	C2, C4, C7
7	2.94 (t)	31.3	C1, C2, C6, C8, C9
8	2.53 (t)	37.9	C1, C7, C9
9	-	174.4	
1′	-	134.1	
2′	6.93 (d, *J* = 2.0)	108.8	C4′, C6′, C7′
3′	-	146.9	
4′	-	145.7	
5′	6.87 (d, *J* = 8.1)	114.3	C1′, C3′
6′	6.88 (dd, *J* = 8.1, 2.0)	119.4	C1′, C2′, C4′, C7′
7′	5.54 (d, *J* = 7.5)	87.9	C2′, C6′, C9′
8′	3.63 (m)	53.7	C3, C1′
9′	3.95 (m)	63.8	C3, C7′, C8′
5-OMe	3.88 (s)	56.1	C5
3′-OMe	3.87 (s)	56.0	C3′

**overlapping peaks*

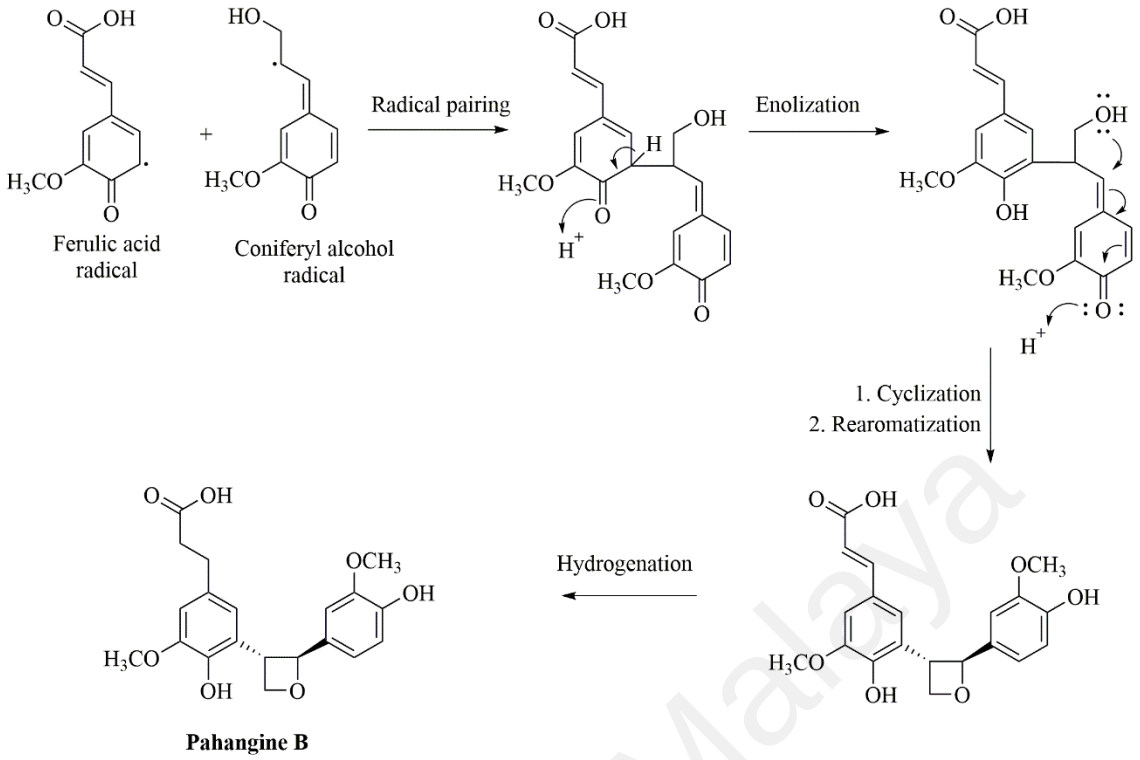

Scheme 4.3: Hypothethical biosynthesis pathway of pahangine B **131**.

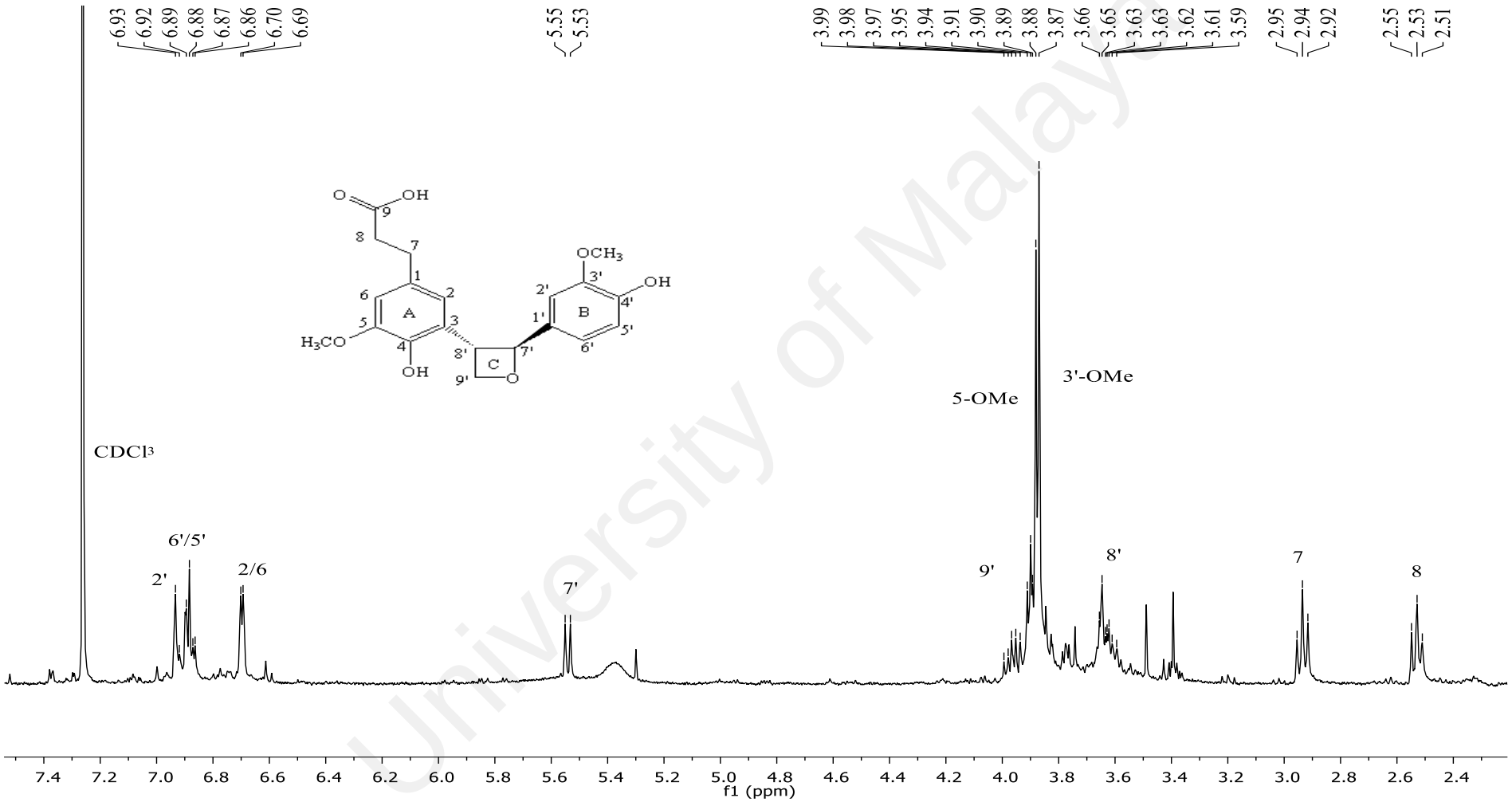

Figure 4.7: ^{1}H NMR spectrum of pahangine B **131**.

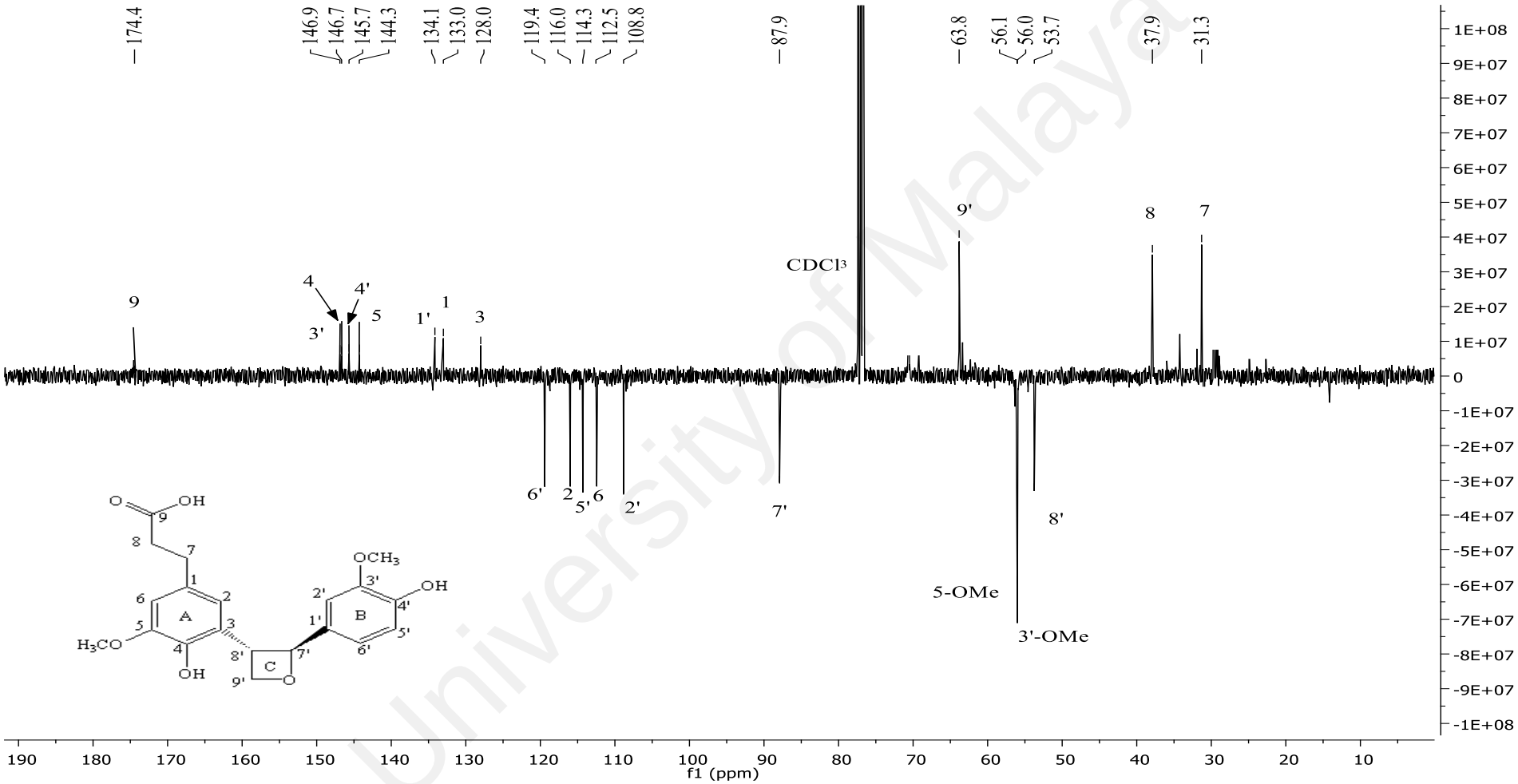

Figure 4.8: DEPT-Q NMR spectrum of pahangine B **131**.

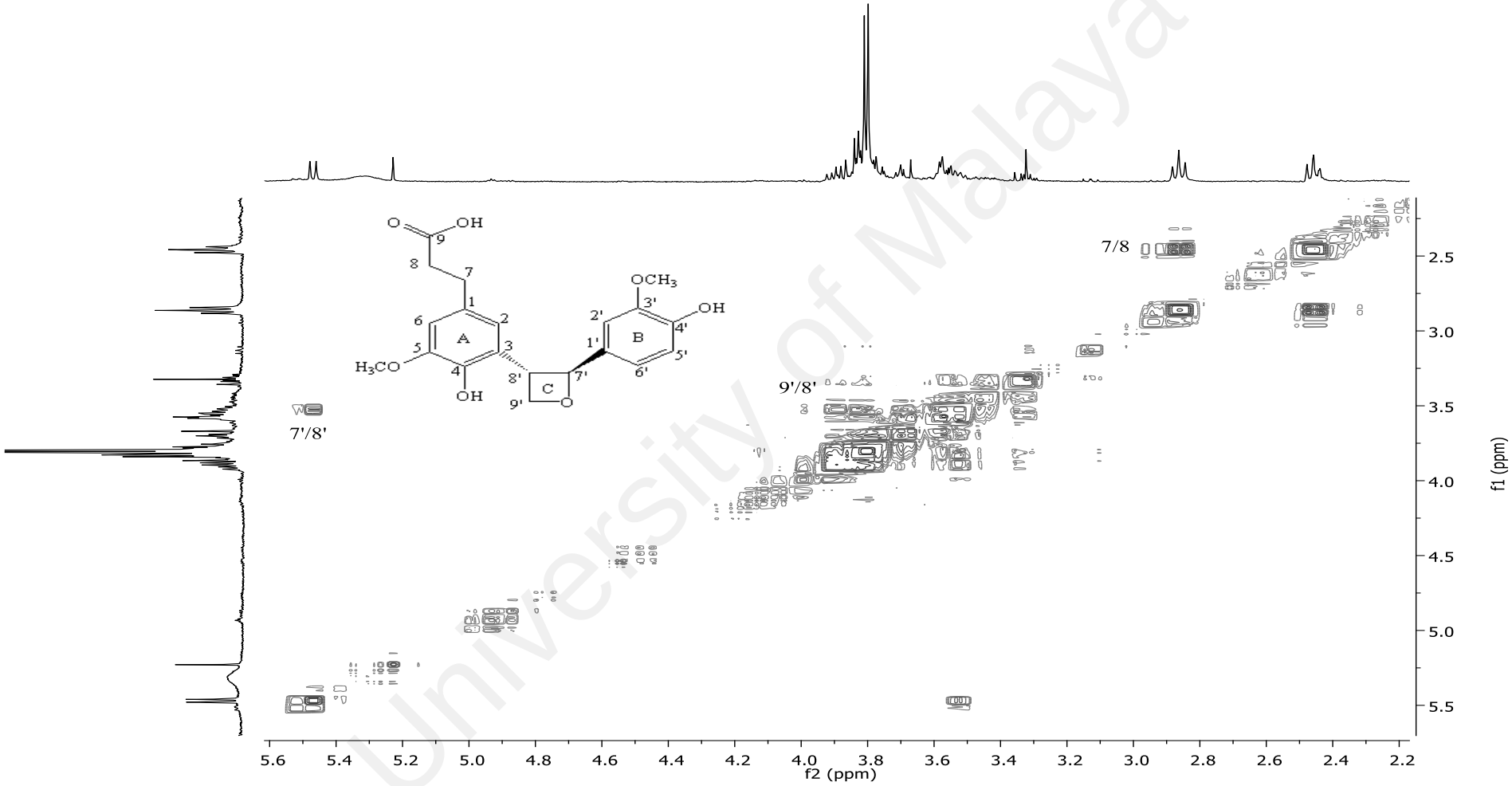

Figure 4.9: COSY NMR spectrum of pahangine B **131**.

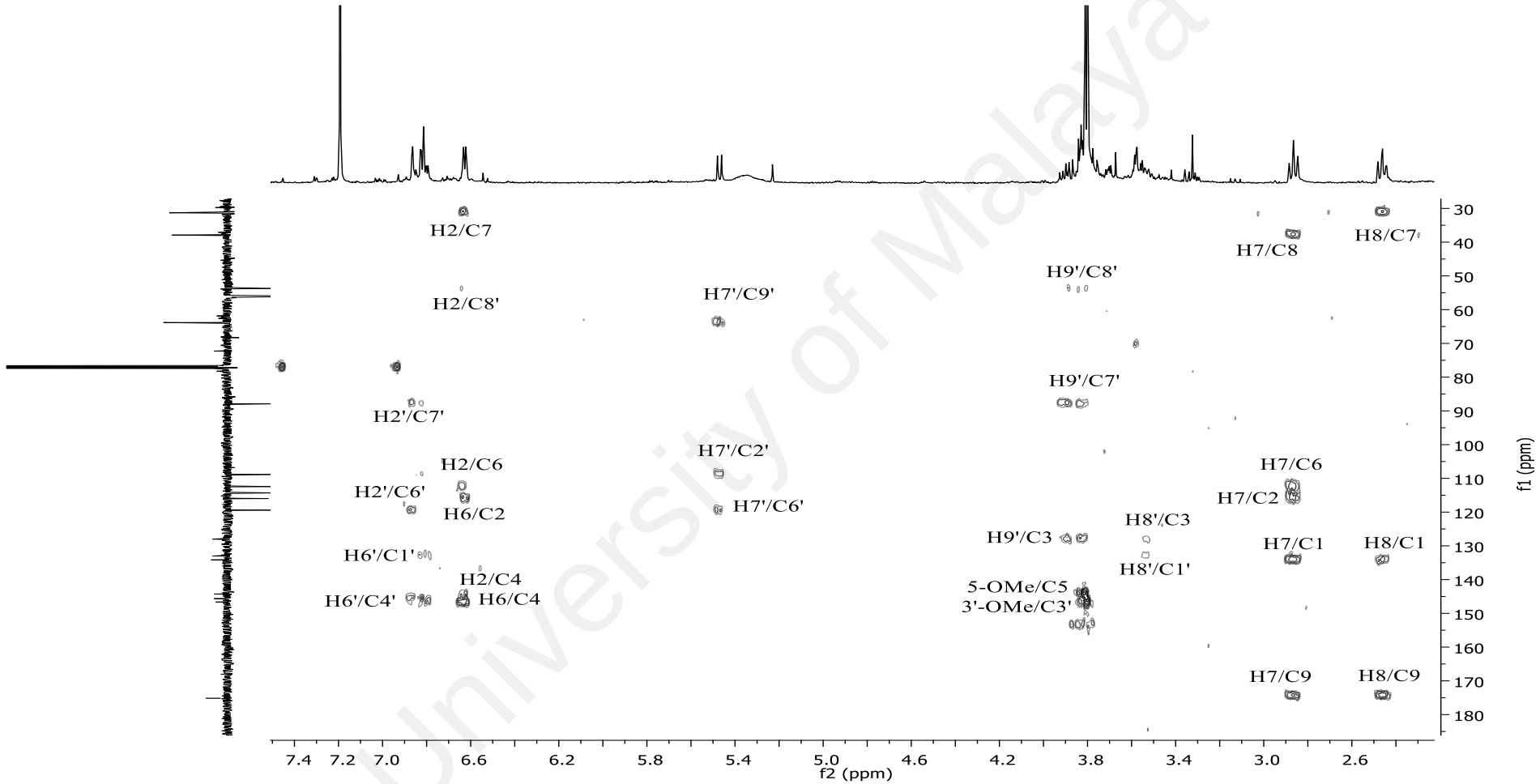

Figure 4.10: HMBC NMR spectrum of pahangine B **131**.

4.1.3 *p*-Coniferaldehyde 123

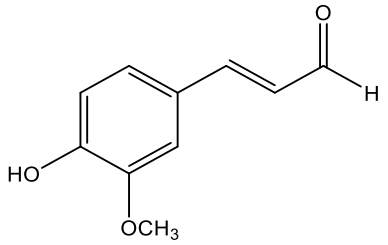

123

Compound **123** was isolated as a colourless solid. The LCMS-IT-TOF spectrum showed the molecular ion peak $[M+H]^+$ at m/z 179.0993 (calcd. for $C_{10}H_{11}O_3$, 179.0703), corresponding to a molecular formula of $C_{10}H_{10}O_3$. The IR spectrum gave an intense absorption at 1720 cm-^{1} due to the carbonyl stretch (Sribuhom et al., 2015).

The ^{1}H NMR spectrum of **123** showed the presence of a methyl group δ_H 3.96 at H-3. It also showed three aromatic protons of a 1,3,4-trisubstituted aromatic ring appearing as two doublets at δ_H 7.08 (d, J = 1.9 Hz) and 6.97 (d, J = 8.2 Hz) and a doublet of doublets at δ_H 7.14 (dd, J = 1.9, 8.2 Hz) which corresponded to H-2, H-5 and H-6, respectively. In addition, H-9 was suggested to be an aldehyde as evidenced by the presence of a doublet which resonated particularly downfield at δ_H 9.67. H-7 appeared as a doublet (J = 7.8 Hz) mainly because it correlated with H-8 which was an α proton of the α,β-unsaturated carbonyl system.

The ^{13}C NMR spectrum displayed ten carbon signals with three quarternary carbons, three aromatic carbons, one mehoxyl, two olefinic carbons, and one carbonyl. The α,β-unsaturated carbonyl system was demonstrated in the ^{13}C NMR spectrum (Figure 4.12) as the methine signals resonated at δ_C 153.2 (C-7) and δ_C 126.6 (C-8). It was noteworthy that the relatively deshielded C-7 olefinic signal was expected as it was the β carbon of α,β-unsaturated carbonyl system.

In the HMBC spectrum, the correlations from H-9 aldehyde signal to C-1 was important, as it substantiated the existence of of α,β-unsaturated carbonyl system. Other

diagnostic correlations were those arose from H-2 and H-6 correlations to C-7, as well as H-7 couplings to C-2, and C-6.

Despite the difference in ^{1}H NMR spectral patterns of **123** and **130**, it however shows some similarity. The similarity can be seen at δ_H 7.41 and δ_H 6.60, was assignable to H-7 and H-8 methine signals which had a similar coupling constant J = 15.8 Hz with **130**, led to the suggestion that **123** also have a *trans* olefinic protons. As for ^{13}C NMR spectrum, unlike **123**, the presence of electron-withdrawing group (H-9) resulted in the carbon shifts towards downfield; C-9 (δ_C 193.7) in comparison to C-9 (δ_C 168.5). Thorough analyses of the 1D and 2D NMR spectra and comparison with the literature (Table 4.4), it can be concluded that **123** was *p*-coniferaldehyde.

Table 4.4: ^{1}H (400 MHz) and ^{13}C (100MHz) NMR data of *p*-coniferaldehyde **123** (δ in ppm) in $CDCl_3$.

	p-coniferaldehyde **123**		*p*-coniferaldehyde (Sribuhom et al., 2015)	
Position	δ_H (*m*, *J* in Hz) in $CDCl_3$	δ_C in $CDCl_3$	δ_H (*m*, *J* in Hz) in $CDCl_3$	δ_C in $CDCl_3$
1	-	126.8	-	126.4
2	7.08 (d, *J* = 1.92)	109.6	7.07 (d, *J* = 1.90)	109.4
3	-	147.1	-	146.9
4	-	149.1	-	148.9
5	6.97 (d, *J* = 8.19)	115.1	6.96 (d, *J* = 8.10)	114.9
6	7.14(dd, *J* = 1.92, 8.19)	124.2	7.13(dd, *J* = 1.90, 8.10)	124.0
7	7.41 (d, *J* = 15.77)	153.2	7.40 (d, *J* = 15.70)	153.0
8	6.60(dd, *J* = 7.76, 15.77)	126.6	6.60(dd, *J* = 7.90, 15.70)	126.6
9	9.67 (d, *J* = 7.76)	193.7	9.66 (d, *J* = 7.90)	193.5
3-OMe	3.96	56.6	3.95	55.9

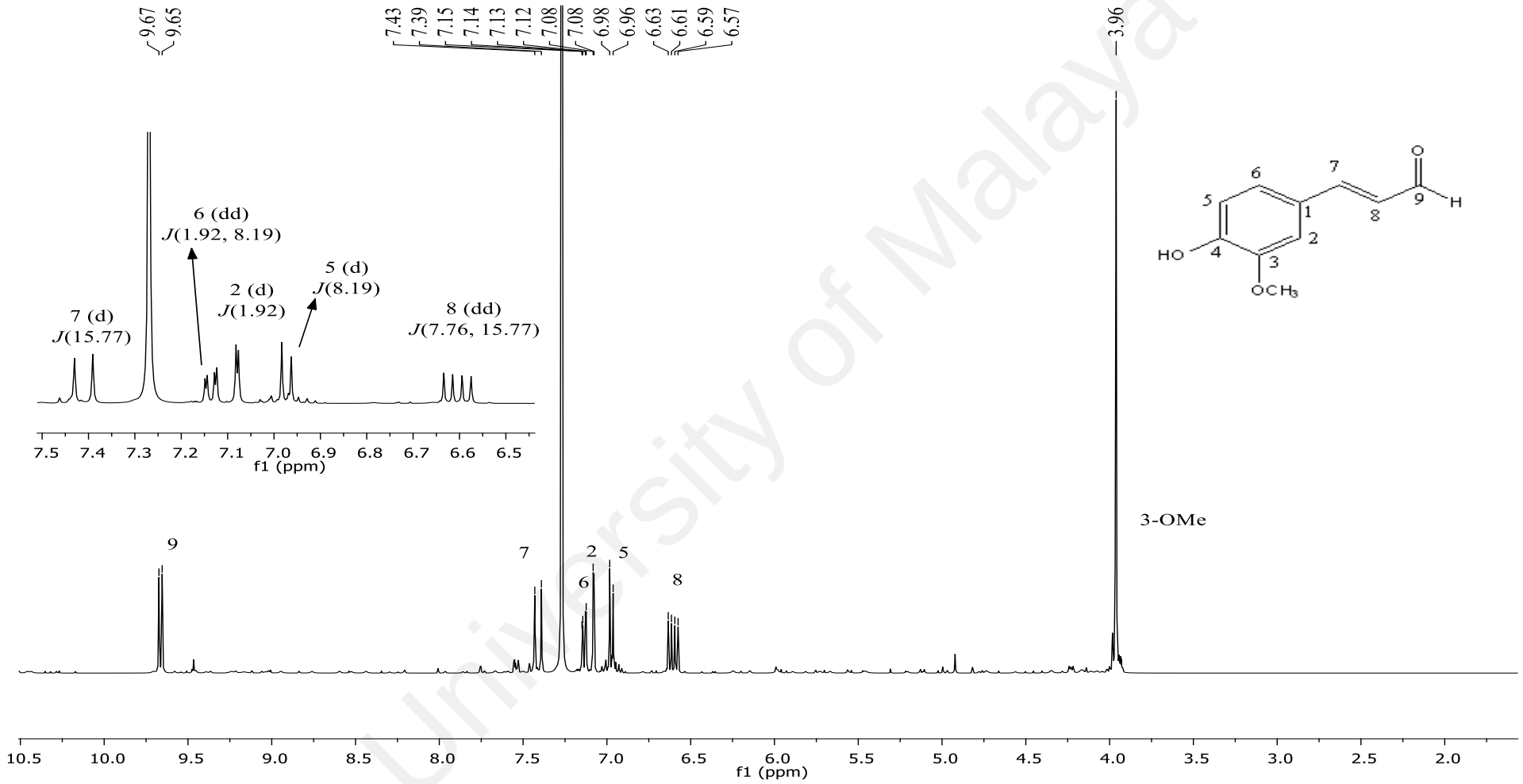

Figure 4.11: ^{1}H NMR spectrum of *p*-coniferaldehyde **123**.

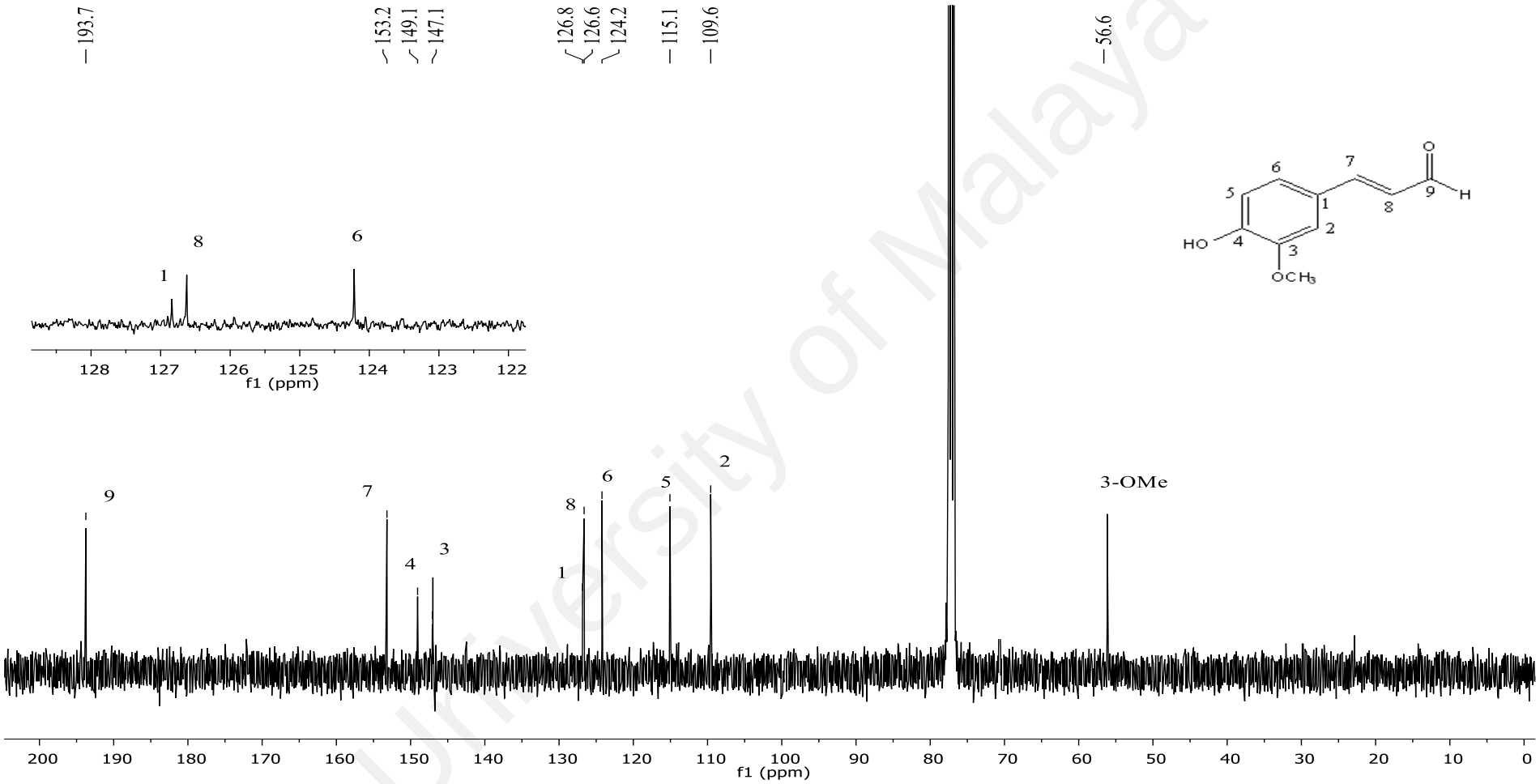

Figure 4.12: ^{13}C NMR spectrum of *p*-coniferaldehyde **123**.

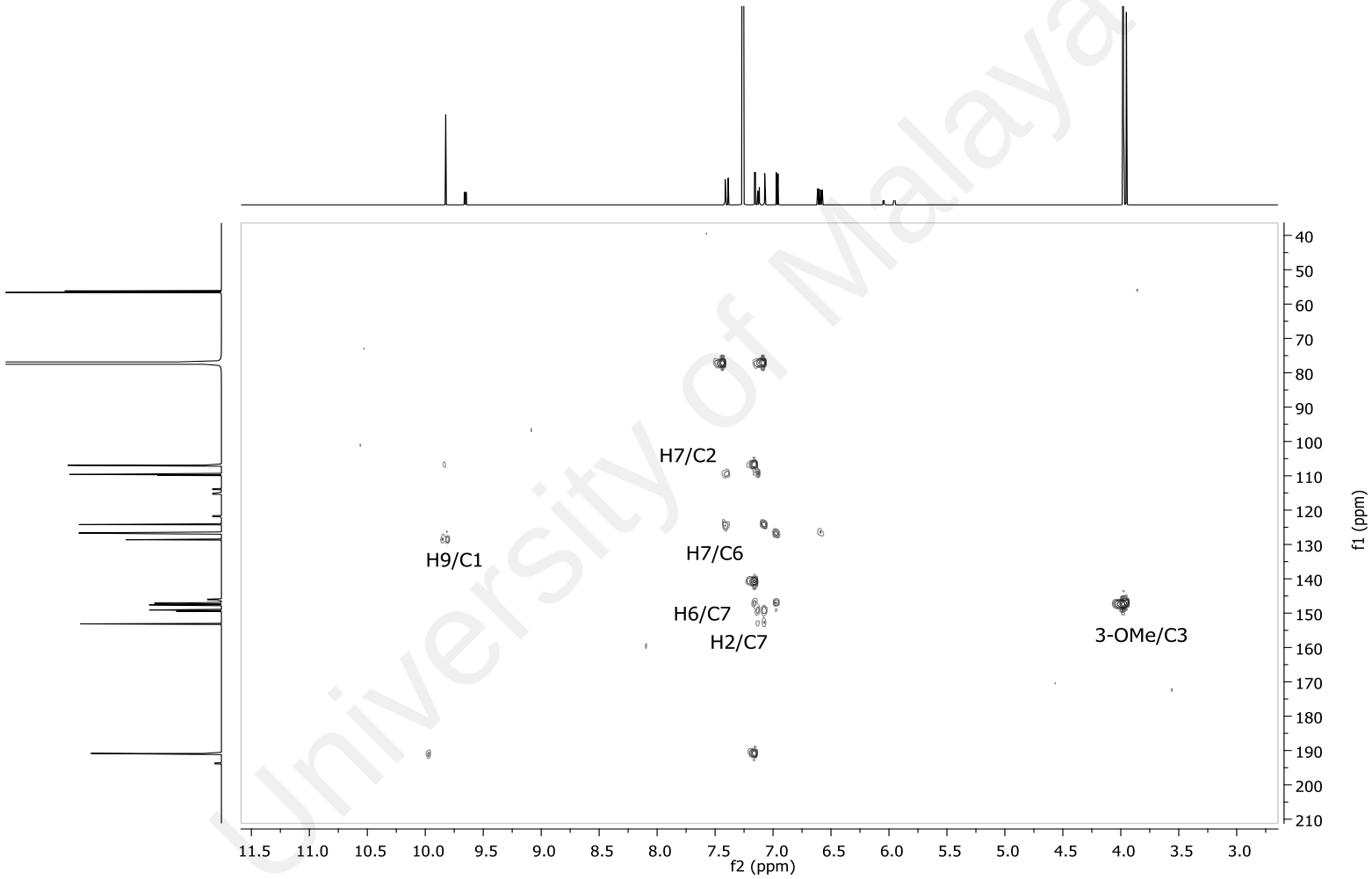

Figure 4.13: HMBC spectrum of *p*-coniferaldehyde **123**.

4.1.4 Tetracosyl ferulate 124

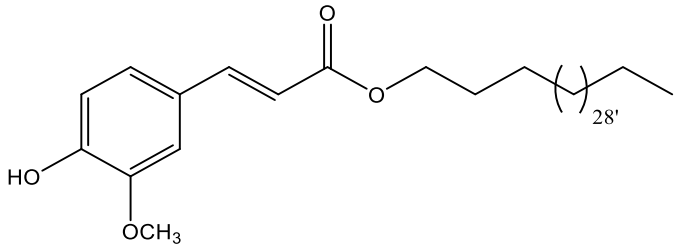

124

Compound **124** was obtained as white amorphous powder. The LCMS-IT-TOF spectrum showed the molecular ion peak $[M+H]^+$ at m/z 615.5507 (calcd. for $C_{40}H_{71}O_4$, 615.5308), corresponding to a molecular formula of $C_{40}H_{70}O_4$ with six degrees of unsaturation. The IR spectrum displayed an absorption bands at 3410 cm^{-1} for hydroxyl group (Addae-Mensah et al., 1992).

The ^{1}H NMR spectrum showed the presence of signals at δ_H 6.91 (d, J = 8.2 Hz), δ_H 7.03 (d, J = 1.9 Hz), and δ_H 7.07 (dd, J = 8.2 and 1.9 Hz) which indicated the presence of a 1,3,4-trisubstituted benzene moiety, corresponding to H-5, H-2 and H-6, respectively. The signals at δ_H 6.29 (d, J = 15.9 Hz, H-8) and δ_H 7.61 (d, J = 15.9 Hz, H-7) showed a *trans* double bond in the molecule. Two triplet signals at δ_H 4.19 and δ_H 0.88 were assigned for H-1′ (J = 6.7 Hz) and terminal methyl protons, H-30 (J = 6.7 Hz). A singlet resonated at δ_H 3.93 corresponded to methoxy group. The multiplet signals which were observed at δ_H 1.20-1.39 revealed the presence of twenty-six methylene groups.

Assignments of the above protons were further established by the COSY spectrum. The signal at δ_H 4.19 for H-1′ showed correlation with the signal at δ_H 1.73 corresponding to H-2′ in the COSY spectrum. The DEPT-Q NMR spectrum showed four quartenary carbons, five methines, one methyl, one methoxy and twenty-nine methylenes. Table 4.5 shows comparison of the assignments of the ^{1}H and DEPT-Q NMR data for **124** and similar data from literature. The table shows that both data were almost identical.

Thus, the structure **124** was identified as tetracosyl ferulate on the basis of LCMS-IT-TOF, ^{1}H and DEPT-Q NMR spectral data and comparison with the literature.

Table 4.5: ^{1}H (400 MHz) and DEPT-Q (100 MHz) data of tetracosyl ferulate **124** (δ in ppm) in $CDCl_3$.

	Tetracosyl ferulate **124**		Tetracosyl ferulate (Addae-Mensah et al., 1992)
Position	δ_H (*m*, *J* in Hz) in $CDCl_3$ (**124**)	δ_C in $CDCl_3$ (**124**)	δ_H (*m*, *J* in Hz) in $CDCl_3$
1	-	127.2	-
2	7.03 (d, *J*=1.9)	109.5	7.04 (d, *J*=2.0)
3	-	146.9	-
4	-	148.0	-
5	6.91 (d, *J*=8.2)	114.9	6.91 (d, *J*=8.5)
6	7.07 (dd, *J*=8.2, 1.9)	123.2	7.07 (dd, *J*=8.5, 2.0)
7	7.61 (d, *J*=15.9)	144.8	7.62 (d, *J*=16.5)
8	6.29 (d, *J*=15.9)	115.8	6.28 (d, *J*=16.5)
9	-	168.0	-
1′	4.19 (t, *J*=6.7)	64.8	4.18 (t, *J*=7.0)
2′	1.73 – 1.54 (m)	24.9	1.69 (m)
3′	2.34 (t, *J*=7.5)	33.7	-
4′		32.1	
5′-27′	1.39 – 1.20 (m)	29.8-28.9	1.25 (m)
28′		26.1	
29′		22.8	
30′	0.88 (t, *J*=6.7)	14.3	0.89 (t, *J*=7.0)
3-OMe	3.93	56.1	3.93

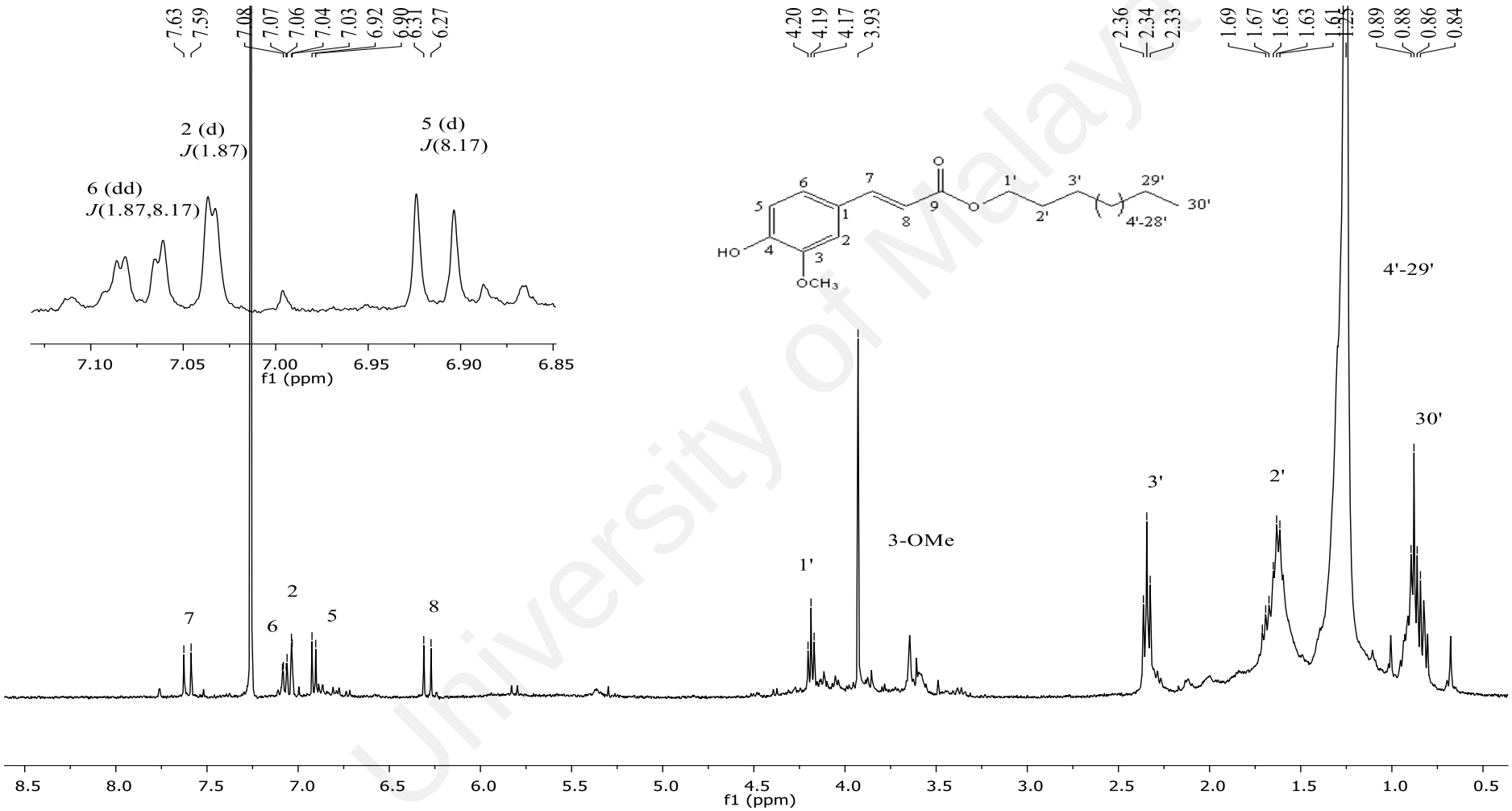

Figure 4.14: ^{1}H NMR spectrum of tetracosyl ferulate **124**.

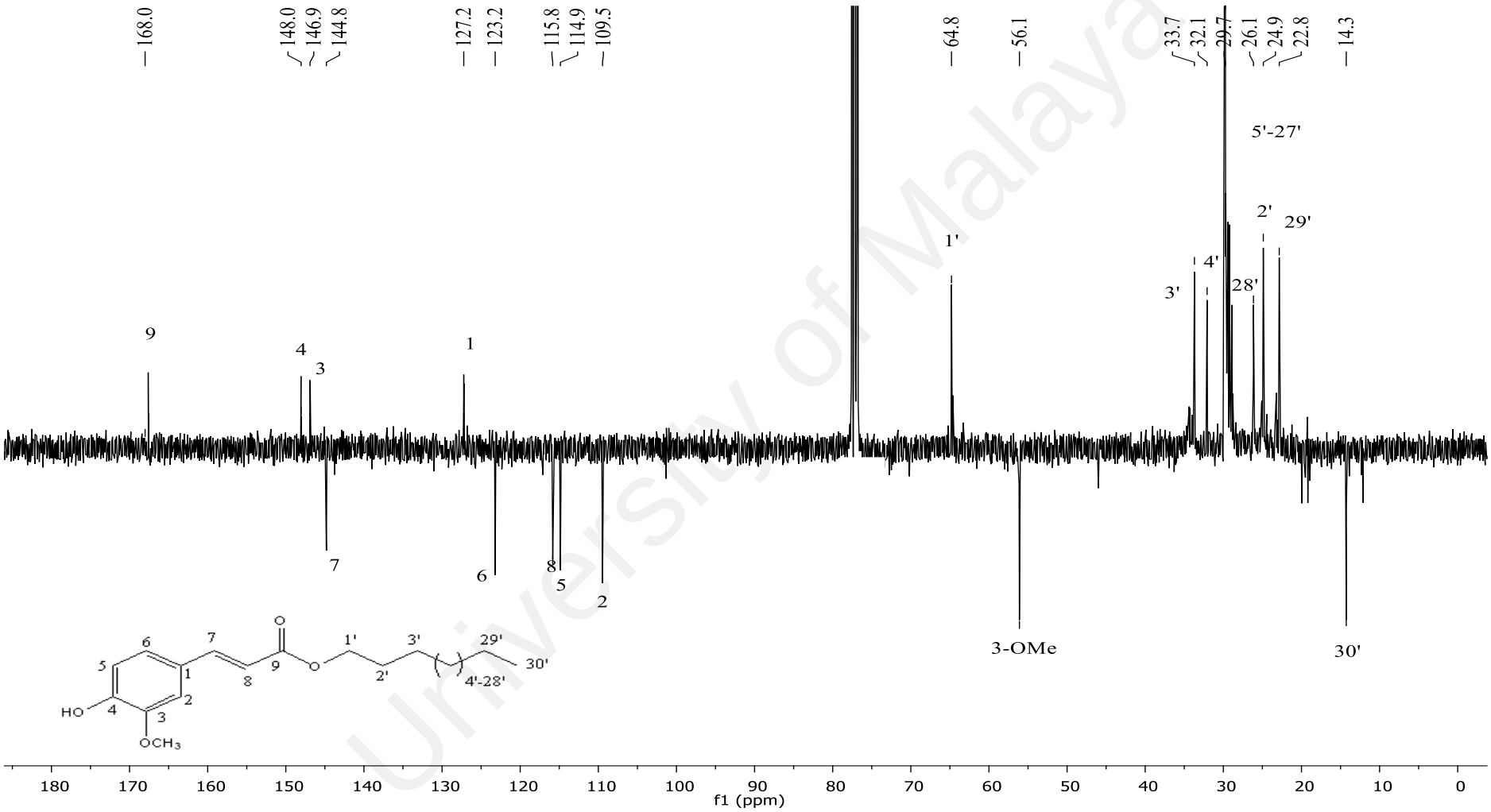

Figure 4.15: DEPT-Q NMR spectrum of tetracosyl ferulate **124**.

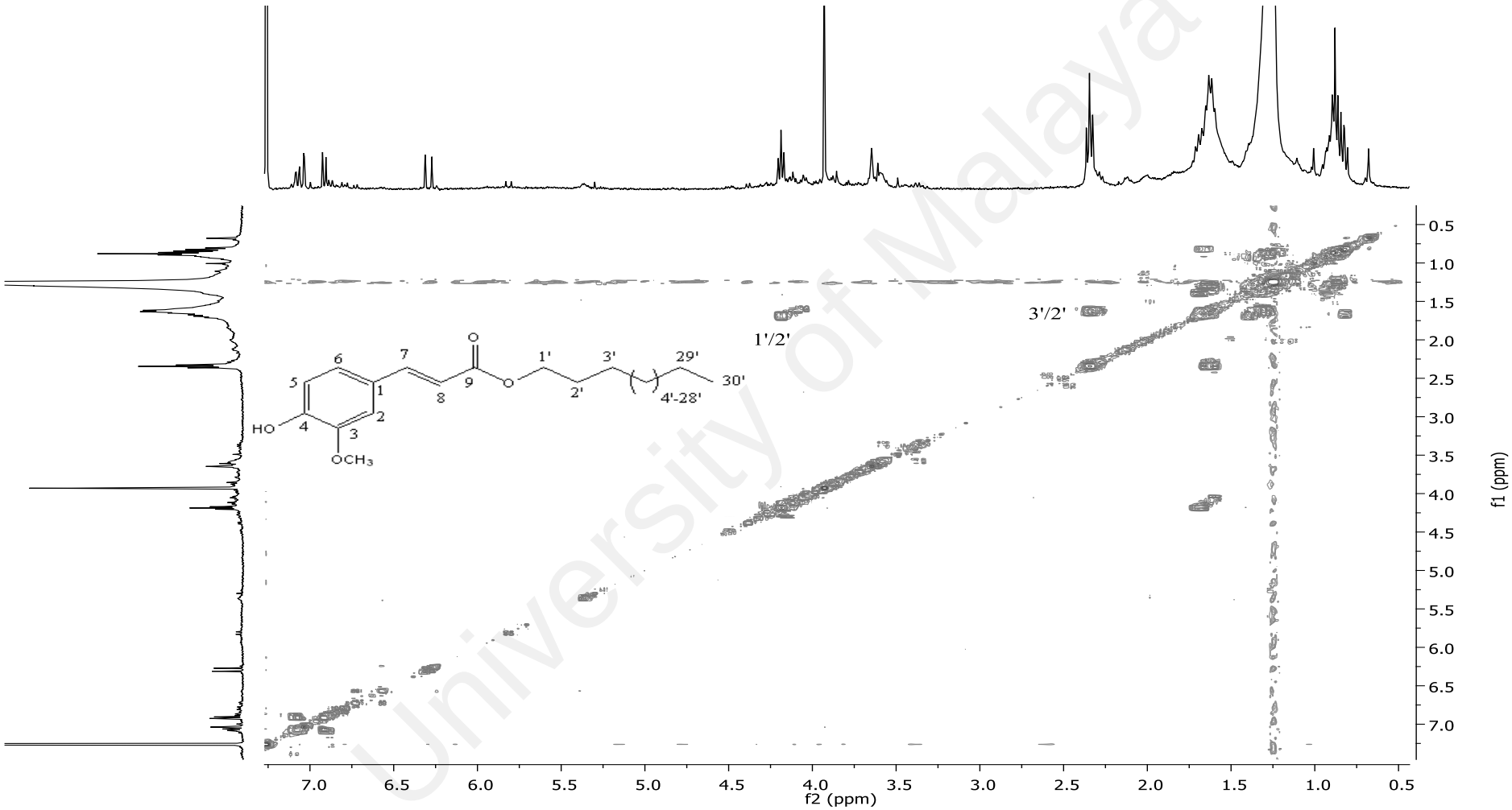

Figure 4.16: COSY NMR spectrum of tetracosyl ferulate **124**.

4.1.5 9-Hydroxy-1-(4-hydroxy-3-methoxyphenyl)propane-7-one 125

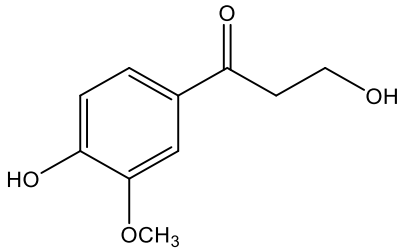

125

Compound **125**, isolated as yellow amorphous powder, was assigned the molecular formula $C_{10}H_{12}O_4$ with five degrees of unsaturation as deduced from its positive LCMS-IT-TOF analysis $[M+H]^+$ at m/z 197.0853 (calcd. for $C_{10}H_{13}O_4$, 197.0736). The IR spectrum revealed absorption bands at 3271 cm^{-1} and 1628 cm^{-1} due to the presence of hydroxyl and conjugated carbonyl functional group, respectively (Westwood et al., 2016).

The ^{1}H NMR spectrum (Figure 4.17) showed three aromatic protons, two aliphatic protons and one methoxy proton signals. The most deshielded proton signals appeared at δ_H 6.97 (d, J = 8.0 Hz), δ_H 7.54 (d, J = 2.7 Hz), and δ_H 7.56 (dd, J = 8.0 and 2.7 Hz) indicated the presence of a 1,3,4-trisubstituted benzene moiety, corresponding to H-5, H-2 and H-6, respectively. The methoxy peak was observed at δ_H 3.96. Furthermore, two triplets were observed at δ_H 3.20 and δ_H 4.03 attributable to aliphatic protons H-9 and H-8, respectively.

Assignments of the above protons were further established by the COSY spectrum. The homonuclear coupling between H-8/H-9 and H-5/H-6 (Figure 4.19), further confirmed the structure of compound **125**. The ^{13}C NMR spectrum (Figure 4.18) showed the presence of ten carbon resonances comprising one carbonyl carbon at most downfield region at δ_C 199.2.

The complete assignments of the ^{1}H NMR and ^{13}C NMR spectroscopic data of compound **125** were achieved with the aid of the COSY, HMBC and HSQC experiments. All of the above-mentioned NMR spectroscopic data of compound **125** and upon

comparison with literature values, was identified as 9-hydroxy-1-(4-hydroxy-3-methoxyphenyl)propane-7-one.

Table 4.6: ^{1}H (400 MHz) and ^{13}C (100MHz) data of 9-hydroxy-1-(4-hydroxy-3-methoxyphenyl)propane-7-one **125** (δ in ppm) in $CDCl_3$.

	9-Hydroxy-1-(4-hydroxy-3-methoxyphenyl)propane-7-one **125**		9-Hydroxy-1-(4-hydroxy-3-methoxyphenyl)propane-7-one (Westwood et al., 2016)	
Position	δ_H (*m*, *J* in Hz) in $CDCl_3$ (**125**)	δ_C in $CDCl_3$ (**125**)	δ_H (*m*, *J* in Hz) in $CDCl_3$	δ_C in $CDCl_3$
1	-	129.8	-	123.8
2	7.54 (d, *J*=2.7)	109.8	7.58-7.50 (m)	109.7
3	-	146.9	-	146.8
4	-	151.0	-	150.9
5	6.97 (d, *J*=8.0)	114.1	6.95 (d, *J*=8.1)	114.1
6	7.56 (dd, *J*=8.0, 2.7)	123.8	7.58-7.50 (m)	129.8
7	-	199.2	-	199.2
8	4.03 (t)	58.5	4.02 (t, *J*=5.3)	56.2
9	3.20 (t)	39.9	3.19 (t, *J*=5.3)	39.9
3-OMe	3.96	56.3	3.96	58.5

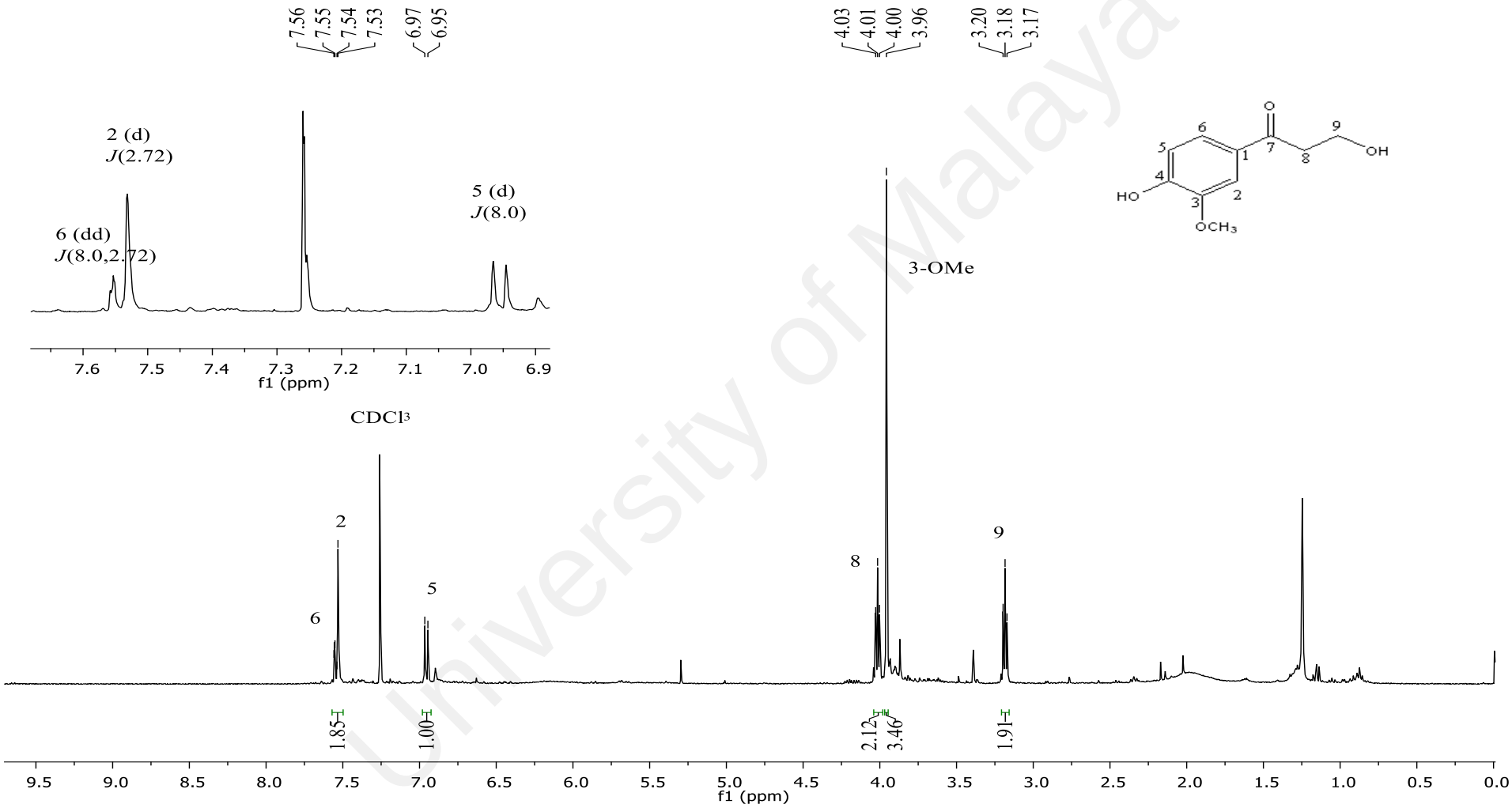

Figure 4.17: ^{1}H NMR spectrum of 9-hydroxy-1-(4-hydroxy-3-methoxyphenyl)propane-7-one **125**.

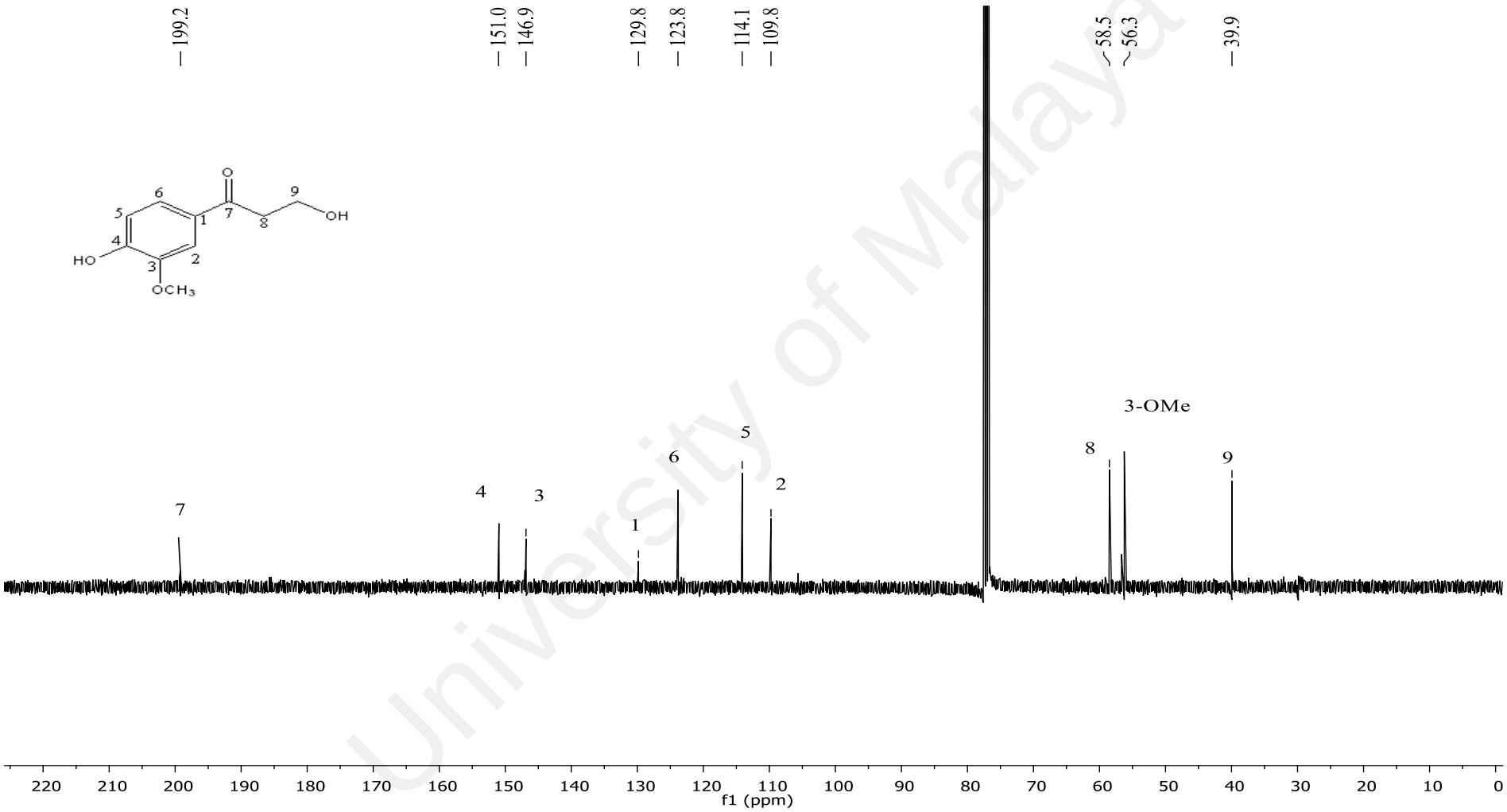

Figure 4.18: ^{13}C NMR spectrum of 9-hydroxy-1-(4-hydroxy-3-methoxyphenyl)propane-7-one **125**.

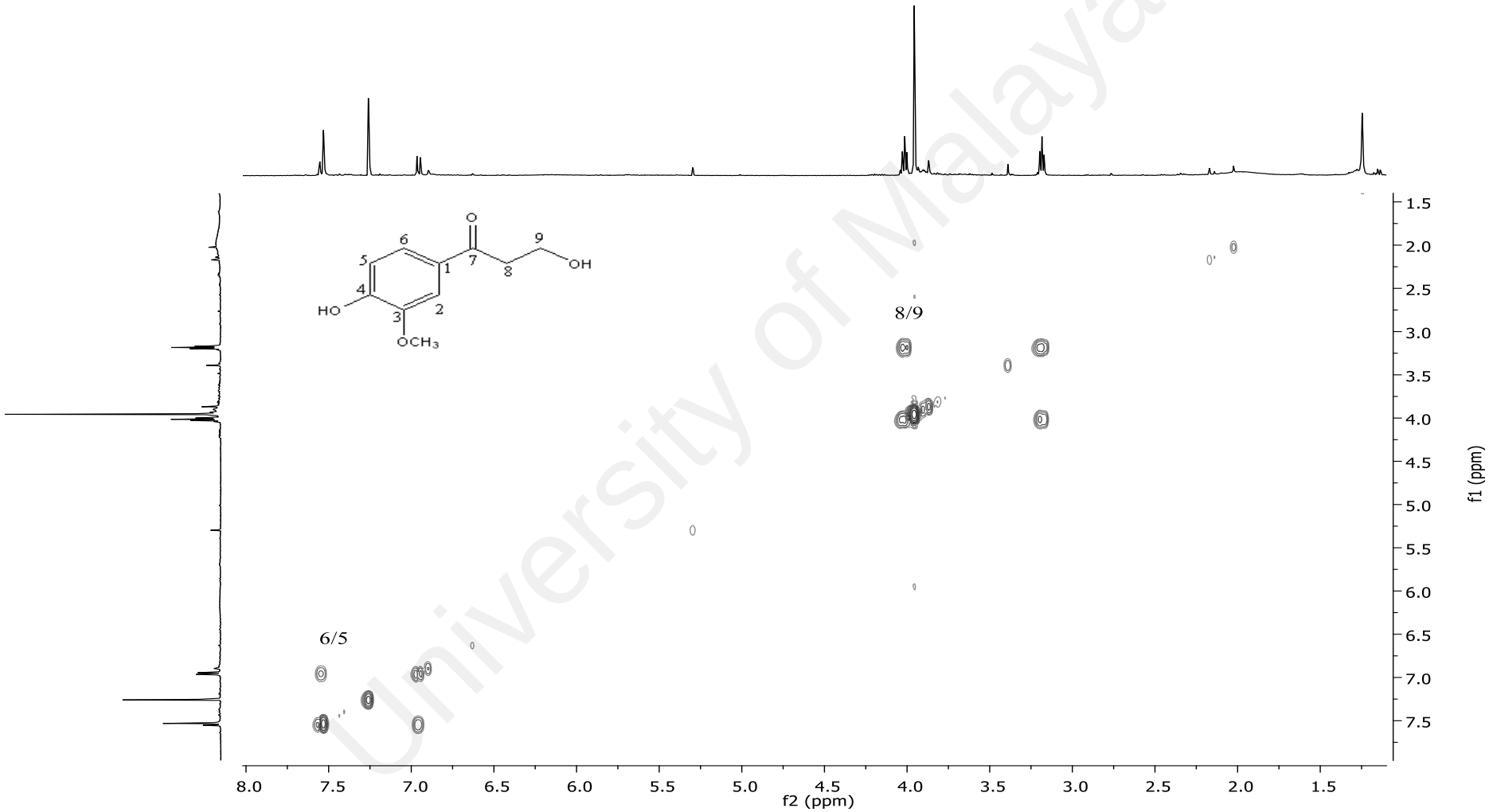

Figure 4.19: COSY spectrum of 9-hydroxy-1-(4-hydroxy-3-methoxyphenyl)propane-7-one **125**.

4.1.6 3,4-Dimethoxybenzoic acid 126

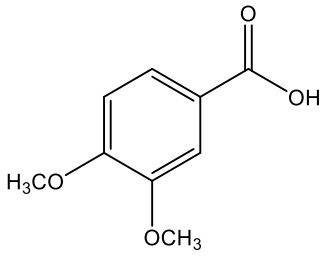

126

Compound **126** was isolated as light yellow amorphous powder. The positive LCMS-IT-TOF analysis exhibited pseudomolecular ion $[M+H]^+$ at m/z 183.0703 (calcd. for $C_9H_{11}O_4$, 183.0613), attributable to the molecular formula of $C_9H_{10}O_4$, consistent with five degrees of unsaturation. The IR spectrum indicated the presence of carboxylic acid moiety at 1725 cm^{-1} (Ezzat et al., 2017).

The ^{1}H NMR (Figure 4.20) and DEPT-Q NMR (Figure 4.21) spectroscopic data of compound **126** were comparable to those of compound **125**, hence suggesting the possibility of compound **126** being structurally related to compound **125**. Similarity can be seen at most deshielded proton signals appeared at δ_H 6.87 (d, J = 8.3 Hz), δ_H 7.46 (d, J = 2.0 Hz), and δ_H 7.32 (dd, J = 8.3 and 2.0 Hz) indicated the presence of a 1,3,4-trisubstituted benzene moiety, corresponding to H-5, H-2 and H-6, respectively. There was however a significant difference as compound **126**, exhibited two methoxy groups at position 3 (δ_H 3.94; δ_C 56.2) and at position 4 (δ_H 3.93; δ_C 56.2).

The complete assignments of the ^{1}H NMR and DEPT-Q NMR spectroscopic data of compound **126** were achieved with the aid of the COSY, HMBC and HSQC experiments. All of the above-mentioned NMR spectroscopic data of compound **126** and upon comparison with literature (Table 4.7), it was identified as 3,4-dimethoxybenzoic acid.

Table 4.7: ^{1}H (400 MHz) and DEPT-Q (100 MHz) NMR data of 3,4-Dimethoxybenzoic acid **126** (δ in ppm) in $CDCl_3$.

	3,4-Dimethoxybenzoic acid **126**		3,4-Dimethoxybenzoic acid (Crestini et al., 2006)	
Position	δ_H (*m*, *J* in Hz) in $CDCl_3$ (**126**)	δ_C in $CDCl_3$ (**126**)	δ_H (*m*, *J* in Hz) in $CDCl_3$	δ_C in $CDCl_3$
1	-	126.0	-	121.9
2	7.46 (d, *J*=2.0)	111.0	7.68 (m)	112.3
3	-	149.2	-	147.1
4	-	152.4	-	151.0
5	6.87 (d, *J*=8.3)	110.4	6.93 (d, *J*=8.7)	114.2
6	7.32 (d, *J*=2.0, 8.3)	120.2	7.68 (m)	123.7
7	-	169.0	-	168.8
3-OMe	3.94	56.2	3.80	54.3
4-OMe	3.93	56.2	3.78	54.1

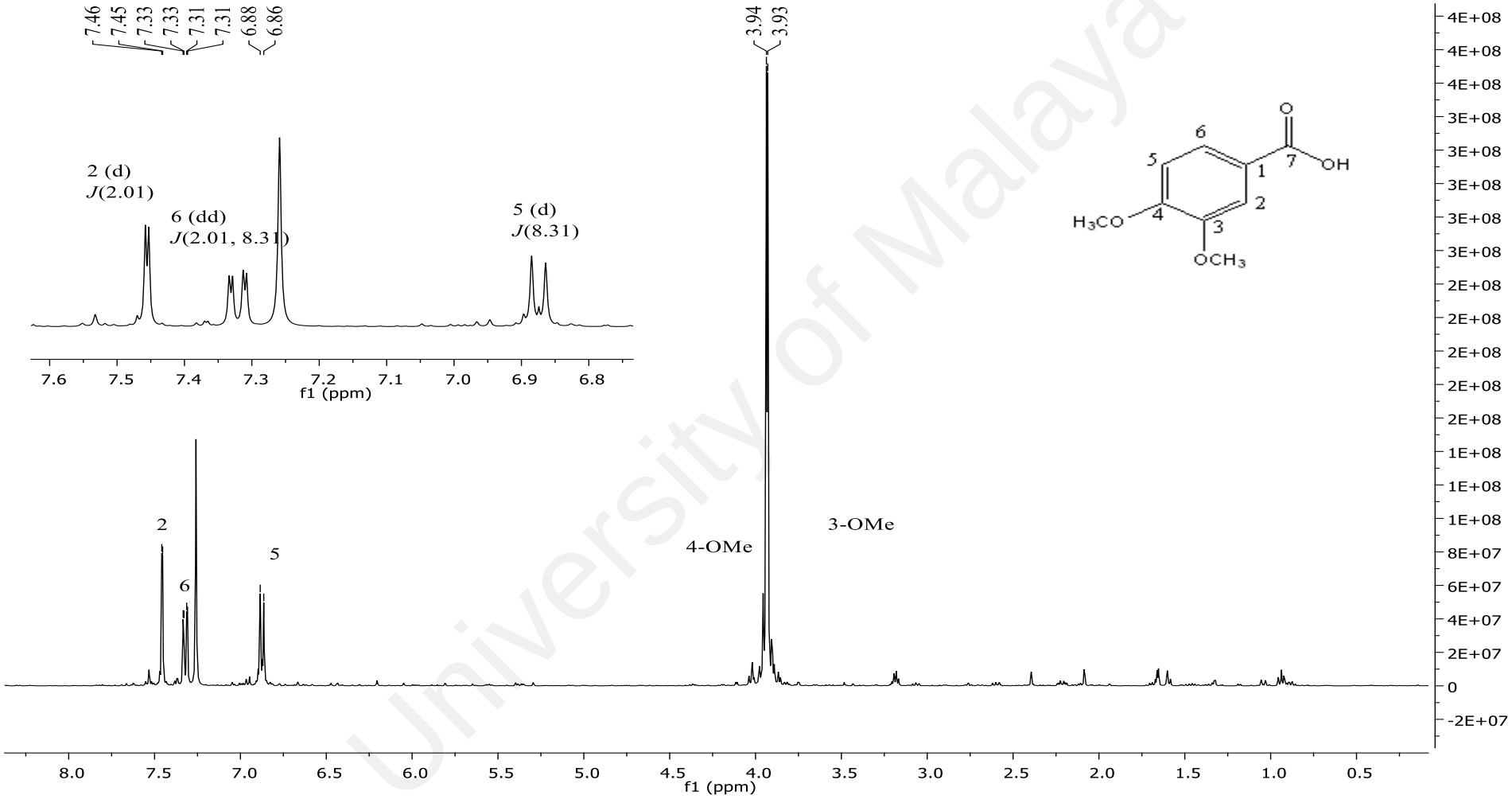

Figure 4.20: ^{1}H NMR spectrum of 3,4-dimethoxybenzoic acid **126**.

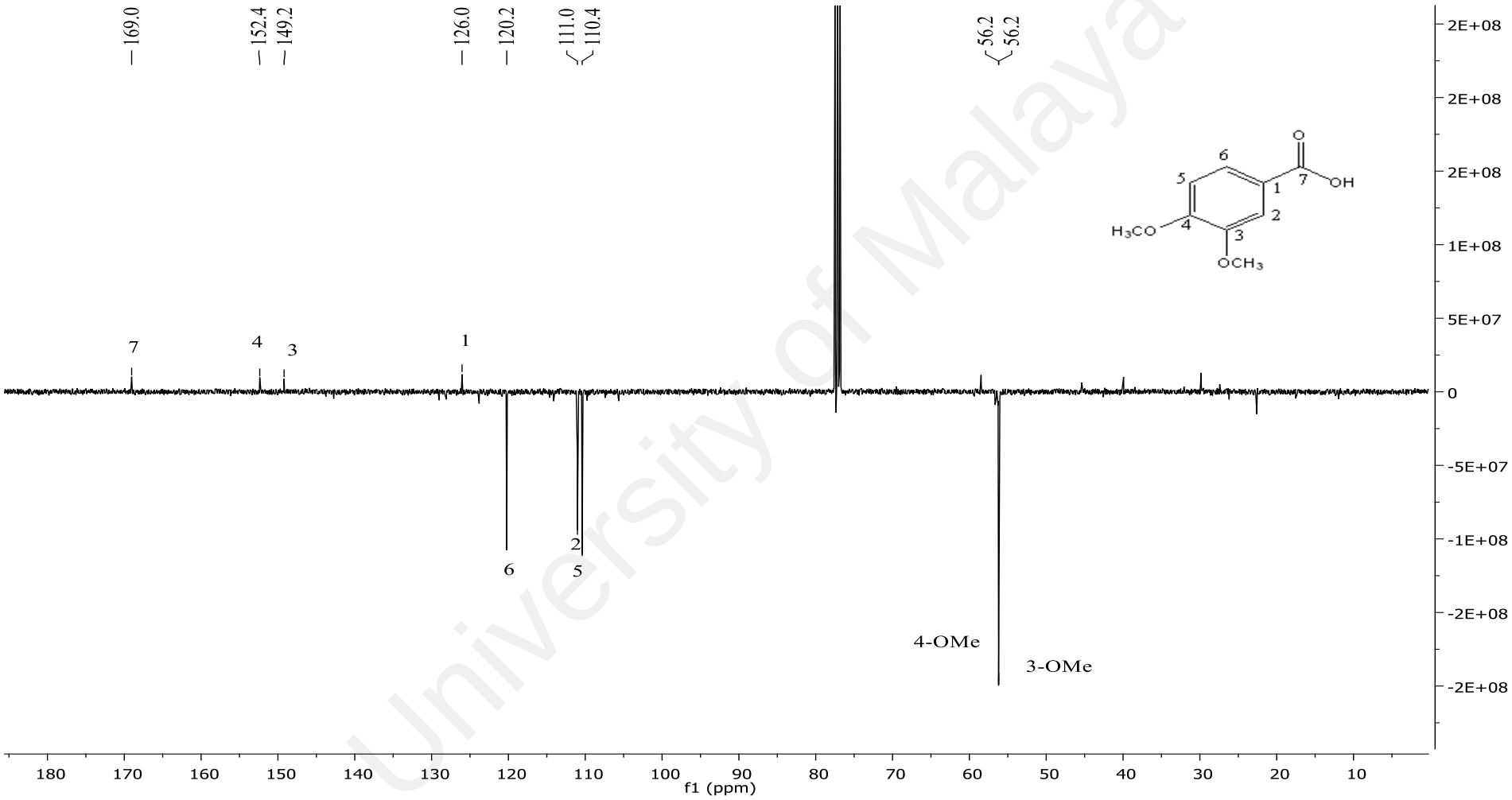

Figure 4.21: DEPT-Q NMR spectrum of 3,4-dimethoxybenzoic acid **126**.

4.1.7 2-(Methoxy)benzoic acid 127

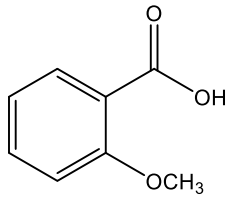

127

Compound **127** was isolated as light yellow amorphous powder. It was assigned a molecular formula of $C_8H_8O_3$ as deduced from its positive LCMS-IT-TOF analysis $[M+H]^+$ at m/z 153.0565 (calcd. for $C_8H_9O_3$, 153.0507), corresponding to five degrees of unsaturation. The IR spectrum indicated the presence of carboxylic acid moiety at 1720 cm^{-1} (X. Wang et al., 2016).

The ^{1}H NMR (Figure 4.22) and DEPT-Q NMR (Figure 4.23) spectroscopic data of compound **127** were comparable to those of compounds **125** and **126**, thus supporting the fact that compound **127** structurally resembled to both compounds. Nevertheless, there was a significant difference between these compounds. In contrary to the two compounds had a 1,3,4-trisubstituted aromatic ring, while compound **127** was a 1,2-disubstituted aromatic ring with δ_H 7.00 (d, J = 7.9 Hz), δ_C 111.5; δ_H 7.49 (d, J = 1.9 and 7.9 Hz), δ_C 133.7; δ_H 7.09 (d, J = 7.9 Hz), δ_C 121.5 and δ_H 8.21 (dd, J = 1.9 and 7.9 Hz) corresponding to H-3, H-4, H-5 and H-6, respectively.

The complete assignments of the ^{1}H NMR and DEPT-Q NMR spectroscopic data of compound **127** were achieved with the aid of the COSY, HMBC and HSQC experiments. Based on the above-mentioned NMR spectroscopic data of compound **127** and upon comparison with literature values (Table 4.8), the compound was identified as 2-(methoxy)benzoic acid.

Table 4.8: ^{1}H (400 MHz) and DEPT-Q (100 MHz) NMR data of 2-(methoxy)benzoic acid **127** (δ in ppm) in $CDCl_3$.

	2-(methoxy)benzoic acid **127**		2-(methoxy)benzoic acid (X. Wang et al., 2016)	
Position	δ_H (*m*, *J* in Hz) in $CDCl_3$ (**127**)	δ_C in $CDCl_3$ (**127**)	δ_H (*m*, *J* in Hz) in $CDCl_3$	δ_C in $CDCl_3$
1	-	120.6	-	117.4
2	-	158.0	-	158.1
3	7.00 (d, *J*=7.9)	111.5	7.07 (d, *J*=6.0)	111.6
4	7.49 (dd, *J*=1.9, 7.9)	133.7	7.13 (t, *J*=6.0)	135.0
5	7.09 (d, *J*=7.9)	121.5	7.58 (t, *J*=6.0)	122.0
6	8.21 (dd, *J*=1.9, 7.9)	132.8	8.17 (d, *J*=6.0)	133.6
7	-	167.3	-	165.7
2-OMe	3.98	56.1	4.08	56.6

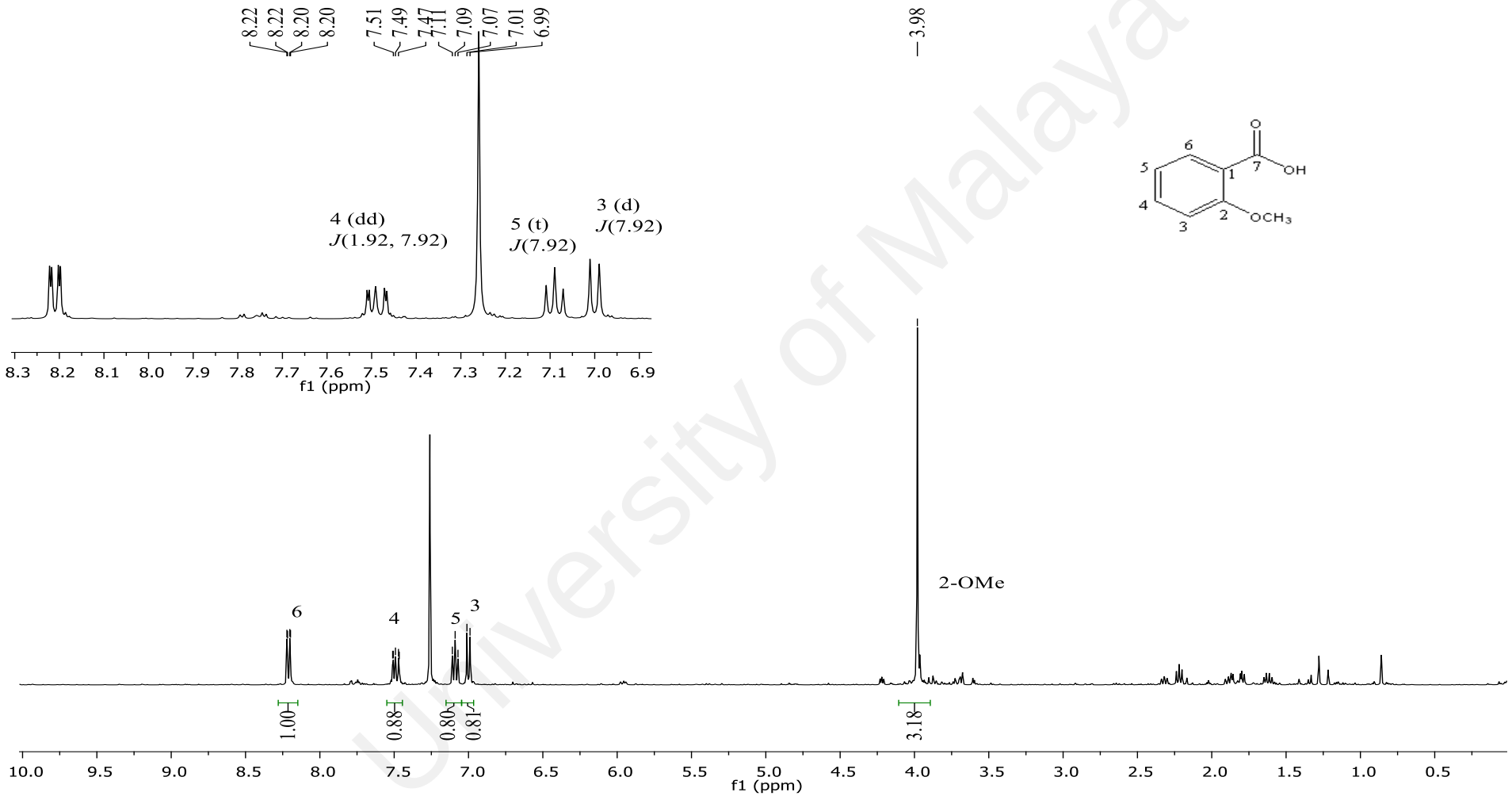

Figure 4.22: ^{1}H NMR spectrum of 2-(methoxy)benzoic acid **127**.

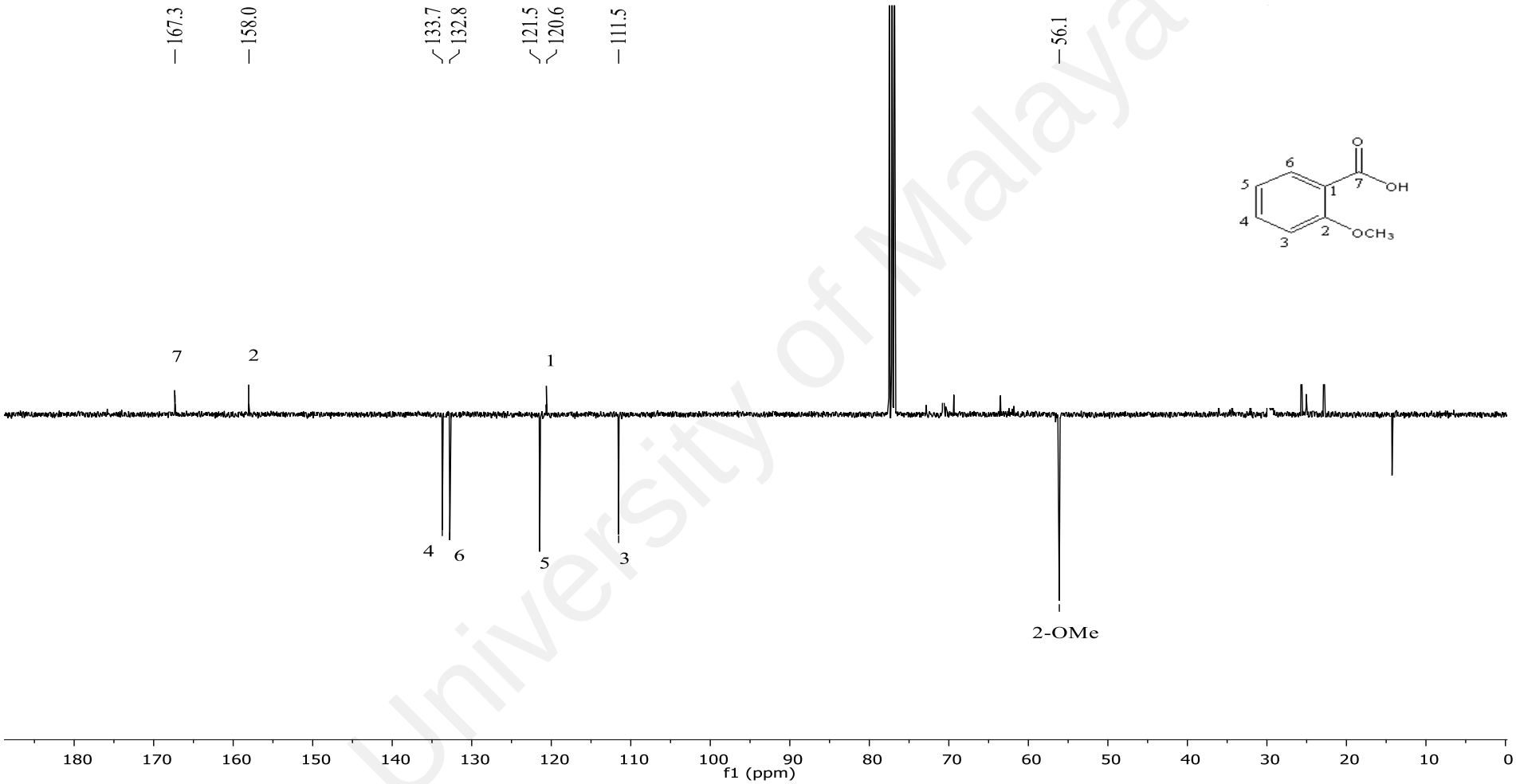

Figure 4.23: DEPT-Q NMR spectrum of 2-(methoxy)benzoic acid **127**.

4.1.8 4-Hydroxybenzaldehyde 128

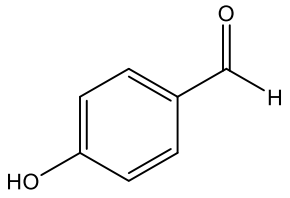

128

Compound **128**, isolated as a yellow amorphous powder. Its positive LCMS-IT-TOF analysis which exhibited pseudo-molecular ion, $[M+H]^+$ at m/z 123.0565 (calcd. for $C_7H_7O_2$, 123.0401) in agreement with the molecular formula of $C_7H_6O_2$, corresponding to five degrees of unsaturation. The IR spectrum revealed absorption bands at ν_{max} 1731 and 3401 cm^{-1}, consistent with the presence of hydroxyl and an aldehyde group, respectively in the molecule (Hsu et al., 2009).

The ^{1}H-NMR (Figure 4.24) and ^{13}C-NMR (Figure 4.25) spectral spectroscopic data of compound **128** were comparable to those of compound **127**, thus, supporting the fact that compound **128** was indeed structurally related to compound **127**. There was however a significant difference on splitting pattern between these two compounds. Unlike compound **127** which had a 1,2-disubstituted aromatic ring, compound **128** revealed the presence of a 1,4-disubstituted aromatic ring with a pair of characteristic AA'BB' doublets [δ_H 7.81 (d, J = 8.4 Hz, H-2 & H-6; δ_C 132.6, C-2 & C-6) and δ_H 6.96 (d, J = 8.4 Hz, H-3 & H-5; δ_C 116.2, C-3 & C-5)].

The complete assignments of the ^{1}H-NMR and ^{13}C-NMR spectroscopic data of compound **128** were achieved with the aid of the COSY, HMBC and HSQC experiments. All of the above-mentioned NMR spectroscopic data of compound **128** and upon comparison with literature values (Table 4.9), it was identified as 4-hydroxybenzaldehyde (Hsu et al., 2009).

Table 4.9: ^{1}H (400 MHz) and ^{13}C (100 MHz) NMR data of 4-hydroxybenzaldehyde **128** (δ in ppm) in $CDCl_3$.

	4-Hydroxybenzaldehyde **128**		4-Hydroxybenzaldehyde (Hsu et al., 2009)	
Position	δ_H (*m*, *J* in Hz) in $CDCl_3$ (**128**)	δ_C in $CDCl_3$ (**128**)	δ_H (*m*, *J* in Hz) in $CDCl_3$	δ_C in $CDCl_3$
1	-	130.4	-	129.9
2	7.81 (d, *J*=8.40)	132.6	7.81 (d, *J*=8.70)	132.3
3	6.96 (d, *J*=8.40)	116.2	6.95 (d, *J*=8.40)	115.9
4	-	161.5	-	161.5
5	6.96 (d, *J*=8.40)	116.2	6.95 (d, *J*=8.40)	115.9
6	7.81 (d, *J*=8.40)	132.6	7.81 (d, *J*=8.70)	132.3
7	-	191.1	9.86	190.9

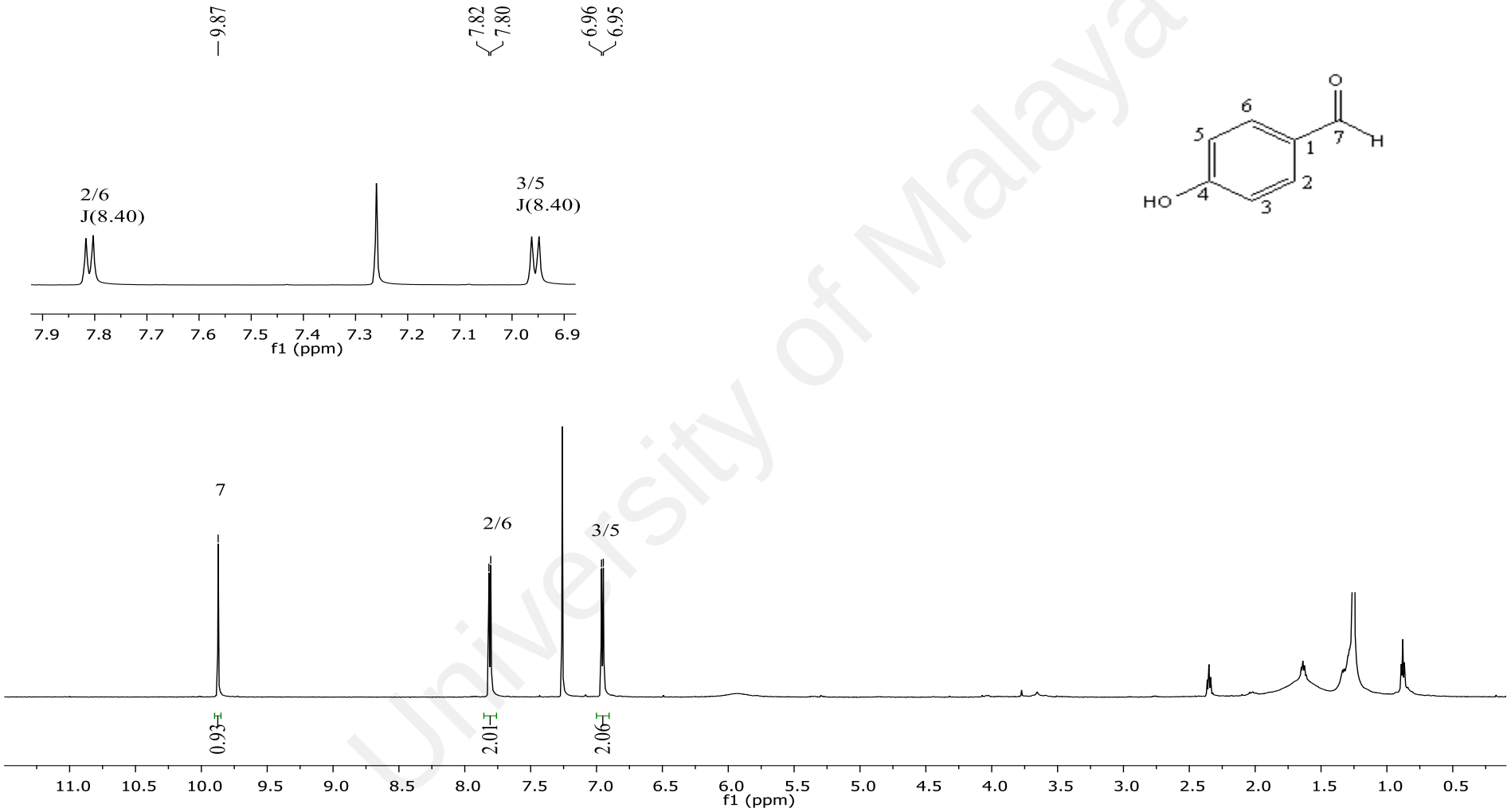

Figure 4.24: ^{1}H NMR spectrum of 4-hydroxybenzaldehyde **128**.

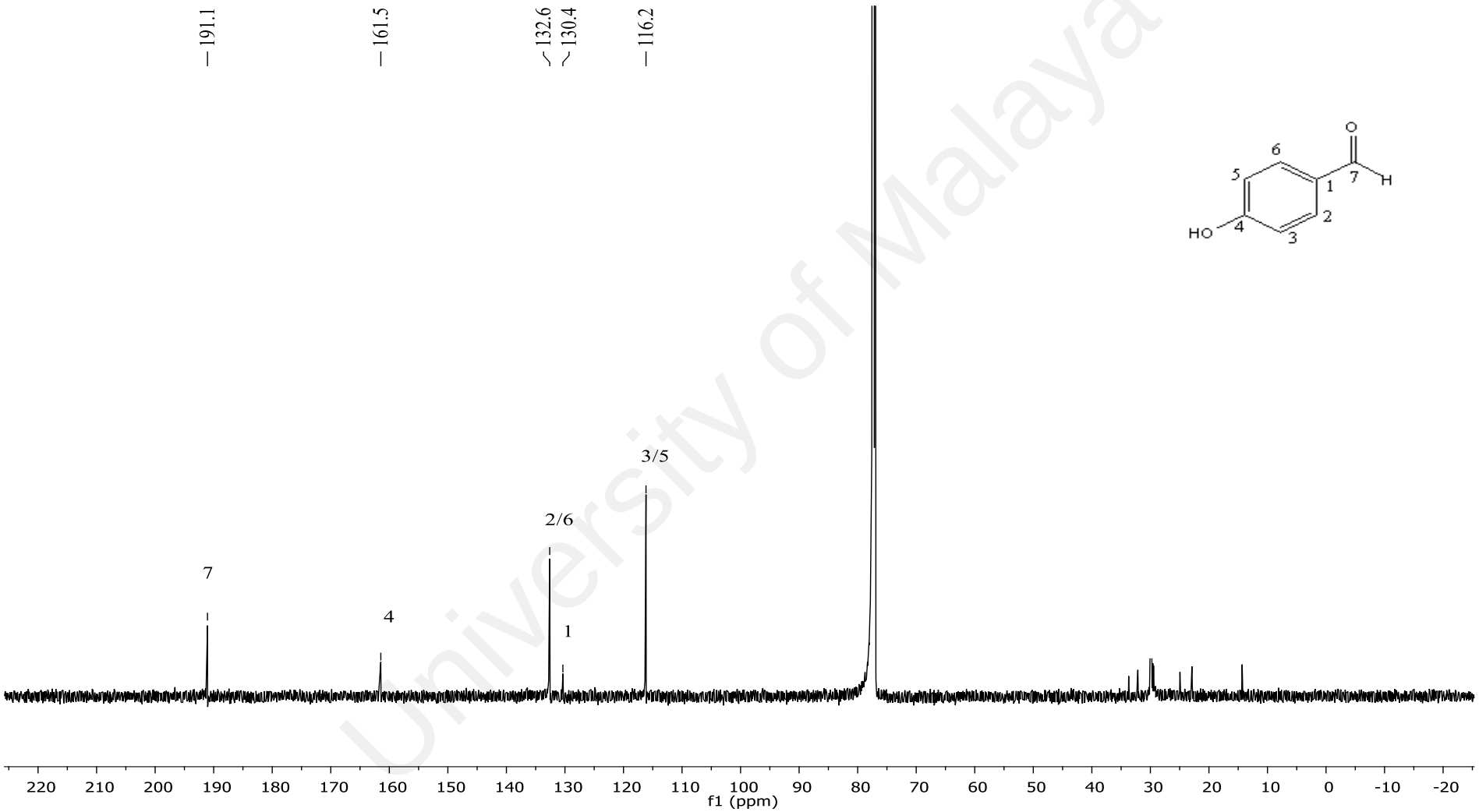

Figure 4.25: ^{13}C NMR spectrum of 4-hydroxybenzaldehyde **128**.

4.1.9 2,6-*Bis*(1-hydroxyethyl)benzoic acid 129

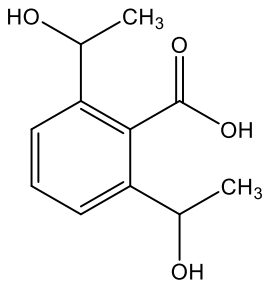

129

Compound **129** was isolated as a yellow amorphous powder and was assigned the molecular formula $C_{11}H_{14}O_4$ with five degrees of unsaturation deduced as from its positive LCMS-IT-TOF analysis $[M+H]^+$ at m/z 211.0954 (calcd. for $C_{11}H_{15}O_4$, 211.0926). The IR spectrum revealed absorption bands at 3251 cm^{-1} and 1704 cm^{-1}, due to hydroxyl groups and carboxylic acid moiety (X. Wang et al., 2016).

The ^{1}H NMR spectrum (Figure 4.26) of compound **129** showed spin systems for 1,2,6-trisubstituted ring [δ_H 7.03 (d, J = 7.6 Hz, H-3; δ_C 116.3, C-3), δ_H 7.55 (dd, J = 7.6 and 8.4 Hz, H-4; δ_C 137.0, C-4) and δ_H 7.01 (d, J = 8.4 Hz, H-5; δ_C 118.0, C-5)]. The multiplet signals in the upfield region were assigned to the methine protons which were observed at δ_H 4.61 attributable to H-8 and H-9. Furthermore, in the most upfield region two sharp overlapping doublets at δ_H 1.53 corresponded to the two methyls at C-8 and C-9.

The ^{13}C NMR spectrum (Figure 4.27) of compound **129** showed eleven carbon peaks with three aromatic carbons, two methine carbons, three quartenary carbons, two methyls and one carbonyl carbon. The deshielded signal at δ_C 162.2 was assigned to the carboxylic acid. Two oxygenated carbon signals detected at δ_C 80.1 and δ_C 69.4, and were ascribable to the aliphatic carbons C-8 and C-9, respectively. Other carbon values are displayed in Table 4.10.

The complete assignments of the ^{1}H NMR and ^{13}C NMR spectroscopic data of compound **129** were achieved with the aid of the COSY, HMBC and HSQC experiments.

COSY spectrum showed correlation of H-9 with H-10 and H-8 with H-11. This implied that H-9 and H-10, H-8 and H-11 are one ^{1}H-^{1}H spin system. Thorough and detailed analysis of the 2D NMR proved that the structure of compound **129** is 2,6-*bis*(1-hydroxyethyl)benzoic acid.

Table 4.10: ^{1}H (400 MHz) and ^{13}C (100 MHz) data of 2,6-*bis*(1-hydroxyethyl)benzoic acid **129** (δ in ppm) in $CDCl_3$.

	2,6-*Bis*(1-hydroxyethyl)benzoic acid **129**		2,6-*Bis*(1-hydroxyethyl)benzoic acid (Liu et al., 2016)	
Position	δ_H (*m*, *J* in Hz) in $CDCl_3$ (**129**)	δ_C in $CDCl_3$ (**129**)	δ_H (*m*, *J* in Hz) in $CDCl_3$	δ_C in $CDCl_3$
1	-	106.8	-	106.4
2	-	141.3	-	141.0
3	7.03 (d, *J*=7.6)	116.3	7.05 (d, *J*=7.6)	116.3
4	7.55 (dd, *J*=7.6, 8.4)	137.0	7.55 (dd, *J*=7.6, 8.4)	137.0
5	7.01 (d, *J*=8.4)	118.0	7.03 (d, *J*=8.4)	118.0
6	-	141.3	-	141.3
7		162.2		162.2
8	4.61 (m)	69.4	4.61 (m)	69.4
9	4.61 (m)	80.1	4.61 (m)	80.1
10	1.53 (d, *J*=6.19)	18.1	1.53 (d, *J*=6.19)	18.1
11	1.53 (d, *J*=6.19)	18.1	1.53 (d, *J*=6.19)	18.1

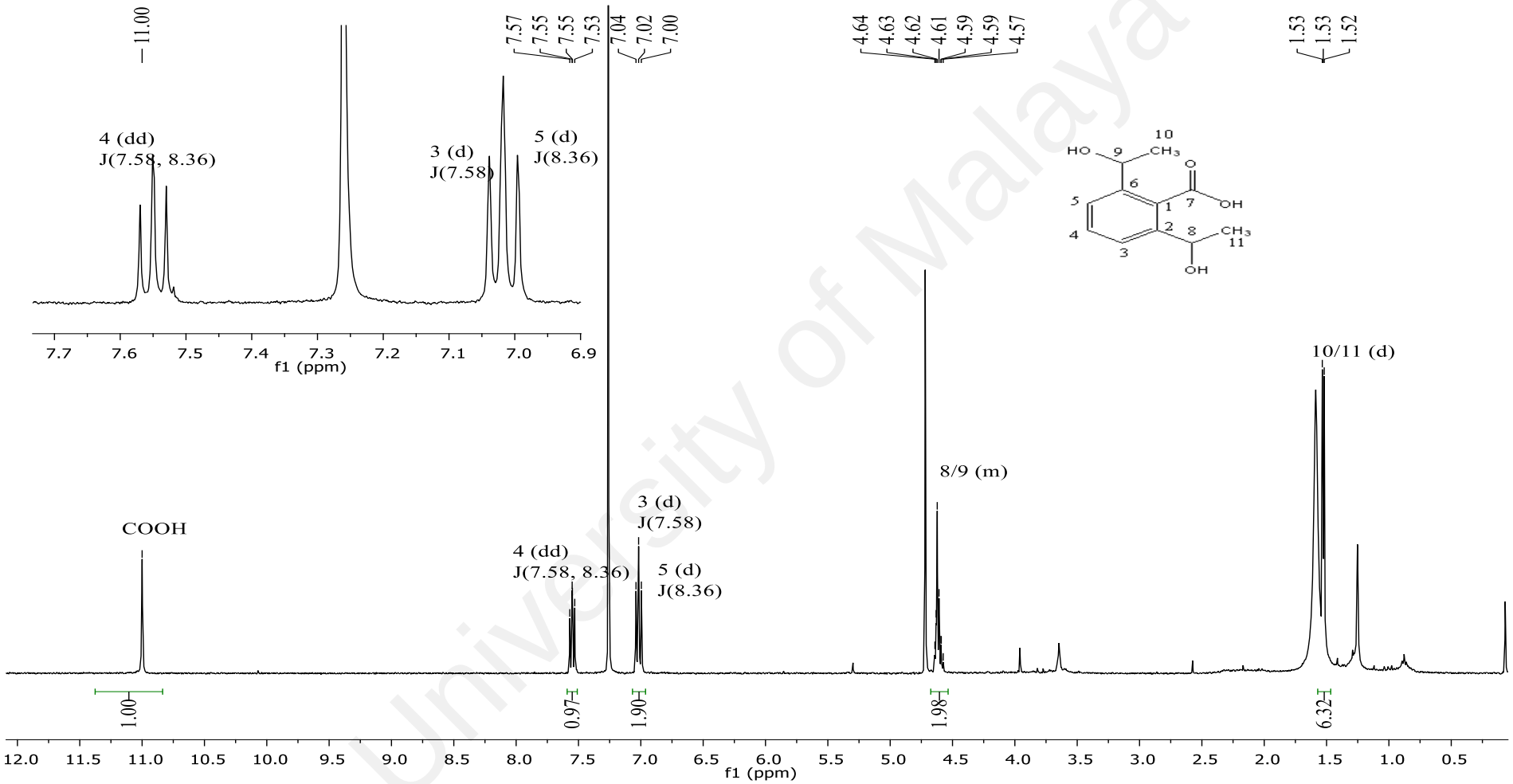

Figure 4.26: ^{1}H NMR spectrum of 2,6-*bis*(1-hydroxyethyl)benzoic acid **129**.

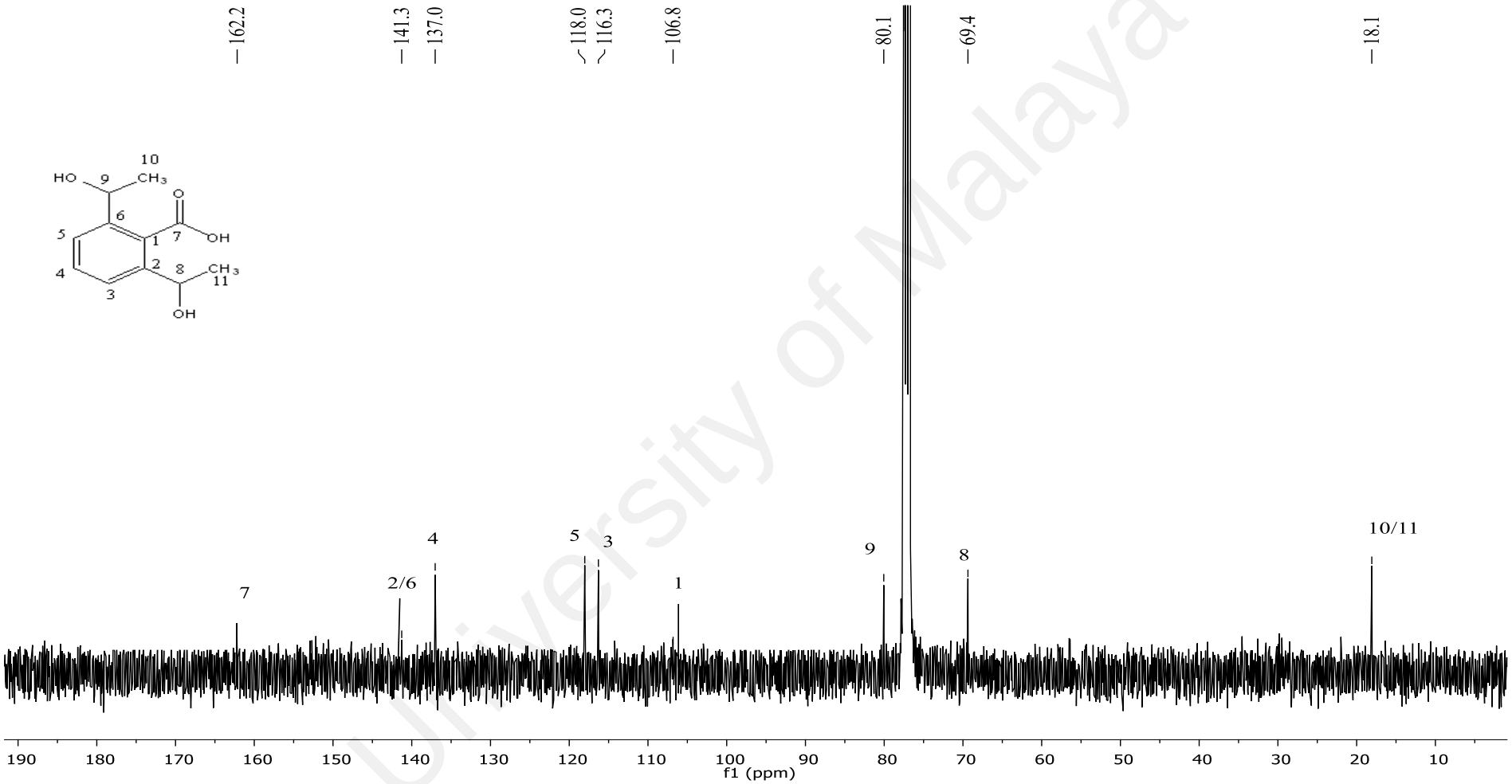

Figure 4.27: ^{13}C NMR spectrum of 2,6-*bis*(1-hydroxyethyl)benzoic acid **129**.

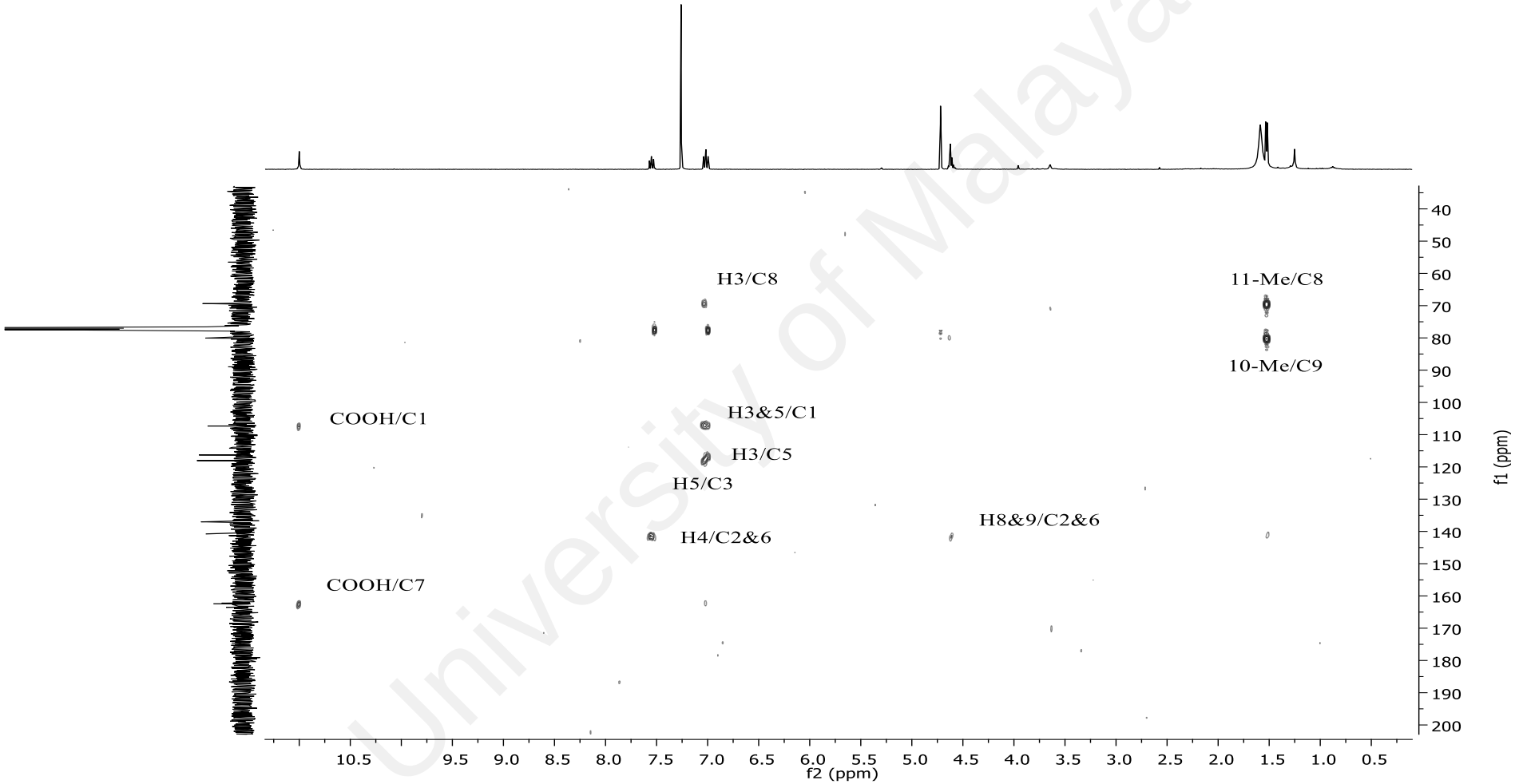

Figure 4.28: HMBC spectrum of 2,6-*bis*(1-hydroxyethyl)benzoic acid **129**.

4.1.10 Vanillic acid 132

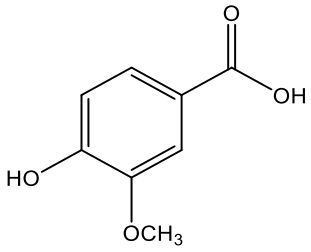

132

Compound **132** was isolated as light yellow amorphous powder. The positive LCMS-IT-TOF analysis exhibited pseudomolecular ion $[M+H]^+$ at m/z 169.0703 (calcd. for $C_8H_9O_4$, 169.0456), attributable to the molecular formula of $C_8H_8O_4$, consistent with five degrees of unsaturation. The IR spectrum indicated the presence of carboxylic acid moiety at 1725 cm^{-1} (Ezzat et al., 2017).

The ^{1}H NMR spectrum (Figure 4.29) and ^{13}C NMR spectrum (Figure 4.30) of compound **132** were comparable to those of compound **126**, hence suggesting the possibility of compound **132** being structurally related to compound **126**. Similarity can be seen at most deshielded proton signals appeared at δ_H 6.97 (d, J = 8.3 Hz), δ_H 7.59 (d, J = 1.9 Hz), and δ_H 7.71 (dd, J = 8.3 and 1.9 Hz) which indicated the presence of a 1,3,4-trisubstituted benzene moiety, corresponding to H-5, H-2 and H-6, respectively. There was however a significant difference as compound **132**, exhibited a three proton singlet at δ_H 3.97 (δ_C 56.3) for C-3 methoxy group.

The complete assignments of the ^{1}H NMR and ^{13}C NMR spectroscopic data of compound **132** were achieved with the aid of the COSY, HSQC, HMBC experiments and upon comparison with literature values (Table 4.11). Based upon these compound **132** it was identified as vanillic acid (Ezzat et al., 2017).

Table 4.11: ^{1}H (400 MHz) and ^{13}C (100 MHz) NMR data of vanillic acid **132** (δ in ppm) in $CDCl_3$.

	Vanillic acid **132**		Vanillic acid (Ezzat et al., 2017)	
Position	δ_H (*m*, *J* in Hz) in $CDCl_3$ (**132**)	δ_C in $CDCl_3$ (**132**)	δ_H (*m*, *J* in Hz) in $CDCl_3$	δ_C in $CDCl_3$
1	-	121.2	-	121.9
2	7.59 (d, *J*=1.8)	112.3	7.68 (m)	112.3
3	-	146.4	-	147.1
4	-	150.9	-	151.0
5	6.97 (d, *J*=8.3)	114.4	6.93 (d, *J*=8.7)	114.2
6	7.71 (dd, *J*=1.8, 8.3)	125.3	7.68 (m)	123.7
7	-	169.6	-	168.8
3-OMe	3.97	56.3	3.90	62.7

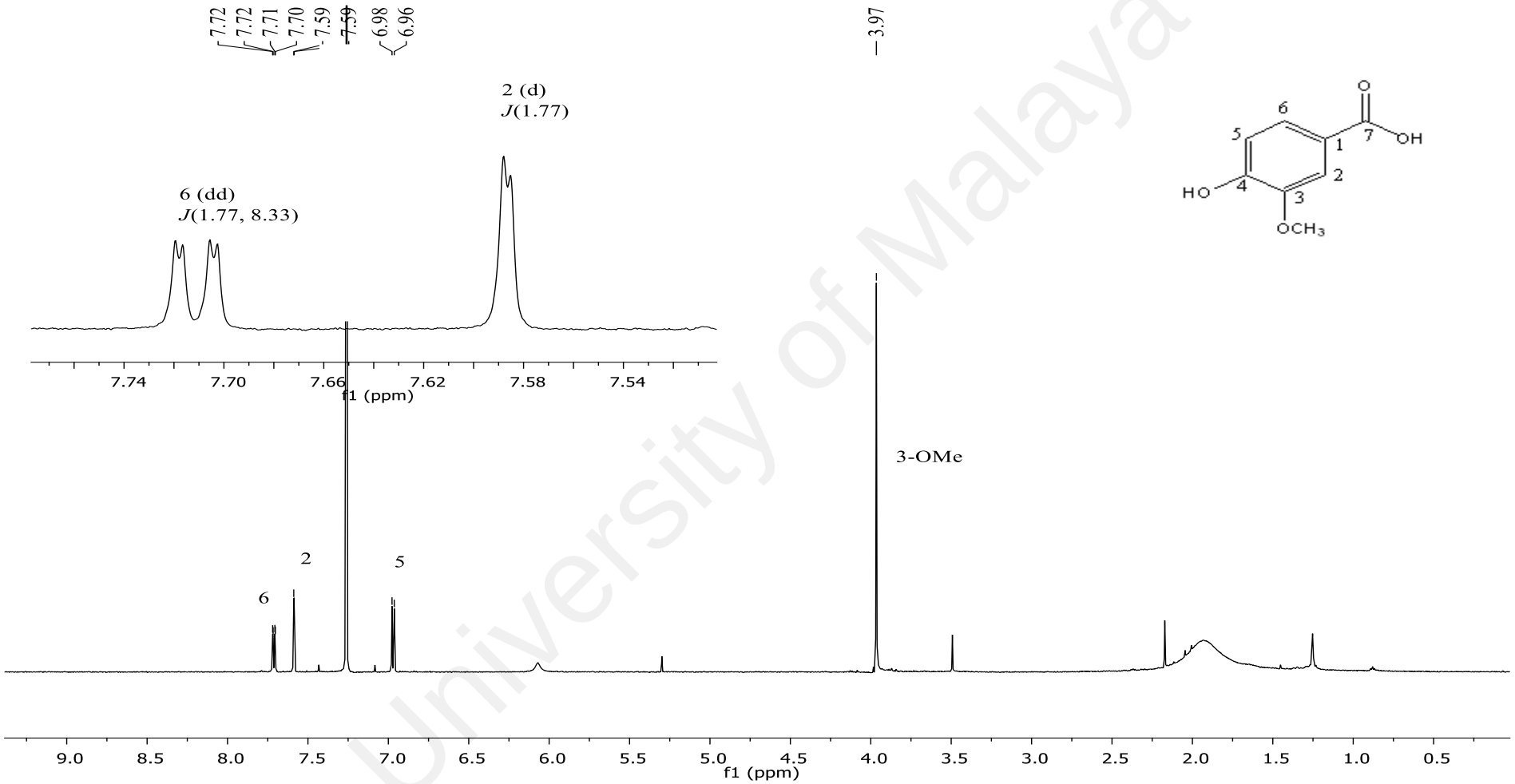

Figure 4.29: ^{1}H NMR spectrum of vanillic acid **132**.

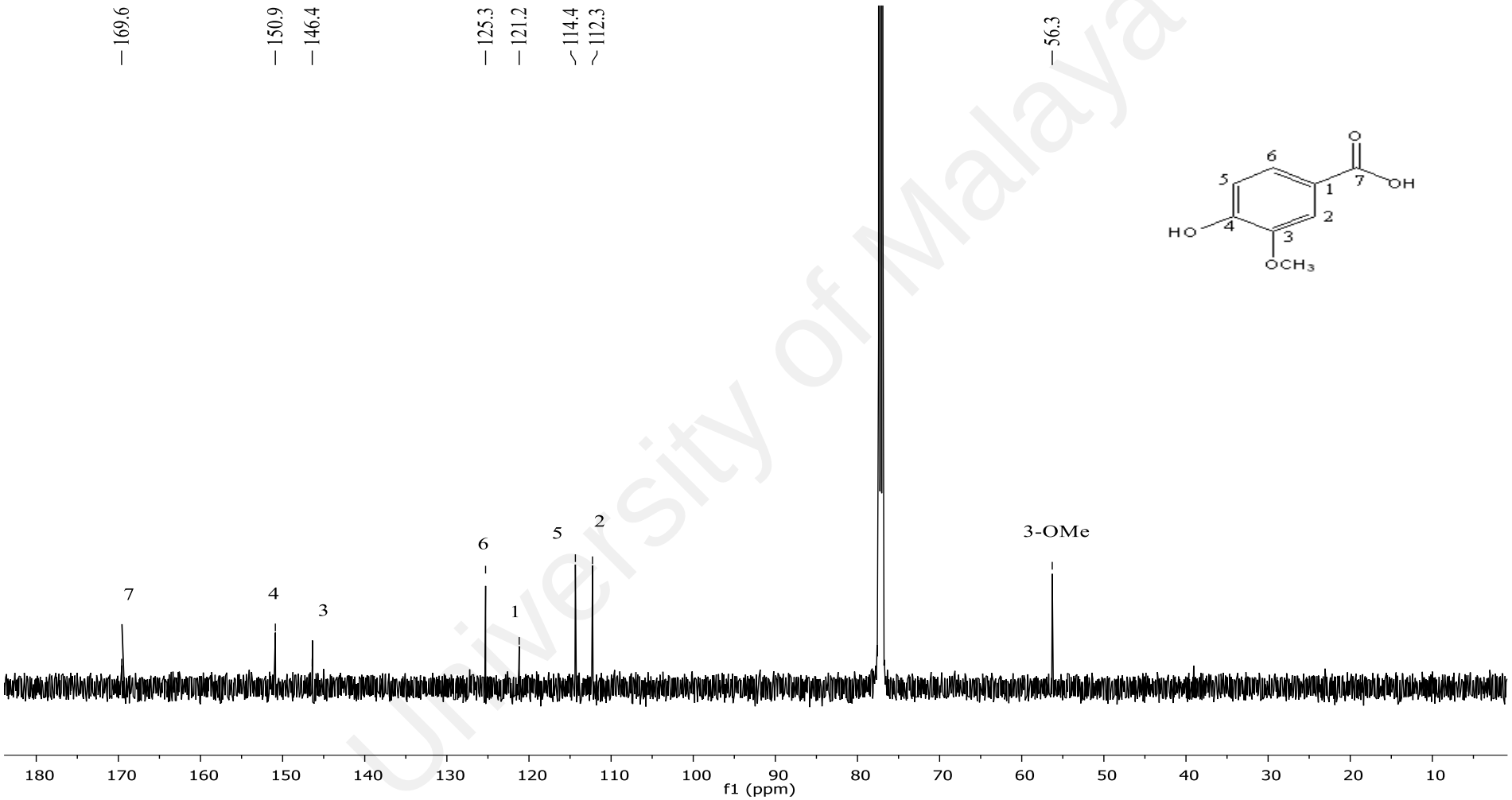

Figure 4.30: ^{13}C NMR spectrum of vanillic acid **132**.

4.1.11 Vanillin 133

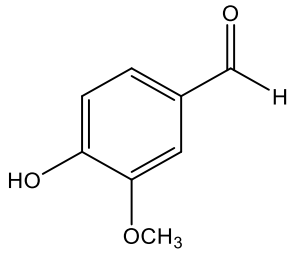

133

Compound **133** was isolated as light-yellow amorphous powder. The positive LCMS-IT-TOF analysis exhibited pseudomolecular ion $[M+H]^+$ at m/z 153.0456 (calcd. for $C_8H_9O_3$, 153.0507), attributable to molecular formula of $C_8H_8O_3$, consistent with five degrees of unsaturation. The IR spectrum revealed absorption bands at ν_{max} 3401 and 1695cm^{-1}, which suggested the presence of hydroxyl and an aldehydic groups (C. Yang et al., 2016).

The ^{1}H NMR spectrum (Figure 4.31) and ^{13}C NMR spectrum (Figure 4.32) of compound **133** were comparable to those of compound **132**, hence suggesting the possibility of these compounds being structurally related to each other. A significant difference can be seen at most deshielded proton δ_H 9.83 (s) and in the upfield region δ_C 191.0, which provided evidence that **133** possessed an aldehyde group. However, similarity can be seen for proton signals which appeared at δ_H 7.05 (d, J = 8.5 Hz), δ_H 7.43 (d, J = 1.8 Hz), and δ_H 7.43 (dd, J = 8.5 and 1.8 Hz). These indicated the presence of a 1,3,4-trisubstituted benzene moiety, corresponding to H-5, H-2 and H-6, respectively.

The complete assignments of the ^{1}H NMR and ^{13}C NMR spectroscopic data of compound **133** were achieved by COSY, HSQC, HMBC experiments. All the above-mentioned NMR spectroscopic data of compound **133** and upon comparison with published data (Table 4.12) it was identified as vanillin.

Table 4.12: ^{1}H (400 MHz) and ^{13}C (100 MHz) NMR data of vanillin **133** (δ in ppm) in $CDCl_3$.

	vanillin **133**		vanillin (C. Yang et al., 2016)	
Position	δ_H (*m*, *J* in Hz) in $CDCl_3$ (**133**)	δ_C in $CDCl_3$ (**133**)	δ_H (*m*, *J* in Hz) in $CDCl_3$	δ_C in $CDCl_3$
1	-	130.1	-	129.9
2	7.43(d, *J*=1.8)	108.9	7.46 (s)	114.4
3	-	147.3	-	147.2
4	-	151.8	-	151.7
5	7.05 (d, *J*=8.5)	114.5	7.07 (d, *J*=8.50)	108.8
6	7.43 (dd, *J*=1.8, 8.5)	127.7	7.45 (s)	127.5
7	9.83	191.0	9.86	190.9
3-OMe	3.97	56.3	3.99	56.1

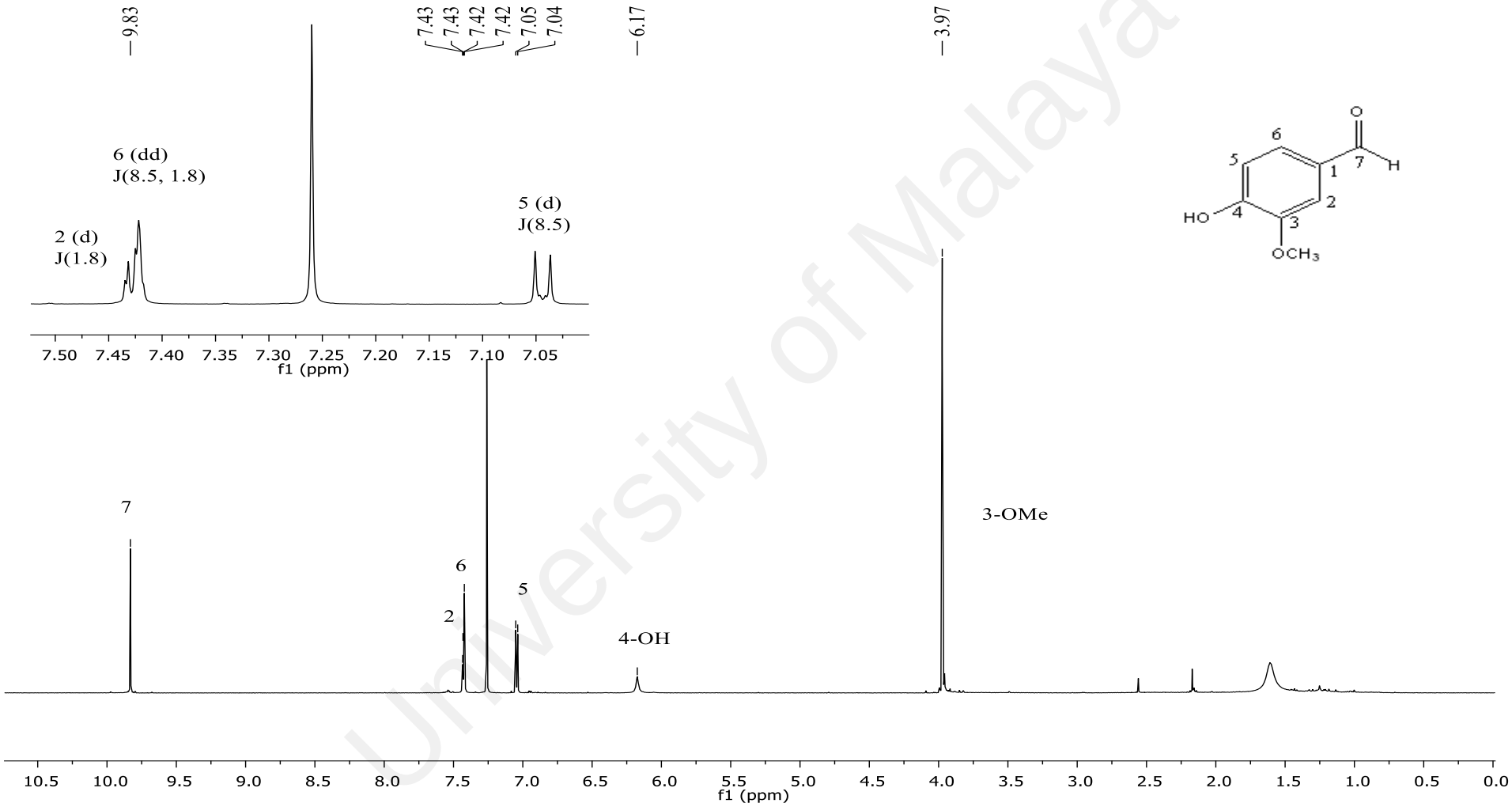

Figure 4.31: ^{1}H NMR spectrum of vanillin **133**.

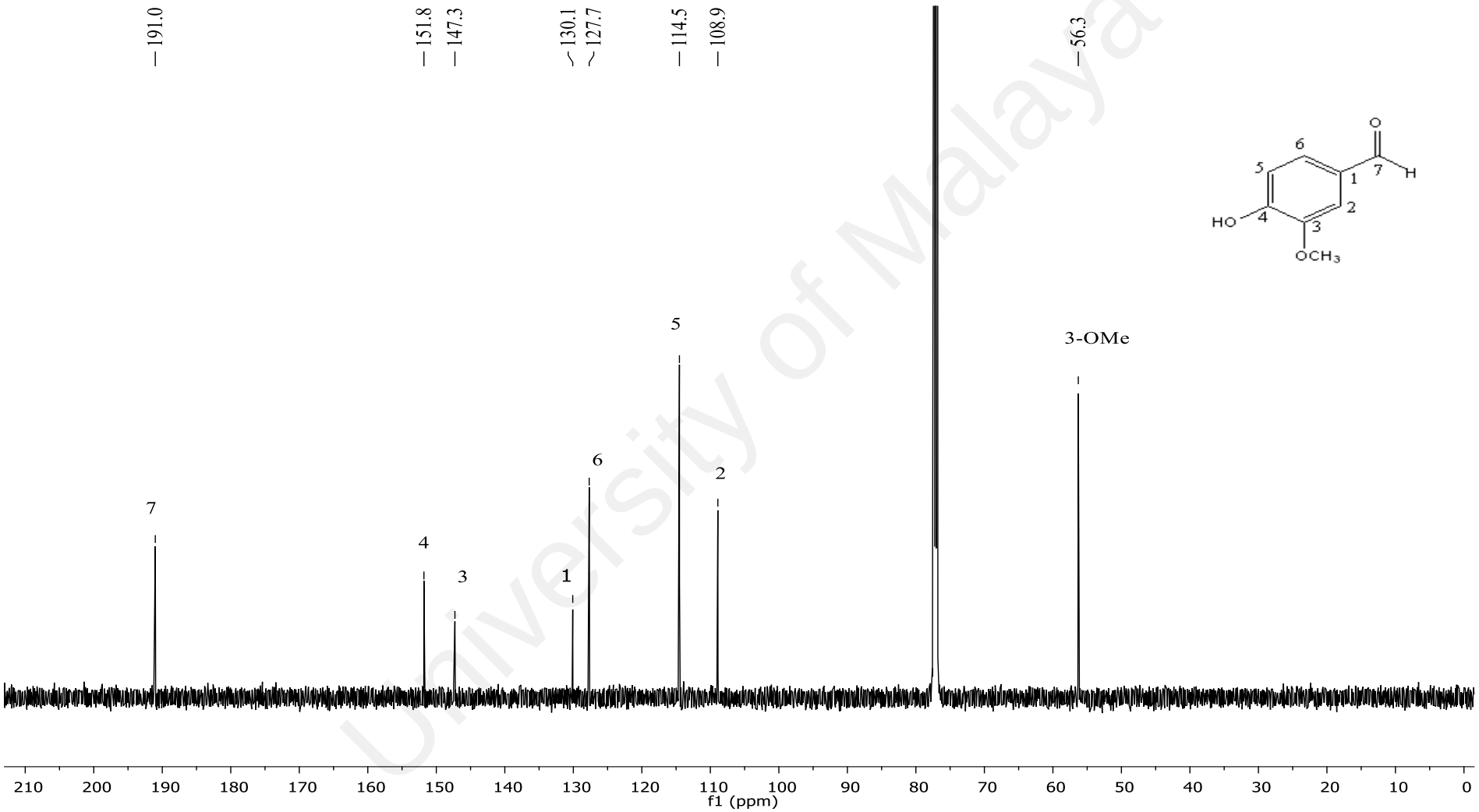

Figure 4.32: ^{13}C NMR spectrum of vanillin **133**.

4.1.12 Methyl orsellinate 134

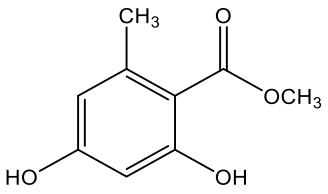

134

Compound **134** was isolated as light-yellow amorphous powder. The positive LCMS-IT-TOF analysis showed a pseudomolecular ion $[M+H]^+$ at m/z 183.0286 (calcd. for $C_9H_{11}O_4$, 183.0613), attributable to the molecular formula $C_9H_{10}O_4$, consistent with five degrees of unsaturation. The IR spectrum displayed absorption bands at ν_{max} 3401 and 1628 cm^{-1}, suggestive of the presence of hydroxyl and conjugated carbonyl groups (Basset et al., 2010).

The ^1H NMR spectrum (Figure 4.33) of compound **134** exhibited the typical spin system for a 1,2,4,6-tetrasubstituted aromatic ring with two-proton system with doublets at δ_H 6.28 (H-3; δ_C 101.4, C-3) and δ_H 6.22 (H-5; δ_C 111.5, C-5), each with a *meta*-mutual coupling of 2.5 Hz. The spectrum also displayed a singlet at δ_H 3.92, corresponding to the methoxy group, while the signal in the most upfield region of the ^1H NMR indicated the presence of the methyl group (δ_H 2.48, H-8).

The ^{13}C NMR spectrum (Figure 4.34) showed the presence of nine carbon signals inclusive of two sp^2 methines, four sp^2 quartenary carbons, one methyl carbon, one methoxy group and one conjugated carbonyl. The conjugated carbonyl and methyl carbon showed signals at δ_C 172.3 and δ_C 24.4, respectively.

The position of the conjugated carbonyl group was revealed from the HMBC (Figure 4.35) correlation between H_3-8 to the carbonyl carbon at δ_C 172.3, which establish the connectivity of carboxyl group at C-7. The position of the methoxyl group was also confirmed by the HMBC correlation of 7-OCH_3/C-7. Finally, the pertinent long-range correlations of H-8/C-1, and H-8/C-5 and J^2 correlation H-8/C-6 as deduced from the

HMBC spectrum also confirmed the connectivity of the methyl group attached to the ring at δ_C 144.1.

The complete assignments of the ^{1}H NMR and ^{13}C NMR spectroscopic data of compound **134** were achieved with the aid of the COSY, HSQC and HMBC experiments (Table 4.13). All the above-mentioned NMR spectroscopic data and upon comparison with literature data, it was identified as methyl orsellinate.

Table 4.13: ^{1}H (400 MHz) and ^{13}C (100 MHz) NMR data of methyl orsellinate **134** (δ in ppm) in $CDCl_3$.

	Methyl orsellinate **134**		Methyl orsellinate (Basset et al., 2010)	
Position	δ_H (*m*, *J* in Hz) in $CDCl_3$ (**134**)	δ_C in $CDCl_3$ (**134**)	δ_H (*m*, *J* in Hz) in $CDCl_3$	δ_C in $CDCl_3$
1	-	105.8	--	104.5
2	-	165.5		165.3
3	6.28 (d, *J*=2.5)	101.4	6.28 (s)	100.9
4	-	160.5	-	160.3
5	6.22 (d, *J*=2.5)	111.5	6.23 (s)	111.3
6	-	144.1	-	144.0
7	-	172.3	-	172.1
8	2.48	24.4	2.49	24.2
7-OMe	3.92	52.0	3.92	51.9

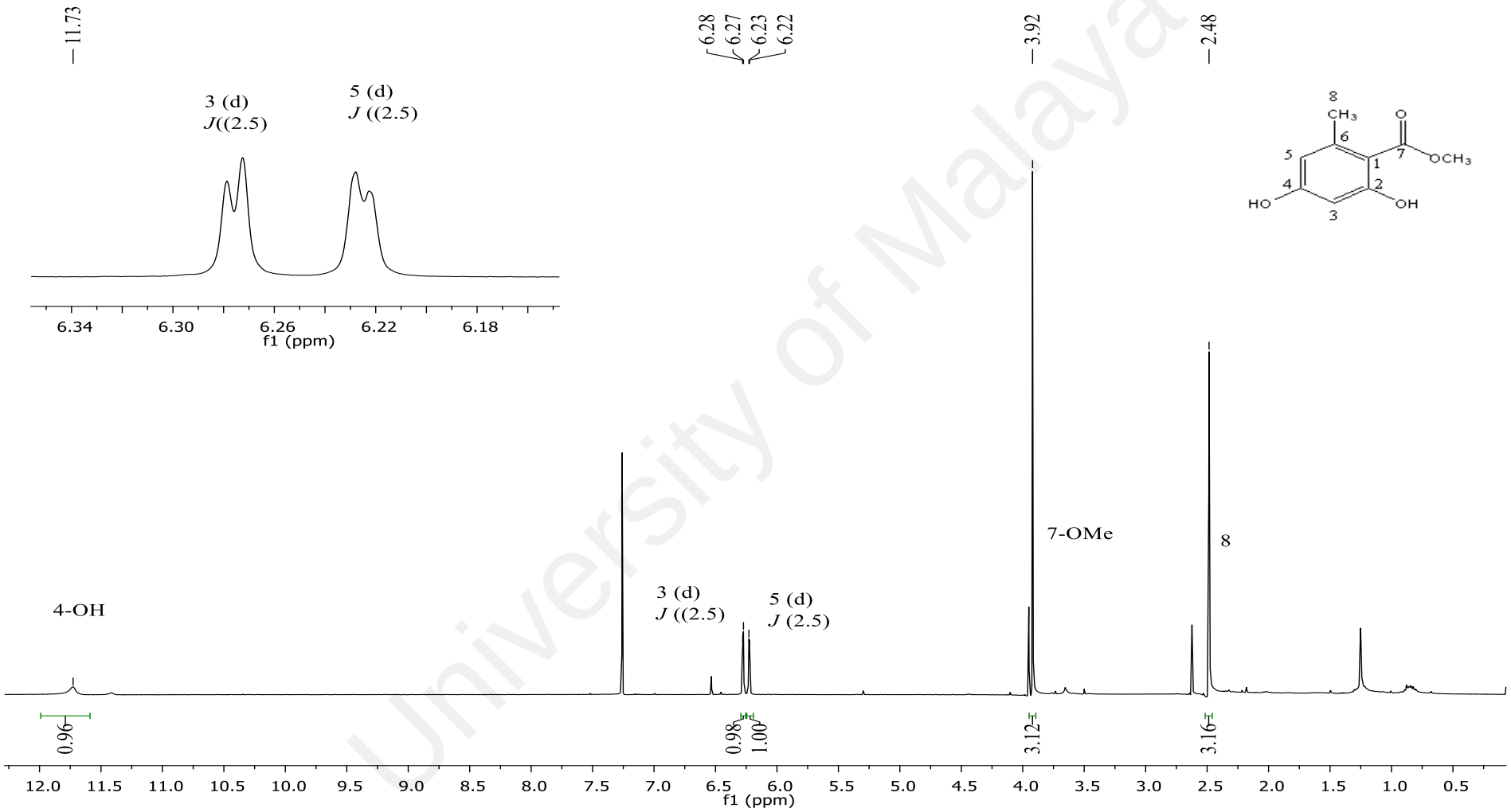

Figure 4.33: ^{1}H NMR spectrum of methyl orsellinate **134**.

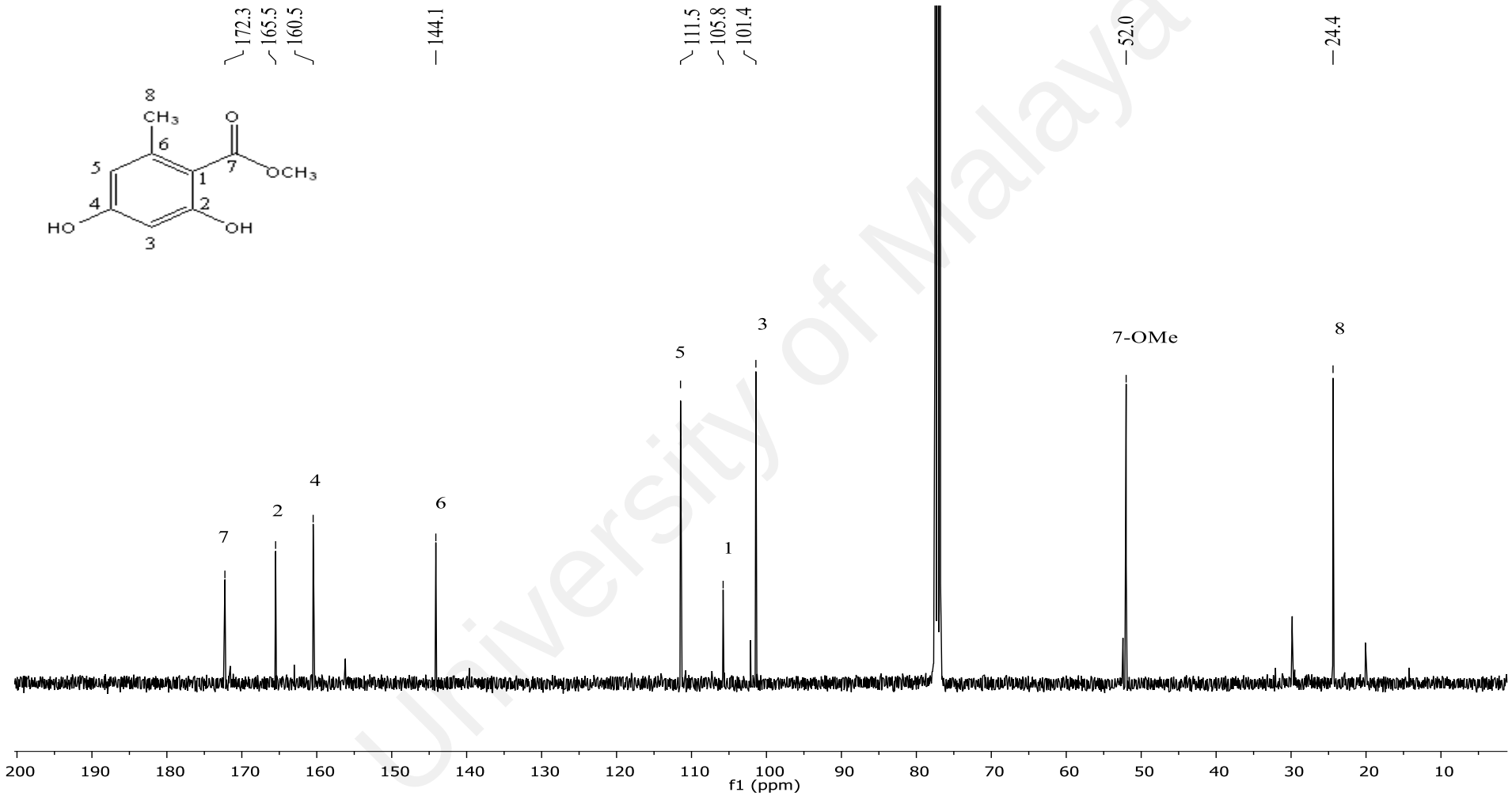

Figure 4.34: ^{13}C NMR spectrum of methyl orsellinate **134**.

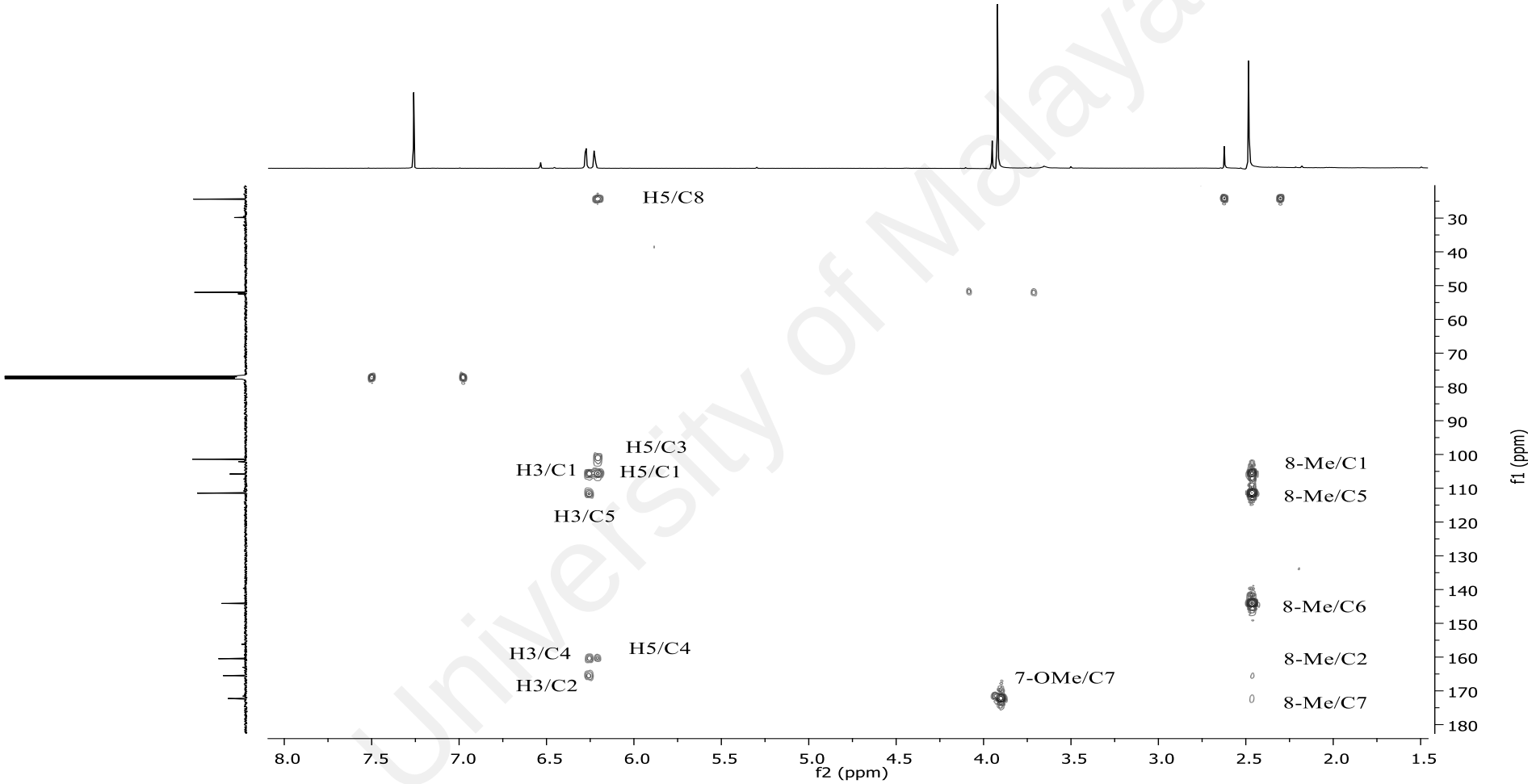

Figure 4.35: HMBC spectrum of methyl orsellinate **134**.

4.1.13 5α-Cholesta-20,24-diene-3β,6α-diol 135

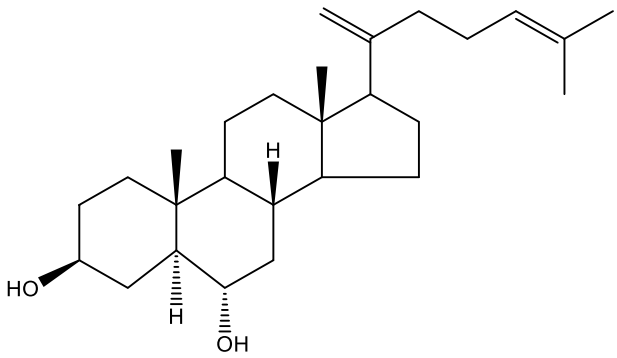

135

Compound **135** was obtained as white amorphous powder. The molecular formula of **135** was determined as $C_{27}H_{44}O_2$ by LCMS-IT-TOF, which provided a molecular ion peak at m/z 401.3434 $[M+H]^+$ (calcd. m/z at 401.3375 for $C_{27}H_{44}O_2$ corresponding to six degree of unsaturation. The IR spectrum indicated an absorption band for hydroxyl group (3430 cm^{-1}), and an olefinic (2941 cm^{-1}) functionalities (Basset et al., 2010).

The ^1H NMR spectrum (Figure 4.36) showed four singlets for the methyl groups resonated at δ_H 0.70 (Me-18), δ_H 0.78 (Me-19), δ_H 1.61 (Me-26), and δ_H 1.62 (Me-27). An olefinic proton resonated at δ_H 5.30 (d, *J*=1.48, H-24) while the exo methylene group protons at δ_H 4.43 and 4.69 (d, *J*=1.48, H-21). This features mentioned were typical of a tetracyclic triterpene, which belonged to the class of cholestane (Revesz et al., 1999). The more downfield chemical shift of the methylene protons of δ_H 2.33 (m, H-22) and δ_H 2.08 (m, H-23) suggested that it adjacent with electron withdrawing group.

The ^{13}C NMR spectrum (Figure 4.37) of **135** coupled with HSQC analysis revealed the presence of twenty-seven carbons, among which four methyls at δ_C 16.4 (C-18), δ_C 15.7 (C-19), δ_C 27.2 (C-26), δ_C 27.3 (C-27), δ_C 26.9 (C-29), and δ_C 23.6 (C-30). Four olefinic carbon signals resonated at δ_C 151.2 (C-20), δ_C 105.4 (C-21), δ_C 121.1 (C-23), δ_C 135.3 (C-24), with two oxygenated carbons at δ_C 73.0 (C-3) and δ_C 73.1 (C-5) were identified.

Through the COSY experiment (Figure 4.38), the exo methylene at δ_H 4.72 (H-21) showed 'W-coupling' with H-17 (δ_H 1.89).and H-22 (δ_H 2.33). An olefinic methine at δ_H 5.30 (H-24) showed vicinal coupling to H-23 (δ_H 2.08), thus confirm the positions of these protons.

The HMBC experiment (Figure 4.39) supported that Me-18 (δ_H 0.70, s) and Me-19 (δ_H 0.78, s) were two methyl that fused between rings, were built from basis correlation with C-12 (δ_C 40.3), C-13 (δ_C 42.0), C-14 (δ_C 49.9), C-17 (δ_C 49.5) and C-1 (δ_C 36.0), C-9 (δ_C 50.1), C-10 (δ_C 38.0) respectively. The formation of germinal methyl between Me-26 (δ_C 23.6) and Me-27 (δ_C 21.3), were deduced from the cross correlation between them with C-24 (δ_C 121.1), and C-25 (δ_C 135.3), respectively. Careful analysis of this experiment suggested that both olefinic moieties were located at C-20(21) and C-24(25) positions. The double bond was deduced from the correlations of H-21 with C-17, C-20 and C-22; and H-24 with C-22.

Complete assignments of all 1D and 2D NMR spectra (Table 4.14) suggested that **135** was 5α-Cholesta-20,24-diene-3β,6α-diol (Gao et al., 2001).

Table 4.14: ^{1}H (400 MHz) and ^{13}C (100 MHz) NMR data of 5α-Cholesta-20,24-diene-3β,6α-diol **135** (δ in ppm) in $CDCl_3$.

	5α-Cholesta-20,24-diene-3β,6α-diol **135**		5α-Cholesta-20,24-diene-3β,6α-diol (Gao et al., 2001)	
Position	δ_H (*m*, *J* in Hz) in $CDCl_3$ (**135**)	δ_C in $CDCl_3$ (**135**)	δ_H (*m*, *J* in Hz) in $CDCl_3$	δ_C in $CDCl_3$
1	1.36 (m)	36.0	1.38 (m)	36.2
2	1.46 (m)	27.3	1.45 (m)	27.4
3	2.63 (m)	73.0	2.67(m)	73.2
4	1.18 (m)	32.3	1.20 (m)	32.3
5	1.21 (m)	46.7	1.25 (m)	46.8
6	2.59 (m)	73.1	2.62 (m)	73.4
7	1.62 (m)	41.2	1.61 (m)	41.4
8	1.21 (m)	27.7	1.24 (m)	27.8
9	0.91 (m)	50.1	0.90 (m)	50.2
10	-	38.0	-	38.2
11	1.52 (m)	24.4	1.54 (m)	24.4
12	1.42 (m)	40.3	1.44 (m)	40.5
13	-	42.0	-	42.2
14	0.97 (m)	49.9	0.96 (m)	49.9
15	1.76 (m)	23.1	1.78 (m)	23.2
16	1.52 (m)	25.1	1.54 (m)	25.2
17	1.89 (m)	49.5	1.87 (m)	49.6
18	0.70 (s)	16.4	0.73 (s)	16.6
19	0.78 (s)	15.7	0.79 (s)	15.6
20	-	151.2	-	151.2
21	4.69, 4.43 (d, *J*=1.48)	105.4	4.70, 4.45 (d, *J*=1.48)	105.3
22	2.33 (m)	37.0	2.35 (m)	37.0
23	2.08 (m)	27.2	2.09 (m)	27.3
24	5.30 (d, *J*=1.48)	121.1	5.30 (d, *J*=1.48)	121.2
25	-	135.3	-	135.4
26	1.61 (s)	23.6	1.63 (s)	23.7
27	1.62 (s)	21.3	1.64 (s)	21.8

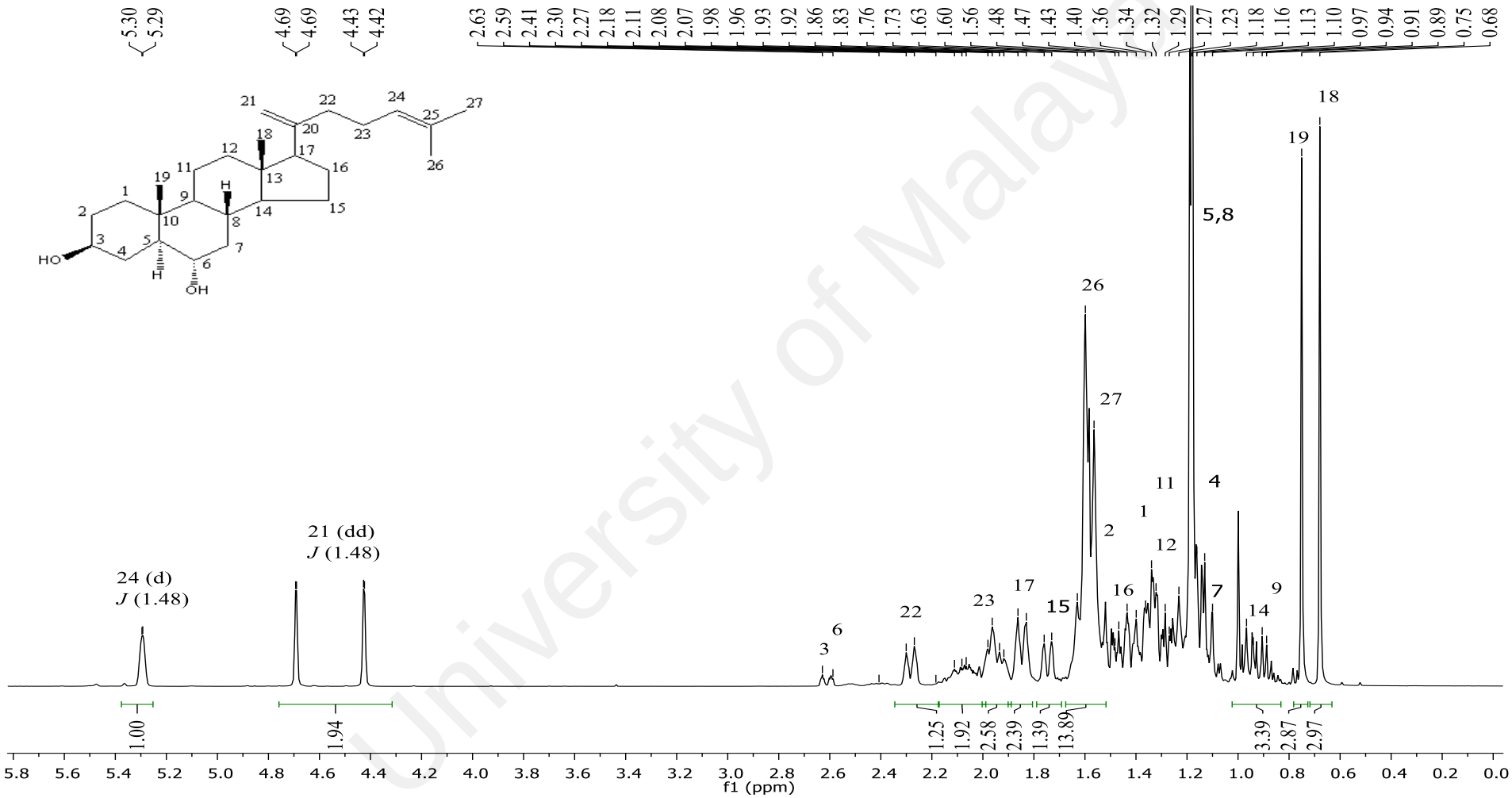

Figure 4.36: ^{1}H NMR spectrum of 5α-Cholesta-20,24-diene-3β,6α-diol **135**.

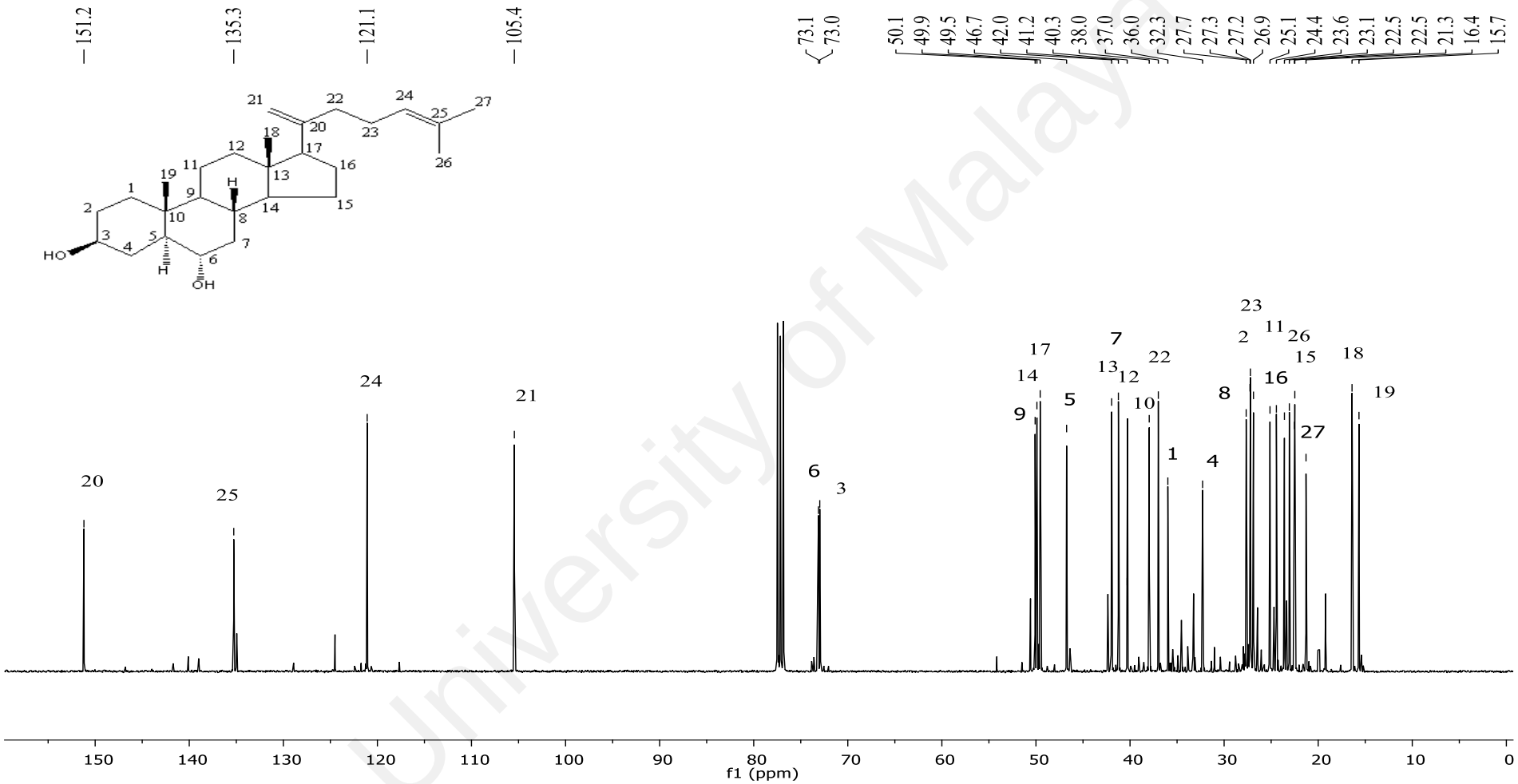

Figure 4.37: ^{13}C NMR spectrum of 5α-Cholesta-20,24-diene-3β,6α-diol **135**.

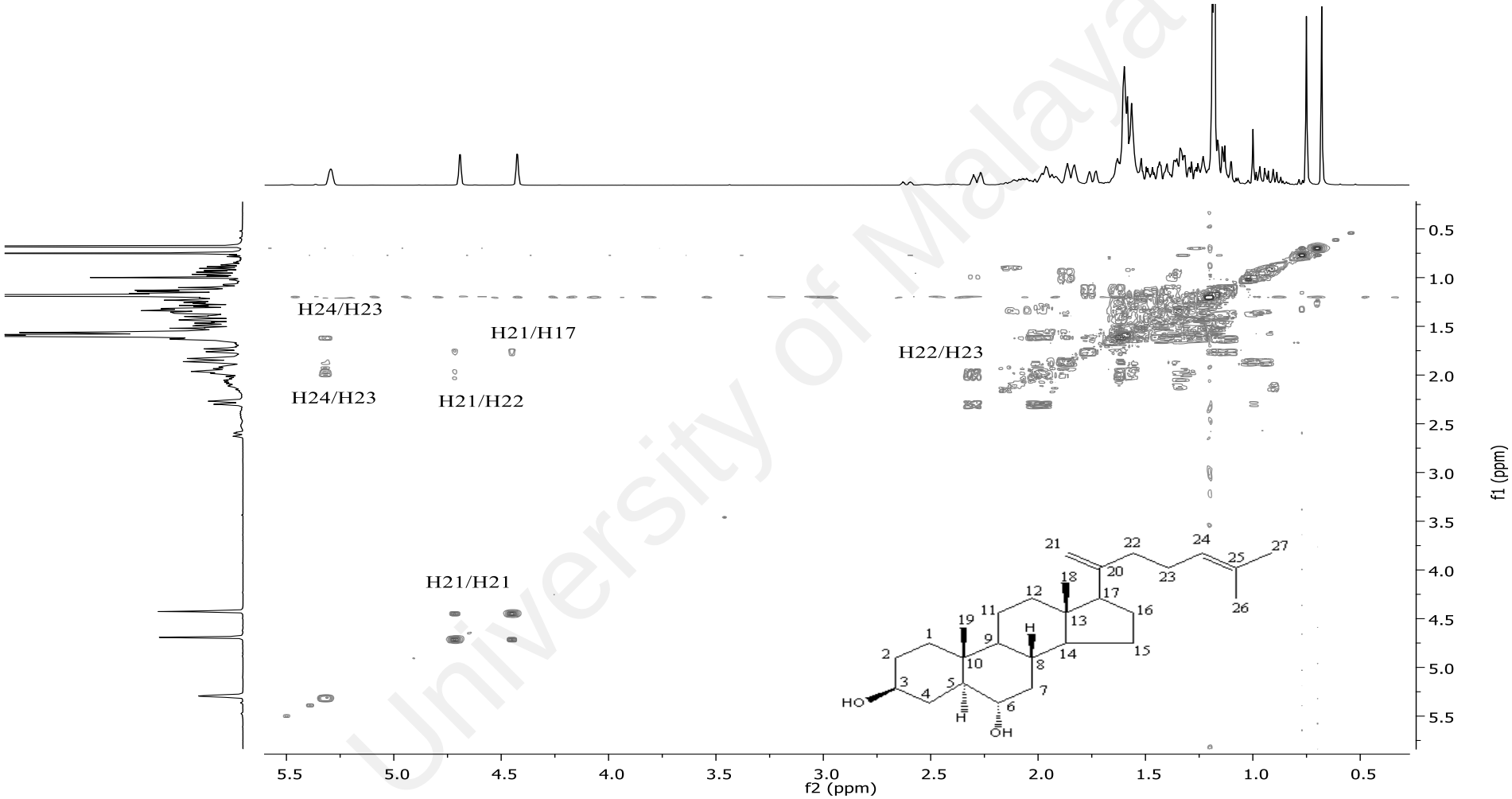

Figure 4.38: COSY spectrum of 5α-Cholesta-20,24-diene-3β,6α-diol **135**.

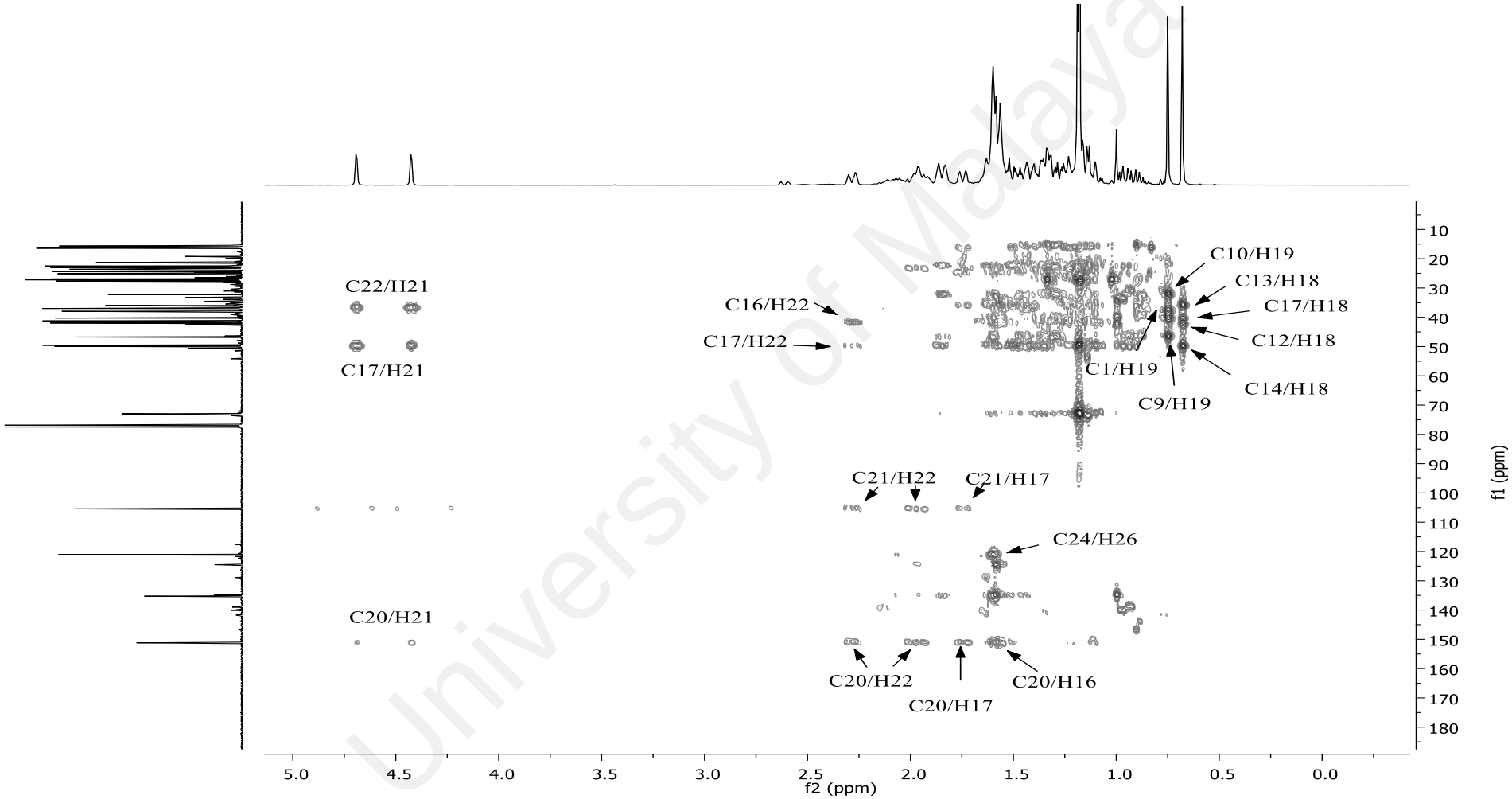

Figure 4.39: HMBC NMR spectrum of 5α-Cholesta-20,24-diene-3β,6α-diol **135**.

4.1.14 4-Hydroxy-6-(9,13,17-trimethyldodeca-8,12,16-trienyl)-2(3H)-benzofuranone 136

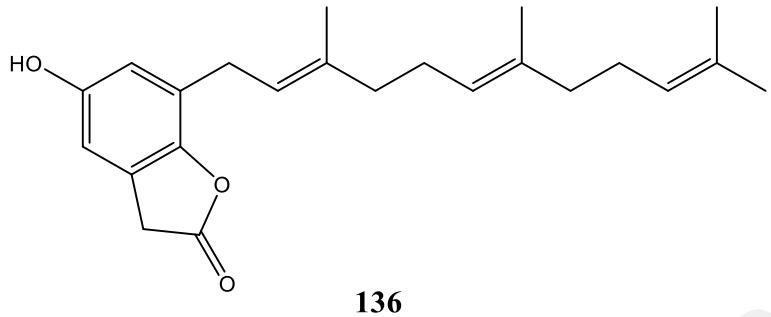

136

Compound **136** was isolated as a pale-yellow amorphous powder. The molecular formula was determined to be $C_{23}H_{30}O_3$ by positive LCMS-IT-TOF (355.2243 $[M+H]^+$, calcd. for 355.2228), indicating nine degrees of unsaturation. The IR spectrum indicated the presence of a highly conjugated system and conjugated carbonyl group absorption at 1470, 1457, and 1725 cm^{-1}. The hydroxyl group was also observed in the IR spectrum at 3402 cm^{-1} (Gu et al., 2007).

The ^1H and ^{13}C NMR spectra demonstrated the presence of a 1,2,3,5-tetrasubstituted aromatic ring with two methines at δ_H 6.58 (s, H-3; δ_C 109.3), δ_H 6.61 (s, H-5; δ_C 115.5); and four quartenary carbons at δ_C 147.0 (C-1), δ_C 123.8 (C-2), δ_C 152.4 (C-4), and δ_C 126.1 (C-6). Three isoprene (C_5-units) formed as indicated by ^1H and ^{13}C NMR signals, three olefinic protons (δ_H 5.09 – 5.30) and six olefinic carbons (δ_C 120.6, 124.1, 124.5, 135.3, 135.5 and 137.9), four vinylic methyls (δ_H 1.59, 1.59, 1.67 and 1.71) with ^{13}C NMR at δ_C 16.2, 16.2, 16.4, 25.8, four methylene carbons (δ_C 25.8, 26.6, 39.8 and 39.9) with eight allylic protons (δ_H 1.96 – 2.12) and two benzylic protons (δ_H 3.34 (d, J=7.3 Hz).

In the HMBC spectrum of **136** (Figure 4.43), the long-range correlations between H-7 (δ_H 3.34, d, J=7.3 Hz) with C-9, C-5 and C-1; H-3 with C-2', C-7, and C-1 indicated that four isoprene units were attached to the aromatic ring, thus confirmed the structure of **136**. Upon comparison of spectral data of **136** with known compound, 5-hydroxy-7-

(3,7,11,15-tetramethylhexadeca-2,6,10,11-tetraenyl)-2(3 *H*)-benzofuranone (Gu et al., 2007), showed similarities except that **136** has one less isoprene unit which was confirmed by the complete assignments of all 1D, 2D NMR spectra and LCMS-IT-TOF. All the above-mentioned NMR spectroscopic data of compound **136** and upon comparison with literature (Table 4.15), was identified as 4-hydroxy-6-(9,13,17-trimethyldodeca-8,12,16-trienyl)-2(3 H)-benzofuranone, which is a new benzofuran isolated from *E. kingiana*.

Table 4.15: ^{1}H (400 MHz) and ^{13}C (100 MHz) NMR data of 4-hydroxy-6-(9,13,17-trimethyldodeca-8,12,16-trienyl)-2(3 H)-benzofuranone **136** (δ in ppm) in $CDCl_3$.

	4-Hydroxy-6-(9,13,17-trimethyldodeca-8,12,16-trienyl)-2(3 H)-benzofuranone **136**		5-Hydroxy-7-(3,7,11,15-tetramethylhexadeca-2,6,10,11-tetraenyl)-2(3 *H*)-benzofuranone (Gu et al., 2007)	
Position	δ_H (*m*, *J* in Hz) in $CDCl_3$ (**136**)	δ_C in $CDCl_3$ (**136**)	δ_H (*m*, *J* in Hz) in $CDCl_3$	δ_C in $CDCl_3$
1'	-	174.6	-	174.6
2'	3.69 (s)	34.0	3.69 (s)	33.9
1	-	147.0	-	146.8
2	-	123.8	-	123.6
3	6.58 (s)	109.3	6.58 (s)	109.2
4	-	152.4	-	152.3
5	6.61 (s)	115.5	6.61 (s)	115.4
6	-	126.1	-	125.9
7	3.34 (d, *J*=7.3)	27.8	3.32 (d, *J*=7.3)	27.7
8	5.30 (d, *J*=7.3)	120.6	5.28 (t, *J*= 7.3)	120.4
9	-	137.9	-	137.5
10	1.96 – 2.10 (m)	39.9	1.96 – 2.13 (m)	39.7
11	1.96 - 2.12 (m)	26.6	1.96 – 2.13 (m)	26.7
12	5.09 - 5.11 (m)	124.5	5.07 – 5.11 (m)	124.4
13	-	135.3	-	135.2
14	1.96 - 2.03 (m)	39.8	1.96 – 2.13 (m)	39.7
15	1.96 - 2.03 (m)	25.8	1.96 – 2.13 (m)	26.0
16	5.09 - 5.11 (m)	124.1	5.07 – 5.11 (m)	124.2
17	-	135.5	-	135.0
18	1.67 (s)	25.8	1.96 - 2.13 (m)	39.7
19	-	-	1.96 - 2.13 (m)	26.5
20	-	-	5.07-5.11 (m)	124.0
21	-	-	-	131.3
22	-	-	1.67	25.7
9-Me	1.71 (s)	16.4	1.70 (s)	16.2
13-Me	1.59 (s)	16.2	1.60 (s)	16.0
17-Me	1.59 (s)	16.2	1.60 (s)	16.0
21-Me	-	-	1.60 (s)	17.6

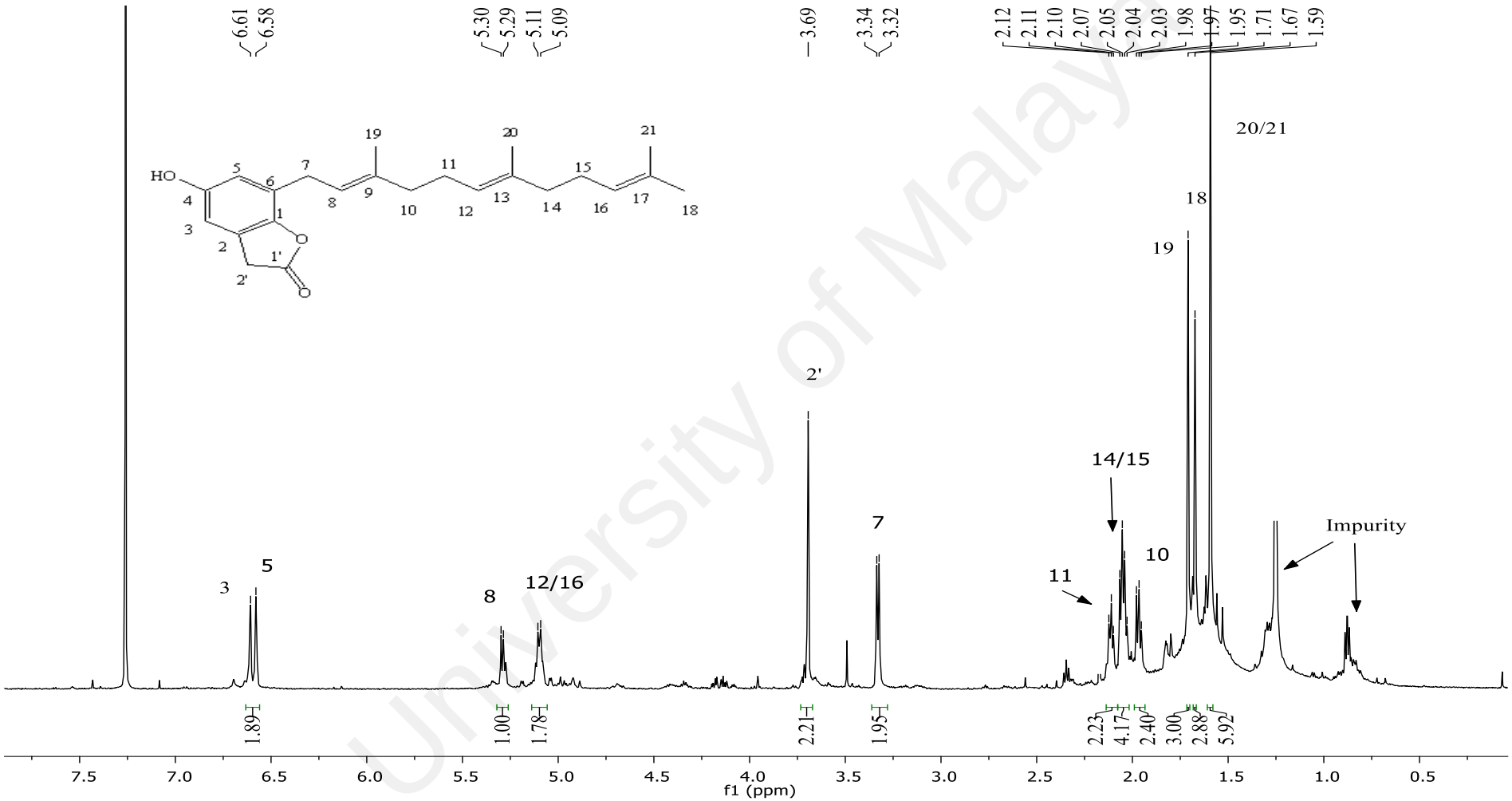

Figure 4.40: ^{1}H NMR spectrum of 4-hydroxy-6-(9,13,17-trimethyldodeca-8,12,16-trienyl)-2(3 H)-benzofuranone **136**.

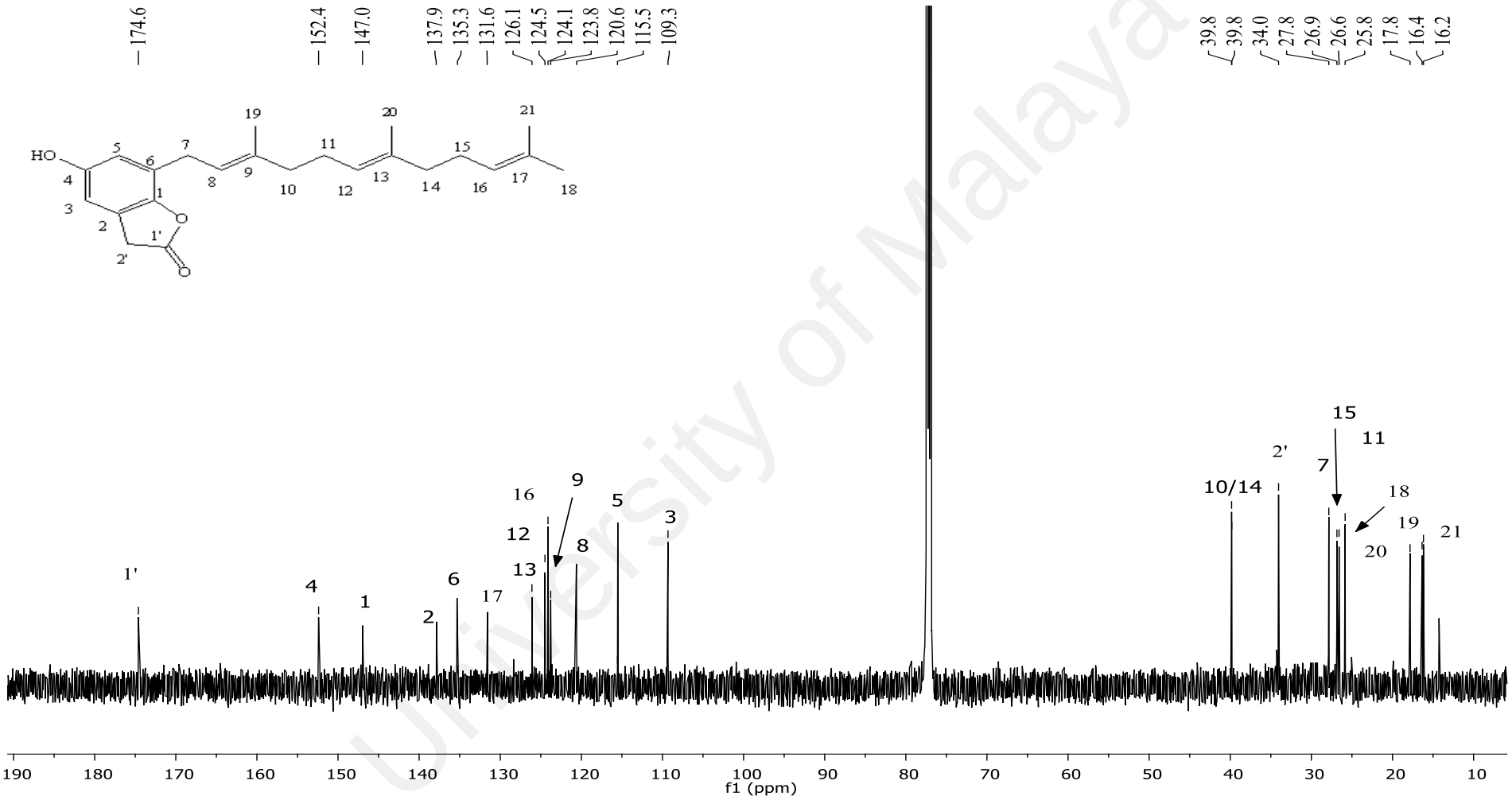

Figure 4.41: ^{13}C NMR spectrum of 4-hydroxy-6-(9,13,17-trimethyldodeca-8,12,16-trienyl)-2(3 H)-benzofuranone **136**.

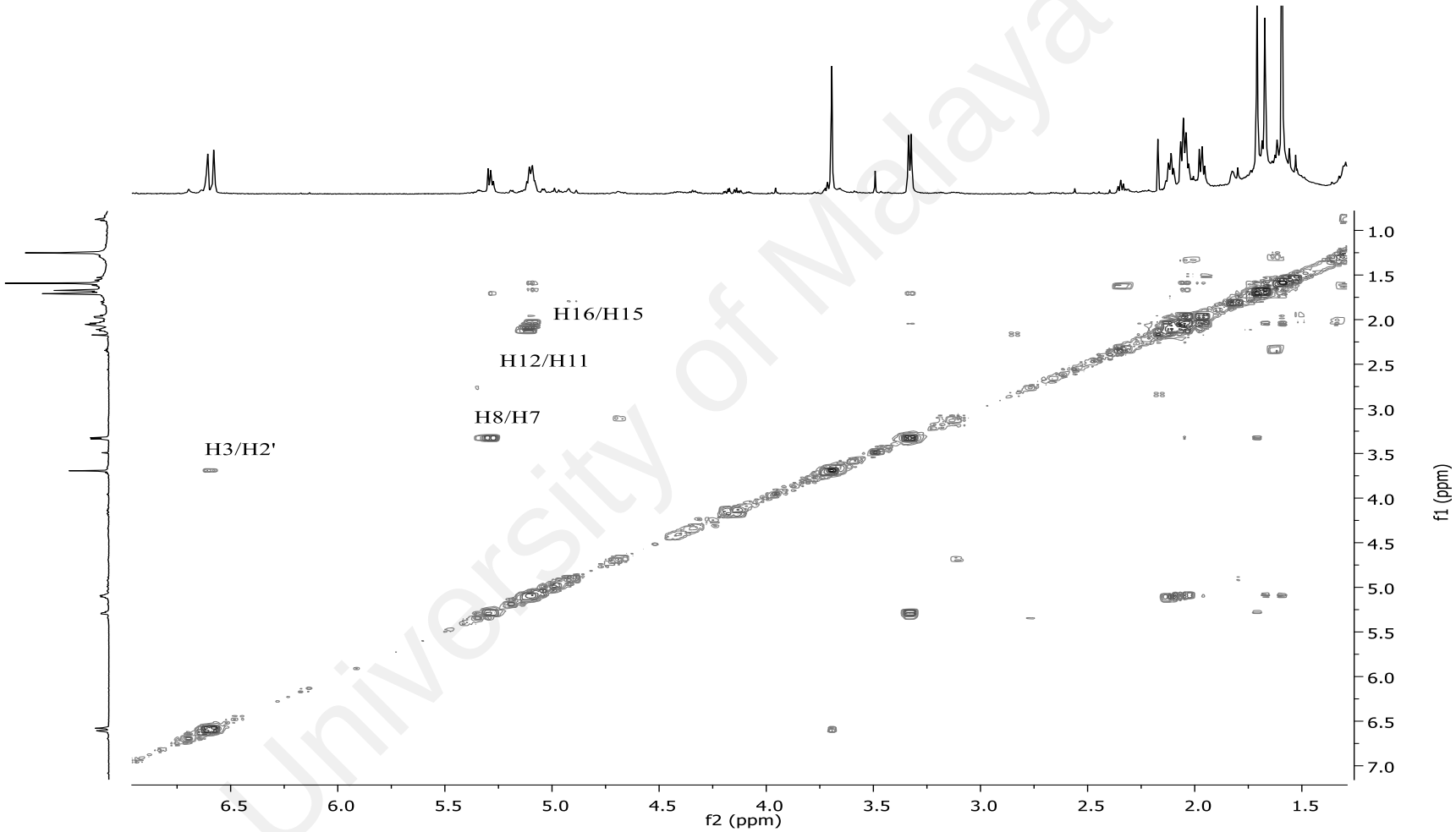

Figure 4.42: COSY NMR spectrum of 4-hydroxy-6-(9,13,17-trimethyldodeca-8,12,16-trienyl)-2(3 H)-benzofuranone **136**.

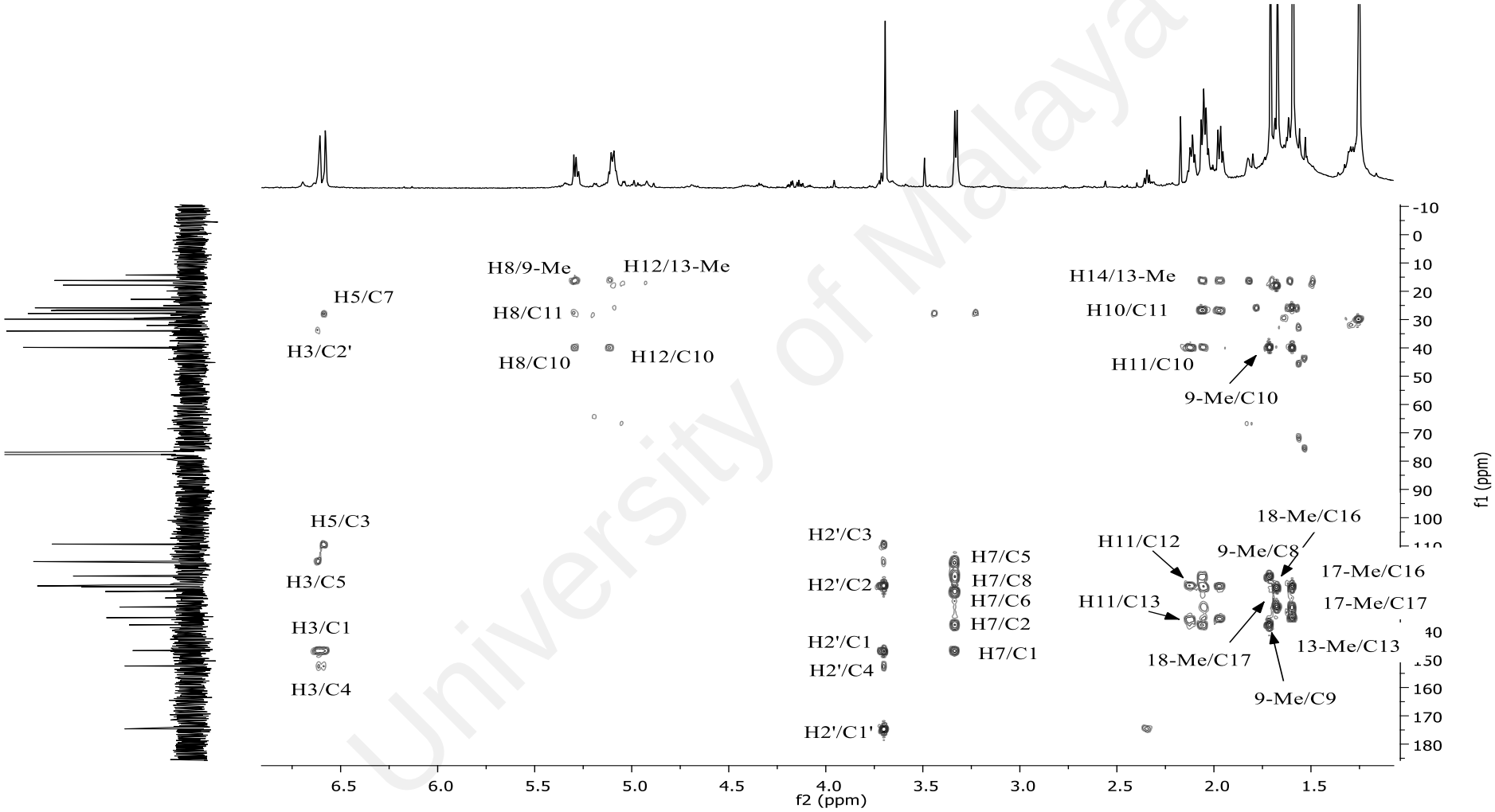

Figure 4.43: HMBC spectrum of 4-hydroxy-6-(9,13,17-trimethyldodeca-8,12,16-trienyl)-2(3 H)-benzofuranone **136**.

4.1.15 (-)-Epicatechin 137

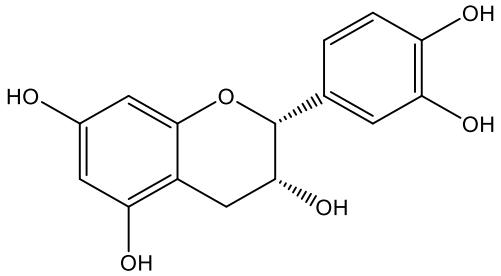

137

Compound **137** was obtained as a white amorphous powder. The molecular formula was determined to be $C_{15}H_{14}O_6$ by positive LCMS-IT-TOF (291.1432 $[M+H]^+$, calcd. for 291.0824), indicating nine degrees of unsaturation. The IR spectrum suggested the presence of a highly conjugated system and hydroxyl group absorption at 1470, 1457, and 3402 cm^{-1} (Q. Wang et al., 2015).

The ^1H NMR spectrum of **137** showed characteristic signal of flavanol-type structures (de Sousa et al., 2015). Then, it displayed five signals in the aromatic region (δ 7.01 – 5.96), and three signals in the aliphatic region (δ 2.76 – 4.60). The coupling constant of the aromatic signals (ring B) indicated one *ortho*-coupled (δ 6.81, d, J = 8.2 Hz, H-5'), one *meta*-coupled (δ 7.01, d, J = 1.9 Hz, H-2'), and one *meta*- and *ortho*-coupled (δ 6.85, dd, J =1.9 and 8.2 Hz, H-6') protons. The remaining aromatic signals (J=2.3 Hz) were attributed to the aromatic protons; H-6 and H-8 in ring A which showed *meta*-coupling to each other at δ 5.98 and δ 5.96, respectively. The signals in the upfield region belonged to the aliphatic protons in ring C which appeared as multiplet at δ 4.60 and 4.22 corresponding for H-2 and H-3. Moreover, two sets of doublet of doublet (dd) at δ 2.89 and 2.76 indicated two protons of ring C, assignable to H-4a and H-4b respectively.

The ^{13}C NMR spectrum of **137** displayed fifteen signals with seven quaternary carbon. All non-quaternary carbons were assigned from the HSQC correlations. The quartenary carbons at δ_C 145.8 (C-3'), 146.0 (C-4'), 157.4 (C-9), 157.7 (C-7) and 158.0 (C-5) suggested that they were oxygenated. Table 4.16 shows the comparison of the assignments of the ^{1}H and ^{13}C NMR data for **137** and similar data from literature. The table shows that both data were almost identical. Thus, the structure **137** was solved as (-)-epicatechin.

Table 4.16: ^{1}H (400 MHz) and ^{13}C (100 MHz) NMR data of (-)-epicatechin **137** (δ in ppm) in MeOD.

	(-)-Epicatechin **137**		(-)-Epicatechin (Q. Wang et al., 2015)	
Position	δ_H (*m*, *J* in Hz) in MeOD (**137**)	δ_C in MeOD (**137**)	δ_H (*m*, *J* in Hz) in $CDCl_3$	δ_C in $CDCl_3$
1	-	-	-	-
2	4.60 (m)	79.9	4.83 (br s)	78.5
3	4.22 (m)	67.6	4.19 (br s)	66.1
4a	2.89 (dd, *J* = 16.7, 4.6)	29.3	2.88 (dd, *J* = 17.0, 4.0)	27.9
4b	2.76 (dd, *J* = 16.7, 2.9)		2.76 (dd, *J* = 17.0, 2.0)	
5	-	158.0	-	150.0
6	5.98 (d, *J* = 2.3)	96.5	5.98 (s)	95.1
7	-	157.7	-	156.6
8	5.96 (d, *J* = 2.3)	95.9	5.95 (s)	94.6
9	-	157.4	-	156.2
10	-	100.1	-	98.7
1′	-	132.3	-	130.9
2′	7.01 (d, *J* = 1.9)	115.3	7.01 (s)	113.9
3′	-	145.8	-	144.5
4′	-	146.0	-	144.4
5′	6.81 (d, *J* = 8.2)	115.9	6.79 (d, *J* = 8.5)	114.6
6′	6.85 (dd, *J* = 8.2, 1.9)	119.4	6.82 (d, *J* = 8.5)	118.1

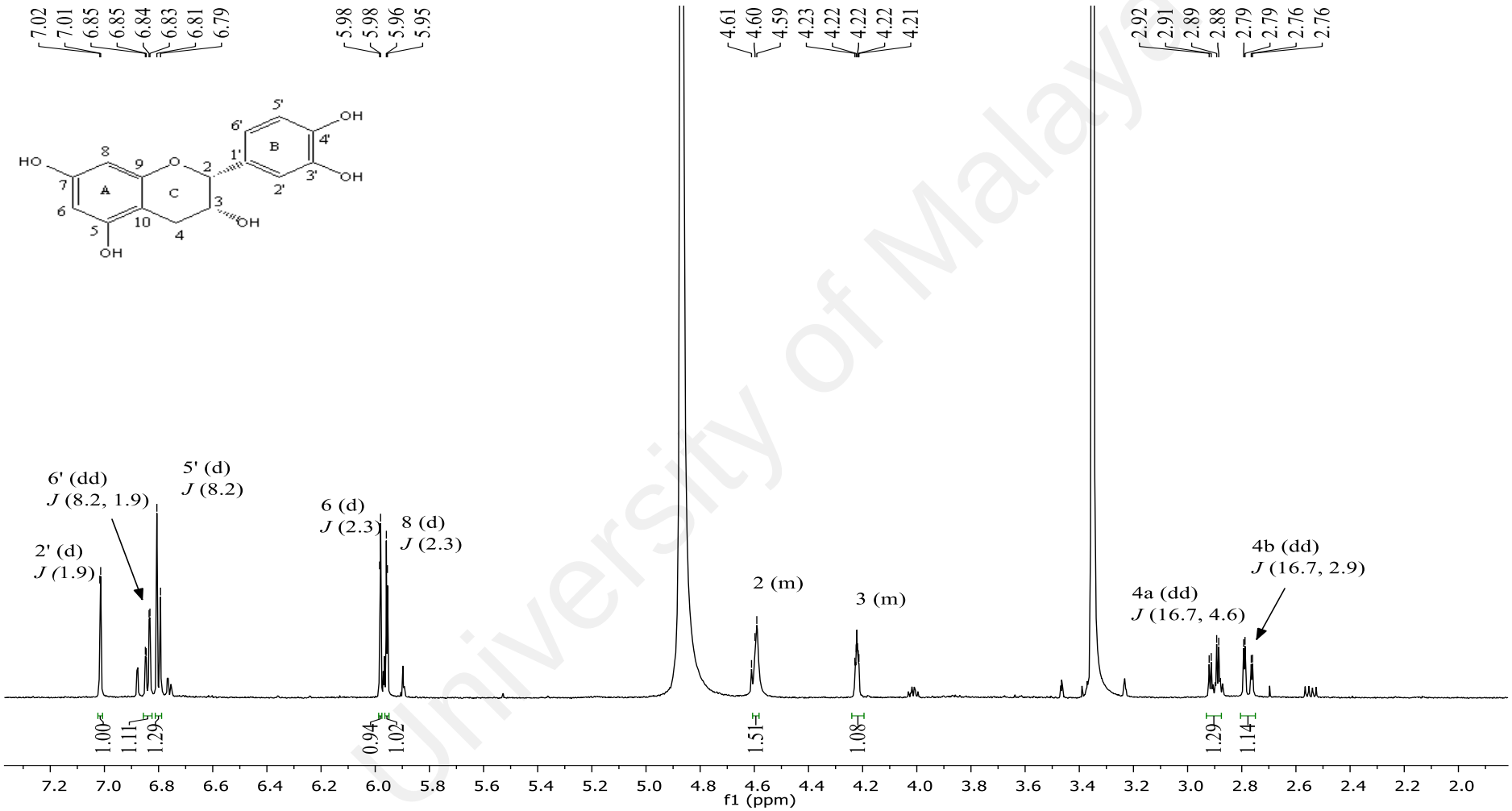

Figure 4.44: ^{1}H NMR spectrum of (-)-epicatechin **137**.

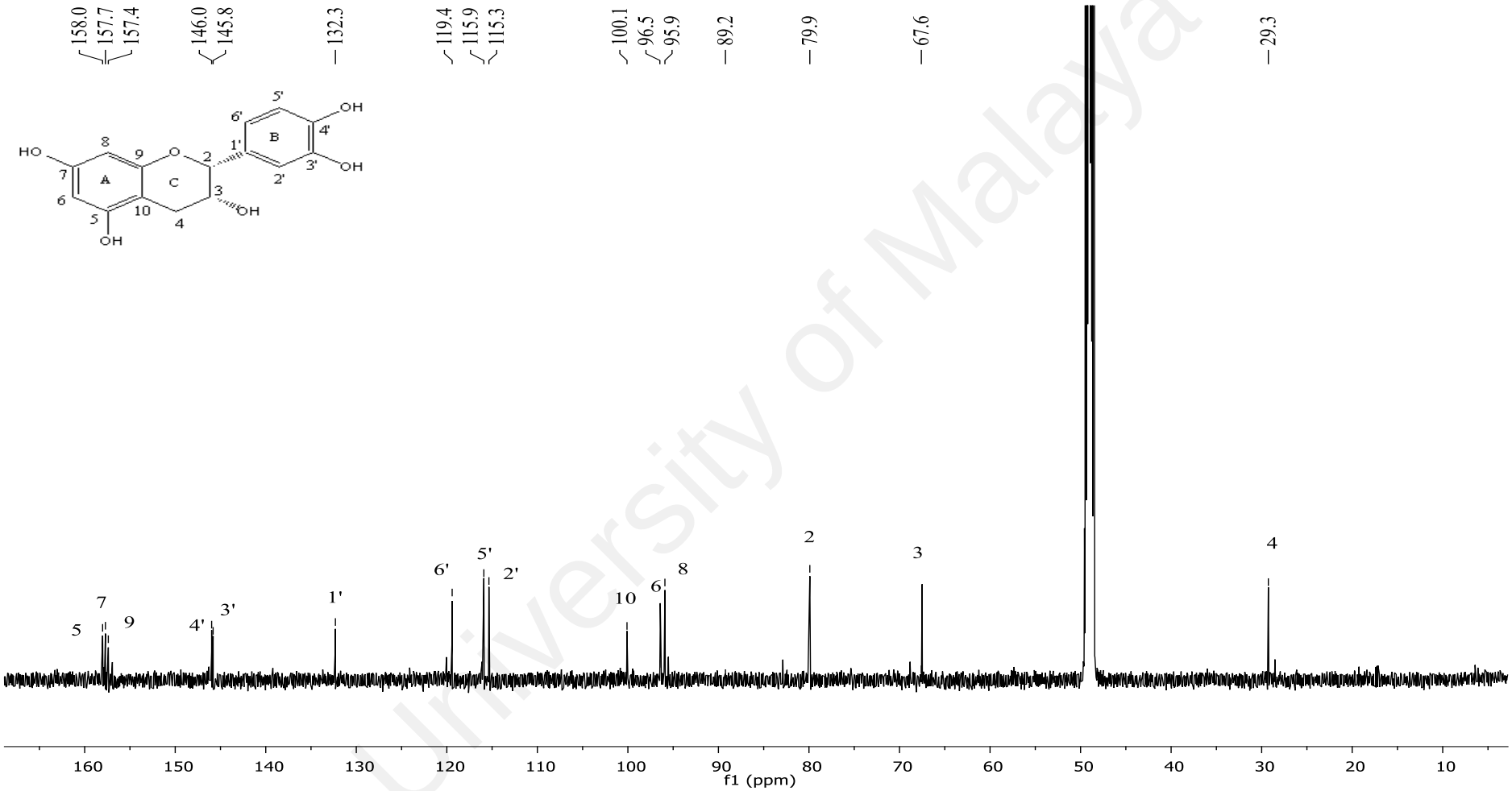

Figure 4.45: ^{13}C NMR spectrum of (-)-epicatechin **137**.

4.1.16 (+)-Catechin 138

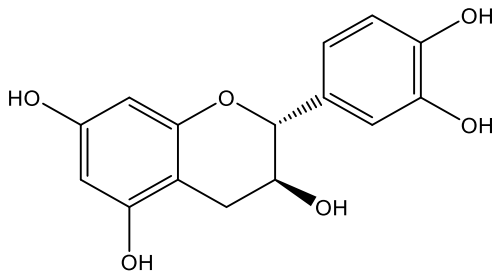

138

Compound **138** was isolated as a white amorphous powder. The molecular formula was deduced to be $C_{15}H_{14}O_6$ by positive LCMS-IT-TOF (291.1432 $[M+H]^+$, calcd. for 291.0824), indicating nine degrees of unsaturation. The IR spectrum revealed the presence of a highly conjugated system and hydroxyl group absorption at 1470, 1457, and 3402 cm^{-1} (Q. Wang et al., 2015).

Both compounds **137** and **138** showed nine ^1H NMR and fifteen ^{13}C NMR resonances. The main distinctive NMR spectral feature of these stereoisomers was the coupling constant between protons H-2 and H-3. In compound **138**, these protons were assigned to be *trans* to each other according to rather large coupling constant at H-2 (J = 7.5 Hz), while in compound **137**, the protons were *cis*-orientated as indicated by the unresolved coupling, i.e. a multiplet signal, at H-2.

The complete assigments of the ^1H NMR and ^{13}C NMR data of compound **138** were achieved by COSY, HSQC, HMBC experiments and comparison with the literature data (Table 4.18) (Q. Wang et al., 2015), thus confirming compound **138** to be (+)-catechin.

Table 4.17: ^{1}H (400 MHz) and ^{13}C (100 MHz) NMR data of (+)-catechin **138**.

	(+)-Catechin **138**		(+)-Catechin (Q. Wang et al., 2015)	
Position	δ_H (*m*, *J* in Hz) in MeOD (**138**)	δ_C in MeOD (**138**)	δ_H (*m*, *J* in Hz) in $CDCl_3$	δ_C in $CDCl_3$
1	-	-	-	-
2	4.60 (d, *J* = 7.5)	83.0	4.60 (d, *J* = 7.5)	80.6
3	4.01 (m)	69.0	4.01 (dd, *J* = 8.0, 7.5)	66.6
4a	2.88 (dd, *J* = 16.1, 5.5)	28.7	2.87 (dd, *J* = 16.5, 5.0)	26.3
4b	2.54 (dd, *J* = 16.1, 8.2)		2.55 (dd, *J* = 16.5, 8.0)	
5	-	157.7	-	154.7
6	5.97 (d, *J* = 2.3)	96.5	5.97 (d, *J* = 1.5)	94.2
7	-	158.0	-	155.6
8	5.90 (d, *J* = 2.3)	95.7	5.89 (d, *J* = 1.5)	93.4
9	-	157.1	-	155.4
10	-	101.1	-	98.7
1′	-	132.4	-	130.0
2′	6.88 (d, *J* = 1.9)	115.4	6.87 (d, *J* = 1.5)	113.1
3′	-	146.4	-	144.1
4′	-	146.4	-	144.0
5′	6.80 (d, *J* = 8.1)	116.2	6.79 (d, *J* = 8.0)	113.9
6′	6.76 (dd, *J* = 8.3, 1.9)	120.2	6.75 (dd, *J* = 8.0, 1.5)	117.9

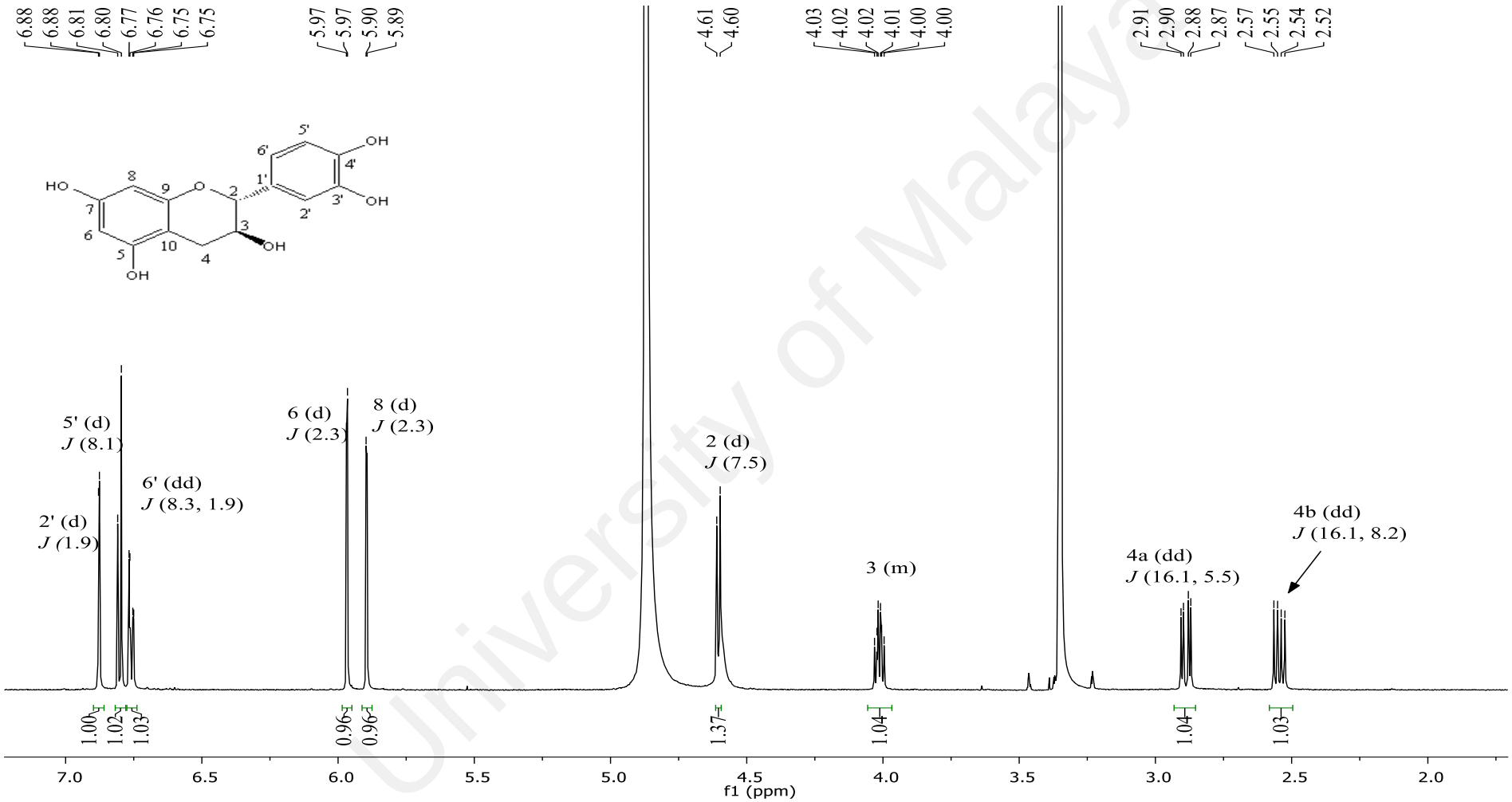

Figure 4.46: ^{1}H NMR spectrum of (+)-catechin **138**.

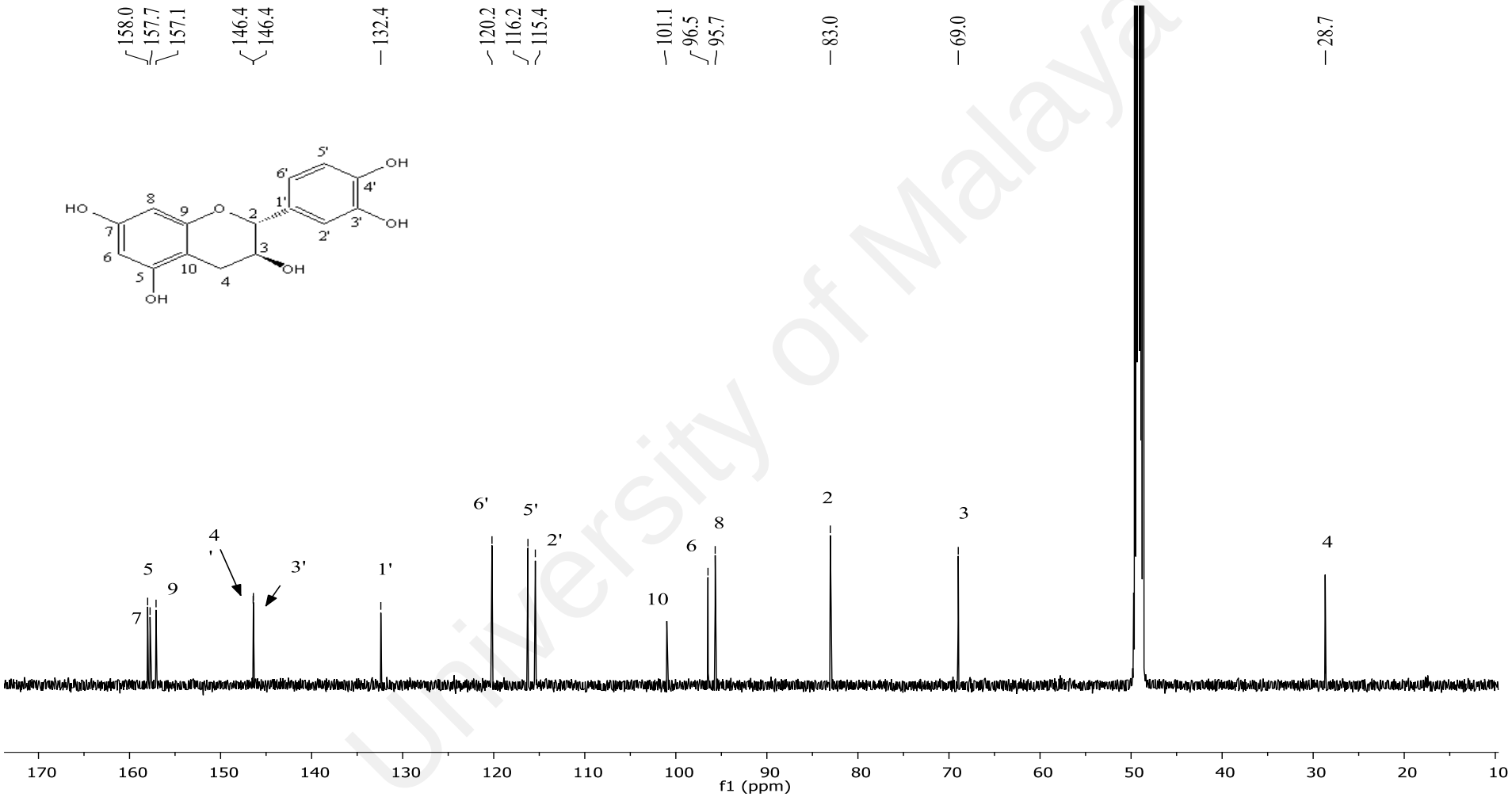

Figure 4.47: ^{13}C NMR spectrum of (+)-catechin **138**.

4.1.17 Cinnamtannin B1 139

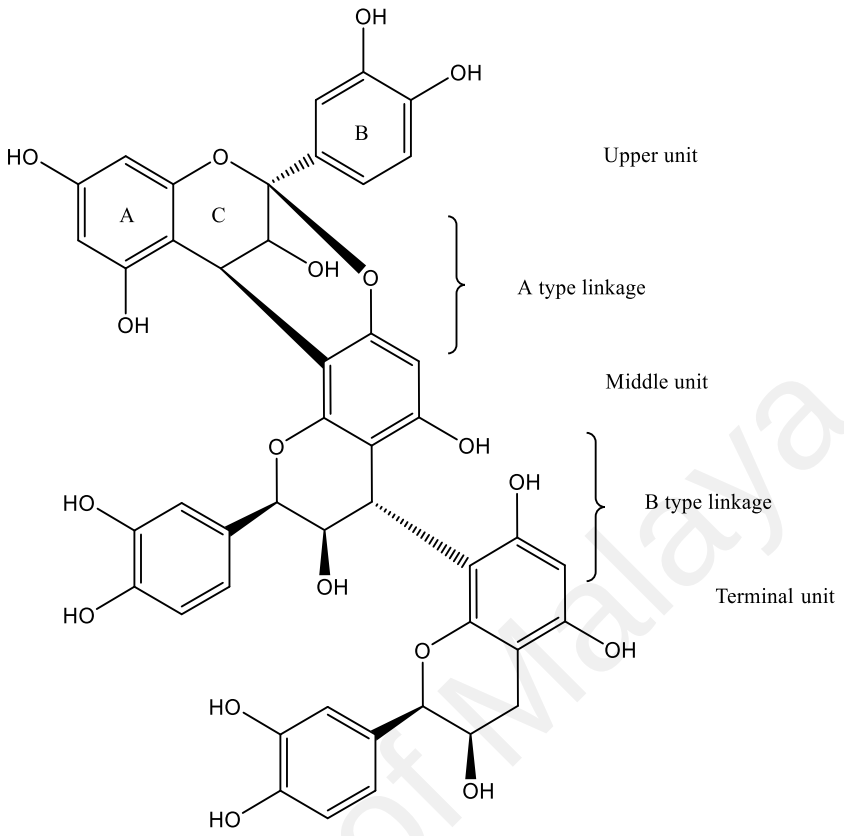

139

Compound **139** was obtained as a pale brown amorphous powder. The UV spectrum of compound **139**, showed absorption maxima at 211 and 278 nm, which suggested the presence of polymeric proanthocyanidins formed from at least two flavan-3-ols units (Li & Deinzer, 2008; C. Xu et al., 2015). The quasi-molecular ion $[M-H]^-$ at *m/z* 863.40 (calcd. for $C_{45}H_{35}O_{18}$, 863.1829) from ESI-MS spectrum (Figure 4.49) suggested compound **139** ($C_{45}H_{35}O_{18}$) to be an oligomeric flavonoid composed of three epicatechin **137** moieties and these moieties were the upper unit (U), middle unit (M) and terminal unit (T) (Jayaprakasha et al., 2006). The fragment ions, at *m/z* 572.75 and 288.68, respectively, indicated that the A-type dimer and epicatechin monomer were formed after quinone methide cleavage of the interflavan bonds. The fragment of *m/z* 450.80 and 410.67 were formed following cleavage of the middle unit through the heterocyclic ring fission mechanism, and the *m/z* 710.95 was formed after cleavage of one of the C-rings

through the *retro*-Diels-Alder fission. The fragmentation patterns indicated that compound **139** is an oligomeric flavonoids and the bonds between the moieties were one A-type and one B-type linkage (Panche et al., 2016). The B-type linkage of proanthocyanidin consist of a single interflavan bond and they are linked through C-4 and C-8 bonds while for two interflavan linkages with an additional ether bond between C-2 and O-7 were assigned to the A-type proanthocyanidin (Rodrigues et al., 2007).

The ^{1}H NMR (Table 4.18, Figure 4.50) spectrum of compound **139** exhibited the presence of three epicatechin **137** moieties. The similarities of the peak can be seen at the most downfield region in the ring B for the upper, middle and terminal units of compound **139** where nine signals appeared at δ 6.80 – 7.30, corresponding to one *ortho*-coupled (d, J = 8.2 Hz, H-5'), one *meta*-coupled (d, J = 1.9 Hz, H-2'), and one *meta*- and *ortho*-coupled (dd, J =2.0 and 8.2 Hz, H-6') protons for each units. The remaining aromatic signals were attributed to H-6 and H-8 in ring A which showed *meta*-coupling with each other at δ 5.96 and 6.01, respectively with a coupling constant of 2.3 Hz. However, this *meta*-coupling only appeared for the upper unit and not in the middle and terminal units. The signals at δ 5.96 and 6.01 were ascribed to H-6 of the middle unit and terminal unit. The remaining eight signals at δ 2.83 – 5.70 could be attributed to the aliphatic protons in ring C.

The double interflavonoid linkage (A-type) between the upper and middle unit was confirmed to be C-4/C-8 and C-2/O-7 based on the loss of proton signals of H-2 and H-4 in the upper unit and H-8 in the middle unit. However, for the second linkage of compound **139**, the loss of a proton at H-4 from the middle unit and H-8 in the terminal unit suggested a B-type linkage presented between the units.

These results are consistent with the structured units, which are all epicatechin with small value of coupling constants (J = 3.3 Hz) for H-3 and H-4. However, due to the minor amount, ^{13}C experiment of compound **139** could not be obtained but according to

the above-mentioned evidence and comparison of the UV, ESI-MS, ^{1}H NMR data and values in the literature (Jayaprakasha et al., 2006), compound **139** was identified as cinnamtannin B1.

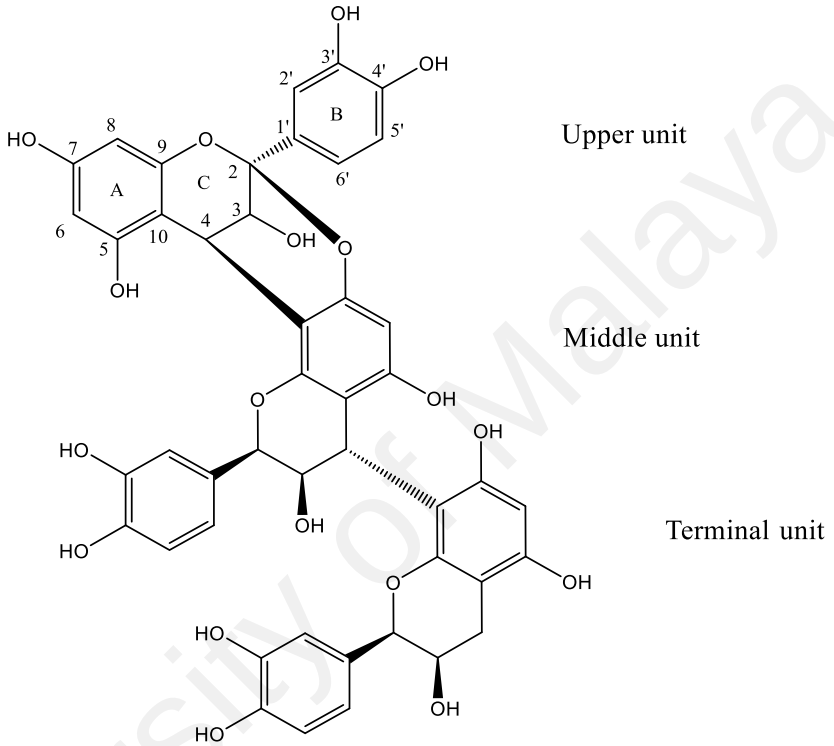

Figure 4.48: Structure of cinnamtannin B1 **139**.

Table 4.18 : ^{1}H (600 MHz) NMR data of cinnamtannin B1 **139**.

	cinnamtannin B1 **139**	cinnamtannin B1 (Jayaprakasha et al., 2006)
Position	δ_H (*m*, *J* in Hz) in MeOD (**139**)	δ_H (*m*, *J* in Hz) in MeOD
Upper unit		
2	-	-
3	3.19 (d, *J* = 3.4)	3.28 (d, *J* = 3.5)
4	4.14 (d, *J* = 3.4)	4.14 (d, *J* = 3.5)
5	-	-
6	5.96 (d, *J* = 2.3)	5.95 (d, *J* = 2.4)
7	-	-
8	6.01 (d, *J* = 2.3)	6.00 (d, *J* = 2.4)
9	-	-
10	-	-
1′	-	-
2′	7.03 (d, *J* = 2.0)	7.02 (d, *J* = 2.0)
3′	-	-
4′	-	-
5′	6.83 (d, *J* = 8.2)	6.83 (d, *J* = 8.2)
6′	6.86 (dd, *J* = 8.2, 2.0)	6.84 (dd, *J* = 8.2, 2.0)
Middle unit		
2	5.70 (br s)	5.69 (br s)
3	4.12 (br d, *J* = 1.6)	4.11 (br d, *J* = 1.2)
4	4.55 (br s)	4.54 (br s)
5	-	-
6	5.80 (br s)	5.79 (br s)
7	-	-
8	-	-
9	-	-
10	-	-
1′	-	-
2′	7.31 (d, *J* = 2.0)	7.30 (d, *J* = 2.0)

'Table 4.18, continued'

	cinnamtannin B1 **139**	cinnamtannin B1 (Jayaprakasha et al., 2006)
Position	δ_H (*m*, *J* in Hz) in MeOD (**139**)	δ_H (*m*, *J* in Hz) in MeOD
Middle unit		
3′	-	-
4′	-	-
5′	6.81 (d, *J* = 8.3)	6.81 (d, *J* = 8.2)
6′	7.18 (dd, *J* = 8.3, 2.0)	7.19 (dd, *J* = 8.2, 2.0)
Terminal unit		
2	4.38 (br s)	4.37 (br s)
3	3.86 (br s)	3.85 (br s)
4	2.83 (m)	2.82 (m)
5	-	-
6	6.10 (br s)	6.09 (br s)
7	-	-
8	-	-
9	-	-
10	-	-
1′	-	-
2′	6.82 (d, *J* = 1.8)	6.81 (d, *J* = 1.7)
3′	-	-
4′	-	-
5′	6.76 (d, *J* = 8.2)	6.74 (d, *J* = 8.2)
6′	6.72 (dd, *J* = 8.2, 1.8)	6.71 (dd, *J* = 8.2, 1.7)

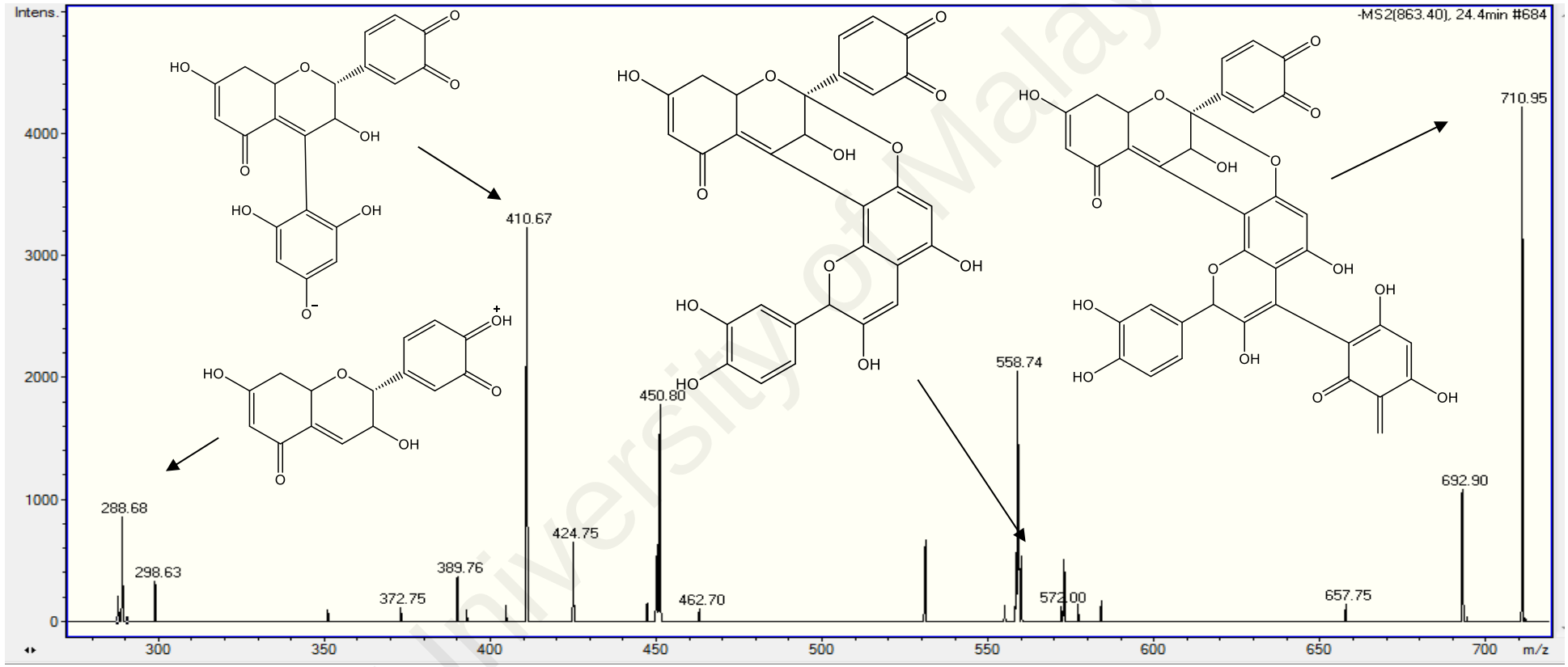

Figure 4.49: ESI-MS spectrum of cinnamtannin B1 **139**.

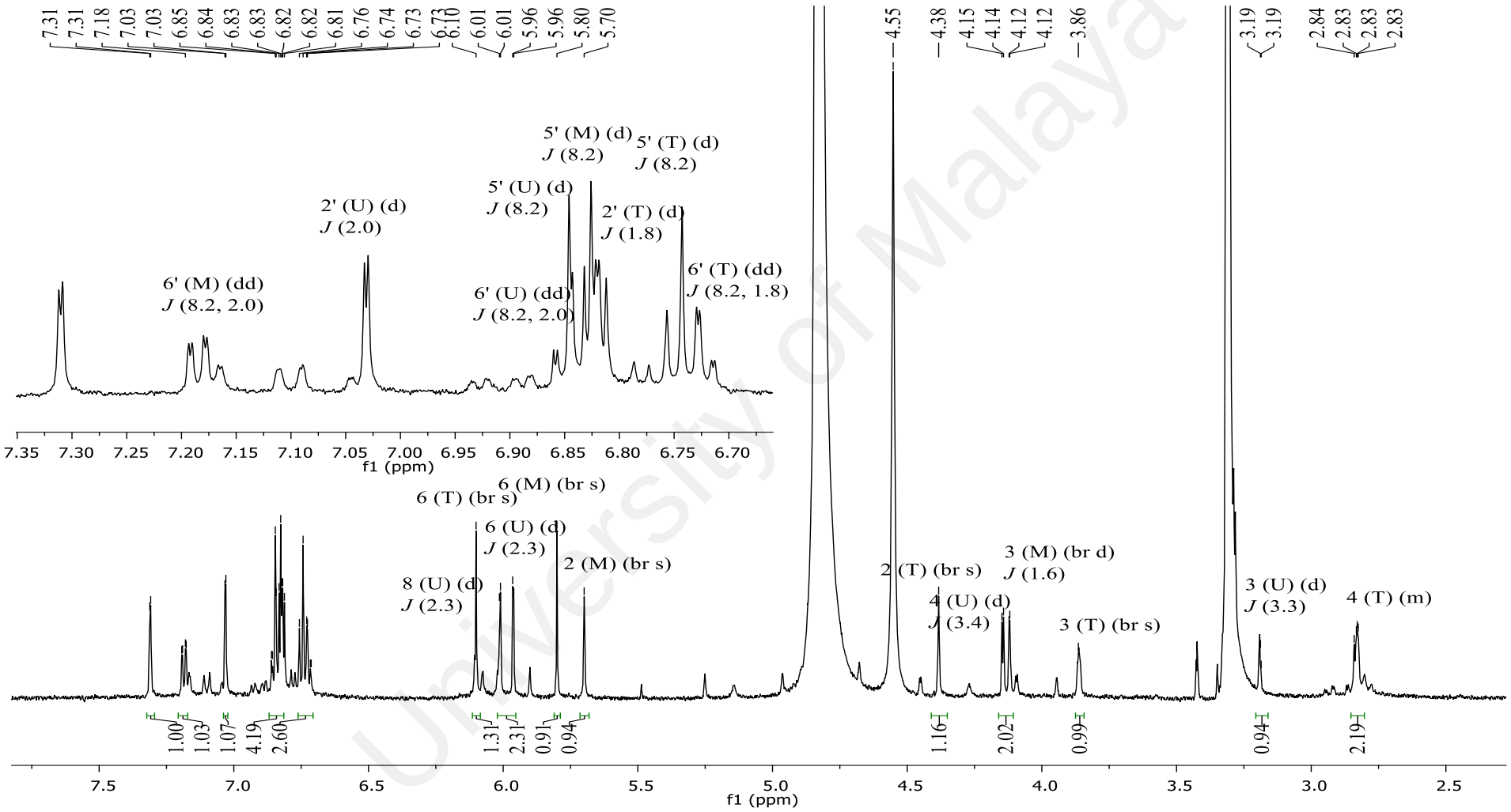

Figure 4.50: ^{1}H NMR spectrum of cinnamtannin B1 **139**.

CHAPTER 5: DENGUE

5.1 Introduction

Dengue is among the most widespread mosquito-borne disease. Mosquito-borne diseases contribute significantly to disease burden, death, poverty, and social debility all over the world particularly in tropical countries. It is endemic in many tropical and sub-tropical parts of the world and is rapidly spreading to other countries (Zandi et al., 2012; Torres et al., 2014).

Malaysia, with a population of 31.1 million and a population density of 95 per km^2, outbreaks of dengue cases are endemic, with increasing cases of dengue over the past two decades (Abd Kadir et al., 2013). According to WHO, the cumulative number of cases reported in 2017 were 27,404 cases, which was lower than in 2016 (41,075 cases), a decline of 33 % (13,670 cases) (WHO, 2017a). As of week 15, there have been a total of 65 deaths related to dengue in 2017, compared to 92 deaths for the same period in 2016, lower by 27 deaths or 29.3 %. Recent statistic of dengue cases and fatalities in Malaysia is ringing the alarm bells across the country.

Dengue is a severe, often fatal, most rapidly emerging febrile disease. It infection is caused by dengue virus (DENV), a *flavivirus* belonging to the Flaviviridae family. DENV is transmitted principally in a cycle that involves humans and mosquito vectors, *Aedes aegypti* and *Aedes albopictus* (Moghaddam et al., 2014). It is an acute infection that kills much faster than AIDS (Torres et al., 2014).

There are four distinct DENV genotypes, DENV-1. DENV-2, DENV-3 and DENV-4, with dengue virus type 2 (DENV-2) being the most prevalent. All four genotypes can cause a wide range of illnesses ranging from a mild febrile infection, self-limited dengue fever to severe dengue hemorrhagic fever and dengue shock syndrome.

5.2 Pathophysiology of dengue fever

Dengue infection is caused by bites of the female *Aedes aegypti* and *Aedes albopictus* mosquito carrying *Flavivirus*. After a person is bitten, the virus incubation period varies between 3 and 14 days (Abd Kadir et al., 2013), after which the person may experience early symptoms such as fever, headache, rash, nausea, and joint and musculoskeletal pain (Guzman & Isturiz, 2010). This classic dengue fever (DF) records temperatures between 29 to 40 °C and usually lasts 5-7 days. During this period, the virus may get into the peripheral bloodstream and, if left untreated, can damage blood vessels and lymph nodes resulting in dengue hemorrhagic fever (DHF) with symptoms such as bleeding from the nose, gums or under the skin. DHF patients also have difficulty in breathing and severe development can lead to dengue shock syndrome (DSS). DSS can result in death if proper treatment is not provided (Gibbons & Vaughn, 2002; Abd Kadir et al., 2013).

Aedes mosquitoes are small and black with white markings on the body and legs. Female mosquitoes need blood from biting humans or animals to produce live eggs. It takes 2-3 days for egg development. The principal vector of dengue has adapted well to the urban environment and always breeds in stagnant containers (Kyle & Harris, 2008). Eggs need moist conditions and mature in 24-72 hour. Mosquito bites are the only route of DENV spread. The transmission of DENV is often from human to human through domestic mosquitoes (Goel et al., 2004). An outbreak starts after a mosquito sucks the blood of a patient with DF/DHF (Figure 5.1). After being transmitted to a new human host by infected mosquitoes, the virus replicates in the lymph nodes and spreads through the lymph and blood to other tissue (Goel et al., 2004).

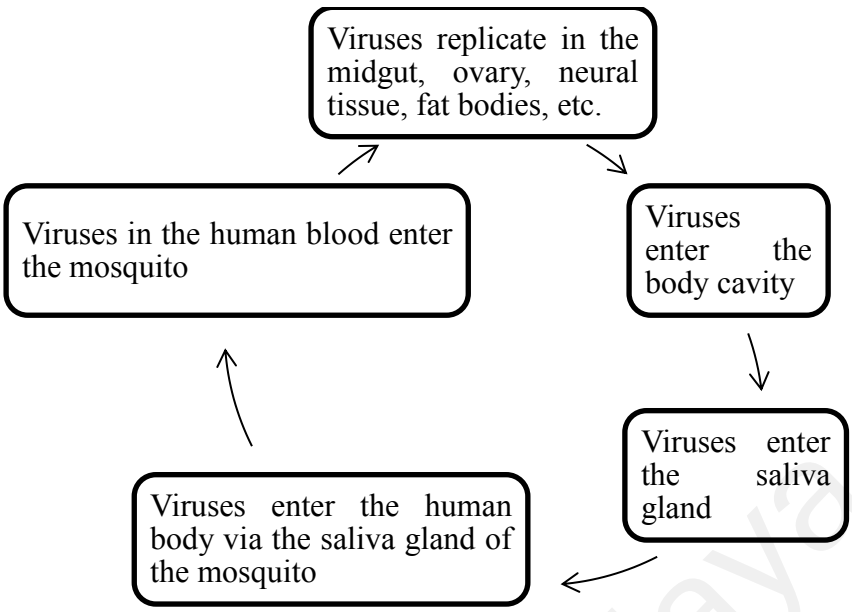

Figure 5.1: Dengue virus transmission cycle.
Source: Goel, A., Patel, D. N., Lakhani, K. K., Agarwal, A., Singla, S., & Agarwal, R. (2004). Dengue fever-a dangerous foe. J Indian Acad Clin Med, 5(3), 247-258

To identify a potential antiviral treatment for DENV, it is necessary to understand the life cycle of the virus. The dengue virion is a small particle with a lipoprotein envelope and an icosahedral nucleocapsid containing a positive single-stranded RNA genome (Goel et al., 2004). Virus infection of the cell begins with binding to the host cell surface. It enters the cell by receptor-mediated endocytosis (Abd Kadir et al., 2013), with the cell membrane forming a sac-like structure known as an endosome. In the endosome, the virus penetrates deep into the cell until the endosome membrane acquires a negative charge, which allows it to fuse with the endosomal membrane to open a port for release of genetic material. At this point, the virus in the cell fluid starts to reproduce. Changes in the acidity of the secretory pathway during this viral journey travel play an important role in its maturation (Figure 5.2) (Abd Kadir et al., 2013).

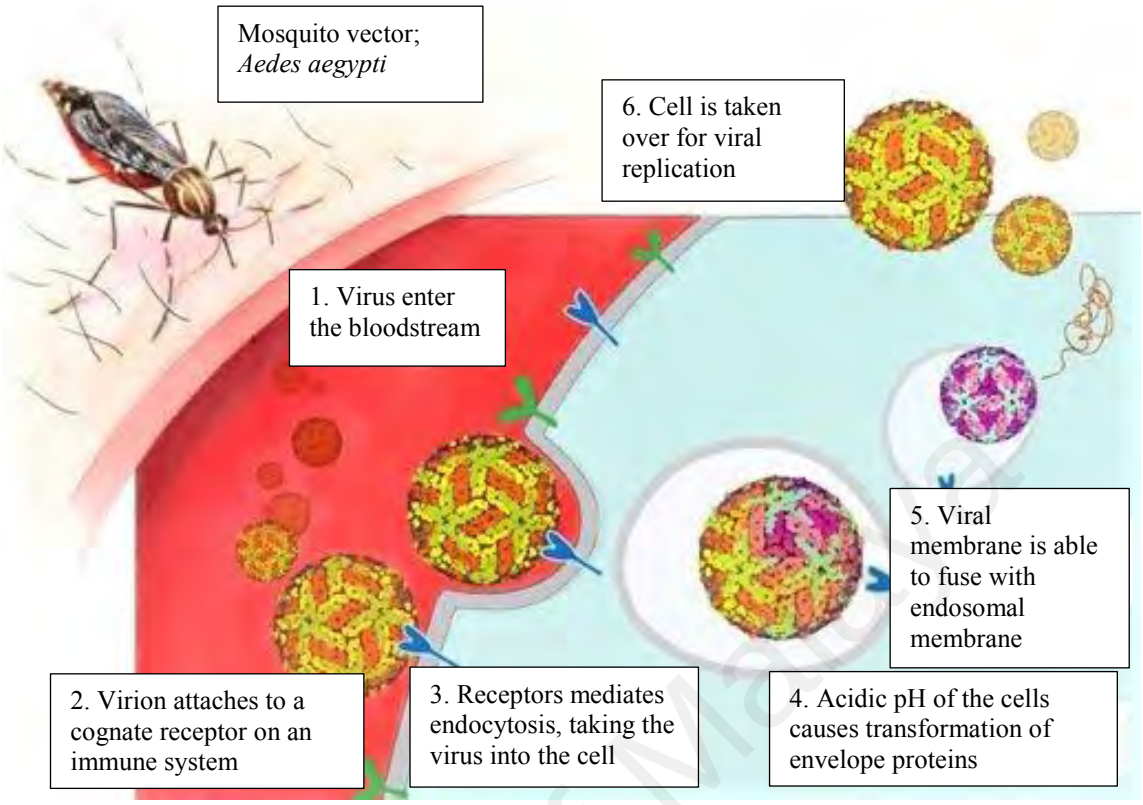

Figure 5.2: Dengue virus infection cycle in cells.
Source: Abd Kadir, S. L., Yaakob, H., & Mohamed Zulkifli, R. (2013). Potential anti-dengue medicinal plants: a review. Journal of Natural Medicines, 67(4), 677-689

5.3 Proteins of dengue virus

The DENV particle is about 50 nm in diameter. The 10,723-nucleotide RNA genome that encodes for structural and non-structural proteins; an uninterrupted open reading frame (ORF), directing the synthesis of a polyprotein precursor (Figure 5.3) (Stevens et al., 2009; Teixeira et al., 2014).

There are two types of proteins for dengue virus. The first type is consisted of structural proteins where the capsid protein (~100 amino acids) is involved in the packaging of viral genome/form nucleocapsid core (NC). The pre-membrane (prM) protein (~165 amino acids) might function as a chaperone for folding and assembly of envelope (E) protein during particle maturation. The E protein (~495 amino acids) constructs the envelope structure of the virus.

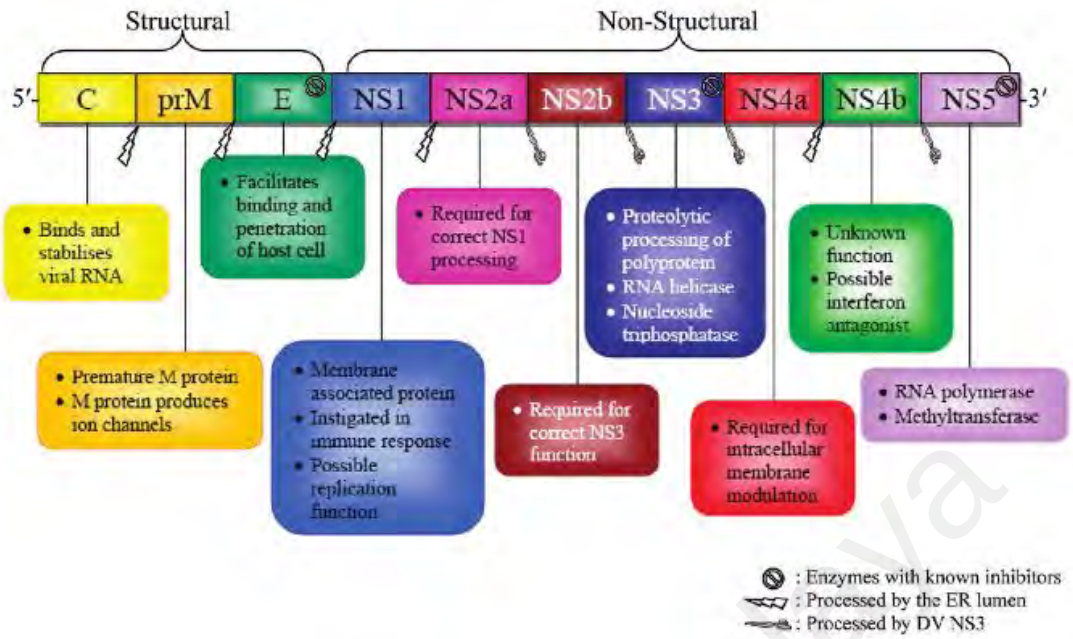

Figure 5.3: Proteins and potential targets, involved in DENV lifecycle.
Source: Stevens, A. J., Gahan, M. E., Mahalingam, S., and Keller, P. A. (2009). The medicinal chemistry of dengue fever. Journal of Medicinal Chemistry, 52(24), 7911-7926

The second type of proteins is nonstructural proteins (NS). Nonstructural proteins are essential for viral replication. NS1 involves in early steps of viral replication (Lindenbach & Rice, 1999), while NS3 shows enzymatic activities, which is involved in the viral polyprotein processing and genome replication. NS3 functions as a serine protease (NS2B/NS3 complex mediate proteolytic processing of polyprotein), 5′-Ribonucleic acid (RNA) triphosphatase (RTPase), nucleoside triphosphatase (NTPase) and helicase (Luo et al., 2008). NS5 exhibit two enzymatic activities which are involved in the methylation of 5′-cap structure of genomic RNA (methyltransferase) and RNA-dependent RNA polymer (Zhou et al., 2007; Dong et al., 2008; Geiss et al., 2009). Due to the improved knowledge on the structures and functions of the proteins, the development of vaccine and therapeutic design currently targeting E, NS1, NS3 and NS5 proteins (Wahab et al., 2007).

5.3.1 Dengue virus NS2B/NS3 protease

In the search for new drugs against this infection, the NS2B/NS3 protease of the dengue virus has been investigated as a molecular target. NS2B is a cofactor of the NS3 serine protease, which is crucial for the *flavivirus* replications that make it a potential target for the development of therapeutics against the dengue virus (Wichapong et al., 2010).

Serine protease utilizes a combination of mechanisms that are common to enzyme catalysis. First, the enzyme binds to the substrate to form an enzyme-substrate Michaelis-Menten complex (E-S complex) utilizing non-covalent bonding interaction such as ionic interactions, dipole-dipole interactions, hydrophobic interactions, hydrogen bonding and Van der Waal's interactions. When the substrate is bound to the active site of the enzyme, the carbonyl group of the scissile amide bond is exposed for catalysis by enzyme.

Recently, varied types of potential inhibitors against the DENV-2 NS2B/NS3 protease have been reported. Previous studies had screen isolated compounds from *Boesebergia rotunda* (L.) which showed potent inhibitory activity against DENV-2 NS2B/NS3 protease with K_i value of 21 μM (Kiat et al., 2006). In addition, flavonoid type compounds extracted from the leaves of *Byrsonima coccolobifolia* also showed moderate inhibitory against DENV-2 NS2B/NS3 with IC_{50} of 15.1 ± 2.2 and 17.5 ± 1.4 μM. respectively (de Sousa et al., 2015).

The availability of the compounds with reported activity values against the dengue virus NS2B/NS3 protease enzyme gave some hopes for the future development of anti-viral treatment for dengue through ligand-based drug design.

5.4 Plants traditionally used as dengue inhibitors

Natural products have become the main foundation of test material in the growth of antiviral drugs based on traditional medical practices. Traditional remedies are based on

native cultural beliefs and knowledge, and are applied to sustain health, prevent, treat and diagnose physical or mental illness. Traditional medicinal plants have been reported to have antiviral activity.

In the Philippines, *Euphorbia hirta*, known locally as "gatas-gatas", is used in traditional medicine to cure dengue fever by people in rural areas (Abd Kadir et al., 2013). It is a common weed in garden beds, and wastelands and is found throughout, Sunda, Sumatra, Peninsular Malaysia, the Philippines and Vietnam. Practitioners of traditional medicines believe that decoction of "gatas-gatas" leaves can reverse viral infection and stop the fever from moving into critical phases, although there are no scientific studies proving its efficiency. Philippine folkloric medicine also cites the use of "gatas-gatas" together with papaya leaf extract which usually boiled as a tea and drank continuously as a cure against dengue. Many people attest to this cure, at least in the Philippines and other Asian countries.

Alternanthera philoxeroides or locally known as "Alligator weed" was also used by the local people in Australia as they believed it will cure the dengue virus. The whole plants were used as decoction by using the fresh amount of the plants and it were smashed to extract the juice for the drinking (Jiang et al., 2005). The lists of the various medicinal plants used as dengue inhibitors are shown in table below.

Table 5.1: Some medicinal plants tested as dengue inhibitors.

Plants	Local name	Locality	Plant parts and uses
Alternanthera philoxeroides (Amaranthaceae)	Alligator weed	Australia	Whole plant: used as decoction by using the fresh amount of the plants and it were smashed to extract the juice for the drinking (Jiang et al., 2005).
Carica papaya (Caricaceae)	Papaya	Central America, Mexico and most tropical countries	Leaves: it being crushed and then strained using a cloth to drink the juice (Mathew et al., 2016).
Euphorbia hirta (Euphorbiaceae)	Gatas-gatas	Phillipines	Leaves: usually boiled as a tea and drank continuously (Abd Kadir et al., 2013).

5.5 Overview of studies on plant species possessing as antiviral inhibitors

To date, 32 varied species have been found having the potential to treat dengue; some of these have not yet been investigated scientifically (Abd Kadir et al., 2013). However, only 11 species namely; *Boesenbergia rotunda* (Zingiberaceae), *Cladosiphon okamuranus* (Chordariaceae), *Cryptonemia crenulate* (Halymeniaceae), *Cryptocarya chartacea* (Lauraceae), *Gymnogongrus griffithsiae* (Phyllophoraceae), *Gymnogongrus torulosus* (Phyllophoraceae), *Leucaena leucocephala* (Fabaceae), *Mimosa scabrella* (Fabaceae), *Tephrosia madrensis* (Fabaceae),and *Zostera marina* (Zosteraceae) where the species that have been successfully isolated compounds which exhibited potent activities against DENV (Sánchez et al., 2000; Kiat et al., 2006; Rees et al., 2008; Allard et al., 2011). The isolated compounds belong to various chemical classes such as sulfated polysaccharides, flavonoids, quercetin and natural chalcone compounds. The details of plants and their isolated compounds were tabulated in Table 5.2.

Generally, many plants worldwide show strong inhibitory effect on dengue virus. However, *B. glabra* and *E. kingiana* have not been studied before against dengue virus. Here, we report the effect on isolated compounds of both plants towards dengue virus specifically on DENV-2 using NS2B/NS3 protease.

Table 5.2: Compounds isolated which possessing antiviral activity, according to the plant species.

Species and site of collection	Chemical constituents isolated	Type of compounds	Biological activities
Boesenbergia rotunda (Zingiberaceae) Thailand	4-Hydroxypanduratin A **140** Panduratin A **141**	Flavonoids	Both compounds showed good competitive inhibitory activities towards DENV-2 NS3 protease with K_i values of 21 and 25 μM, respectively (Kiat et al., 2006).
Cladosiphon okamuranus (Chordariaceae) Japan	Fucoidan **142**	Polysaccharide	The compound was found to potentially inhibit DENV-2 infection. The virus infection was tested in BHK-21 cells in a focus-forming assay. It reduced infectivity by 20 % at 10 μ*g* mL^{-1} as compared with untreated cells (Hidari et al., 2008).

'Table 5.2, continued'

Species and site of collection	Chemical constituents isolated	Type of compounds	Biological activities
Cryptonemia crenulata (Halymeniaceae) Brazil	Galactan **143**	Polysaccharide	Galcatan **143** were selective inhibitors of DENV-2 multiplication in Vero cells with IC_{50} values of 1.0 μ*g* mL^{-1}, where the IC_{50} values for the reference polysaccharides heparin and DS8000 were 1.9 and 0.9 μ*g* mL^{-1}, respectively (Talarico et al., 2005).
Cryptocarya chartacea Kosterm (Lauraceae) France	Chartaceones C **144** Chartaceones D **145** Chartaceones E **146** Chartaceones F **147**	Flavonoids	All these compounds demonstrated inhibitory activity against DENV NS5 RNA-dependent RNA polymerase, with IC_{50} values ranging from 1.8 to 4.2 μM (Allard et al., 2011).
Gymnogongrus griffithsiae (Phyllophoraceae) Brazil	Kappa carrageenan **148**	Polysaccharide	The compound inhibits DENV-2 multiplication at the IC_{50} values of 0.9 μ*g* mL^{-1}, which is the same as the IC_{50} value for the commercial polysaccharides DS8000 (Talarico et al., 2005).

'Table 5.2, continued'

Species and site of collection	Chemical constituents isolated	Type of compounds	Biological activities
Gymnogongrus torulosus (Phyllophoraceae) Brazil	Galactan **143**	Polysaccharide	It was active against DENV-2 in Vero cells, with IC_{50} values in the range of 0.19 – 1.7 μ*g* mL^{-1} (Pujol et al., 2002).
Leucaena leucocephala (Fabaceae) Brazil	Galactomannans **149**	Polysaccharides	This compound showed moderate activity against DENV-1 in vivo. In vitro experiments with DENV-1 in C6/36 cell culture assays showed that the concentration producing a 100-fold decrease in virus titer of DENV-1 was 37 mg L^{-1} (Ono et al., 2003).
Mimosa scabrella (Fabaceae) Brazil	Galactomannans **149**	Polysaccharides	In vitro experiments with DENV-1 in C6/36 cell culture assays showed galactomannans **150** with concentration of 347 mg L^{-1} produced a 100-fold decrease in virus titer of DENV-1 (Ono et al., 2003).

'Table 5.2, continued'

Species and site of collection	**Chemical constituents isolated**	**Type of compounds**	**Biological activities**
Tephrosia madrensis (Fabeaceae); Mexico	glabranine **150** 7-*O*-methylglabranine **151**	Flavonoids	Both compounds exert strong inhibitory effects on dengue virus replication in LLC-MK2 cells. 7-*O*-methylglabranine **151** inhibited the replication of virus by 10% with 6 µM and by 75% with 12 µM and 25 µM; inhibitory effects were observed at lower concentrations, **151** were more conspicuous than with glabranine **150** (Sánchez et al., 2000).
Zostera marina (Zosteraceae); Sri Lanka	Zosteric acid **152**	Cinnamic acid	It showed a modest IC_{50} of approximately 2.3 mM against DENV-2 (Rees et al., 2008).

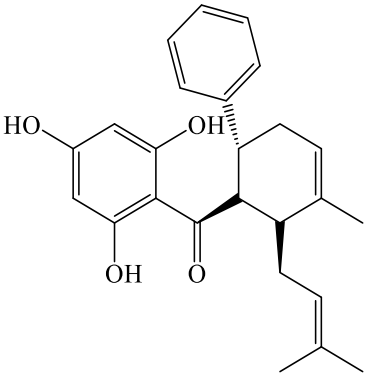

140

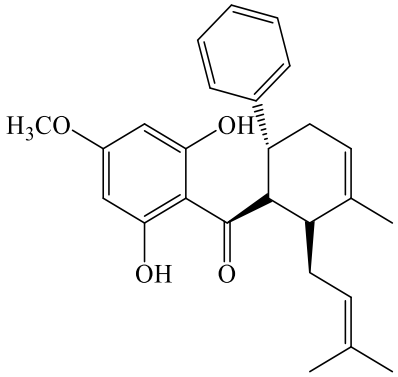

141

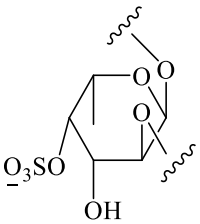

142

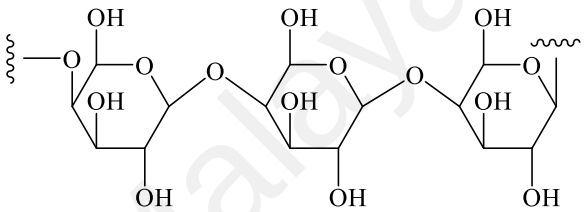

143

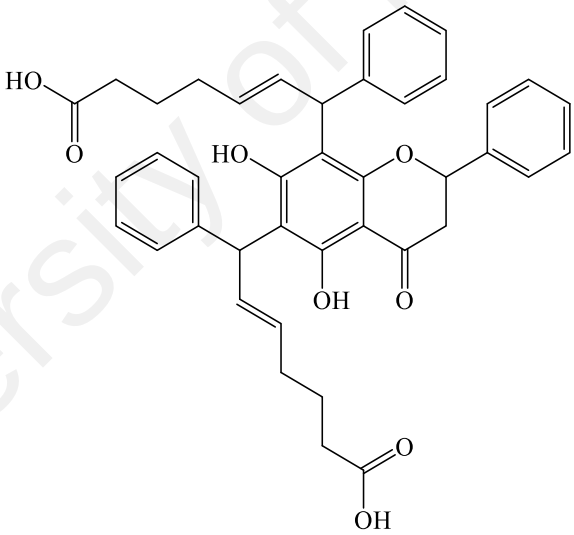

144

Scheme 5.1: Isolated compounds which exhibited potent activities against DENV.

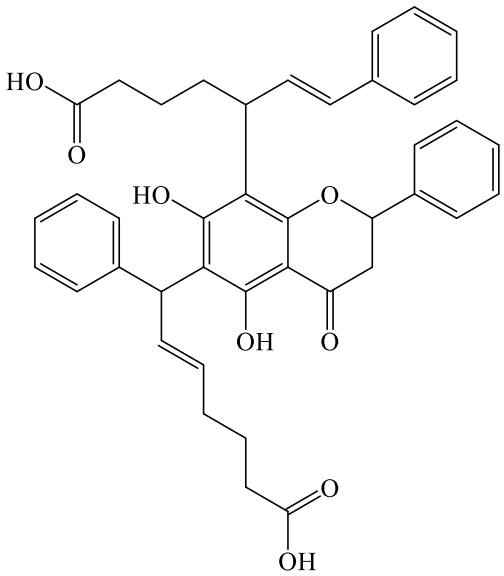

145

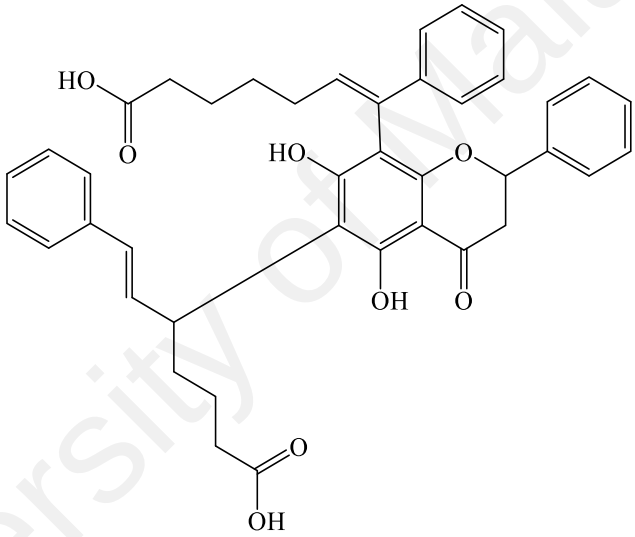

146

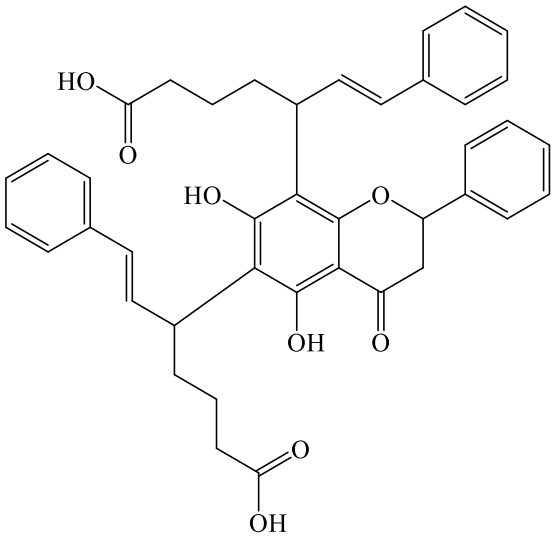

147

'Scheme 5.1, continued'

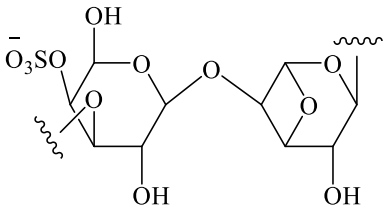

148

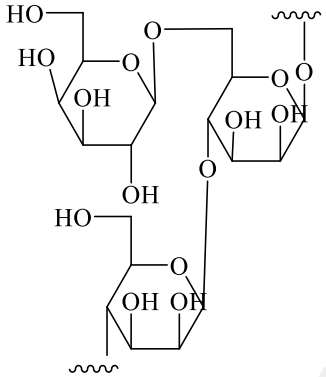

149

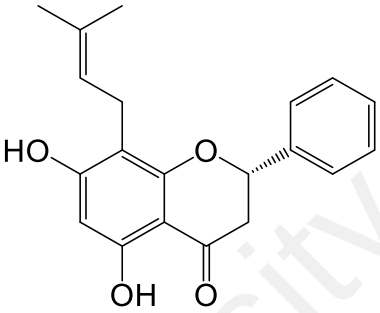

150

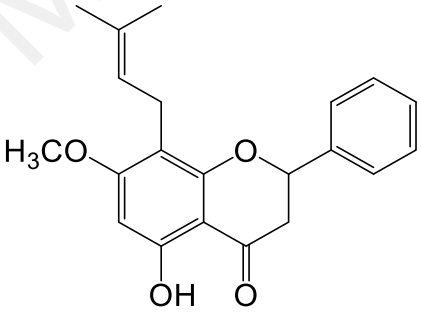

151

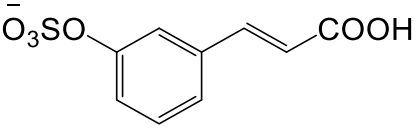

152

'Scheme 5.1, continued'

5.6 Material and methods for *in vitro* DENV-2 protease inhibition assay

Briefly, the preparation of the materials and methods for the assay are discussed in subchapter below.

5.6.1 Preparation of DENV-2 NS2B/NS3 protease

Protease inhibition study was performed *in vitro* using purified DENV-2 NS2B/NS3 protease (Nawi, 2015; Abdul et al., 2016), and the bioassay protocol was employed as described by Nawi and A. W. H et al. with minor modification (Nawi, 2015; Abdul et al., 2016).

5.6.2 Preparation of the substrate (Boc-Gly-Arg-Arg-MCA)

The substrate was prepared by mixing 800 µL of dimethyl sulfoxide (DMSO) into the vial containing 5.2 mg (8.0 µmol) of the titled compound, which has been lyophilized as an amorphous powder from aqueous solution. The vial was kept tight and shake until all the contents are dissolved. This preparation will furnish a 10 mM solution of the titled compound.

5.6.3 Preparation of Tris buffer (200 mM Tris – HCl, pH 8.5)

12.14 g of Tris base was dissolved in 300 ml autoclaved ultrapure water. The solution was adjusted to pH 8.5 with concentrated HCl and made up to a final volume of 500 ml with autoclaved ultrapure water, filtered through a 0.45 µm filter and stored at 4 °C.

5.6.4 Methods for *in vitro* DENV-2 protease inhibition assay

The protease activity assay was conducted at a constant concentration of the protease, constant concentrations of substrate, and constant concentrations of the

compounds with the values of 0.5 µM, 10 mM in DMSO solution, and 200 ppm, respectively. The reaction mixtures were prepared in black 96-well plates. Each reaction mixture consisted of 200 mM Tris buffer with the total volume of 100 µL. Tris buffer was pipetted to the wells, followed by compounds and by the enzyme into well plate. The mixtures were pre-incubated at 37 °C, shaken at 200 rpm for 10 minutes. Then, the substrate was added to wells and incubated at 37 °C and shaken at 200 rpm for 60 minutes.

After the completion incubation time completed, the well plate was analyzed, and the fluorescence was detected using the Promega Glomax Multi Detection System microplate reader with excitation and emission wavelengths at 365 and 410-460 nm, respectively. Percentage of inhibition was calculated using the following formula:

Percentage of inhibition: $= \frac{Absorbance\ of\ control - Absorbance\ of\ sample}{Absorbance\ of\ control}\ x\ 100\%$

For IC_{50} determination, the same protocol was used as described before with serial dilutions of inhibitors in the range of 0.78 to 200 µg/mL with varied concentrations of the compounds between 6.25 to 200 ppm.

5.7 Results and discussion

The dichloromethane extracts (DCME) of *B. glabra* and *E. kingiana* have shown moderate inhibitory activity against NS2B/NS3 protease of DENV-2 with percentage of inhibition of 51.28 ± 13.90% and 65.05 ± 3.73% at 200 ppm respectively as compared to the standard quercetin **153** with a value of 90.91 ± 2.61% inhibition at 200 ppm. Therefore, all compounds with sufficient amount from both plants, *B. glabra* and *E. kingiana* were subjected to *in vitro* analysis against NS2B/NS3 protease of DENV-2 with the intention of identifying the compounds which could be responsible in giving rise to the activities.

From *B. glabra*, only two compounds, 9-hydroxy-1-(4-hydroxy-3-methoxyphenyl)propane-7-one **125** and pahangine A **130** were tested and calculated for their percentage of inhibition towards the protease. Percentage of inhibition for 9-hydroxy-1-(4-hydroxy-3-methoxyphenyl)propane-7-one **125** and pahangine A **130** were 48.54 ± 7.45% and 28.59 ± 7.78%, respectively. Both compounds showed weak inhibition towards the protease with percentage of inhibition less than 50%. The percentage of inhibition for each compound together with crude extracts of *B. glabra* standard at 200 ppm is shown in Table 5.3 below.

Table 5.3: Percentage inhibition of the DCME and compounds isolated from *B. glabra* against DENV-2 NS2B/NS3 protease.

Compounds isolated	**Percentage inhibition (%)**
Dichloromethane extracts (DCME) of *B. glabra*	51.28 ± 13.91
9-Hydroxy-1-(4-hydroxy-3-methoxyphenyl)propane-7-one **125**	48.54 ± 7.45
Pahangine A **130**	28.59 ± 7.78
Quercetin **153**(standard)	90.90 ± 9.13

Meanwhile, for *E. kingiana*, five compounds were subjected to *in vitro* assays against NS2B/NS3 protease of DENV-2; methyl orsellinate **134**, 5α-Cholesta-20,24-diene-3β,6α-diol **135**, 4-hydroxy-6-(9,13,17-trimethyldodeca-8,12,16-trienyl)-2(3 H)-benzofuranone**136**, (-)-epicatechin **137**, and (+)-catechin **138**. Percentage of inhibition for methyl orsellinate **134**, 5α-Cholesta-20,24-diene-3β,6α-diol **135**, 5-hydroxy-7-(3,7,11-trimethyldodeca-2,6,10-trienyl)-2(3*H*)-benzofuranone **136**, (-)-epicatechin **137**, and (+)-catechin **138** were 16.42 ± 2.92%, 49.21 ± 7.40%, 61.23 ± 6.96%, 69.92 ± 3.34% and 62.02 ± 6.19%, respectively. Among all compounds, only three compounds were moderately inhibiting the protease with percentage of inhibition more than 50%. The

percentage of inhibition for each compound together with crude extracts of *E. kingiana* and standard at 200 ppm is shown in Table 5.4 below.

Table 5.4: Percentage inhibition of the DCME and compounds isolated from *E. kingiana* against DENV-2 NS2B/NS3 protease.

Sample	Percentage inhibition (%)
Dichloromethane extracts (DCME) of *E. kingiana*	65.05 ± 3.73
Methyl orsellinate **134**	16.42 ± 2.92
5α-Cholesta-20,24-diene-3β,6α-diol **135**	49.21 ± 7.40
5-Hydroxy-7-(3,7,11-trimethyldodeca-2,6,10-trienyl)-2(3*H*)-benzofuranone **136**	61.23 ± 6.96
(-)-Epicatechin **137**	69.92 ± 3.34
(+)-Catechin **138**	62.02 ± 6.19
Quercetin **153**(standard)	90.90 ± 9.13

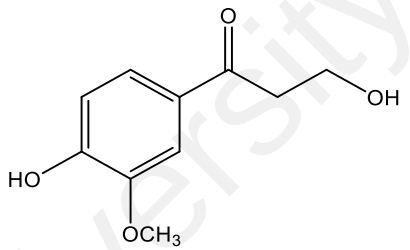

125

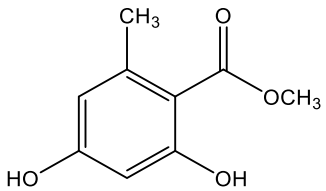

134

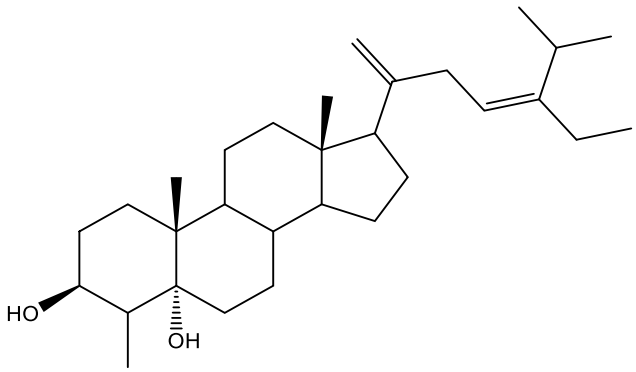

135

Scheme 5.2: Structure of compounds which subjected to *in vitro* against NS2B/NS3 protease of DENV-2.

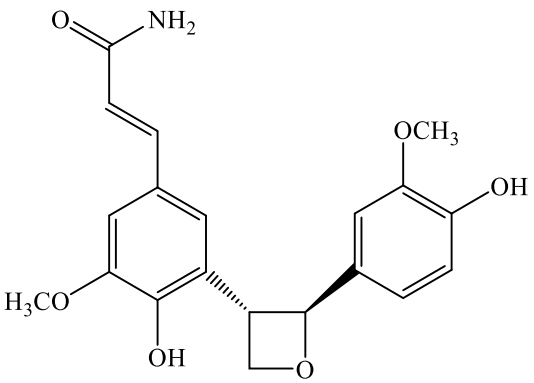

130

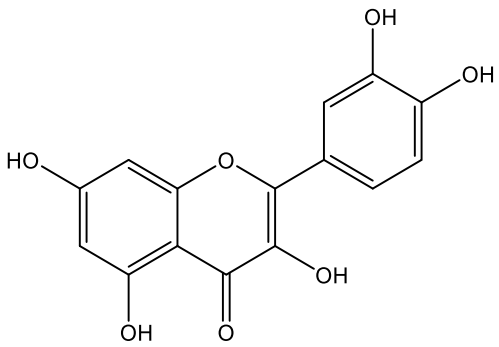

153

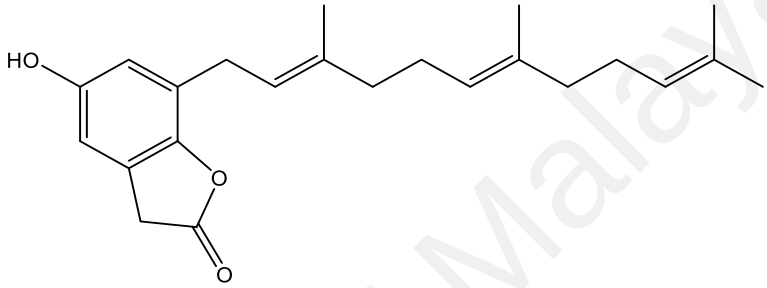

136

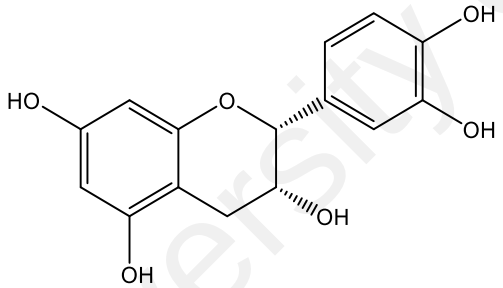

137

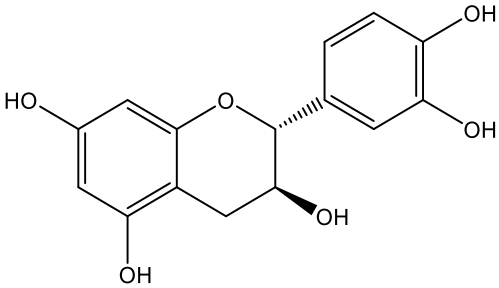

138

'Scheme 5.2, continued**'**

Based on the percentage of inhibition for both plants, only compounds from *E. kingiana*, 4-hydroxy-6-(9,13,17-trimethyldodeca-8,12,16-trienyl)-2(3 H)-benzofuranone**136**, (-)-epicatechin **137**, and (+)-catechin **138** gave percentage inhibition more than 50%, hence these compounds were further evaluated in order to determine their respective IC_{50} values.

Subsequently, 4-hydroxy-6-(9,13,17-trimethyldodeca-8,12,16-trienyl)-2(3 H)-benzofuranone**136**, (-)-epicatechin **137**, and (+)-catechin **138** with the percentage of inhibition more than 50% (Scheme 5.3) were further evaluated to determine their respective IC_{50} values along with the reference standard, quercetin **153** (Table 5.5). 4-hydroxy-6-(9,13,17-trimethyldodeca-8,12,16-trienyl)-2(3 H)-benzofuranone**136** (IC_{50} = 403.14 ± 33.03 μM), (-)-epicatechin **137** (IC_{50} = 170.10 ± 5.94 μM), and (+)-catechin **138** (IC_{50} = 184.13 ± 2.11 μM), moderately inhibited the NS2B/NS3 protease of DENV-2 with (-)-epicatechin **137** being the most moderately inhibited the protease among all isolated compounds.

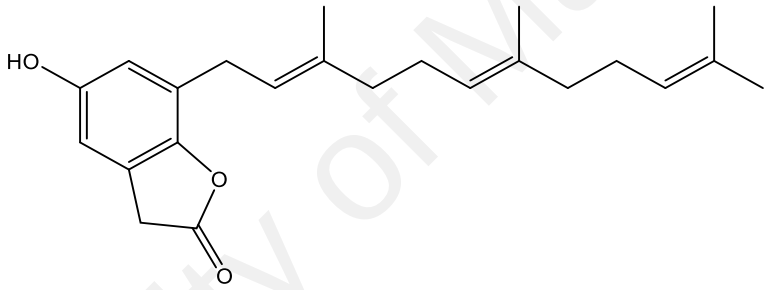

136

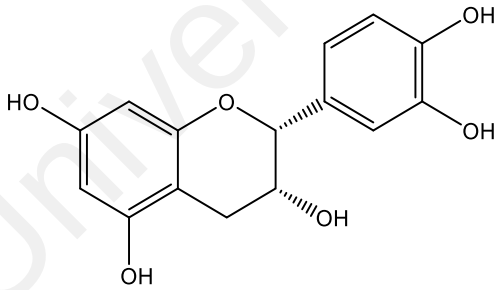

137

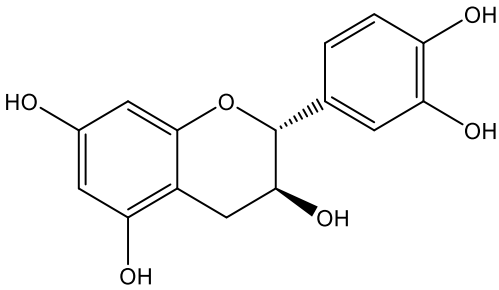

138

Scheme 5.3: Structure of compounds that exhibited more than 50 % inhibition towards the DENV-2 NS2B/NS3 protease.

Table 5.5: IC_{50} values on active compounds.

Compounds	**IC_{50} (μM)**
4-Hydroxy-6-(9,13,17-trimethyldodeca-8,12,16-trienyl)-2(3 H)-benzofuranone**136**	403.14 ± 33.03
(-)-Epicatechin **137**	170.10 ± 5.94
(+)-Catechin **138**	184.13 ± 2.11
Quercetin **153** (standard)	9.48 ± 9.13

Hence, to understand the interaction of active compounds (4-hydroxy-6-(9,13,17-trimethyldodeca-8,12,16-trienyl)-2(3 H)-benzofuranone**136**, (-)-epicatechin **137**, and (+)-catechin **138**) with the DENV-2 NS2B/NS3 protease, molecular docking (MD) were performed. This will provide much clear picture of the site at which the active compounds bind to the protease.

CHAPTER 6: MOLECULAR DOCKING OF ACTIVE COMPOUNDS ON DENV-2 NS2B/NS3 PROTEASE

6.1 Introduction

With the development of computer science and structure biology, structure-based drug design has become one of routine approaches of drug discovery today (Hao et al., 2012). At the same time, high-throughput protein purification, crystallography and nuclear magnetic resonance spectroscopy techniques have been established and contributed to many structural details of proteins and protein-ligand complexes. These developments allow the computational strategies to cover all aspects of drug discovery today, such as virtual screening (VS) techniques for hit identification and methods for main optimization (Meng et al., 2011). VS is a more direct and rational drug discovery approach and has the benefit of low cost and effective screening compare with traditional experimental high-throughput screening (HTS).

VS can be classified into ligand-based and structure-based methods. Ligand-based methods is when a set of active ligand molecules is identified, and few or no structural information is accessible for targets, such as pharmacophore modeling and quantitative structure activity relationship (QSAR) methods can be used. As to structure-based drug design, MD is one of the most frequently used in methods because of its ability to predict, with a substantial degree of accuracy, the conformation of small-molecule ligands within the appropriate binding site (Ferreira et al., 2015). To investigate the mechanism of action, docking studies were performed for the active compounds.

6.2 Dengue virus NS2B/NS3 protease: insight into molecular interaction

Dengue virus type 2 (DENV-2), the most prevalent of the four serotypes, contains a single-stranded RNA and encodes a large single polyprotein precursor of 3,391 amino acid residues which consists of three structural proteins (C, prM, and E) and seven

nonstructural proteins (NS1, NS2A, NS2B, NS3, NS4A, NS4B and NS5) (Frecer & Miertus, 2010). In this study, the NS2B/NS3 protease of the DENV-2 has been investigated as molecular target. It was reported by Wichapong, the MD simulations of NS2B/NS3 protease (Figure 6.1) discovered that strong interaction between the C-terminal domain of NS2B and NS3 support the stability of the loop regions of the NS3 protease (Wichapong et al., 2010).

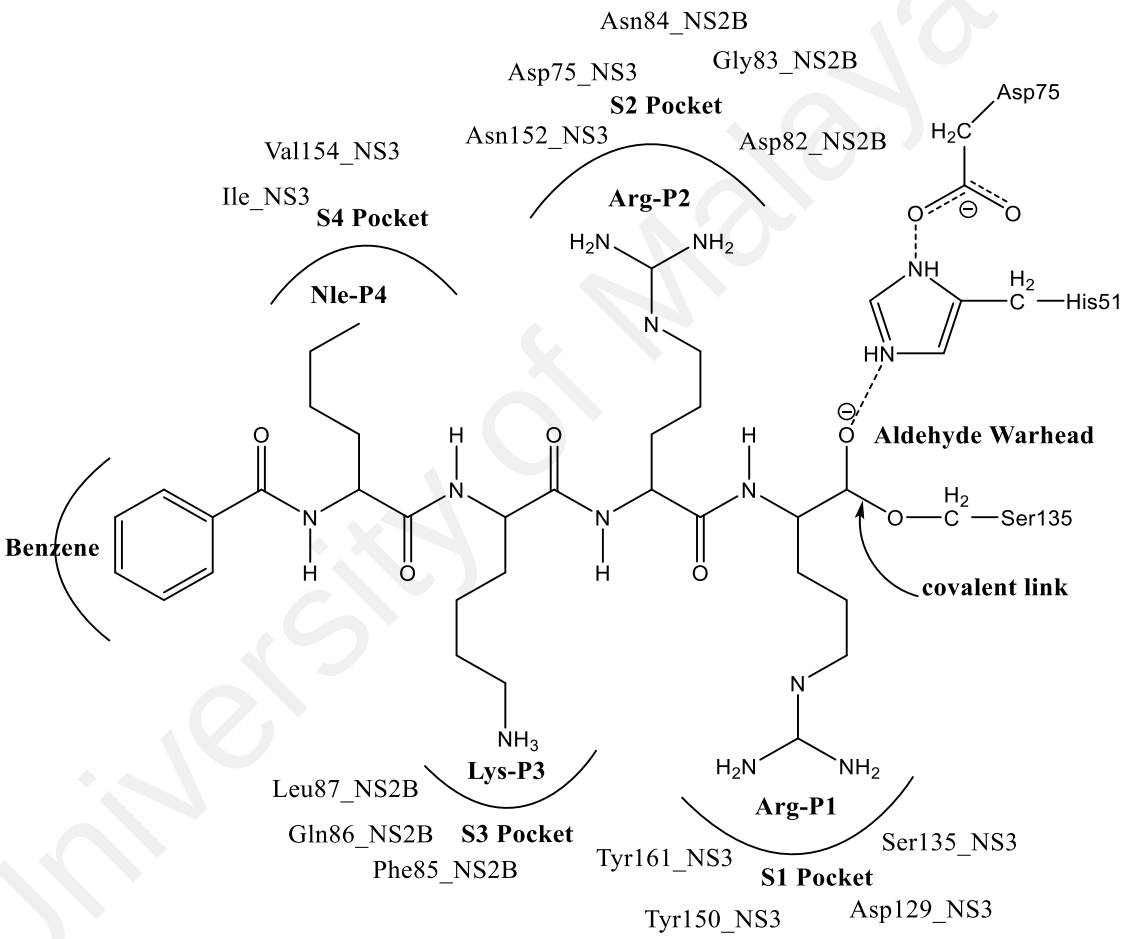

Figure 6.1: Schematic representation of the DENV-2 NS2B/NS3 protease.
Source: Wichapong, K., Pianwanit, S., Sippl, W., & Kokpol, S. (2010). Homology modeling and molecular dynamics simulations of Dengue virus NS2B/NS3 protease: insight into molecular interaction. J Mol Recognit, 23(3), 283-300

The enzymatic NS3 protease is a trypsin-like serine protease shown to harbor a classic serine protease catalytic triad consist of residues His51, Asp75, and Ser135. This interaction also involved the binding of the Arg-P2 residue of the inhibitor and the residue

of the S2 pocket. These results show that the C-terminal domain of NS2B is not only vital for the interaction with the P2 residue of the inhibitor but also plays a noteworthy role for binding to NS3 protease.

Furthermore, the interaction of the inhibitor with the S1 pocket involves only residue from the NS3 domain. Contrarily, both, residue from the C-terminal domain of NS2B as well as Asp75 and Asn152 from NS3, are significant for maintaining the interaction with the P2 residue of the inhibitor at the S2 pocket. At the S3 pocket, the main interactions are detected between the P3 residue and Gly153 as well as Tyr161 from NS3. Hydrophobic interaction only can be observed at the S4 pocket of the NS3 domain.

6.3 Materials and methods

4-hydroxy-6-(9,13,17-trimethyldodeca-8,12,16-trienyl)-2(3 H)-benzofuranone**136**, (-)-epicatechin **137**, and (+)-catechin **138** were studied to MD for prediction of predominant binding mode of a ligand with 3D structures of DENV-2 NS2B/NS3 protease that is considered a key technique. The enzyme NS2B and NS3 were used as receptor and the chemical compounds (4-hydroxy-6-(9,13,17-trimethyldodeca-8,12,16-trienyl)-2(3 H)-benzofuranone**136**, (-)-epicatechin **137**, and (+)-catechin **138**) were act as ligand molecule. The effectiveness of three compounds can be determined via the docking studies by calculating their minimization value. This will give broad perspective for better understanding of their activity. Briefly, MD of the active inhibitors was carried out using Autodock 3.0.5 and AutoDockTools (ADT).

6.3.1 3D structure preparation of the DENV-2 NS2B/NS3 protease

A homology model of the DENV-2 NS2B/NS3 protease was obtained from the Research Collaboratory for Structural Bioinformatics – Protein Data Bank (RCSB-PDB) database (PDB ID:2FOM) for structure-based design purposes. The selected 3D structure

was downloaded in PDB format file. The enzyme was then prepared under the protein preparation protocol implemented in Discovery Studio 2.5 (Accelry Inc., CA, USA) suite of program. After that, the geometry optimization and energy minimization of DENV-2 NS2B/NS3 protease was conducted by removing the water molecules. Then, the protonation of the DENV-2 NS2B/NS3 protease was done through 'Protonate 3D' feature, followed by optimization of the partial charge and energy minimization. The optimized, minimized 3D structure of DENV-2 NS2B/NS3 protease then was saved in the .pdbqt format.

6.3.2 Ligands preparation

For the ligands, the two-dimensional structure of the 4-hydroxy-6-(9,13,17-trimethyldodeca-8,12,16-trienyl)-2(3 H)-benzofuranone**136**, (-)-epicatechin **137**, and (+)-catechin **138** was built using Hyperchem 8 and subjected to energy minimization with a convergence criterion of 0.05 kcal/(molA). Non-polar hydrogens and lone pairs were then merged, and each atom was assigned with Gasteiger partial charges. A grid box was generated at the center of the active site gorge with 60x60x60 points along the *x*, *y* and *z* axes. The rest parameters were set at default setting.

6.3.3 Molecular docking simulation of DENV-2 NS2B/NS3 protease and ligands

The MD simulation of DENV-2 NS2B/NS3 protease and the ligands were done by using Autodock 3.0.5 software. At first, the docking simulation process began by selecting the 'Dock' feature from the 'Compute' panel. The rest parameters were set at default setting. After the docking control, parameters and models to display were set to the receptor and ligand molecule. The output was set to predict 100 solutions. The docking result can be saved in .mdb file format. The obtained log files were read in ADT

to analyze the results of docking. The overall steps of molecular docking simulation were simplified in the Scheme 6.1.

The lowest binding energy conformation in all clusters was considered as the most favorable docking pose. The determination of the best ligand from docking simulation was decided on their molecular interaction with the lowest docked energy (by observing the protein-ligand complex) that generated from the simulation (Verma et al., 2015). The lowest energy minimized value is the most suitable for drug stability.

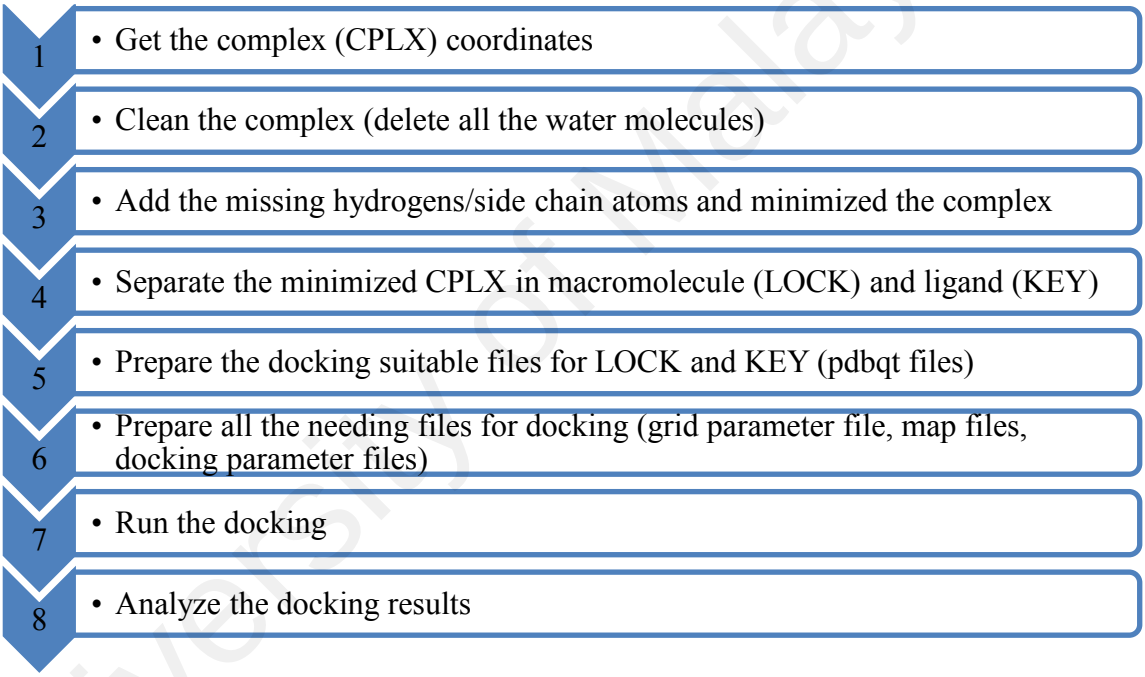

Scheme 6.1: Overall steps of molecular docking simulations.

6.4 Results and discussion

Binding energy evaluation provided a correlation to the activity performed at the experimental stage. The best docked pose with the lowest binding energy was selected from series of poses generated after calculating their binding energy. The more negative the binding energy, the better the binding activity. In another word, the binding between the ligand and the enzyme will be more stable. The binding energy of the 4-hydroxy-6-(9,13,17-trimethyldodeca-8,12,16-trienyl)-2(3 H)-benzofuranone**136**, (-)-epicatechin

137, (+)-catechin **138** and quercetin **153** (standard) have given a docking score of -6.31, -6.17, -6.00 and -6.53 kcal with the modelled DENV-2 NS2B/NS3 protease, respectively.

As per discussed in previous chapter (chapter 5.7), although (-)-epicatechin **137** being the most potent compared to the other isolated compounds, the standard quercetin **153** showed highest inhibition. It may cause by the interaction of hydrogen bonding between carbonyl group at C-4 of the quercetin **153** with aldehyde warhead (His51) at catalytic triad in the interacting site of the DENV-2 NS2B/NS3 protease, while other isolated active compounds (4-hydroxy-6-(9,13,17-trimethyldodeca-8,12,16-trienyl)-2(3 H)-benzofuranone**136**, (-)-epicatechin **137**, and (+)-catechin **138**) not bind at catalytic triad. Catalytic triad is where all the reaction occurs. Interaction with the aldehyde warhead at the catalytic triad (His51, Asp75 and Ser135) were needed to have effectiveness inhibition of the enzyme activity (Yin et al., 2006). The only common interaction for all active compounds (4-hydroxy-6-(9,13,17-trimethyldodeca-8,12,16-trienyl)-2(3 H)-benzofuranone**136**, (-)-epicatechin **137**, and (+)-catechin **138**) with the standard quercetin **153** was the hydrogen bonding between oxygen atoms in each compound with Asn152 at S2 pocket.

Being diastereomers; (-)-epicatechin **137**, and (+)-catechin **138**, both showed similar interaction with Asp129 and Tyr161 of the DENV-2 NS2B/NS3 protease at S1 pocket. However, (-)-epicatechin **137** showed a slightly more activity as compared to (+)-catechin **138**, which may due to the type of the bonding with Tyr161 of the DENV-2 NS2B/NS3 protease. (-)-epicatechin **137** showed 4 hydrogen bonding interaction of hydroxyl group while (+)-catechin **138** only have 3 hydrogen bonding and 1 π- π stacking interaction with the DENV-2 NS2B/NS3 protease. Having more hydrogen bonding interactions resulted for (-)-epicatechin **137** being more active as hydrogen bonding was more stable compare to the π- π stacking interaction in the (+)-catechin **138**. The least potent, 4-hydroxy-6-(9,13,17-trimethyldodeca-8,12,16-trienyl)-2(3 H)-

benzofuranone**136**, may cause from only showed 2 hydrogen bonding with Asp129 and Ser135 at S1 pocket.

Apart from the type of interaction, distance of the enzyme and ligands at the active sites within 3 Å region was also plays a vital role for the good interaction. Summary of the binding energy and distance of the enzyme and ligands at the active sites was tabulated in Table 6.1. The binding sites of the DENV-2 NS2B/NS3 protease and the ligands were illustrated in Figure 6.2, Figure 6.3 and Figure 6.4.

Based on foregoing discussion, it can be concluded that hydrogen bonding interactions, and π- π stacking interaction of the active ligands with the above discussed residues are important for activity and potency of the inhibitors especially interaction at the catalytic triad.

Hence, from the computational analysis mainly MD simulations, it has showed more clearly on their binding mode of the activity profile which comprise protease and ligand interaction. Further, *in vitro* and *in vivo* studies on dengue virus are necessary to confirm their efficacy and to evaluate their drug potency.

Table 6.1: Binding interaction data for the active compounds towards DENV-2 NS2B/NS3 protease.

Ligand/Compound	Binding Energy (kcal)	Interacting site	Residue	Type of interaction	Distance (Å)	Ligand Interacting
4-hydroxy-6-(9,13,17-trimethyldodeca-8,12,16-trienyl)-2(3 H)-benzofuranone**136**	-6.31	S1 pocket	Asp129	Hydrogen	2.19	Hydroxyl group at C-5
			Ser135	Hydrogen	1.78	Carbonyl group at C-1
(-)-epicatechin **137**	-6.17	S1 pocket	Asp129	Hydrogen	1.91	Hydroxyl group at C-7
			Asp129	Hydrogen	2.19	Hydroxyl group at C-7
			Tyr161	Hydrogen	2.09	Hydroxyl group at C-3
		S2 pocket	Asn152	Hydrogen	1.81	Hydroxyl group at C-3’
			Asn152	Hydrogen	1.88	Hydroxyl group at C-4’
(+)-catechin **138**	-6.00	S1 pocket	Asp129	Hydrogen	1.83	Hydroxyl group at C-5
			Ser135	Hydrogen	2.44	Hydroxyl group at C-3
			Tyr161	Pi-Pi	3.41	Aromatic ring A
		S2 pocket	Asn152	Hydrogen	1.95	Hydroxyl group at C-3’
			Asn152	Hydrogen	2.11	Hydroxyl group at C-4’
quercetin **153**	-6.53	Aldehyde warhead	His51	Hydrogen	2.19	Carbonyl group at C-4
		S1 pocket	Ser135	Hydrogen	1.71	Carbonyl group at C-4
			Ser135	Hydrogen	1.77	Hydroxyl group at C-5
		S2 pocket	Asn152	Hydrogen	1.84	Hydroxyl group at C-3’

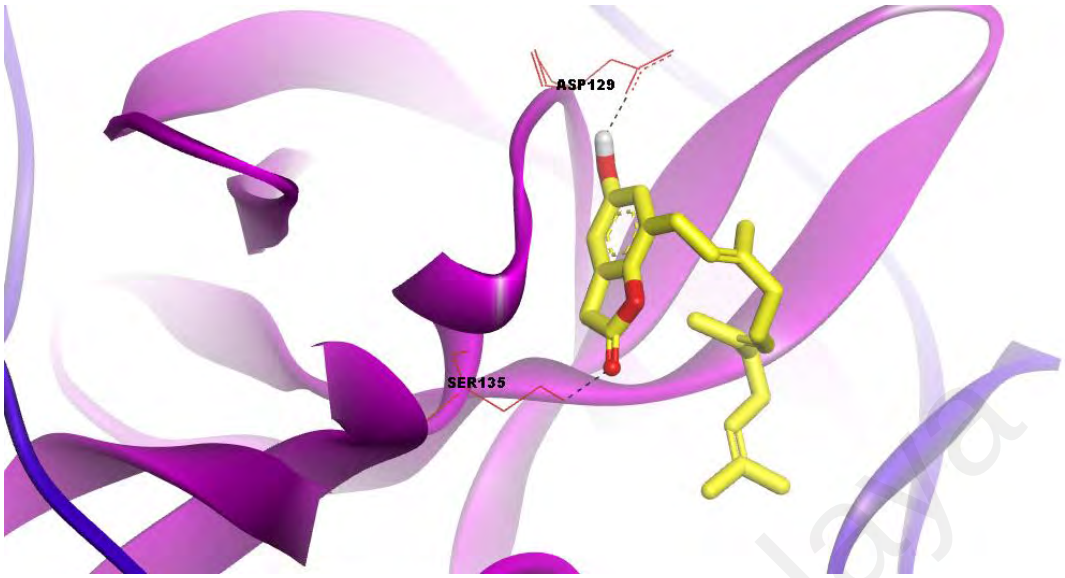

Figure 6.2: Binding residue of DENV-2 NS2B/NS3 protease (ribbon purple and blue) that react with 4-hydroxy-6-(9,13,17-trimethyldodeca-8,12,16-trienyl)-2(3 H)-benzofuranone**136** (yellow).

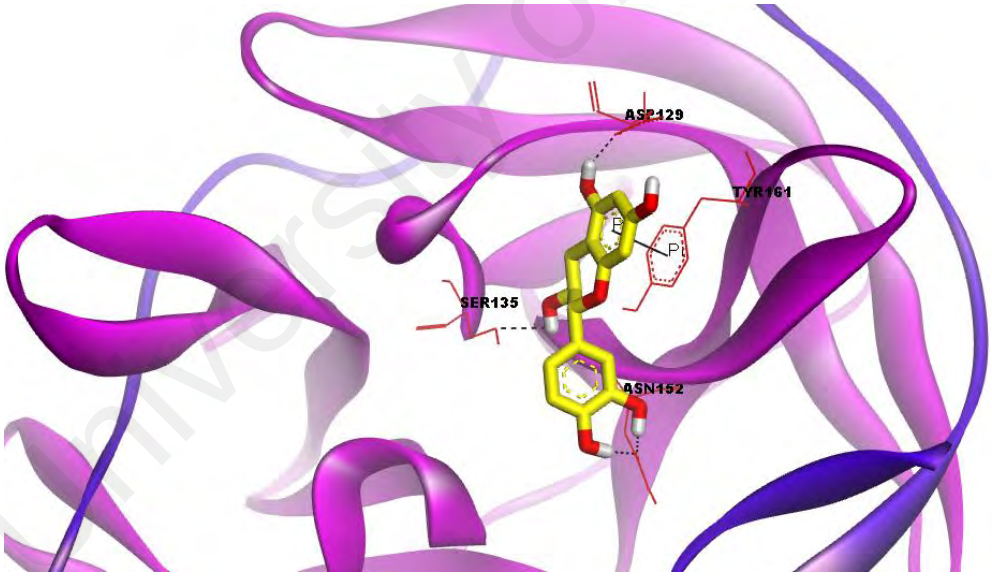

Figure 6.3: Binding residue of DENV-2 NS2B/NS3 protease (ribbon purple and blue) that react with (-)-epicatechin **137** (yellow).

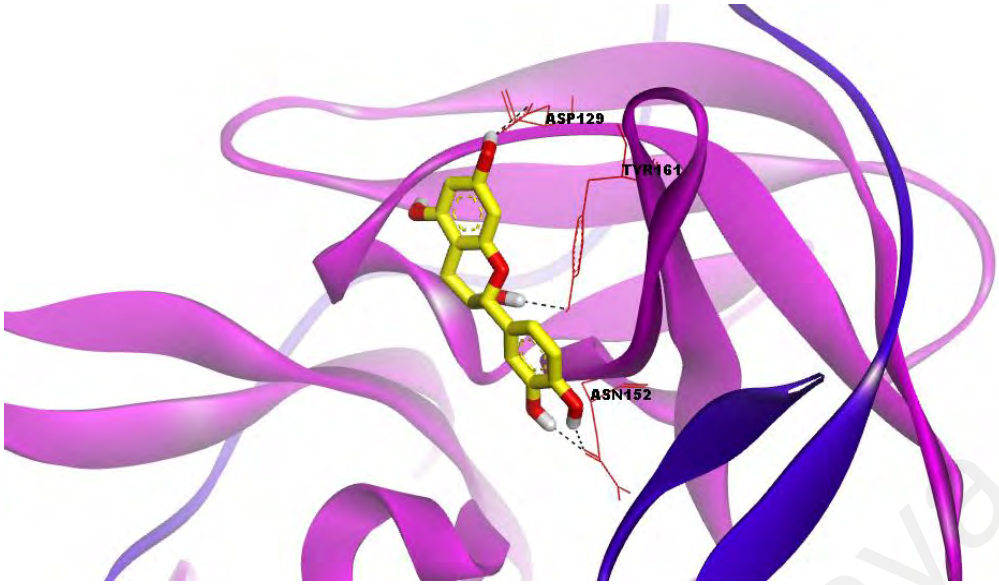

Figure 6.4: Binding residue of DENV-2 NS2B/NS3 protease (ribbon purple and blue) that react with (+)-catechin **138** (yellow).

CHAPTER 7: CONCLUSION

The chemistry of the Lauraceae family has attracted great interest to many scientists with the isolations of structurally interesting and bioactive chemical constituents. However, the phytochemical studies on the genus *Beilschmiedia* and *Endiandra* continues to fall behind with other more popular genera such as *Alseodaphne*, *Cinnamomum*, *Persea* and *Phoebe* over the years. To date, only 15 species among 250 species for the genus *Beilschmiedia* and only 8 species out of 125 species for the genus *Endiandra* have been chemically investigated. Previous investigations towards *B. glabra*, they have led isolation diverse types of chemical constituents such as alkaloids, butanolides, steroids, sesquiterpenes, and triterpenes. Meanwhile for *E. kingiana*, these plants are reported to contain endiandric acid derivatives only.

Even though there are previous investigations towards *B. glabra* and *E. kingiana*, the reports on the biological activities are still limited. Instead as for *B. glabra*, the crude extracts of these species (with the number of active compounds isolated from them are still limited) exhibit antifungal, antibacterial, antimicrobial, antioxidant, and anti-inflammatory; meanwhile, as for *E. kingiana*, only cytotoxic activity and antiapoptotic have been reported to date. Among all reports on the biological activities towards *B. glabra* and *E. kingiana*, however none were on the dengue antiviral activity. This is the first study on the dengue antiviral activity specifically on the DENV-2 NS2B/NS3 protease towards both plants.

The dichloromethane extracts (DCME) of the dried barks of *B. glabra* and *E. kingiana* at 200 ppm was found to inhibit the NS2B/NS3 protease of DENV-2 at 51.28 ± 13.90% and 65.05 ± 3.73%, respectively. Since the DCME of the dried barks of *B. glabra* and *E. kingiana* showed moderate inhibition towards the NS2B/NS3 protease of DENV-2, both extracts were subjected to repeated column chromatography over silica gel, preparative TLC and HPLC, to yield seventeen compounds. Their structures were elucidated using

various spectroscopic techniques such as 1D NMR (^{1}H, ^{13}C, DEPT-Q), 2D NMR (COSY, HSQC, HMBC, NOESY), UV, mass spectrometry and comparison with literature reviews for the known compounds.

Among seventeen compounds which were isolated, two neolignans (*B. glabra*) and one benzofuran (*E. kingiana*) were reported as new compounds. The two new neolignans were pahangine A **130** and pahangine B **131**, which featured an oxetane ring in the molecules and the new benzofuran was identified as 4-hydroxy-6-(9,13,17-trimethyldodeca-8,12,16-trienyl)-2(3 H)-benzofuranone**136**. The remaining compounds were isolated from *B. glabra* and *E. kingiana* which each yielded seven compounds respectively. The seven compounds isolated from *B. glabra* were *p*-coniferaldehyde **123**, tetracosyl ferulate **124**, 9-hydroxy-1-(4-hydroxy-3-methoxyphenyl)propane-7-one **125**, 3,4-dimethoxybenzoic acid **126**, 2-(methoxy)benzoic acid **127**, 4-hydroxybenzaldehyde **128**, 2,6-*bis*(1-hydroxyethyl)benzoic acid **129**. The seven remaining compounds were from the *E. kingiana* namely vanillic acid **132**, vanillin **133**, methyl orsellinate **134**, 5α-Cholesta-20,24-diene-3β,6α-diol **135**, (-)-epicatechin **137**, (+)-catechin **138** and cinnamtannin B1 **139**.

Therefore, seven compounds with sufficient amount from both plants were then subjected to *in vitro* against NS2B/NS3 protease of DENV-2 with the intention of identifying the compounds which could be responsible in giving rise to the activities. Seven compounds namely; 9-hydroxy-1-(4-hydroxy-3-methoxyphenyl)propane-7-one **125** (*B. glabra*), pahangine A **130** (*B. glabra*), methyl orsellinate **134** (*E. kingiana*), 5α-Cholesta-20,24-diene-3β,6α-diol **135** (*E. kingiana*), 4-hydroxy-6-(9,13,17-trimethyldodeca-8,12,16-trienyl)-2(3 H)-benzofuranone**136** (*E. kingiana*), (-)-epicatechin **137** (*E. kingiana*), and (+)-catechin **138** (*E. kingiana*).

Among all compounds, only 4-hydroxy-6-(9,13,17-trimethyldodeca-8,12,16-trienyl)-2(3 H)-benzofuranone**136**, (-)-epicatechin **137**, and (+)-catechin **138** exhibited more than 50

% inhibition towards the DENV-2 NS2B/NS3 protease with the percentage inhibition of 61.23 % ± 7.0, 69.93 % ± 3.3, and 62.02 % ± 6.2 respectively. Subsequently, 4-hydroxy-6-(9,13,17-trimethyldodeca-8,12,16-trienyl)-2(3 H)-benzofuranone**136**, (-)-epicatechin **137**, and (+)-catechin **138** were further evaluated to determine their respective IC_{50} values. The IC_{50} values showed that 4-hydroxy-6-(9,13,17-trimethyldodeca-8,12,16-trienyl)-2(3 H)-benzofuranone**136** (IC_{50} = 403.14 ± 33.03), (-)-epicatechin **137** (IC_{50} = 170.10 ± 5.94), and (+)-catechin **138** (IC_{50} = 184.13 ± 2.11), moderately inhibited the NS2B/NS3 protease of DENV-2 with (-)-epicatechin **137** being the most potent among the three compounds. One may observe that the inhibiting potential of 4-hydroxy-6-(9,13,17-trimethyldodeca-8,12,16-trienyl)-2(3 H)-benzofuranone**136**, (-)-epicatechin **137**, and (+)-catechin **138** decreased with increased of the number of hydroxyl groups, the position of these hydroxyl groups and the number of aromatic rings in the molecules which were found to play a role in influencing the activities.

Molecular docking studies were also attempted in the move to better understand how the chemical groups in these molecules (4-hydroxy-6-(9,13,17-trimethyldodeca-8,12,16-trienyl)-2(3 H)-benzofuranone**136**, (-)-epicatechin **137**, and (+)-catechin **138**) may have influenced their activities. Based on molecular docking studies, (-)-epicatechin **137** being slightly more active compared to (+)-catechin **138**, although both being iastereomers whicht may due to the type of the bonding with Tyr161 of the DENV-2 NS2B/NS3 protease at S1 pocket. (-)-Epicatechin **137** showed 4 hydrogen bonding interaction of hydroxyl group while (+)-catechin **138** only have 3 hydrogen bonding and 1 π- π stacking interaction with the DENV-2 NS2B/NS3 protease. Having hydrogen bonding interactions resulted for (-)-epicatechin **137** being more active as hydrogen bonding was more stable compare to the π- π stacking interaction in the (+)-catechin **138**. The least potent, 4-hydroxy-6-(9,13,17-trimethyldodeca-8,12,16-trienyl)-2(3 H)-benzofuranone**136**, may cause from only showed 2 hydrogen bonding with Asp129 and Ser135 at S1 pocket.

In conclusion, this study showed that (-)-epicatechin **137**, and (+)-catechin **138** are promising candidates in the search for natural drugs which can be employed to inhibited DENV-2 NS2B/NS3 protease. Therefore, one may suggest (-)-epicatechin **137**, and (+)-catechin **138** as potential candidates for further development of anti-dengue drugs, in the treatment of dengue. Hence, from the molecular docking simulations, it has showed more clearly on the binding mode of the activity profile which comprise protease and ligand interaction. Further, *in vitro* and *in vivo* studies on dengue virus are necessary to confirm their efficacy and to evaluate their drug potency.

REFERENCES

Abd, K. S. L., Yaakob, H., and Mohamed, Z. R. (2013). Potential anti-dengue medicinal plants: a review. *Journal of Natural Medicines, 67*(4), 677-689.

Abdul, W. H., Hariono, M., Tan, M. L., and Kamarulzaman, E. E. B. (2016). Thioguanine derivatives: google patents. World Intellectual Property Organization. Malaysia.

Addae-Mensah, I., Achenbach, H., Thoithi, G. N., Waibel, R., and Mwangi, J. W. (1992). Epoxychiromodine and other constituents of *Croton megalocarpus*. *Phytochemistry, 31*(6), 2055-2058.

Allard, P. M., Dau, E. T., Eydoux, C., Guillemot, J. C., Dumontet, V., Poullain, C., Canard, B., Gueritte, F., and Litaudon, M. (2011). Alkylated flavanones from the bark of *Cryptocarya chartacea* as dengue virus NS5 polymerase inhibitors. *Journal of Natural Products, 74*(11), 2446-2453.

Apel, C., Geny, C., Dumontet, V., Birlirakis, N., Roussi, F., Pham, V. C., Huong, D. T. M., Nguyen, V. H., Chau, V. M., and Litaudon, M. (2014). Endiandric acid analogues from *Beilschmiedia ferruginea* as dual inhibitors of Bcl-xl/bak and Mcl-1/bid interactions. *Journal of Natural Products, 77*(6), 1430-1437.

Azmi, M. N., Gény, C., Leverrier, A., Litaudon, M., Dumontet, V., Birlirakis, N., Guéritte, F., Leong, K. H., Halim, S. N. A., and Mohamad, K. (2014). Kingianic acids a–g, endiandric acid analogues from *Endiandra kingiana*. *Molecules, 19*(2), 1732-1747.

Azmi, M. N., Péresse, T., Remeur, C., Chan, G., Roussi, F., Litaudon, M., and Awang, K. (2016). Kingianins o–q: pentacyclic polyketides from *Endiandra kingiana* as inhibitor of Mcl-1/bid interaction. *Fitoterapia, 109*, 190-195.

Bandaranayake, W. M., Banfield, J., Black, D. S. C., Fallon, G., and Gatehouse, B. (1981). Constituents of *endiandra* species. I. Endiandric acid, a novel carboxylic acid from *Endiandra introrsa* (lauraceae), and a derived lactone. *Australian Journal of Chemistry, 34*(8), 1655-1667.

Banfield, J. E., Black, D., Collins, D. J., Hyland, B. P., Lee, J. J., and Pranowo, S. R. (1994). Constituents of some species of *Beilschmiedia* and *Endiandra* (lauraceae): new endiandric acid and benzopyran derivatives isolated from *B. oligandra*. *Australian Journal of Chemistry, 47*(4), 587-607.

Banning, J. W., Salman, K. N., and Patil, P. N. (1982). A pharmacological study of two bisbenzylisoquinoline alkaloids, thalistyline and obamegine. *Journal of Natural Products, 45*(2), 168-177.

Basset, J.-F., Leslie, C., Hamprecht, D., White, A. J. P., and Barrett, A. G. M. (2010). Studies on the resorcylates: biomimetic total syntheses of (+)-montagnetol and (+)-erythrin. *Tetrahedron Letters, 51*(5), 783-785.

Brossi, A. (1987). *The Alkaloids: Chemistry And Physiology,* (31) (pp 86-90). Academic Press: Florida.

Burkill, I. H. (1966). *A Dictionary of the Economic Products of the Malay Peninsula. 2*(2) (pp 25-36). Unit Ministry of Agriculture Malaysia: Malaysia.

Chang, H.-S., Cheng, M.-J., Wu, M.-D., Chan, H.-Y., Hsieh, S.-Y., Lin, C.-H., Yech, Y.-J., and Chen, I.-S. (2017). Secondary metabolites produced by an endophytic fungus cordyceps ninchukispora from the seeds of *Beilschmiedia erythrophloia* Hayata. *Phytochemistry Letters, 22*, 179-184.

Chaverri, C., and Cicció, J. F. (2010). Essential oils from *Beilschmiedia pendula* (sw.) Hemsl. (lauraceae) from costa rica. *The Journal Of Essential Oil Research, 22*(3), 259-262.

Chen, J.-J., Chou, E.-T., Duh, C.-Y., Yang, S.-Z., and Chen, I.-S. (2006). New cytotoxic tetrahydrofuran- and dihydrofuran-type lignans from the stem of *Beilschmiedia tsangii*. *Planta Medica, 72*(4), 351-357.

Chen, J.-J., Chou, E.-T., Peng, C. F., Huang, H. Y., Yang, S.-Z., and Chen, I.-S. (2007). Novel epoxyfuranoid lignans and antitubercular constituents from the leaves of *Beilschmiedia tsangii*. *Planta Medica, 73*, 567-571.

Chen, J.-J., Kuo, W.-L., Sung, P.-J., Chen, I.-S., Cheng, M.-J., Lim, Y.-P., Liao, H.-R., Chang, T.-H., Wei, D.-C., and Chen, J.-Y. (2015). Beilschamide, a new amide, and cytotoxic constituents of *Beilschmiedia erythrophloia*. *Chemistry of Natural Compound, 51*(2), 302-305.

Cheuka, P. M., Mayoka, G., Mutai, P., and Chibale, K. (2017). The role of natural products in drug discovery and development against neglected tropical diseases. *Molecules, 22*(1), 5851-5841.

Chouna, J. R., Alango Nkeng-Efouet, P., Ndjakou Lenta, B., Duplex Wansi, J., Neumann, B., Stammler, H.-G., Fon Kimbu, S., and Sewald, N. (2011). Beilschmiedic acids F and G, further endiandric acid derivatives from *Beilschmiedia anacardioides*. *Helvetica Chimica Acta, 94*(6), 1071-1076.

Chouna, J. R., Nkeng-Efouet, P. A., Lenta, B. N., Devkota, K. P., Neumann, B., Stammler, H.-G., Kimbu, S. F., and Sewald, N. (2009). Antibacterial endiandric acid derivatives from *Beilschmiedia anacardioides*. *Phytochemistry, 70*(5), 684-688.

Chouna, J. R., Nkeng-Efouet, P. A., Lenta, B. N., Wansi, J. D., Kimbu, S. F., and Sewald, N. (2010). Endiandric acid derivatives from the stem bark of *Beilschmiedia anacardioides*. *Phytochemistry Letters, 3*(1), 13-16.

Cordell, G. A. (2002). *Medicinal Natural Products: A Biosynthetic Approach, 2*(65) (pp 305). Chicago: American Chemical Society.

Corner, E. J. H. (1988). *Wayside Tree of Malaya, 3*(1) (pp 45). Kuala Lumpur: The Malayan Nature Society.

Davis, R. A., Barnes, E. C., Longden, J., Avery, V. M., and Healy, P. C. (2009). Isolation, structure elucidation and cytotoxic evaluation of endiandrin B from the Australian

rainforest plant *Endiandra anthropophagorum*. *Bioorganic Medicinal Chemistry, 17*(3), 1387-1392.

Davis, R. A., Carroll, A. R., Duffy, S., Avery, V. M., Guymer, G. P., Forster, P. I., and Quinn, R. J. (2007). Endiandrin a, a potent glucocorticoid receptor binder isolated from the australian plant *Endiandra anthropophagorum*. *Journal of Natural Products, 70*(7), 1118-1121.

De Sousa, L. R., Wu, H., Nebo, L., Fernandes, J. B., da Silva, M. F., Kiefer, W., Kanitz, M., Bodem, J., Diederich, W. E., Schirmeister, T., and Vieira, P. C. (2015). Flavonoids as noncompetitive inhibitors of dengue virus NS2B-NS3 protease: inhibition kinetics and docking studies. *Bioorganic Medicinal Chemistry, 23*(3), 466-470.

Dong, H., Zhang, B., and Shi, P. Y. (2008). Flavivirus methyltransferase: a novel antiviral target. *Antiviral Research, 80*(1), 1-10.

Ezzat, M. I., Ezzat, S. M., El Deeb, K. S., and El Fishawy, A. M. (2017). In vitro evaluation of cytotoxic activity of the ethanol extract and isolated compounds from the corms of *Liatris spicata* (l.) Willd on Hepg2. *Natural Product Research, 31*(11), 1325-1328.

Fabiani, C., Murray, A. P., Corradi, J., and Antollini, S. S. (2018). A novel pharmacological activity of caffeine in the cholinergic system. *Neuropharmacology, 135*, 464-473.

Ferreira, L. G., dos Santos, R. N., Oliva, G., and Andricopulo, A. D. (2015). Molecular docking and structure-based drug design strategies. *Molecules, 20*(7), 13384-13421.

Fischer, D. C. H., Goncalves, M. I., Oliveira, F., and Alvarenga, M. A. (1999). Constituents from *Siparuna apiosyce. Fitoterapia, 70*(3), 322-323.

Fleming, S. A., and Gao, J. J. (1997). Stereocontrol of paterno-büchi photocycloadditions. *Tetrahedron Letters, 38*(31), 5407-5410.

Frecer, V., and Miertus, S. (2010). Design, structure-based focusing and in silico screening of combinatorial library of peptidomimetic inhibitors of dengue virus NS2B/NS3 protease. *Journal of Computer Aided Molecular Design, 24*(3), 195-212.

Geiss, B. J., Thompson, A. A., Andrews, A. J., Sons, R. L., Gari, H. H., and Keenan, S. M. (2009). Analysis of flavivirus NS5 methyltransferase cap binding. *Journal of Molecular Biology, 385*(5), 1643-1654.

Gibbons, R. V., and Vaughn, D. W. (2002). Dengue: an escalating problem. *The British Medical Journal, 324*.

Gibbs, R. D. (1974). *Chemotaxonomy of flowering plant,* (1) (pp 85): McGill-Queen's University Press.

Goel, A., Patel, D. N., Lakhani, K. K., Agarwal, A., Singla, S., and Agarwal, R. (2004). Dengue fever-a dangerous foe. *Journal Indian Academy of Clinical Medicine, 5*(3), 247-258.

Gu, Q., Wang, R.-R., Zhang, X.-M., Wang, Y.-H., Zheng, Y.-T., Zhou, J., and Chen, J.-J. (2007). A new benzofuranone and anti-HIV constituents from the stems of *Rhus chinensis*. *Planta Medica, 73*(3), 279-282.

Gubler, D. J. (1998). Dengue and dengue hemorrhagic fever. *Clinical Microbiology Reviews, 11*(3), 480-496.

Guzman, A., and Isturiz, R. E. (2010). Update on the global spread of dengue. *International Journal of Antimicrobial Agents, 36*.

Hao, G. F., Yang, G. F., and Zhan, C. G. (2012). Structure-based methods for predicting target mutation-induced drug resistance and rational drug design to overcome the problem. *Drug Discovery Today, 17*(19-20), 1121-1126.

Harborne, J. B. (2007). *The Flavonoids Advances in Research Since 1986* (1) (pp 54). United States of America: Routledge.

Hassandarvish, P., Rothan, H. A., Rezaei, S., Yusof, R., Abubakar, S., and Zandi, K. (2016). In silico study on baicalein and baicalin as inhibitors of dengue virus replication. *Royal Society of Chemistry Advances, 6*(37), 31235-31247.

Havsteen, B. H. (2002). The biochemistry and medical significance of the flavonoids. *Pharmacology and Therapeutics, 96*, 67-202.

He, H., Hu, L., and Liu, F. (1999). Chemical constituents of *Colchicum autumnale*. *Huaxue Yanjiu Yu Yingyong, 11*(5), 509-510.

Hidari, K. I. P. J., Takahashi, N., Arihara, M., Nagaoka, M., Morita, K., and Suzuki, T. (2008). Structure and anti-dengue virus activity of sulfated polysaccharide from a marine alga. *Biochemical and Biophysical Research. Communications, 376*(1), 91-95.

Hsu, P. J., Miller, J. S., and Berger, J. M. (2009). Bakuchiol, an antibacterial component of *Psoralidium tenuiflorum*. *Natural Product Research, 23*(8), 781-788.

Huang, R., Harrison, L. J., and Sim, K. Y. (1999). A triterpenoid with a novel abeodammarane skeleton from *Dysoxylum cauliflorum*. *Tetrahedron Letters, 40*, 1607-1610.

Huang, Y. T., Chang, H. S., Wang, G. J., Lin, C. H., and Chen, C. H. (2012). Secondary metabolites from the roots of *Beilschmiedia tsangii* and their anti-inflammatory activities. *International Journal of Molecular Sciences, 13*, 16430-16443.

Javad, S., Sarwar, S., Jabeen, K., Iqbal, S., and Tariq, A. (2016). Enhanced extraction of an anticancer drug, vinblastine, from *Catharanthus roseus*. *Pure and Applied Biology, 5*(3), 608-614.

Jayaprakasha, G. K., Ohnishi-Kameyama, M., Ono, H., Yoshida, M., and Jaganmohan Rao, L. (2006). Phenolic constituents in the fruits of *Cinnamomum zeylanicum* and their antioxidant activity. *Journal of Agricultural and Food Chemistry, 54*(5), 1672-1679.

Jiang, W.-L., Luo, X.-L., and Kuang, S.-J. (2005). Effects of alternanthera philoxeroides griseb against dengue virus *in vitro*. *Di Yi Jun Yi Da Xue Xue Bao, 25*(4), 454-456.

Keng, H. (1978). *Order and families of Malayan seed plants* (2) (pp 78). Singapore: University Press.

Kiat, T. S., Pippen, R., Yusof, R., Ibrahim, H., Khalid, N., and Rahman, N. A. (2006). Inhibitory activity of cyclohexenylchalcone derivatives and flavonoids of fingerroot, *Boesenbergia rotunda* (l.), towards dengue-2 virus NS3 protease. *Bioorganic Medicinal Chemistry Letters, 16*.

Kitagawa, I., Minagawa, K., Zhang, R. S., Hori, K., Doi, M., Inoue, M., Ishida, T., Kimura, M., Uji, T., and Shibuya, H. (1993). Dehatrine, an antimalarial bisbenzylisoquinoline alkaloid from the indonesian medicinal plant *Beilschmiedia madang*, isolated as a mixture of two rotational isomers. *Chemical and Pharmaceutical Bulletin, 41*(5), 997-999.

Kochummen, K. M. (1997). *Tree Flora of Pasoh Forest,* (44) (pp 121). Kuala Lumpur: Forest Research Institute Malaysia.

Kuete, V., Tankeo, S. B., Saeed, M. E. M., Wiench, B., Tane, P., and Efferth, T. (2014). Cytotoxicity and modes of action of five cameroonian medicinal plants against multi-factorial drug resistance of tumor cells. *Journal of Ethnopharmacology, 153*(1), 207-219.

Kyle, J. L., and Harris, E. (2008). Global spread and persistence of dengue. *Annual Review of Microbiology, 62*, 71-92.

Lenta, B. N., Chouna, J. R., Nkeng-Efouet, P. A., Kimbu, S. F., Tsamo, E., and Sewald, N. (2011). Obscurine: a new cyclostachine acid derivative from *Beilschmiedia obscura*. *Natural Product Communications, 6*(11), 1591-1592.

Lenta, B. N., Tantangmo, F., Devkota, K. P., Wansi, J. D., Chouna, J. R., Soh, R. C. F., Neumann, B., Stammler, H.-G., Tsamo, E., and Sewald, N. (2009). Bioactive constituents of the stem bark of *Beilschmiedia zenkeri*. *Journal of Natural Products, 72*(12), 2130-2134.

Leverrier, A., Awang, K., Guéritte, F., and Litaudon, M. (2011). Pentacyclic polyketides from *Endiandra kingiana* as inhibitors of the Bcl-Xl/Bak interaction. *Phytochemistry, 72*(11), 1443-1452.

Leverrier, A., Dau, M. E. T. H., Retailleau, P., Awang, K., Guéritte, F., and Litaudon, M. (2010). Kingianin a: a new natural pentacyclic compound from *Endiandra kingiana*. *Organic Letters, 12*(16), 3638-3641.

Li, H.-J., and Deinzer, M. L. (2008). The mass spectral analysis of isolated hops a-type proanthocyanidins by electrospray ionization tandem mass spectrometry. *Journal of Mass Spectrometry, 43*(10), 1353-1363.

Lindenbach, B. D., and Rice, C. M. (1999). Genetic interaction of flavivirus nonstructral proteins NS1 and NS4A as a determinant of replicase function. *Journal of Virology, 73*(6), 4611-4621.

Luo, D., Xu, T., Watson, R. P., Scherer-Becker, D., Sampath, A., and Jahnke, W. (2008). Insights into RNA unwinding and ATP hydrolysis by the flavivirus NS3 protein. *The EMBO Journal, 27*(23), 3209-3219.

Mabberley, D. J. (2008). *Mabberley's plant-book: a portable dictionary of plants, their classifications, and uses,* (4) (pp 853). Cambridge: Cambridge University Press.

Mathew, A., Paluri, V., Venkateswaramurthy, N., and Sambath kumar, R. (2016). A review of newer therapy in dengue fever. *International Journal of Research Pharmacology and Pharmacotherapeutics, 5*(2), 170-177.

Meneses, R., Ocazionez, R. E., Martinez, J. R., and Stashenko, E. E. (2009). Inhibitory effect if essential oils obtained from plants grown in colombia on yellow fever virus replication *in vitro*. *Annals of Clinical Microbiology and Antimicrobials, 8*(8), 67-69.

Meng, X.-Y., Zhang, H.-X., Mezei, M., and Cui, M. (2011). Molecular docking: a powerful approach for structure-based drug discovery. *Current Computer-Aided Drug Design, 7*(2), 146-157.

Moghaddam, E., Teoh, B.-T., Sam, S.-S., Lani, R., Hassandarvish, P., Chik, Z., Yueh, A., Abubakar, S., and Zandi, K. (2014). Baicalin, a metabolite of baicalein with anti-viral activity against dengue virus. *Scientific Reports, 4*, 5452.

Mollataghi, A., A. Hadi, A. H., and Cheah, S.-C. (2012). (-)-Kunstleramide, a new antioxidant and cytotoxic dienamide from the bark of *Beilschmiedia kunstleri* Gamble. *Molecules, 17*, 4197-4208.

Mollataghi, A., Coudiere, E., Hadi, A. H. A., Mukhtar, M. R., Awang, K., Litaudon, M., and Ata, A. (2012). Anti-acetylcholinesterase, anti-α-glucosidase, anti-leishmanial and anti-fungal activities of chemical constituents of *Beilschmiedia species*. *Fitoterapia, 83*(2), 298-302.

Mollataghi, A., Hadi, A. H. A., Awang, K., Mohamad, J., Litaudon, M., and Mukhtar, M. R. (2011). (+)-Kunstlerone, a new antioxidant neolignan from the leaves of *Beilschmiedia kunstleri* Gamble. *Molecules, 16*(8), 6582.

Narender, T. (2012). Recent advances in the natural products drug discovery. *Journal of. Pharmacognosy, 3*(2), 108-111.

Nawi, M. S. M. (2015). *Ligand based drug discovery of novel dengue-2 NS2B-NS3 protease inhibitors*. Universiti Sains Malaysia: Malaysia.

Ndjakou Lenta, B., Chouna, J. R., Nkeng-Efouet, P. A., and Sewald, N. (2015). Endiandric acid derivatives and other constituents of plants from the genera *Beilschmiedia* and *Endiandra* (Lauraceae). *Biomolecules, 5*(2), 910-942.

Newman, D. J., Cragg, G. M., and Snader, K. M. (2000). The influence of natural products upon drug discovery (Antiquity to late 1999). *Natural Product Reports, 17*(3), 215-234.

Ng, F. S. P. (1989). *Tree flora of Malaya; a manual for foresters* (3) (pp 79). Malaysia: Longman Malaysia.

Ng, F. S. P., and Phillipson, J. D. (1989). *Tree flora of Malaya; a manual for foresters* (4) (pp 69). Malaysia: Longman Malaysia.

Nishida, S. (1999). Revision of *Beilschmiedia* (Lauraceae) in the neotropics. *Annals of the Missouri Botanical Garden, 86*(3), 657-701.

Nishida, S. (2008). Taxonomic revision of *Beilschmiedia* (Lauraceae) in Borneo. *Blumea - Biodiversity, Evolution and Biogeography of Plants, 53*(2), 345-383.

Nkeng-Efouet, P. A., and Rao, V. (2012). Phytochemicals from *Beilschmiedia anacardioides* and their biological significance. *Phytochemicals-a global perspective of their role in nutrition and health, 53*(2), 345-383.

Ono, L., Wollinger, W., Rocco, I. M., Coimbra, T. L. M., Gorin, P. A. J., and Sierakowski, M.-R. (2003). *In vitro* and *in vivo* antiviral properties of sulfated galactomannans against yellow fever virus (Beh111 strain) and dengue 1 virus (hawaii strain). *Antiviral Research, 60*(3), 201-208.

Panche, A. N., Diwan, A. D., and Chandra, S. R. (2016). Flavonoids: an overview. *Journal of Nutritional Science, 5*, 4715-4732.

The Plant List. (2013). Published on the Internet; http://www.theplantlist.org/ (accessed 1st January).

Pudjiastuti, P., Mukhtar, M. R., Hadi, A. H. A., Saidi, N., Morita, H., Litaudon, M., and Awang, K. (2010). (6,7-dimethoxy-4-methylisoquinolinyl)-(4'-methoxyphenyl)-methanone, a new benzylisoquinoline alkaloid from *Beilschmiedia brevipes*. *Molecules, 15*, 2339-2346.

Pujol, C. A., Estevez, J. M., Carlucci, M. J., Ciancia, M., Cerezo, A. S., and Damonte, E. B. (2002). Novel dl-galactan hybrids from the red seaweed *Gymnogongrus torulosus* are potent inhibitors of herpes simplex virus and dengue virus. *Antiviral Chemistry and Chemotheraphy, 13*(2), 83-89.

Rees, C. R., Costin, J. M., Fink, R. C., McMichael, M., Fontaine, K. A., Isern, S., and Michael, S. F. (2008). *In vitro* inhibition of dengue virus entry by *p*-sulfoxy-cinnamic acid and structurally related combinatorial chemistries. *Antiviral Research, 80*(2), 135-142.

Revesz, L., Hiestand, P., La Vecchia, L., Naef, R., Naegeli, H. U., Oberer, L., and Roth, H. J. (1999). Isolation and synthesis of a novel immunosuppressive 17*α*-

substituted dammarane from the flour of the palmyrah palm (*Borassus flabellifer*). *Bioorganic and Medicinal Chemistry Letters, 9*(11), 1521-1526.

Ridley, H. N. (1922). *The flora of the Malay Peninsula. By Henry N. Ridley, with illus. by J. Hutchinson* (Vol. 1). London: L. Reeve and co., ltd.

Rodrigues, C. M., Rinaldo, D., dos Santos, L. C., Montoro, P., Piacente, S., Pizza, C., Hiruma-Lima, C. A., Brito, A. R., and Vilegas, W. (2007). Metabolic fingerprinting using direct flow injection electrospray ionization tandem mass spectrometry for the characterization of proanthocyanidins from the barks of *Hancornia speciosa*. *Rapid Communication Mass Spectrometry, 21*(12), 1907-1914.

Rohwer, J. G., Richter, H. G., and Werff, H. v. d. (1991). Two new genera of neotropical Lauraceae and critical remarks on the generic delimitation. *Annals of the Missouri Botanical Garden, 78*(2), 388-400.

Salleh, W. M. N. H. W., Ahmad, F., Khong, H. Y., and Zulkifli, R. M. (2016). Chemical constituents and bioactivities from the leaves of *Beilschmiedia glabra* kosterm (Lauraceae). *Marmara Pharmaceutical Journal, 20*, 401-407.

Salleh, W. M. N. H. W., Ahmad, F., Khong, H. Y., Zulkifli, R. M., Chen, J.-J., Nahar, L., Wansi, J. D., and Sarker, S. D. (2016). Beilschglabrines A and B: two new bioactive phenanthrene alkaloids from the stem bark of *Beilschmiedia glabra*. *Phytochemistry letters, 16*, 192-196.

Salleh, W. M. N. H. W., Ahmad, F., Yen, K. H., and Zulkifli, R. M. (2015). A review on chemical constituents and biological activities of the genus *Beilschmiedia* (Lauraceae). *Tropical Journal of Pharmaceutical Research, 14*(11), 2139-2150.

Salleh, W. M. N. H. W., Ahmad, F., Yen, K. H., and Zulkifli, R. M. (2016). Anticholinesterase and anti-inflammatory constituents from *Beilschmiedia pulverulenta* Kosterm. *Natural Product Sciences, 22*(4), 225-230.

Salleh, W. M. N. H. W., Ahmad, F., Yen, K. H., Zulkifli, R. M., and Sarker, S. D. (2016). Madangones A and B: Two new neolignans from the stem bark of *Beilschmiedia madang* and their bioactivities. *Phytochemistry Letters, 15*, 168-173.

Salleh, W. M. N. H. W., Ahmada, F., Yen, K. H., and Zulkifli, R. M. (2015). Chemical compositions and biological activities of essential oils of *Beilschmiedia glabra*. *Natural Product Communications, 10*(7), 1297-1300.

Sampath, A., and Padmanabhan, R. (2009). Molecular targets for flavivirus drug discovery. *Antiviral Research, 81*(1), 6-15.

Sánchez, I., Gómez-Garibay, F., Taboada, J., and Ruiz, B. H. (2000). Antiviral effect of flavonoids on the dengue virus. *Phytotheraphy Research, 14*, 56.

Saphier, S., Hu, Y., Sinha, S. C., Houk, K. N., and Keinan, E. (2005). Origin of selectivity in the antibody 20F10-catalyzed yang cyclization. *Journal of the American Chemical Society, 127*(1), 132-145.

Satake, H., Koyama, T., Bahabadi, S., Matsumoto, E., Ono, E., and Murata, J. (2015). Essences in metabolic engineering of lignan biosynthesis. *Metabolites, 5*(2), 270.

Satake, H., Ono, E., and Murata, J. (2013). Recent advances in the metabolic engineering of lignan biosynthesis pathways for the production of transgenic plant-based foods and supplements. *Journal of Agricultural and Food Chemistry, 61*(48), 11721-11729.

Savithramma, N., Rao, M. L., and Ankanna, S. (2011). Screening of traditional medicinal plants for secondary metabolites. *International Journal of Research in Pharmaceutical Sciences (Madurai, India), 2*(4), 643-647.

Sribuhom, T., Sriphana, U., Thongsri, Y., and Yenjai, C. (2015). Chemical constituents from the stems of *Alyxia schlechteri. Phytochemistry Letters, 11*, 80-84.

Stevens, A. J., Gahan, M. E., Mahalingam, S., and Keller, P. A. (2009). The medicinal chemistry of dengue fever. *Journal of Medicinal Chemistry, 52*(24), 7911-7926.

Sulaiman, S. N., Zahari, A., Liew, S. Y., Litaudon, M., Issam, A. M., Wahab, H. A., and Awang, K. (2018). Pahangine A and B, two new oxetane containing neolignans from the barks of *Beilschmiedia glabra* Kosterm (Lauraceae). *Phytochemistry Letters, 25*, 22-26.

Symons, G. M., Hudson, C. J., and Livermore, M. L. (2018). *Papaver somniferum* plants for the production of codeine. *Journal of Medicinal Chemistry, 52*(1), 59.

Talarico, L. B., Pujol, C. A., Zibetti, R. G., Faría, P. C., Noseda, M. D., Duarte, M. E., and Damonte, E. B. (2005). The antiviral activity of sulfated polysaccharides against dengue virus is dependent on virus serotype and host cell. *Antiviral Research, 66,* 67-69.

Talontsi, F. M., Lamshoeft, M., Bauer, J. O., Razakarivony, A. A., Andriamihaja, B., Strohmann, C., and Spiteller, M. (2013). Antibacterial and antiplasmodial constituents of *Beilschmiedia cryptocaryoides*. *Journal of Natural Products, 76*(1), 97-102.

Teixeira, R., Pereira, W., Oliveira, A., da Silva, A., de Oliveira, A., da Silva, M., da Silva, C., and de Paula, S. (2014). Natural products as source of potential dengue antivirals. *Molecules, 19*(6), 8151.

Teponno, R. B., Kusari, S., and Spiteller, M. (2016). Recent advances in research on lignans and neolignans. *Natural Product Reports, 33*(9), 1044-1092.

Torres, R. C., Garbo, A. G., and Walde, R. Z. M. L. (2014). Larvicidal activity of *Persea americana* Mill. against *Aedes aegypti*. *Asian Pacific Journal of Tropical Medicine, 7*(1), 167-170.

Tsuchiya, H. (2017). Anesthetic agents of plant origin: a review of phytochemicals with anesthetic activity. *Molecules, 22*(8), 1369/1361-1369/1334.

Tuan, P. A., Kim, Y. S., Kim, Y., Thwe, A. A., Li, X., Park, C. H., Lee, S. Y., and Park, S. U. (2016). Molecular characterization of flavonoid biosynthetic genes and

accumulation of baicalin, baicalein, and wogonin in plant and hairy root of *Scutellaria lateriflora*. *Saudi Journal of Biological Sciences*. *5*(7), 70.

Van Der Werff, H. (2003). A synopsis of the genus *Beilschmiedia* (Lauraceae) in Madagascar. *Adansonia, 25*(1), 77-92.

Verma, R., Jatav, V. K., and Sharma, S. (2015). Identification of inhibitors of dengue virus (DENV1, DENV2 AND DENV3) NS2B/NS3 serine protease: a molecular docking and simulation approach. *Asian Journal of Pharmaceutical and Clinical Research, 8*(1), 287-292.

Vogt, T. (2010). Phenylpropanoid biosynthesis. *Molecular Plant, 3*(1), 2-20.

Wahab, H. A., Yusof, R., and Rahman, N. A. (2007). A search for vaccines and therapeutic for dengue: a review. *Current Computer-Aided Drug Design, 3*, 101-112.

Wang, Q., Wu, R., Wu, J., Dai, N., and Han, N. (2015). A new alkaloid from *Helianthemum ordosicum*. *Magnetic Resonance in Chemistry, 53*(4), 314-316.

Wang, X., Chen, R.-X., Wei, Z.-F., Zhang, C.-Y., Tu, H.-Y., and Zhang, A.-D. (2016). Chemoselective transformation of diarylethanones to arylmethanoic acids and diarylmethanones and mechanistic insights. *Journal of Organic Chemistry, 81*(1), 238-249.

Westwood, N. J., Lancefield, C. S., and Tran, F. (2016). Depolymerization of oxidized lignin. *American Chemical Society*, 27, 90-93.

Whitmore, T. C., and Ng, F. S. P. (1989). *Tree flora of Malaya: a manual for foresters.* (5) (pp 52). *Malaysia*: Longman.

WHO. (2017a). *Update on the Dengue situation in the Western Pacific Region*. Published on the Internet; http://www.wpro.who.int/emerging_diseases (accessed 1st January).

Wiart, C. (2006). *Medicinal Plants of Asia and the Pacific.* (pp 132). United States of America: Taylor and Francis.

Wichapong, K., Pianwanit, S., Sippl, W., and Kokpol, S. (2010). Homology modeling and molecular dynamics simulations of dengue virus NS2B/NS3 protease: insight into molecular interaction. *Journal of Molecular Recognition, 23*(3), 283-300.

Xu, C., Yang, B., Zhu, W., Li, X., Tian, J., and Zhang, L. (2015). Characterisation of polyphenol constituents of *Linderae aggregate* leaves using HPLC fingerprint analysis and their antioxidant activities. *Food Chemistry, 186*, 83-89.

Xu, R., Fazio, G. C., and Matsuda, S. P. T. (2004). On the origins of triterpenoid skeletal diversity. *Phytochemistry (Elsevier), 65*(3), 261-291.

Yang, C., Peng, W., Yang, B., Zhang, J., and Chen, Y. (2016). A new sesquiterpenoid from *Polyalthia petelotii*. *Natural Product Research, 30*(14), 1565-1570.

Yang, P.-S., Cheng, M.-J., Chen, J.-J., and Chen, I.-S. (2008). Two new endiandric acid analogs, a new benzopyran, and a new benzenoid from the root of *Beilschmiedia erythrophloi*a. *Helvetica Chimica Acta, 91*(11), 2130-2138.

Yang, P.-S., Cheng, M.-J., Peng, C.-F., Chen, J.-J., and Chen, I.-S. (2009). Endiandric acid analogs from the roots of *Beilschmiedia erythrophloia*. *Journal of Natural Products, 72*(1), 53-58.

Yin, Z., Patel, S. J., Wang, W.-L., Wang, G., Chan, W.-L., Rao, K. R. R., Alam, J., Jeyaraj, D. A., Ngew, X., Patel, V., Beer, D., Lim, S. P., Vasudevan, S. G., and Keller, T. H. (2006). Peptide inhibitors of dengue virus NS3 protease. Part 1: Warhead. *Bioorganic Medicinal Chemistry Letters, 16*(1), 36-39.

Zakaria, M., and Mohd, M. A. (1994). *Traditional Malay Medicinal Plants*. Kuala Lumpur: Fajar Bakti.

Zandi, K., Teoh, B.-T., Sam, S.-S., Wong, P.-F., Mustafa, M. R., and AbuBakar, S. (2012). Novel antiviral activity of baicalein against dengue virus. *BMC Complementary and Alternative Medicine, 12*(1), 214.

Zhou, Y., Ray, D., Zhao, Y., Dong, H., Ren, S., and Li, Z. (2007). Structure and function of flavivirus NS5 methyltransferase. *Journal of Virology, 81*(8), 3891-3903.

LIST OF PUBLICATIONS

Articles published in ISI-cited journals:

Sulaiman, S. N., Zahari, A., Liew, S. Y., Litaudon, M., Issam, A. M., Wahab, H. A., and Awang, K. (2018). Pahangine A and B, two new oxetane containing neolignans from the barks of *Beilschmiedia glabra* Kosterm (Lauraceae). *Phytochemistry Letters, 25*, 22-26.

Phytochemistry Letters 25 (2018) 22–26

Contents lists available at ScienceDirect

Phytochemistry Letters

journal homepage: www.elsevier.com/locate/phytol

Pahangine A and B, two new oxetane containing neolignans from the barks of *Beilschmiedia glabra* Kosterm (Lauraceae)

Syazreen Nadia Sulaiman[a], Azeana Zahari[a,b], Sook Yee Liew[c], Marc Litaudon[d], Issam A.M.[a], Habibah A. Wahab[c], Khalijah Awang[a,b,*]

[a] Department of Chemistry, Faculty of Science, University of Malaya, 50603 Kuala Lumpur, Malaysia
[b] Centre of Natural Products and Drug Discovery (CENAR), University of Malaya, 50603 Kuala Lumpur, Malaysia
[c] Chemistry Division, Centre for Foundation Studies in Science, University of Malaya, 50603 Kuala Lumpur, Malaysia
[d] Centre de Recherche de Gif, Institut de Chimie des Substances Naturelles, CNRS-ICSN UPR 2361, Université Paris-Saclay, Avenue de la Terrasse, 91198 Gif-sur-Yvette Cedex, France
[e] School of Pharmaceutical Sciences, Universiti Sains Malaysia, 11800 Universiti Sains Malaysia, Pulau Pinang, Malaysia

ARTICLE INFO

Keywords:
Beilschmiedia glabra
Oxetane
Pahangine A
Pahangine B
Lauraceae

ABSTRACT

Phytochemical investigation on the barks of *Beilschmiedia glabra* Kosterm led to the isolation of two new oxetane containing neolignans, Pahangine A (**1**) and Pahangine B (**2**) together with eight known compounds. The structures of isolated compounds were elucidated by extensive spectroscopic analysis including 1D and 2D NMR (^{1}H–^{1}H COSY, HSQC, and HMBC), DEPT-Q NMR, and by comparing with the published data. A possible biosynthetic pathway for the formation of **1** and **2** was proposed.

1. Introduction

Beilschmiedia is a genus of the family Lauraceae which is an evergreen tree, distributed in Peninsular Malaysia, Sumatra and Borneo (Nishida, 2008). The Lauraceae family is known as a rich source of lignans and neolignans (Azmi et al., 2014; Azmi et al., 2016; Giang et al., 2006; Li et al., 2004; Monte Neto et al., 2008). The term "lignan" refers to a dimer generated by a *β–β′* (8–8′) oxidative coupling of two phenylpropane units, whereas the term "neolignan" should be used for a compound formed by other than 8−8′ coupling (Cardullo et al., 2016). To date, only two *Beilschmiedia* species have been reported to produce neolignans such as kunstlerone, madangones A and madangones B (Mollataghi et al., 2011; Salleh et al., 2016). Thus, this manuscript communicates the isolation and characterization of two unprecedented oxetane containing neolignans from *Beilschmiedia glabra* (*B. glabra*); Pahangine A (**1**) and Pahangine B (**2**). To the best knowledge of the author, this is the first report on the presence of oxetane containing neolignans in Lauraceae. Eight known compounds; coniferaldehyde (Sribuhom et al., 2015), ferulic acid tetracosyl ester (Addae-Mensah et al., 1992), 3-hydroxy-1-(4-hydroxy-3-methoxyphenyl) propan-1-one (Westwood et al., 2016), 3-methoxy-4-methylbenzoic acid (Nguyen et al., 2005), 2-methoxybenzoic acid (Wang et al., 2016), vanillic acid (Ezzat et al., 2017), vanillin (Pouysegu et al., 2010), and 4-hydroxybenzaldehyde (Hsu et al., 2009) were also isolated from this plant.

2. Result and discussion

Pahangine A (**1**) was obtained as a yellow amorphous solid, $[\alpha]_D^{25} = +37.5$. The molecular formula $C_{20}H_{21}NO_6$ was assigned as deduced from its positive LCMS-IT-TOF spectrum (*m/z* 372.1447 $[M+H]^+$; calcd. for $C_{20}H_{22}NO_6$, 372.1442), consistent with 11 ° of unsaturation (DoU); which can be accounted to ring A (4 DoU), ring B (4 DoU), oxetane ring C (1 DoU) and two double bonds (2 DoU). The IR spectrum of **1** indicated the presence of hydroxyl (3354 cm^{-1}) and conjugated carbonyl (1670 cm^{-1}) functionalities. The DEPT-Q spectrum (Table 1) revealed the presence of twenty carbons; seven sp^2 quaternary carbons, seven sp^2 methines, two sp^3 methines, one sp^3 methylene, two methoxyls and one carbonyl carbon of an amide. The signals at δ_C 88.9 (C-7′), δ_C 54.1 (C-8′) and δ_C 63.7 (C-9′) were characteristic of sp^3 carbons of an oxetane (Fleming and Gao, 1997). The ^{1}H NMR spectrum (Table 1) of **1** established the existence of two olefinic protons, five aromatic signals and two methoxyl groups (δ_H 3.77, and δ_H 3.66). The two *trans* olefinic protons resonated at δ_H 8.11 and δ_H 6.98, with a pair of doublets having a coupling constant of 15.7 Hz. The aromatic protons in ring A, H-2 and H-6, appeared as broad singlets at δ_H 7.37 and δ_H 7.15 while, three aromatic protons in ring B, H-2′, H-5′ and H-6′ gave signals of an ABX spin system at δ_H 7.31 (d, J = 1.8), δ_H 7.22 (d, J = 8.1 Hz) and δ_H 7.21 (dd, J = 8.1 and 1.8 Hz) respectively. The ^{1}H NMR spectrum also revealed signals of two methylene protons

* Corresponding author at: Department of Chemistry, Faculty of Science, University of Malaya, 50603 Kuala Lumpur, Malaysia.
E-mail address: khalijah@um.edu.my (K. Awang).

https://doi.org/10.1016/j.phytol.2018.03.008
Received 18 October 2017; Received in revised form 15 February 2018; Accepted 1 March 2018
Available online 13 March 2018

APPENDIX

Appendix A: Percentage inhibition graph for 4-hydroxy-6-(9,13,17-trimethyldodeca-8,12,16-trienyl)-2(3 H)-benzofuranone **136**

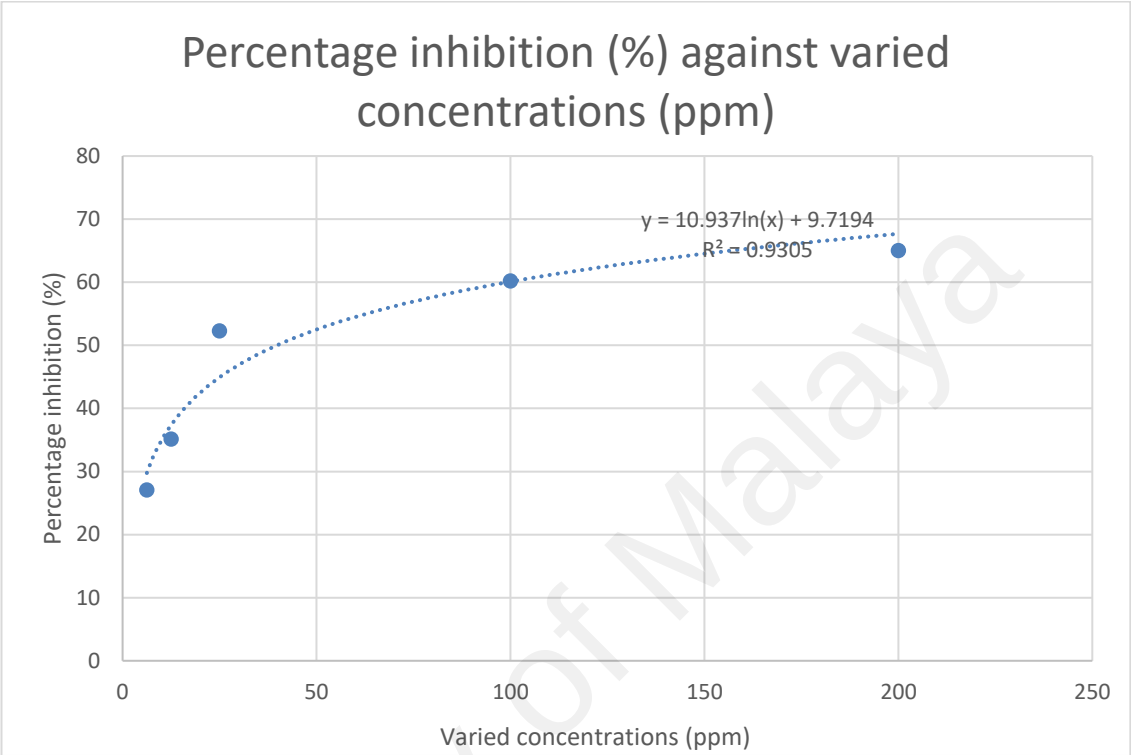

Appendix B: Percentage inhibition graph for (-)-epicatechin **137**

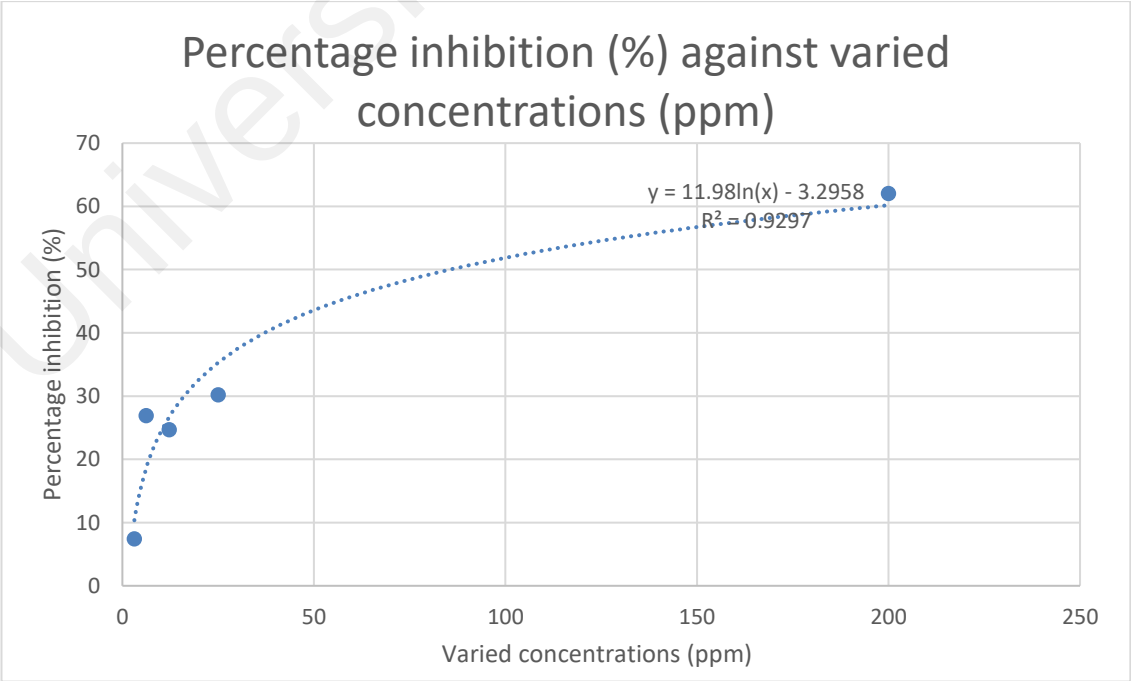

Appendix C: Percentage inhibition graph for catechin **138**